THE ULTIMATE LOAD BEHAVIOUR

OF

COMPOSITE STEEL-CONCRETE BRIDGE DECK STRUCTURES

A THESIS

SUBMITTED TO THE UNIVERSITY OF EDINBURGH

FOR THE DEGREE OF

DOCTOR OF PHILOSOPHY

BY

VUNDELA MALAKONDA REDDY,
B.E., M.Sc.(Eng)., A.M.I.E.

Department of Civil Engineering
and Building Science.

April, 1968.

Acknowledgements

The writer has great pleasure in expressing his gratitude to Professor A. W. Hendry for granting the opportunity to undertake the study under his personal supervision and guidance. Professor Hendry's valuable suggestions and encouregement were of immense help in developing the work which forms the basis of this thesis.

The writer thanks the Association of Commonwealth Universities, London, for the award of financial assistance in the form of a Commonwealth Scholarship from September 1965 to July 1968.

The writer is thankful to the Chairman and Board of Governors, Regional Engineering College, Warangal, India, for sponsoring him for higher studies abroad.

The writer wishes to thank Dr. R. Royles, Dr. S.R. Davies, Mr. R.M. Birse and Mr. W. Dudgeon for their valuable suggestions and help in experimental programme.

The help and assistance of Miss P. Anderson and Miss Elizabeth Turner for photographic work and of all the workshop personnel, especially Mr. R.S. Elder are gratefully acknowledged.

Appreciation is due to all my colleagues for their willing co-operation and help. My special thanks are due to Mr. Chris Chambers for his valuable help in preparing the diagrams in the thesis.

Last, but not least, thanks are due to Miss Elizabeth Geddie for assistance and skilful typing of this thesis.

CONTENTS

List of Figures

Abstract

This thesis is concerned with the Ultimate load behaviour of Composite steel-concrete bridge deck structures and the application of yield-line theory to assess their ultimate capacity. The yield-line theory was applied successfully to analyse the reinforced concrete slabs but its extension to the analysis of structures, where T-beam action is present, is still under exploratory stage. In the introduction, the relative merits of elastic and plastic methods of analysis and their complementary nature are discussed.

A brief review of yield-line theory is given in Chapter 2. It includes an account of the historical development of yield-line theory and the assumptions and the important theorems on which the theory is based.

A theory for the ultimate strength of a Composite beam is developed in Chapter 3. Formulae allowing for strain-hardening of steel and ignoring the same are derived. There is a close agreement between the theory and experiment.

Upper bound solutions by consideration of collapse mechanisms are developed in Chapter 4. Punching shear failure and the effect of composite action on punching load are discussed.

General formulae for the ultimate load of simply supported Composite beam bridges by two alternative methods namely (i) the Equivalent orthotropic slab method and (ii) the Beam and Slab Method are derived.

In order to check the validity of the above theory, eight model bridges along with control beams were built and tested to destruction. The test results are discussed in Chapter 7. The theoretical results compare well with the experimental values.

The conclusions indicate that yield-line theory can be a satisfactory basis for the ultimate load analysis of Composite beam bridge deck structures.

Notation

A_f =Area of flange of steel section, sq.in,

A_r =Area of reinforcement in slab per unit width, sq.in,

A_s =Area of steel section, sq.in,

A_{sc} =Area of steel section in compression, sq.in,

A_w =Area of web of steel section, sq.in,

a =Side length of loaded area, in,

a_e, a_p, a_s as shown in Fig.3.5,

$a_f = A_f/A_s$,

a_x =Component of vector"a" in X-direction,

a_y =Component of vector"a" in Y-direction,

$a_w = A_w/A_s$,

B =Width of flange of Composite beam, in,

Be =Effective width, in,

b =Width of slab, in,

b_x =Component of vector"b" in X-direction,

b_y =Component of vector"b" in Y-direction,

C =Total compressive force, tons,

C_c =Compressive force due to concrete only,

C_r =Compressive force due to reinforcement of slab,

C_u = Cube strength of concrete, psi,

D = Depth of Composite section, in,

d = Depth of steel section, in,

d_l = Effective depth, in,

d_s = Diameter of shear connector, in,

E = Young's Modulus of steel,

E_{sh} =Strain-hardening modulus of steel,

e = Strain,

e_{cu} =Concrete edge strain at maximum moment,

e_e =Steel edge strain at maximum moment,

e_y = Strain in steel at first yield,

e'_y = Strain at top of steel section,

e_s = Strain at beginning of strain-hardening ,

F_1, F_2 : Quantities defined in Computer programme,

f = Ratio of depth of Composite section to depth of steel section,

f'_c = Cylinder strength of concrete, psi,

f_s = Strain-hardening stress,

f_u = Ultimate stress,

f_y = Yield stress,

f'_y = Stess at top of steel section,

g = Ratio of thickness of slab to depth of Composite section,

H = Width of bridge deck,

H_e = Equivalent width of bridge deck,

h = Spacing of beams, in,

h_s = Height of shear connector, in,

i_1, i_2 : Coefficients indicating the variation of moments,

jd = Lever arm, in,

k, k_1 : Quantities defined in Computer programme,

K = Gauge factor,

L = Span of bridge, in,

l = Length of yield line,

l_1 = Longest side length of a rectangular loaded area,

l_s = Distance of load point from the face of the column.

l_x = Projection of l on X-axis,

l_y = Projection of l on Y-axis,

M_c = Ultimate moment of Composite beam, ton-in,

M_{ce} = Ultimate moment of outer Composite beam, ton-in,

$M_x = ma_x$,

$M_y = \mu ma_y$,

$M'_x = m'b_x$,

$M'_y = \mu' m'b_x$,

m = Ultimate transverse +ve moment per unit width of slab, ton-in,

m' = Ultimate transverse -ve moment per unit width of slab, ton-in,

m_i = Magnitude of a typical moment key line,

m_n = Normal moment per unit length of yield line at a point,

m_{ns} = Twisting moment per unit length of yield line at a point,

N_c = Number of shear connectors,

n = Ratio of neutral axis depth to depth of Composite section,

= Sensitivity Factor,

P = Ultimate load, tons,

P_1, P_2 : Quantities defined in Computer programme,

P_A, P_B etc.; Collapse loads from Modes A, B etc.,

$P_{Flex.}$ = Collapse load at flexural failure, tons,

$P_{Min.}$ = Minimum collapse load, tons,

P_{Punch} = Punching load, tons,

P_{Test} = Ultimate load obtained from test, tons,

$p = A_r/d_1$ = Proportion of reinforcement,

p_o = Balanced proportion of reinforcement,

Q_c = Ultimate capacity of one shear connector in Push-out Test,

Q_{uc} = Useful capacity of one shear connector, lbs,

R = Value of Resistance of strain Gauge,

= Value read from Graph in Fig.2.4,

$r = e_s/e_y$,

$r' = A_r\ 100/d_1 \propto C_{ub}$,

$s = E/E_{sh}$,

s_1 = Shortest length of loaded rectangular area, in,

T = Total tensile force, in steel,

t = Thickness of slab, in,

U = Input voltage,

$u = e_{cu}/\ e_y$,

v_1 = Ultimate shear stress at a distance equal to effective depth,

v_o = Ultimate shear stress at a distance equal to half effective depth of slab,

v_o = Ultimate shear stress at zero distance from loaded area,

W = Load,

W_c = Collapse load,

w = Load per unit area,

x = Distance from the load point to the negative yield line parallel to to the beam.

Symbols

α =Flexural parameter defined in reference(92)

α'=Coefficient given by Eq.(2.2) or read from Fig.2.3,

β =Coefficient given by Eq.(2.3) or read from Fig.2.3,
=Torsional parameter defined in reference(92),

β_1=Coefficient indicating the reduction in compressive strength of concrete due to in-plane shear stresses,

Δ = Deflection at the point x,y,

ν = Poisson's ratio,

λ = x/L,

ρ =h/L,

θ_n=Normal rotation of yield line at apoint,

θ_x=Component of θ_n in X-direction,

θ_y=Component of θ_n in Y-direction,

ζ =Ratio of distance between the loads to the span,in,

μ =Ratio of +ve longitudinal to transverse moment,

μ'=Ratio of -ve longitudinal to transverse moment,

μ_e as given by Eq.(4.3)

$\mu_i=(\mu_e+i_2\mu')/(1+i_2)$

$\mu_s=(\mu+i_2\mu')/(1+i_2)$

ϕ,ψ are angles made by yield lines,

δ_1 = Deflection under the load.

CHAPTER 1

1.1 INTRODUCTION

The subject of this thesis is the investigation of the Ultimate Load Behaviour of Composite Steel-Concrete Bridge Deck Structures subjected to one or several concentrated loads. The ultimate load analysis is of recent origin and is being put forward as an alternative approach in design.

In the past, the structural engineering design has been based principally on elastic analysis in which the design criterion is the permissible stress at the adversely stressed part of a structure. The "Safety Factor" which is the ratio of ultimate stress to permissible stress is, no doubt, a measure of the safety of a structure against failure, but it does not indicate precisely how safe is a structure. In other words, it is not possible to calculate by the elastic analysis how much load a structure will carry before it collapses because the structure, no longer, behaves elastically at higher stresses near collapse. The designers were aware of the illogical nature of this design criterion in the orthodox elastic design but did not come forward with an alternative design method until Baker and colleagues (1,2) published their investigations relating to steel structures.

When the ultimate load method is adopted, the structure is analysed when it is in plastic state and when it is about to fail. It is, therefore, possible by this method to predict the load at which a structure will fail and design it to carry the working load, which is a chosen fraction of the failure load. Thus, in the ultimate load method, the ratio of loads rather than stresses, is considered and the ratio of the failure load to the working load is called the "load factor" rather than the "safety factor". The load factor, as defined above, is a real guide to the true safety of the structures.

and can be chosen depending on the degree of safety needed for a particular structure. Apart from the relief from the fundamental defect inherent in elastic method, the advantages claimed for the ultimate load method are its simplicity, the relative ease with which it can be applied to analyse even the most complicated structure and the relative unimportance of such items as sinking of supports, the presence of residual stresses and the worst loading patterns, which cause complications in elastic design. However, it should be admitted that ultimate load analysis has not yet been universally accepted and it is likely to remain complementary and not competitive to the elastic analysis.

The ideal method of design would be first to design the structure with a specified load factor and then to ensure that under working load conditions the deflection, crack widths, steel and concrete stresses are satisfactory. Alternatively the structure might be designed by elastic method and then checked by the ultimate load analysis to find if the load factor is satisfactory. Whichever of these two alternatives is adopted, the ultimate load analysis has to be applied to assess the collapse load of a structure which is essential for the following reasons:

(i) to give the true safety of a structure under specified loads,

(ii) to enable safe designs to be prepared for complicated structures, where a simple design procedure is not available.

and (iii) to assist in an improved understanding of the behaviour of a structure under service conditions, which may lead to a greater economy of design.

1.2 Simple plastic theory.

In a simply supported beam loaded to failure in flexure, a "plastic

hinge" or a region in which the ultimate moment is developed and rotation takes place at a sensibly constant moment, will develop at some point within the span. At this point, the curvature becomes relatively much greater than at other points and hence, for purposes of analysis, the curvature can be assumed to be concentrated at the hinge and the remaining portions of the beam may be assumed straight. An analogous behaviour can be observed in the case of a slab loaded to failure; the curvature tends to be concentrated along a series of straight lines in which the ultimate moment is developed and the remaining portions of the slab remain plane. Since, at ultimate load conditions, some or all of the steel reinforcement is yielding, the lines along which the ultimate moment is developed are referred to as yield lines. Thus, the plastic theory applied to slabs is called "yield-line theory".

1.2.1 The simple plastic theory well-established for steel structures had been described in many texts (2,3,4). The assumptions and theorems on which this theory is founded, are briefly stated here so that they could readily be compared with those of "yield-line theory" which is an extention of the plastic theory for the analysis of reinforced concrete slabs but which has been developed independently by Johansen (5,6).

(a) The assumptions made in simple plastic theory are as follows:

(i) The idealised moment-curvature relationship is as shown in Fig. 1.1 The stress-strain relationship is also idealised on the same lines. The properties in compression are assumed to be the same as those in tension. When the moment at a cross section is sufficiently large so that the material there yields completely, very large deflections occur without increase in bending moment and the cross section behaves as a hinge. Collapse of the structure occurs

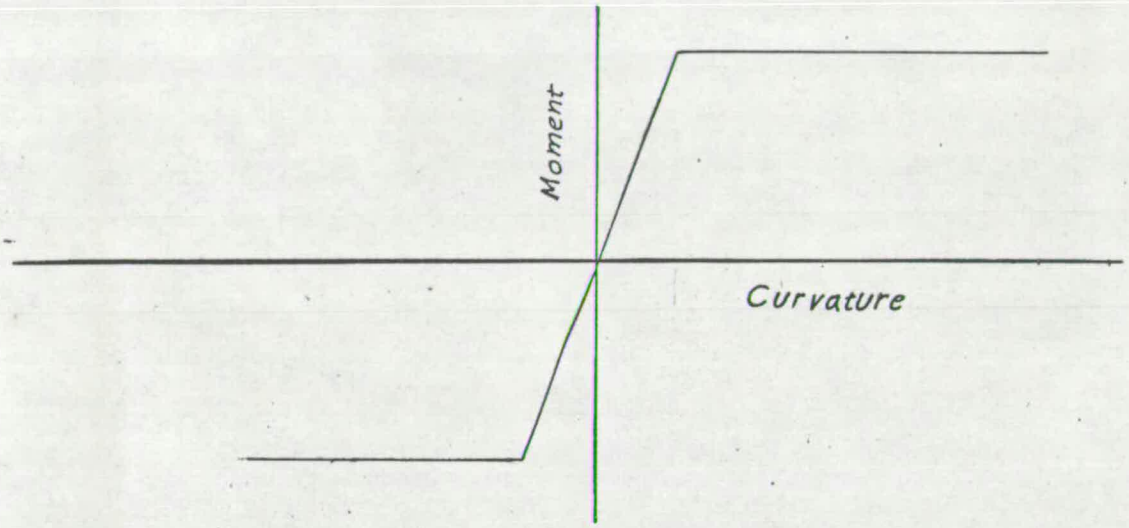

Fig.1.1 Idealised Moment-curvature relationship for steel

when a sufficient number of plastic hinges has formed to transform the structure into a mechanism.

(ii) The deformations are small implying unaltered geometry, which does not invalidate the equilibrium equations.

(iii) The redistribution of moment will occur from the more heavily stressed sections of the structure to the less heavily stressed ones.

(iv) The effects of axial force, shear, instability, repeated loading and brittle fracture may be neglected.

(b) The following are the theorems:

As stated by Neal (3), the "Static theorems" is

"For a given frame and loading, if there exists any distribution for bending moment through out the frame which is both safe and statically admissible with a set of loads W, the value of W must be less than or equal to the collapse load Wc."

This theorem defines what is known as "lower bound" to the collapse load.

The "kinematic theorem" as stated by Neal (3) is

"For a given frame subjected to a set of loads W, the value of which is found to correspond to any assumed mechanism must be either greater than or equal to the collapse load Wc".

This theorem defines the "upper-bound" to the collapse load. These theorems have been proved by Greenberg and Prager (7)

The "Uniqueness theorem" which is a combination of the previous two theorems is

"If for a given frame and loading at least one safe and statically admissible bending moment distribution can be found and in this distribution the bending moment is equal to the fully plastic moment at enough cross sections to cause

failure of the frame as a mechanism due to rotations of plastic hinges at these sections, the corresponding load will be equal to the collapse load Wc".

A formal proof of this theorem is given by Horne (8).

From the assumption (i) it is obvious that the material of which the structure is made should have constant yield point and should be capable of sustaining the yield stress up to several times the elastic strain at first yield, especially when there are extensive collapse mechanisms. Only mild steel satisfies this requirement. As a matter of fact it is the ductile or plastic property of steel observed in tests that had prompted the pioneers in the field to think on these lines and develop a theory ideally suited to steel structures. However, there is a growing tendency to apply this theory to reinforced concrete structures (9,10) on the assumption that reinforced concrete can have or can be designed to have sufficient rotational capacity. Tests carried by Ernst (11) seem to indicate that sufficient rotation will always be achieved with reinforced concrete sections. Corley (12) points out that the ultimate curvature and inelastic rotation occuring in the hinging region near the section of maximum moment of a reinforced beam provided with binding steel in compression zone could be much greater than those calculated on the assumption of a maximum concrete compressive strain of 0.003. But still there exists doubt as to whether or not sufficient rotation can be obtained from a reinforced or prestessed concrete structure to allow all the plastic hinges to form before failure of one of these hinges occurs.

A heavily reinforced concrete section brings much more of the concrete into play and fails by crushing of concrete, which is a sudden failure. This is true in the case of beams and frames which are likely to be reinforced with a more percentage of steel than slabs. A lightly reinforced slab, on the

other hand, is assumed to fail in tension, the steel reinforcement following the stress-strain pattern required for the plastic theory, thus allowing the whole pattern of yield lines to form before its collapse. There is sufficient test data to indicate that it is a satisfactory assumption, on which Johansen (6), who did the main pioneer work for the development of plastic design for reinforced concrete slabs, has based his "Yield-line theory".

1.3 Scope of the present investigation

This investigation forms part of a programme to apply simplified yield-line theory to obtain upper-bound solutions for simply supported Composite steel-concrete Bridge deck structures. A composite structure as cited in the thesis, is a reinforced concrete slab resting on and acting compositely with longitudinal steel girders; The steel girders are designed as T-beams in which the slab also acts as a compression flange of the beam. Jones and Wood (13) elaborate on the main problem that centres round the permissible use of T-beams in the plastic theory of bending. They add that, though at first the excess of concrete in what is termed the beam seems hardly conducive to ideal plasticity, such T-beams are likely to be "under-reinforced" when they form part of a slab, the predominating failure (apart from shear failure) being tension failure of the steel, so that the moment of resistance is sensibly held constant at failure. They further point out that the ultimate moment of resistance is not very sensitive to the assumed width of "flange" and from this point of view there would seem to be little objection to the careful use of T-beams within yield-line theory. They further state that whilst it is admitted that idealised plastic theories for slab and T-beam action combined are open to criticism, nevertheless the hidden effects of membrane action are

likely to cover up the defects of the theory.

No attempt is made to take advantage of membrane action in this investigation, which is mainly concerned with the study of collapse mechanisms involving the supporting beams in which case no beneficial membrane action (apart from T-beam action) is likely to develop (13).

Lower-bound solutions are not attempted since it is extremely difficult to find satisfactory stress fields to conform to the rigorous rules of Limit Analysis.

The literature on punching shear failure is reviewed and the effect of composite action of beams on punching load is discussed.

CHAPTER 2

REVIEW OF YIELD-LINE THEORY

The reason for the growing international popularity of yield-line theory, perhaps, lies in the fact that it is basically an engineers' intuitive approach to a problem, based on results of repeated experiment. It has been accepted without an exhaustive study of some of its foundations because it is attractively simple and matches well established solutions in extremes of its range of application. It should be of interest to know its historical development in relation to other techniques for assessing the ultimate strength of slabs.

2.1 Resume of previous work

As early as 1890, Bach (14) advanced a simplified theory of failure and a corresponding method of calculation has been given by Suenson (15). In 1922, Ingerslav (16) introduced the simplified yield-line theory for thin plates and derived for the first time the correct solution (worst case) for the collapse load of a rectangular slab. But he gave the shear forces in the yield lines zero value and so the method could not be applied to all cases. The acknowledged pioneer of yield-line theory is Johansen (5,6) who extended the theory to cover much more general cases and provided an immense number of practical examples. He developed the "Work" method for calculating the collapse load and an alternative "Equilibrium" method involving nodal forces, which gave the same collapse load but which provided additional information.

A review of the work carried out by Ingerslav (16) was published in 1953 by Hognestad (17). In 1957, Mansfield (18) employed the calculus of variations and found the worst lay out for a system of yield-lines involving non-circular "fans" of any shape. His intentions behind this approach were

ingenious in that if the gravest possible upper-bound solution was found, then that would be the solution without being concerned with lower-bound solutions. But he was unaware that Johansen (5) in 1943 had achieved similar solutions using the nodal force theory. The inference is that nodal force theory (equilibrium method) and the calculus of variations applied directly to the work equation are absolutely equivalent (13).

Until the rigorous rules for Limit Analysis of Prager (19,20) were discovered, there was a doubt as to the nature of the solutions obtained from both the Work and Equilibrium methods. Neither of the two methods produced a unique pattern of yield lines, which yielded the lowest failure load. The above rules indicated that the lowest collapse load had been reached, if one could find a coincidental "upper" and "lower" bound solution. The conditions required to establish an upper or lower-bound solution were essentially as follows:

(a) upper-bound solution - which gives an unsafe or else correct value of the collapse load.

1. A valid mechanism of collapse must be found which satisfies the mechanical boundary conditions.
2. The internal dissipation of energy on yield lines must equal the expenditure of energy due to the external loads (Work Equation).
3. Either the material stays rigid or else deforms plastically
4. Where deformations take place the direction of the strains is defined by the mechanism. The direction of the strains must in turn define the yield stresses required to calculate the dissipation of energy. (This is known as the yield criterion

(b) Lower-bound solution - which gives an oversafe or else correct value of the collapse load.

5. A complete stress field must be found everywhere satisfying the differential equation of equilibrium.

6. The forces and moments at the edges must satisfy the boundary conditions.

7. At no point can the principal stresses violate the yield criterion.

From these rules, it was discovered that, though a lower-bound technique was also based on equilibrium, Johansen's so-called "Equilibrium" method was not a lower-bound solution since his method specified the stress state only along the yield lines and not everywhere in the slab, as required by item 5. Wood (21) proved the equivalence of nodal force theory to the work equation plus differentiation. The work of Kemp (22), Morley (23) and Wood (24) also showed that it was theoretically possible to transform the latter into the language of the former, though in some cases the transformation was extremely laborious. It now becomes clear that the two methods given by Johansen are the alternative forms of only one method namely the Work Equation plus differentiation, though as claimed by Wood (21) and Zones (25), the Equilibrium Method is much simpler to apply in certain cases.

Thus, yield line theory, whichever technique is used, should only be regarded as an upper-bound solution. It may be mentioned in this context that, by employing simplified stress fields and satisfying items 5 and 6, Hillerborg (26) produced a rival and relatively simple method (Strip Method), which is not discussed here.

All that remains now is to see whether it is possible to produce coincidental upper-bound and lower-bound solutions, which conform to the rules of Limit Analysis. Wood (21), Sawczuk and Jaeger (27) in spite of an internationally sustained effort could collect only a very few such solutions. Zones and Wood (13) point out that so far, trivial cases excepted, there is no known coincidental upper and lower-bound solution for orthotropic slabs. They further point out that any hopes of establishing such solutions for all cases have to be abandoned, if the stringent rules of Limit Analysis have to be applied and that yield-line theory must be accepted for what it is. This has led to a newly proposed "normal moment" yield criterion (22,24) in which only the value of the normal moment on yield lines is specified, without reference to the principal moments, which means that yield-line theory and Limit Analysis must go their own separate ways, since they can not yet employ a common yield criterion. The indications are that a new yield criterion such as that proposed by Baus and Tolaccia (28) might more easily be built into yield-line theory than into a rigorous Limit Analysis. Although much has been written (29 to 35) and discussed recently on a general yield-criterion for reinforced concrete slabs, Johansen's original "stepped" yield criterion is still in common use. How this criterion has been adapted to the analysis of slabs in the thesis will be discussed later in this chapter.

2.2 Experimental Confirmation

Analysis of extensive test results carried out by Johansen (6), Wood (21) and Sawczuk and Jaeger (27) reveals a conservatism about yield-line theory, especially in the cases where strong forces (membrane action) are developed in the plane of the slab (36,37), though occasionally (38) suggestions have been made to reduce slightly the required moments of resistance on account of

membrane stresses. Recent tests in Holland (39) have also shown that yield-line theory is reliable even for irregularly shaped slabs. Nylander (40) studied the cases where, with heavy point loads or column reactions, punching shear is encountered.

2.3 Assumptions, Definitions and Notation and Theorems

At the outset, it must be admitted that "yield-line theory" is indeed a great simplification of the true behaviour of a reinforced concrete slab. If a completely accurate assessment of the failure load of a slab is to be made, it is necessary to know the complete stress and deformation relations, which occur under any combination of force and moment, which is out of the scope of this thesis. The alternative to an exact solution is to evolve one in which certain simplifying assumptions are made.

Assumptions

(a) The concrete slab is so lightly reinforced that failure occurs in tensi the reinforcing steel following the stress-strain relation required for simple plastic theory. The stress-strain curves for steel and concrete are shown in Fig. 2.1 and the cross section of slab in Fig. 2.2. The ultimate moment per unit width of slab is given by

$$m = A_r f_y \left(d_1 - \frac{\beta A_r f_{yr}}{a^1 f^1_c} \right) \quad \ldots\ldots\ldots\ldots\ldots\ldots (2.1)$$

or

$$m = A_r f_y \left(d_1 - \frac{3A_r f_{yr}}{4C_u} \right) \quad \ldots\ldots\ldots\ldots\ldots\ldots (2.1a)$$

where A_r = Area of steel per unit width of slab in sq. in.

f_{yr} = Yield stress of reinforcing steel in p.s.i.

f^1_c = Cylinder strength of concrete in p.s.i.

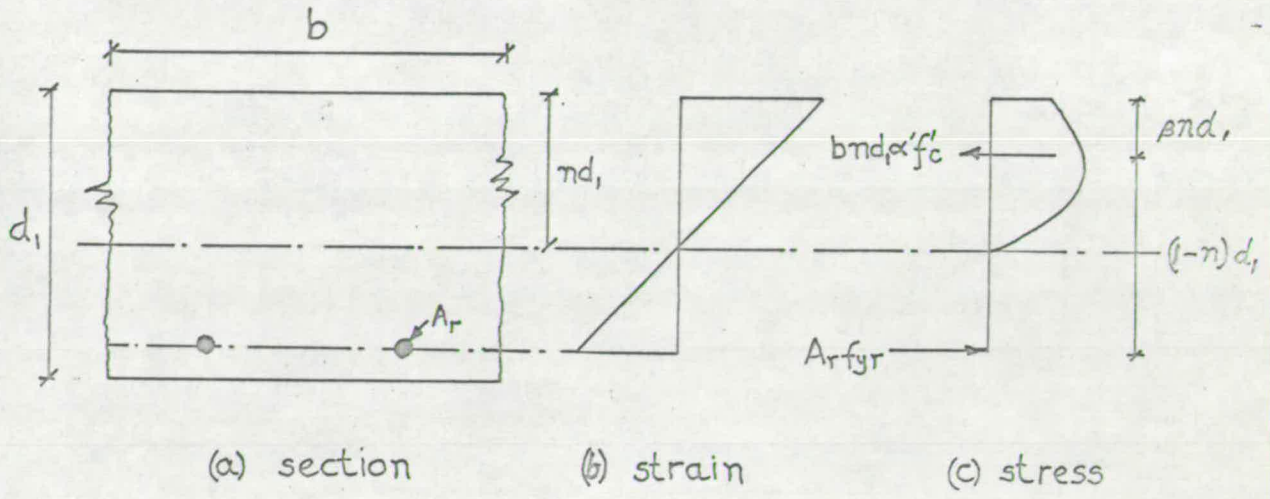

FIG. 2.2 ultimate moment of slab in pure bending

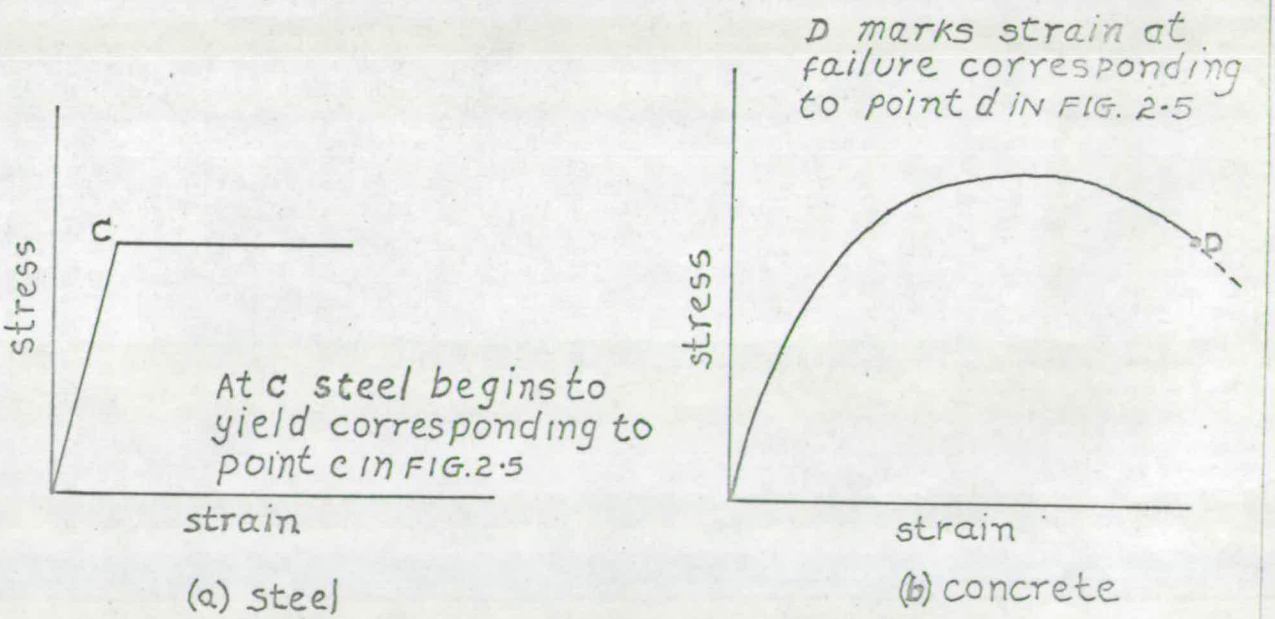

FIG. 2·1

d_1 = Effective depth of section in inches

C_u = Cube strength of concrete in p.s.i.

α^1 and β are coefficients obtained from the graph originally given by Hognestad (41) and reproduced in fig. 2.3, or from the expressions

$$\alpha^1 = \frac{3900 + 0.35 f_c'}{3200 + f_c'} \quad \ldots\ldots\ldots\ldots\ldots\ldots\ldots\ldots \quad (2.2)$$

$$\beta = 0.5 - \frac{f_c'}{80{,}000} \quad \ldots\ldots\ldots\ldots\ldots\ldots\ldots\ldots \quad (2.3)$$

when it is assumed that $f_c' = 0.85\ C_u$, both Equations (2.1) and (2.1a) give values of m which are more or less the same. When the slab is reinforced with high tensile steel without definite yield point (42) the ultimate moment per unit width is given by

$$m = \frac{R}{\alpha C_{ub}} \alpha C_{ub} d_1^2 \quad \ldots\ldots\ldots\ldots\ldots\ldots\ldots\ldots \quad (2.1b)$$

Where C_{ub} = Ultimate strength of concrete in bending in p.s.i.

αC_{ub} = Average concrete strength at failure and is given by the following expressions,

$0 < C_u < 3000$, $\quad \alpha C_{ub} = C_u \left(0.84 - \frac{0.1\ C_u}{1000}\right)$

$3000 < C_u < 7000$, $\quad \alpha C_{ub} = C_u \left(0.62 - \frac{0.027\ C_u}{1000}\right)$

$C_u > 7000$, $\quad \alpha C_{ub} = 0.44\ C_u$

$\frac{R}{\alpha C_{ub}}$ is read from the graph reproduced in Fig. 2.4, knowing the value of r^1,

Where $r^1 = \frac{A_r\ 100}{d_1\ \alpha C_{ub}}$

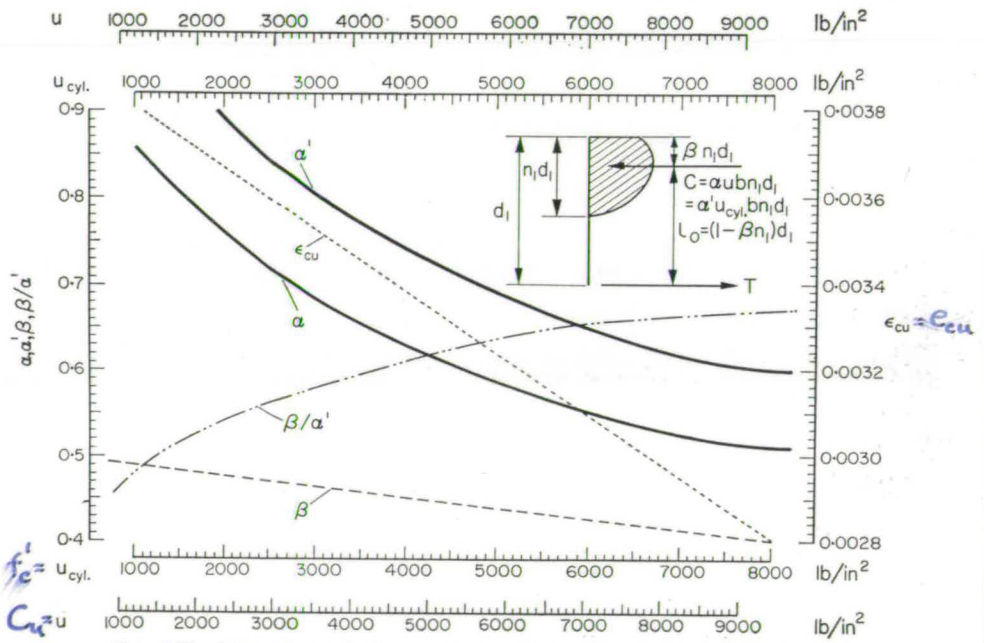

FIG. 2.3 Ultimate load characteristics of stress block for concrete in flexural compression.

FIG. 2.3

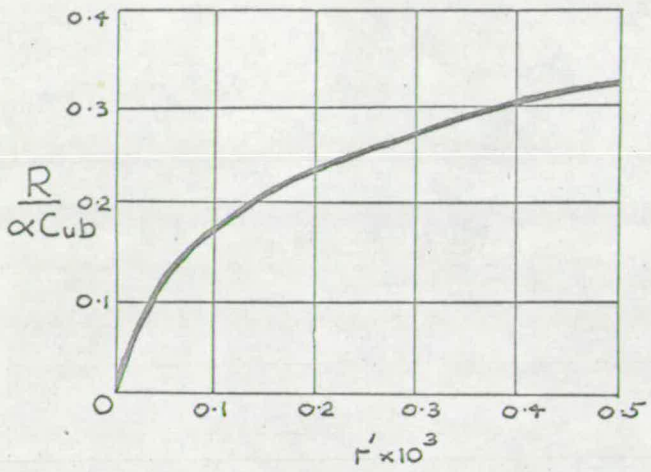

FIG.2·4 Relation between $R/\alpha C_{ub}$ and r' for sections reinforced with high tensile steel without a definite yield point

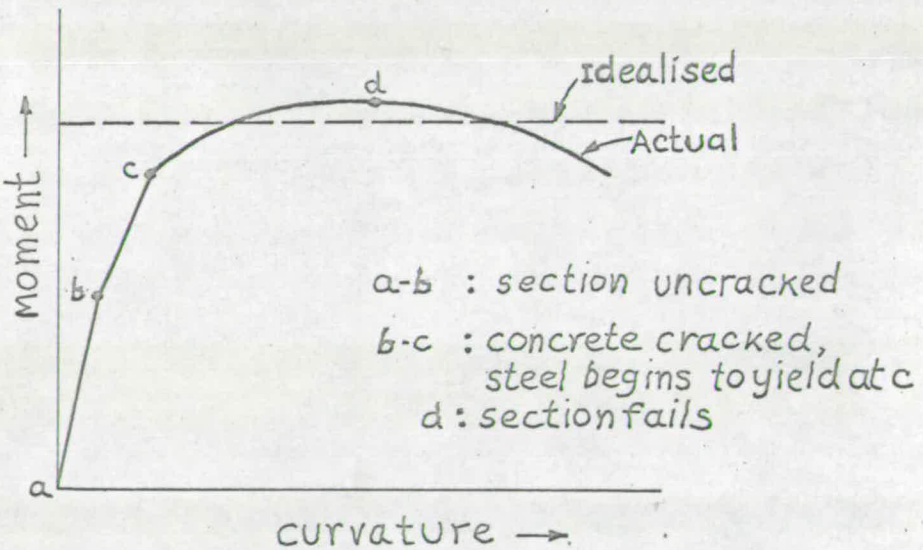

FIG.2·5 Moment-curvature relationship for a reinforced slab

(b) The ultimate or collapse load can be arrived at by consideration of bending action only, the actions of all other stress components having been neglected.

(c) The elastic deformations are small compared to plastic ones and are ignored.

(d) The moment-curvature relationship is idealised as shown in Fig. 2.5. It follows "rigid-plastic" theory, which means that, the elastic deformations having been neglected, the material stays rigid (no deformation) or else goes plastic.

(e) The plastic deformations occur only along yield lines where the reinforcement yielded, while the parts into which the slab is divided by yield lines remain plane.

The comments on the assumptions are as follows:

(a) Where the concrete is overreinforced or where high tensile steel without definite yield point is used as reinforcement, the plastic theory for simple structures may still be permissible but it can not be on par with the excellent response of steel structures to idealised plastic theory, with quite extensive mechanisms (21).

(b) It may not be worth while to attempt to obtain an exact solution for the value of the failure moment since it involves writing down and solving the relevant equilibrium equations compatible with the deformation system as well as satisfying the boundary conditions, which is prohibitive. Fortunately, the test results indicate that the ultimate moment calculated assuming bending action only is conservative and hence is on the safe side.

(c) As observed by Morice (43) in his discussion on test results some elastic deformations do take place in the areas between yield lines and

so these areas do not, in fact, remain plane as assumed. All the rotation does not occur on the assumed yield lines and other cracks form near the main ones. He attributes these as the probable reason for the formation of curved yield lines in places where straight ones are predicted.

- 14 -

(d) From the assumption (e), it follows that the deformed slab usually consists of a series of inclined planes and since inclined planes meet in straight lines, it is obvious that yield lines are straight. A curved yield line may be looked upon as the limiting case of yield lines forming a polygon.

Definitions and Notation

(a) Isotropically reinforced slab is one in which the ultimate moment per unit length is the same in two orthogonal directions. It also indicates that moment can be taken to be the same in any direction.

(b) Orthotropically reinforced slab is one in which the ultimate moment per unit length is different in two orthogonal directions.

The terms isotropic and orthotropic may be applied to either top or bottom reinforcement.

(c) A normal moment is that moment which is normal to the yield line or which acts on a section parallel to yield line.

(d) A twisting moment is that moment which is tangential to the yield line or which acts on a section perpendicular to yield line.

(e) Moment key notation (Fig. 2.6)

The moment key line at the side of the slab is an abbreviated form of the statement "the normal moment per unit length on a yield line in this

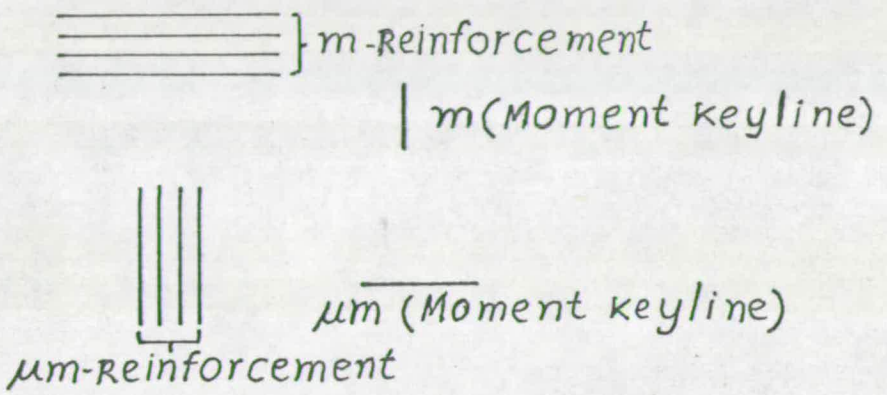

FIG. 2·6

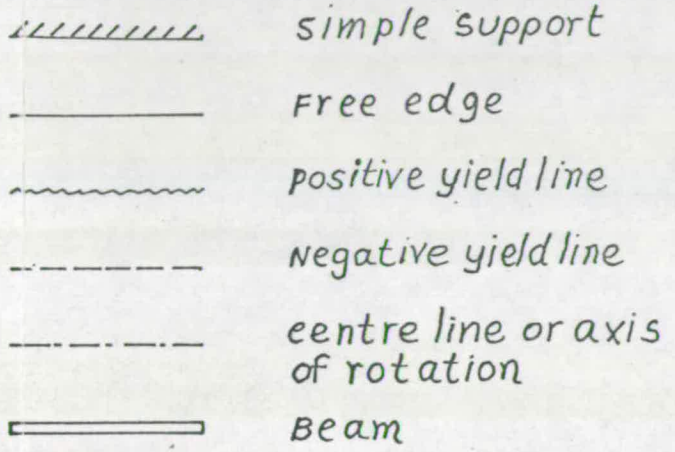

FIG. 2·8

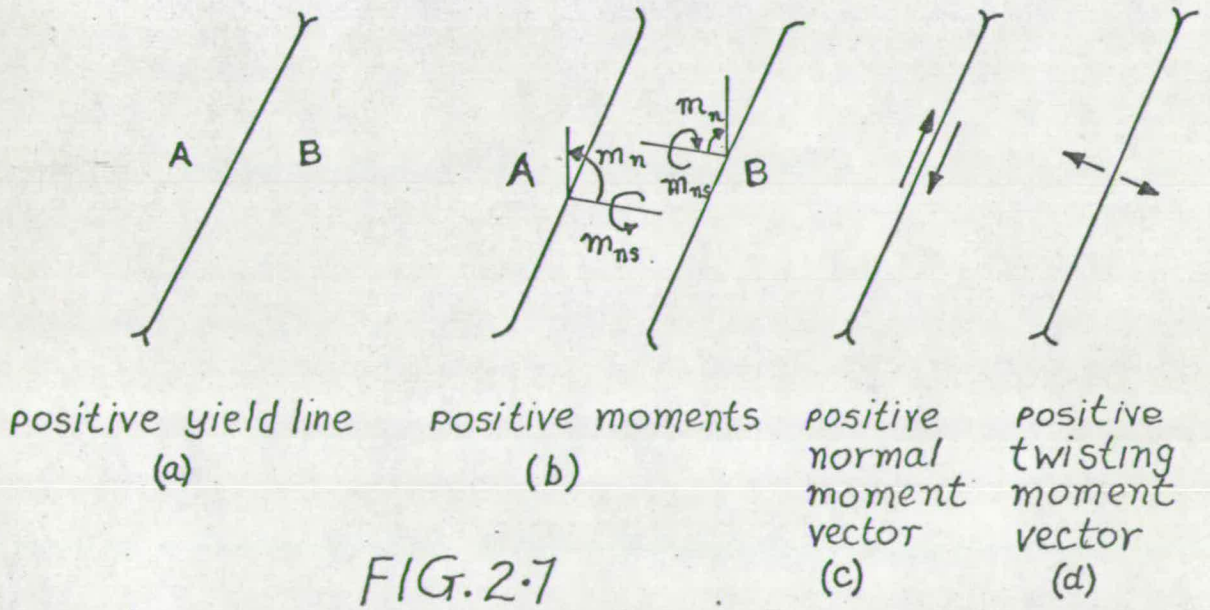

FIG. 2·7

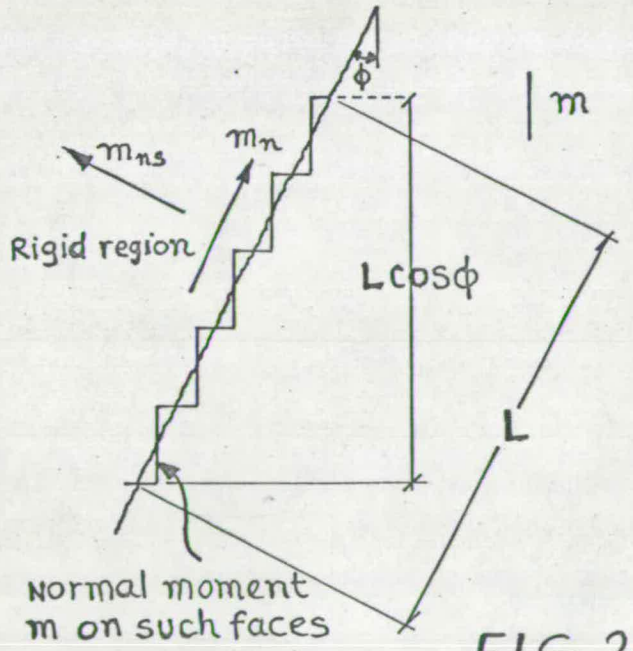

FIG. 2·9

direction is the value given".

A solid "key line" implies positive bending strength (i.e.) it refers to tension reinforcement in the bottom of the slab and a "broken key line" for negative strength (i.e.) top reinforcement in tension.

(f) Sign Convention for moments (Fig. 2.7)

The sign convention for normal and twisting moments is that the moments acting on a region in the direction given in Fig. 2.7 (b) are regarded as positive. Thus the normal moment m_n, when the bottom of the slab is in tension (sagging moment) is positive. The moment vector notation used is an anti-clockwise notation.

(g) General Convention (Fig. 2.8)

The general convention that will be adopted to indicate the type of support and type of yield line is shown in Fig. 2.8.

2.4 Johansen's "stepped" yield criterion (Fig. 2.9)

(a) The basic assumptions underlying it are as follows:

(i) The normal and twisting moments on a yield line can be obtained by considering each band of reinforcement in turn and adding the individual effects.

(ii) For each band of reinforcement taken on its own, the yield line may be considered to be divided into small steps parallel to, and at right angles to the reinforcement as shown in Fig. 2.9.

(iii) All reinforcement crossing the yield line is assumed to yield.

(iv) All reinforcement is assumed to stay in its original straight line when the steel yields (i.e.) there is no kinking or change in horizontal direction of steel crossing the yield line.

(v) When each band of reinforcement is considered on its own, on small steps at right angles to the reinforcement there is only a normal moment per unit length "m" whose value is given by equation (2.1), (2.1a) or (2.1b), while on the steps parallel to the reinforcement, there is neither normal nor twisting moment.

(vi) The values of normal and twisting moments on the yield line are such that they are equivalent to components of the normal moments on the steps.

(b) Evaluation of normal moment m_n and twisting moment m_{ns}.

The normal and twisting moments per unit length of yield line are given by

$$m_n = m \cos^2 \phi \quad \ldots\ldots\ldots\ldots\ldots\ldots\ldots \quad (2.4)$$

$$m_{ns} = m \sin \phi \cos \phi \quad \ldots\ldots\ldots\ldots\ldots\ldots\ldots \quad (2.5)$$

Where m = Moment as shown by Moment key line in Fig. 2.6.

ϕ = Angle measured clockwise from m on tc the yield line.

When there are several sets of reinfocement crossing a yield line, the total value of m_n and m_{ns} will be the sum of the separate effects of reinforcement so that in general

$$m_n = \sum_{i=1}^{n} m_i \cos^2 \phi_i \quad \ldots\ldots\ldots\ldots\ldots\ldots\ldots \quad (2.4a)$$

$$m_{ns} = \sum_{i=1}^{n} m_i \sin \phi \cos \phi_i \quad \ldots\ldots\ldots\ldots\ldots\ldots \quad (2.5a)$$

Where m_i is the magnitude of a typical moment key line and ϕ is the angle

measured clockwise from the moment key line m_i on to the yield line. In applying the above equations, only the m_i values having the same sign as that of the yield line are considered.

2.5 General discussion on yield criterion

The yield criterion (13) that has already been established for reinforced concrete, namely

$$m_n = \sum_{i=1}^{n} m_i \cos^2 \phi_i$$

is quite sufficient as the definition of the yield criterion so long as it is coupled with the statement that only normal rotations θ_n are allowed.

The value indicated for the twisting moment on yield lines,

$$m_{ns} = \sum_{i=1}^{n} m_i \sin \phi_i \cos \phi_i$$

is not a necessary part of yield-line theory.

In the present investigation, neither "square" criterion for isotropic reinforcement nor the "stepped" criterion for orthotropic reinforcement will be adopted in their entirety. The value of the normal moment m_n will be accepted as reliable for a designer.

2.6 Important Theorems on yield lines

Theorem I The yield line between two parts of a slab must pass through the point of intersection of their axis of notation, which usually lie along lines of support or pass over any columns.

Theorem II The yield pattern is determined by the axes of rotation of the various parts of the slab and the ratios between them.

Theorem III The yield pattern corresponds to a maximum absolute value of the ultimate moment per unit length.

The proofs of the above theorems are given by Johansen (6).

2.7 Affinity or Transformation Theorems (Fig. 2.10)

The affinity theorems are applicable only to slabs which are reinforced such that the upper and the lower reinforcements run in the same directions.

If these directions are chosen as co-ordinate axes, the ultimate moments m and -m' will be in sections parallel to the X-axis, with μm and $-\mu' m'$ in sections parallel to the Y-axis. Fig. 2.10 shows an arbitrary part of a slab in which the resultant of the positive ultimate moments is so determined by the vector "a" that the components parallel to the axis are $M_x = ma_x$, $M_y = \mu m a_y$, in which a_x and a_y are the components of "a" in the direction of the axes. In the same way, the resultant of the negative ultimate moments is determined by the vector "b", the components being $M'_x = m' b_x$ and $M'_y = \mu' m' b_y$

Theorem IV is applicable in the cases where $\mu' = \mu$ and also to slabs with simple reinforcement in which m' and $\mu' m' = 0$.

Theorem V requires that $a \equiv b$ for every part of the slab but it is possible for $\mu' \neq \mu$

Theorem IV

In an orthotropic slab with the ultimate moments per unit length m, μm for the bottom reinforcement and -m', $-\mu m'$ for the top, the directions of reinforcement being the same for top and bottom, m and m' can be calculated by transforming the orthotropic slab to a corresponding isotropic slab; the dimensions of isotropic slab in the directions of vectors m and -m' are obtained from those of the orthotropic slab by dividing by $\sqrt{\mu}$. The load per unit area is the same for both slabs and the yield patterns correspond.

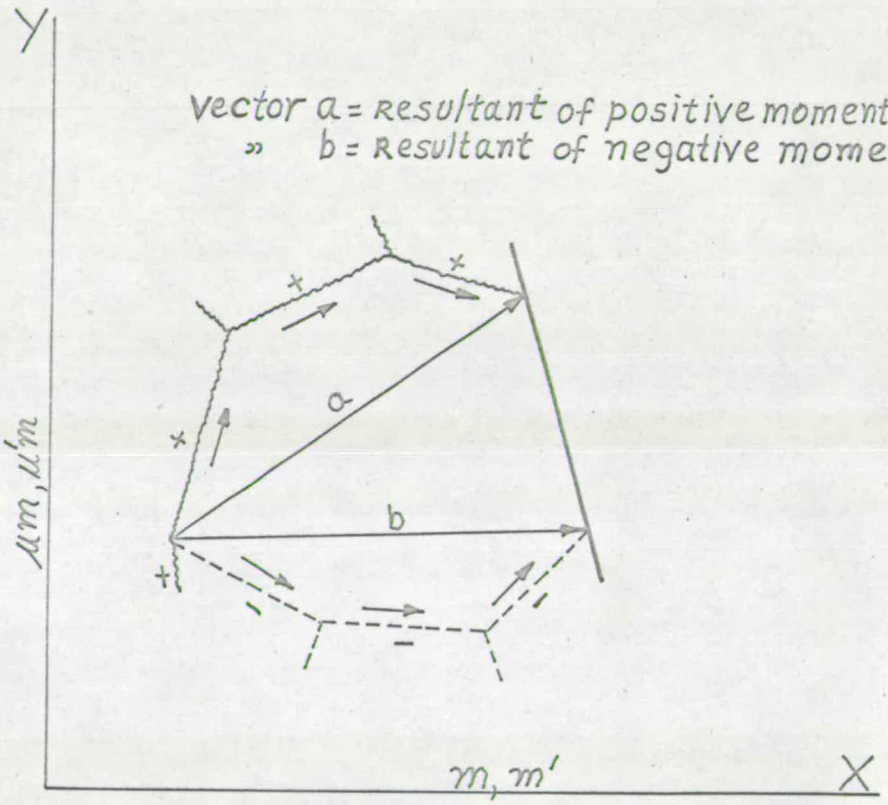
Y
vector a = resultant of positive moments
» b = resultant of negative moments
a
b
μm, μ'm
m, m'
X

FIG. 2·10

A single force P may be looked upon as being a load concentrated over a small area ΔA. For the transformed slab, the corresponding area will be $\Delta A/\sqrt{\mu}$ and the force $P/\sqrt{\mu}$.

Theorem V In an orthotropic slab with the ultimate moments per unit length m, μm for the bottom reinforcement and -m', μ'm' for the top, the directions of reinforcement being the same for top and bottom, and in which the resultants of the positive and negative ultimate moments for each part of the slab can be defined by one and the same vector, m and -m' can be calculated as for an isotropic transformed slab as in Theorem IV except that μ_i replaces μ, where

$$\mu_i = \frac{\mu m + \mu' m'}{m + m'} \quad \ldots\ldots\ldots\ldots\ldots\ldots \quad (2.6)$$

The load per unit area is the same for both slabs, and the yield patterns again correspond.

2.8 The Work Equation

"If a displacement system is given to a slab having a valid failure mechanism, then the work done by the external loads is equal to the work done in the yield lines in taking up the displacement system."

The mathematical form of the above statement is called the Work Equation and is given by the expression

$$\Sigma\left[\iint w\,\Delta dx\,dy\right] = \Sigma\left[\theta_n \int m_n ds\right] \quad \ldots\ldots\ldots\ldots\ldots \quad (2.7)$$

Each region Each line.

Where w is the load/unit area at the point x,y on a rigid region and

Δ is the deflection at the same point

m_n is the normal moment/unit length at a point on a yield line,

θ_n is the normal rotation of the yield line at that point

and ds is a short length of yield line at that point.

The rotation θ_n along a straight yield line is constant and m_n, until specifically stated otherwise, is assumed constant along a yield line.

Therefore equation (2.7) will reduce to

$$\Sigma\left[\iint w\Delta \, dx \, dy\right] = \Sigma[(m_n \, l \, \theta_n)] \quad \text{(Each region; Each line)} \qquad \ldots\ldots\ldots\ldots\ldots\ldots \quad (2.7a)$$

where l is the length of a yield line.

Using vector component method (13), the equation (2.7a) can be rewritten as

$$\sum_{A}^{N}\left[\iint w\Delta \, dx \, dy\right] = \sum_{A}^{N}[\Sigma(m_x \, l_x \, \theta_x) + \Sigma(m_y \, l_y \, \theta_y)] \quad \text{(Each region; Each region)} \qquad \ldots\ldots\ldots \quad (2.7b)$$

where $\Sigma(m_x l_x \theta_x)_A$ implies that the quantity $(m_x l_x \theta_x)$ is calculated for each line round the boundary of rigid region A and the values so calculated are summed after assigning the correct sign. The expressions in y are similar and the letter suffixes B .... N refer to other rigid regions.

$(M_x)_A$ = moment/unit length, in the direction of the X-axis chosen for rigid region A, for a yield line on the boundary of region A.

$(l_x)_A$ = projection of that yield line on to the chosen X-axis for rigid region A.

$(\theta_x)_A$ = rotation of rigid region A about the X-axis.

CHAPTER 3

ULTIMATE STRENGTH OF A COMPOSITE BEAM

3.1 INTRODUCTION

A composite beam bridge can be looked upon as a structure (Fig. 3.1) consisting of a number of single composite beams jointed together and made to interact by the continuity of transverse reinforcement through the flange slab. If, therefore, the ultimate strength of a single composite beam subjected to longitudinal bending is determined, it can be related to the ultimate strength of the bridge as a whole. The behaviour of a composite beam, when it is part of a bridge is complex and can be simplified by using the concept of "effective width", which will be discussed later.

Tests indicate that strain-hardening (44 to 52) where occurs, results in a considerable increase of collapse load and so it is proposed to also allow for its effect on maximum moment.

Before a general formula for ultimate moment of resistance of a composite beam is derived, it is necessary to investigate,

(a) the secondary modes of failure and their prevention in order to realise the full theoretical maximum moment.

(b) the state of deformation in concrete and steel at or near collapse.

(c) the effect of slip on the maximum moment.

and (d) the effective width of slab acting with the beam.

(a) the possible secondary modes of failure include,

(i) longitudinal splitting of slab along the shear connectors.

(ii) vertical separation of the slab and beam.

(iii) lateral buckling of the joist.

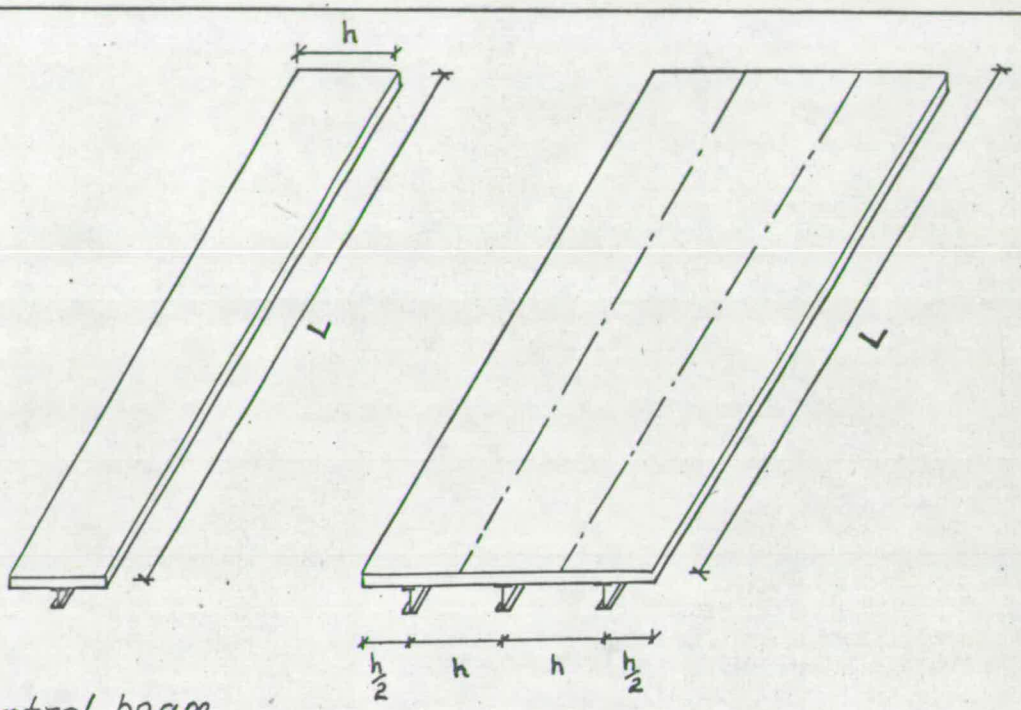

control beam

(a)

composite beam bridge

A-series

(b)

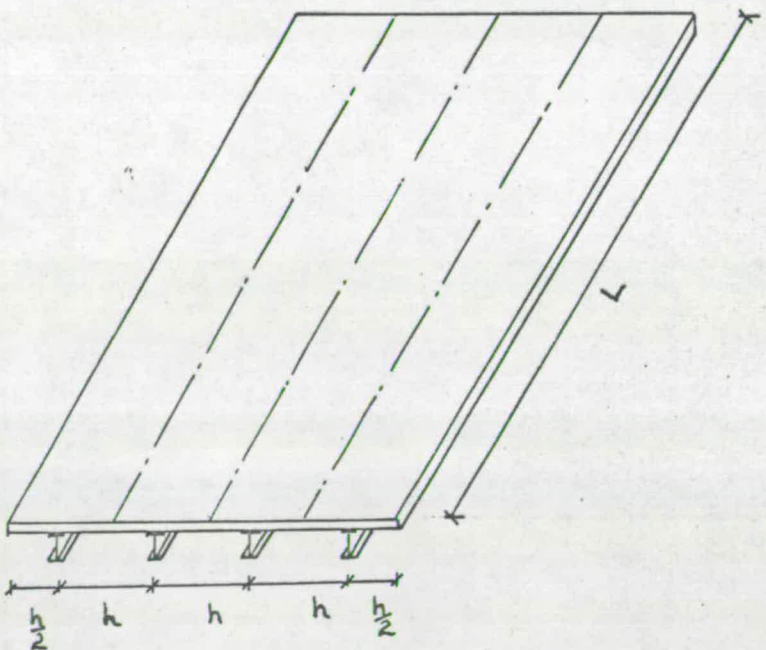

composite beam bridge

B-series

(c)

FIG. 3·1

The failure of type (i) was observed by Adekola (53), Barnard and Johnson (54) and Siess (55). Adekola pointed out that the cause of this failure was the transverse tensile stress along the length of the beam and suggested that a minimum transverse reinforcement of 0.4% with adequate bond length was sufficient to prevent such failure at working load. The author tested composite beams with the ratio of flange width to span equal to 0.4 and 0.167, the transverse reinforcement being the same in both cases. The former developed longitudinal cracks (Fig. 3.2) before the collapse load reached where as they were completely absent in the latter (Fig. 3.3), which indicates that a proper choice of width to span ratio, for a given percentage of transverse reinforcement is also essential to prevent this type of failure.

The failure of type (ii) can be prevented by proper design and proportioning of shear connectors. Headed studs and other types of shear connectors have been standardised (56) to have sufficient horizontal projection to prevent the slab from lifting up.

The type of failure (iii) does not appear serious in the case of simply supported structures since the entire flange which is in compression, acts with the steel member up to its failure.

(b) The State of deformation at or near collapse.

Almost all beams tested by Chapman and Balakrishnan (57) have exhibited strain-hardening. The experimental moments exceeded the theoretical moments calculated using C.P.117 (modified) by 10 to 30%. The measured concrete strains at or near collapse were about 20 to 60% greater than those at spalling of concrete and the corresponding loads were about 5 to 12.5% greater. Chapman (58) observed that when the strain at the top surface of the concrete slab reached a value of about 0.38%, spalling of concrete began and the ultimate strength of

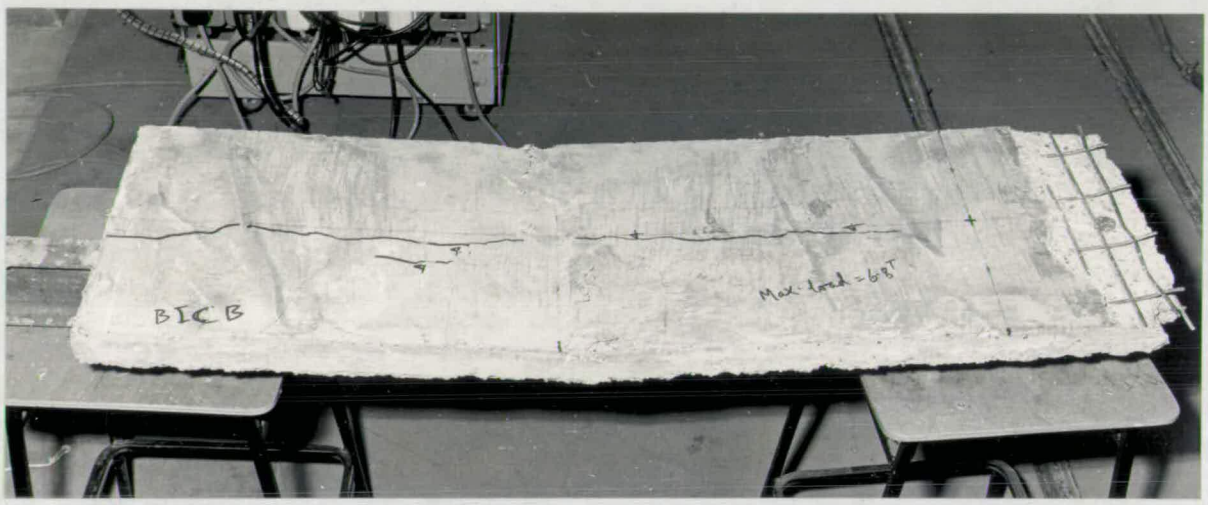

FIG.3.2 Part of Control Beam BICB after failure
Span=2'-6"
Width=1-0"
Maximum Load(Central)=6.8tons
Longitudinal crack first observed at 5.5tons.

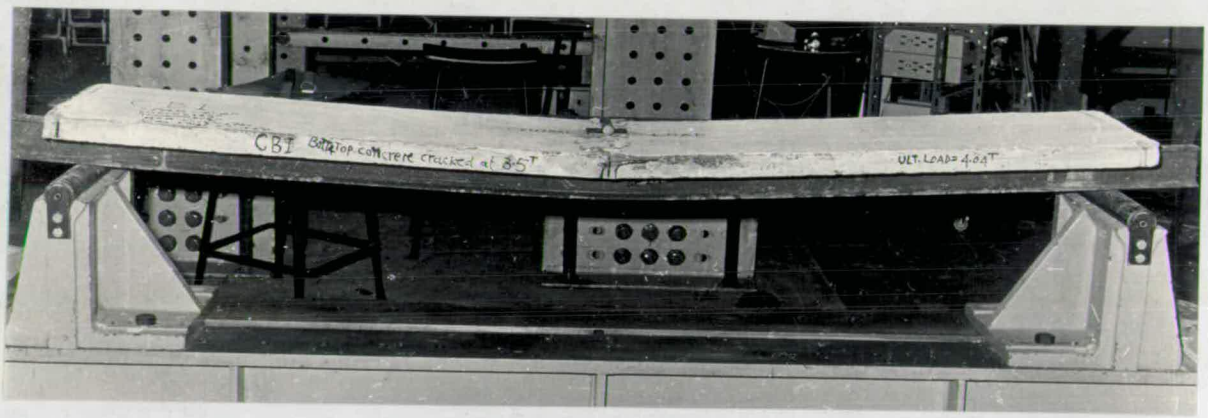

Fig.3.3 Control beam AICB after failure
Span=6'-0"
Width=1-0"
Maximum Central Load=4.04tons
Concrete crushing first started at 3.5tons.

the section was then almost fully mobilised. As the curvature of the section was further increased, the load carried remained approximately constant and the crushing of the slab extended downwards whilst strain-hardening began in the bottom flange of the beam. The present tests confirm this observation particularly in the cases where strain-hardening is found to have occurred.

The beams tested by Barnard and Johnson (54) did not reach the strain-hardening stage at collapse. They observed that the shape of the stress-strain curve for concrete had virtually no effect on the value of maximum moment but had an important effect on the value of e_{cu}, the concrete edge strain at which maximum moment was reached. They further observed that when the neutral axis was in the slab at maximum moment, the assumption that steel was fully plastic had led to over-estimation of maximum moment by a maximum of 11%; but in most practical cases the error was less than 5%.

(c) Effect of Slip

Barnard and Johnson (54) pointed out that the theory for maximum moment provided a safe estimate even when large slip strains were present. Slutter and Driscoll (59) stated that if the sum of the ultimate strengths of all shear connectors in the shear span was sufficient to satisfy the equilibrium conditions at ultimate load, then the theoretical ultimate moment could be obtained, which implies that the effect of slip can be ignored, if sufficient shear connection is provided.

(d) Effective Width

The analysis of a Composite beam and slab system is really a three-dimensional problem. In this investigation, the three-dimensional nature of the problem is by-passed by treating the slab as a thin plate forming the compression flange of the steel joist, which is analysed by the theory of

simple bending. In a compound structure of beams made integral with a slab, under transverse load, the free bending of the beams is to some extent reduced both by the bending of the slab and, when the neutral plane of the slab does not contain the neutral axes of the beams, by forces induced in the plane of the slab as a result of bending. Some authors (60,61) have suggested that this restriction on free bending of a beam can be simulated by introducing the concept of "effective width" in which a certain proportion of the slab acts, in bending, with the beam. The advantage of this artifice is that, if the magnitude of the effective width is found, the rest is analysed by the simple bending theory. It is probably true to say that the need for such a concept has been felt because the amount of computation required in the rational design of a composite structure was otherwise prohibitive. Allen and Severn (62) suggested that a basis for calculation of effective width could be the equality of maximum deflection or of the maximum stress in the beam. Adekola (53) defined the effective width of a slab as that width of the slab which would sustain a force equal to the actual force in the slab, if the longitudinal stress across the slab were constant and equal in magnitude to the theoretical longitudinal stress at middle surface of the slab at its junction with the steel joist. By Harmonic Analysis, he obtained the effective widths of slab at mid span for a single composite beam and for a slab continuous over many steel joists as 0.303 and 0.308 of span respectively. He also pointed out that the effective width was about 12 times the thickness of the slab, in which case the shear lag effect (63) was negligibly small. Timoshenko (64) defined the effective width of compression flange as that width which replaced the actual width such that the elementary theory of bending applied to such a transformed beam

cross section gave the correct value of maximum bending stress which was uniform across the effective width. He obtained the expression for the effective width B_e as

$$B_e = \frac{L}{\pi(1.5 - \nu - \nu^2/2} \quad \ldots\ldots\ldots\ldots\ldots\ldots \quad (3.1)$$

Where ν = Poisson's ratio

L = Span of the beam

Taking $\nu = 0$ for concrete, it can be shown that

$$B_e = \frac{L}{4.17} \quad \ldots\ldots\ldots\ldots\ldots\ldots\ldots\ldots \quad (3.2)$$

Adekola and Timoshenko derived their values assuming that the structure is in elastic state and so they are not strictly applicable at or near ultimate load conditions.

Kemp (65) defined the effective width under ultimate load conditions as that width which, in stress block analysis with ultimate compressive stress of $0.74\ c_u$, resulted in the same concrete force with the same line of action as was found from his more complex theoretical model of the behaviour of the beam. He made simplifying assumptions in order to make allowance for the variation of neutral axis depth across the breadth of the slab due to in-plane shear forces and transverse bending and for the reduction in the compressive strength (66,67) due to longitudinal cracking and to shear stress on transverse planes and derived the effective width as

$$B_e = (1 - 0.96\ B/L)\ B \quad \text{when } B/L < 0.31 \quad \ldots\ldots\ldots \quad (3.3)$$

where B = Actual width of flange.

Kemp's formula can be expressed in a more general form as

$$B_e = \left[1 - 0.625 \frac{\alpha'}{\beta} (1 - \beta_1^2) \frac{B}{L}\right] B \quad \ldots\ldots\ldots\ldots \quad (3.4)$$

$$\text{when } B/L < \frac{0.8\beta}{(1 + \beta_1)\alpha'} \quad \ldots\ldots\ldots\ldots\ldots\ldots \quad (3.5)$$

Where α' and β are coefficients read from graphs based on Hognestad's stress block (41,68) reproduced in Fig. 2.3 or calculated from the expressions (2.2) and (2.3) respectively and β_1 is the coefficient which takes account of the reduction in compressive strength of concrete due to in-plane shear stresses and is derived elsewhere (66,67).

If $\beta_1 = 0.4$, the equation (3.4) will reduce to

$$B_e = (1 - 0.525 \frac{\alpha'}{\beta} \frac{B}{L}) B \quad \ldots\ldots\ldots\ldots\ldots\ldots \quad (3.6)$$

$$\text{when } B/L < 0.57 \; \beta/\alpha' \quad \ldots\ldots\ldots\ldots\ldots\ldots \quad (3.7)$$

Kemp's formula (Equation (3.3)) is a particular case of general equation (3.4) when $\beta_1 = 0.4$ and $\alpha'/\beta = 1.85$, which nearly corresponds to a value of $f'_c = 2000$ PSI.

Johnson (69) suggests a simpler formula, $B_e = (1 - B/L)B$ .. (3.8)

C.P.117 part 2 (70) gives the following formula for effective width:

$$B_e = \frac{B}{\sqrt{1 + 12\left(\frac{B}{L}\right)^2}} \quad \ldots\ldots\ldots\ldots\ldots\ldots \quad (3.9)$$

The equations (3.6), (3.8) and (3.9) are plotted in Fig. 3.4. It will be interesting to note that they all give reasonably close values in the range of B/L values encountered in practical bridge problems.

ACI-ASCE Committee 333 (71) recommend the effective width of concrete flange should not exceed one-fourth of the span length of the beam, and the

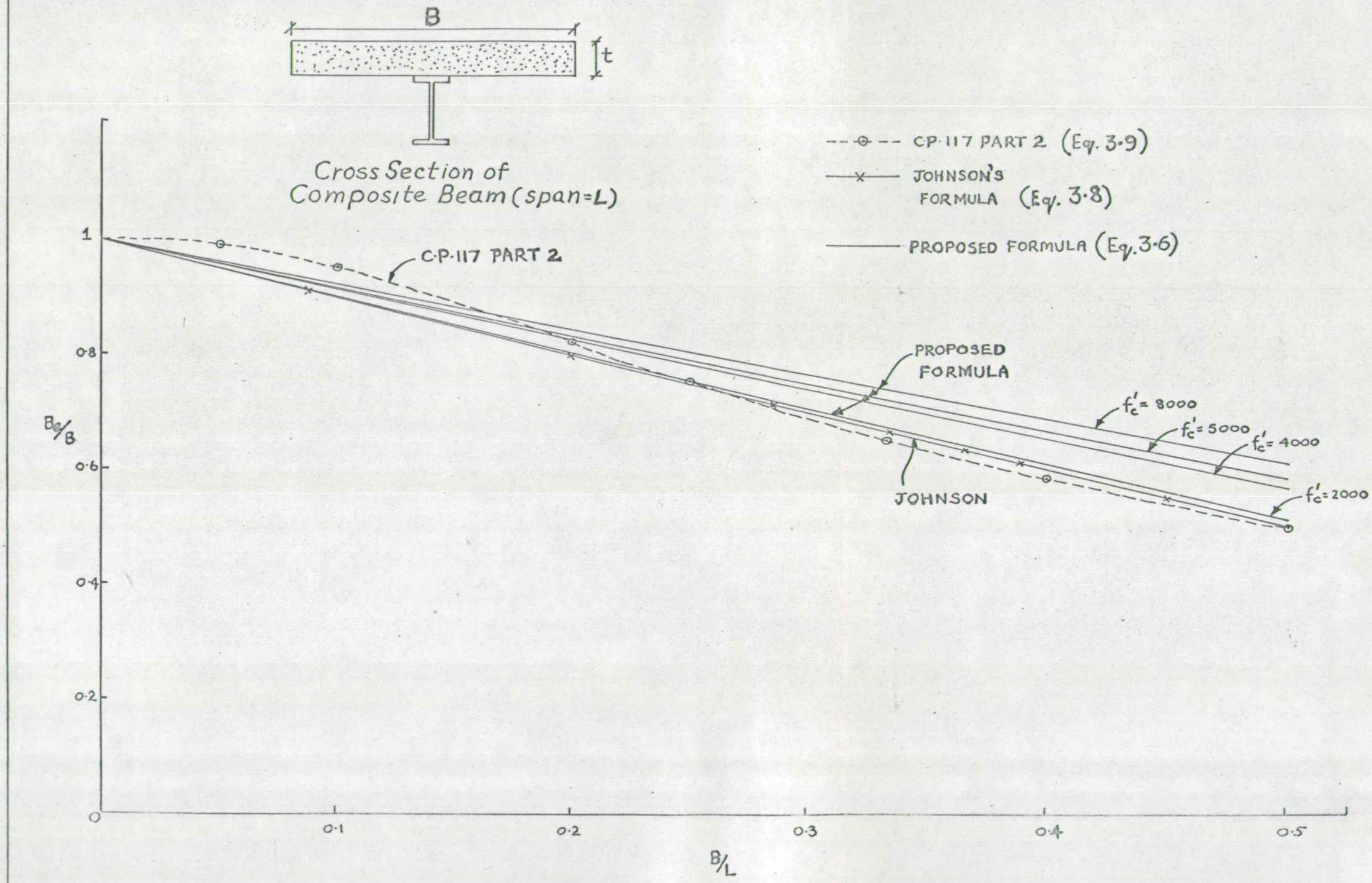
B
t
Cross Section of
Composite Beam (span=L)
CP·117 PART 2 (Eq. 3·9)
JOHNSON'S
FORMULA (Eq. 3·8)
PROPOSED FORMULA (Eq. 3·6)
CP·117 PART 2
PROPOSED
FORMULA
JOHNSON
f_c'= 8000
f_c'= 5000
f_c'= 4000
f_c'= 2000
1
0·8
0·6
0·4
0·2
0
B_e/B
0·1
0·2
0·3
0·4
0·5
B/L

FIG 3·4

overhanging width on either side of the prefabricated beam should not exceed 8 times the thickness of the slab nor one-half the clear distance to the next beam. Brendel (72) presents in his paper the code requirements for effective width that are in force in European and other countries. From all these formulae, one point emerges out that the effective width is a function of either span length, thickness of slab or both. The proposed formula (Equation (3.7)) is mainly a function of $^{B}/_{L}$ but takes into account the variation in strength of concrete.

3.2 Assumptions

In the light of above discussion and from other considerations, the following assumptions are made in deriving a formula for ultimate moment of resistance of a composite beam:

(i) The moment of resistance is provided by two stress blocks in which the concrete above neutral axis is stressed to the crushing strength of the material and the steel is stressed to its yield strength.

(ii) strains produced by welding of shear connectors, shrinkage of concrete, creep under load and temperature changes are not considered. In practice, they are quite uncertain and can not easily be predicted.

(iii) the stress-strain properties of steel are obtained from tensile tests on specimens. Steel has the same properties in tension and compression. The ultimate load characteristics of stress block for concrete in flexural compression are as given in Fig. 2.3.

(iv) the ultimate moment is mobilised when the maximum edge strain reaches the value obtained from Fig.2.3 or given by

$$e'_{cu} = 0.004 - f'_{c}/6.5 \times 10^{6} \quad \ldots\ldots\ldots\ldots\ldots \quad (3.10)$$

(v) the shear connection between the slab and the joist is rigid so that there is no distortion of strain distribution at the interface. In other words, the slip between the slab and the joist is neglected.

(vi) the effective width of slab acting with the beam is equal to the value given be equation (3.6) or (3.9).

(vii) the steel joist is represented by three reactangular areas of steel to calculate tensile forces and the flange are concentrated at points "d" apart where d is the depth of the steel section. Vide Fig. 3.5(a).

(viii) concrete below neutral axis is ignored.

(xi) the longitudinal reinforcement at bottom of slab is ignored as it is not likely to yield, being nearer the neutral axis. The longitudinal reinforcement at top of the slab yields and contributes to the ultimate moment of the beam.

3.3 Derivation of formulae allowing for strain-hardening

Assuming the idealised strain and stress distribution shown in Fig. 3.5 and Fig. 3.6, general formulae for the ultimate moment are derived.

Case (i) Neutral axis within the slab and steel section partly elastic

Vide Fig. 3.5(b) and Fig. 3.5(c)

The moment of resistance is given by

$$M_c = A_s f_y (D - d/2) + a_f A_s f_s D + a_w a_s f A_s \frac{f_s}{2}\left(1 - \frac{a_s}{3}\right) D$$

$$- a_f A_s (f_y - f'_y) t - a_w a_e f A_s \frac{(f_y - f'_y)}{2}\left(\frac{a_e}{3} D + t\right)$$

$$- \alpha' B_e n D f'_c \beta n D - A_r f_{yr} a_r \quad \ldots\ldots\ldots\ldots\ldots\ldots \quad (3.11)$$

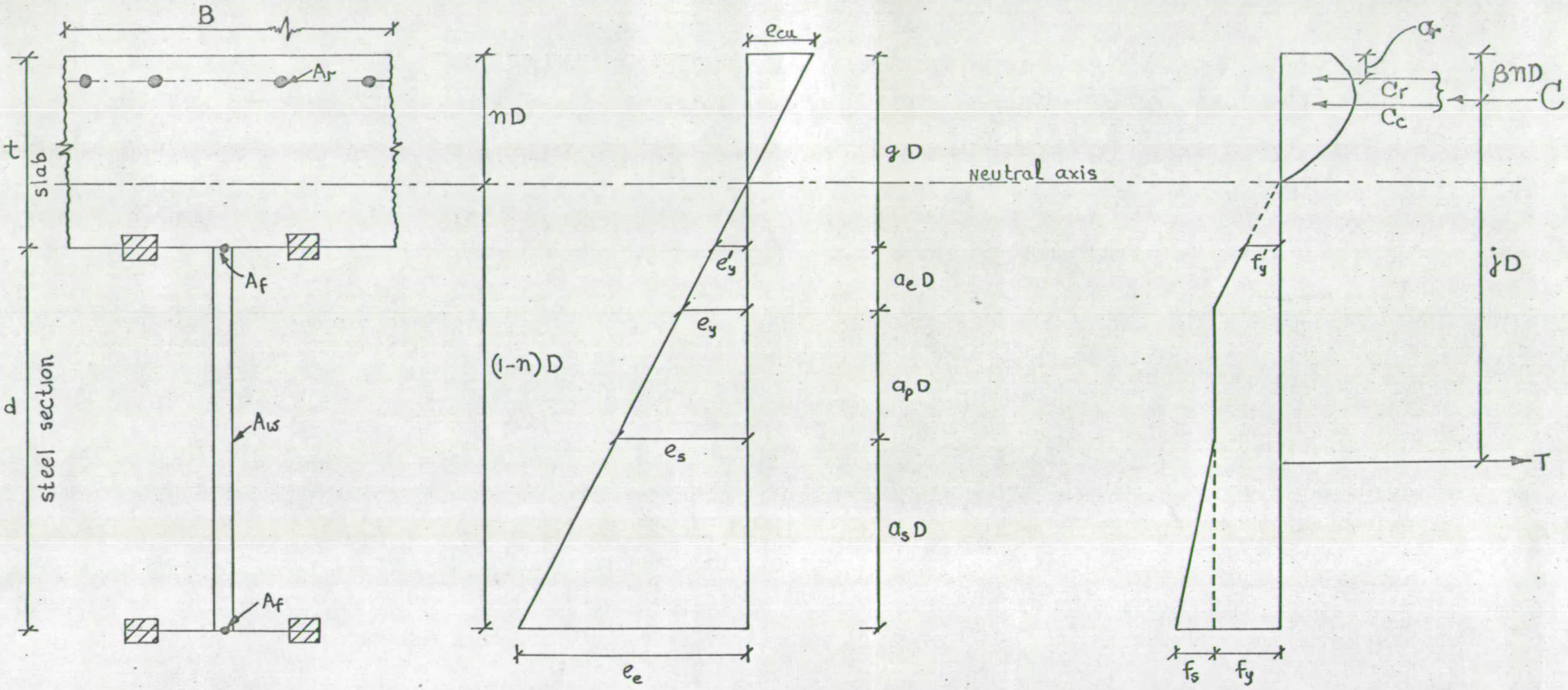

(a) Idealised cross section

A_f = Area of flange

A_w = Area of web

(b) Idealised strain diagram

(c) Idealised stress diagram

C_r = Force in slab reinforcement

C_c = Force in concrete

$C = C_c + C_r$

f_y = yield stress of steel

f'_y = steel stress of interface

f_s = stress in steel due to strain-hardening

T = Total tension

CASE(1) NEWTRAL AXIS WITHIN SLAB
steel section partly elastic
WITH STRAIN-HARDENING

FIG. 3·5

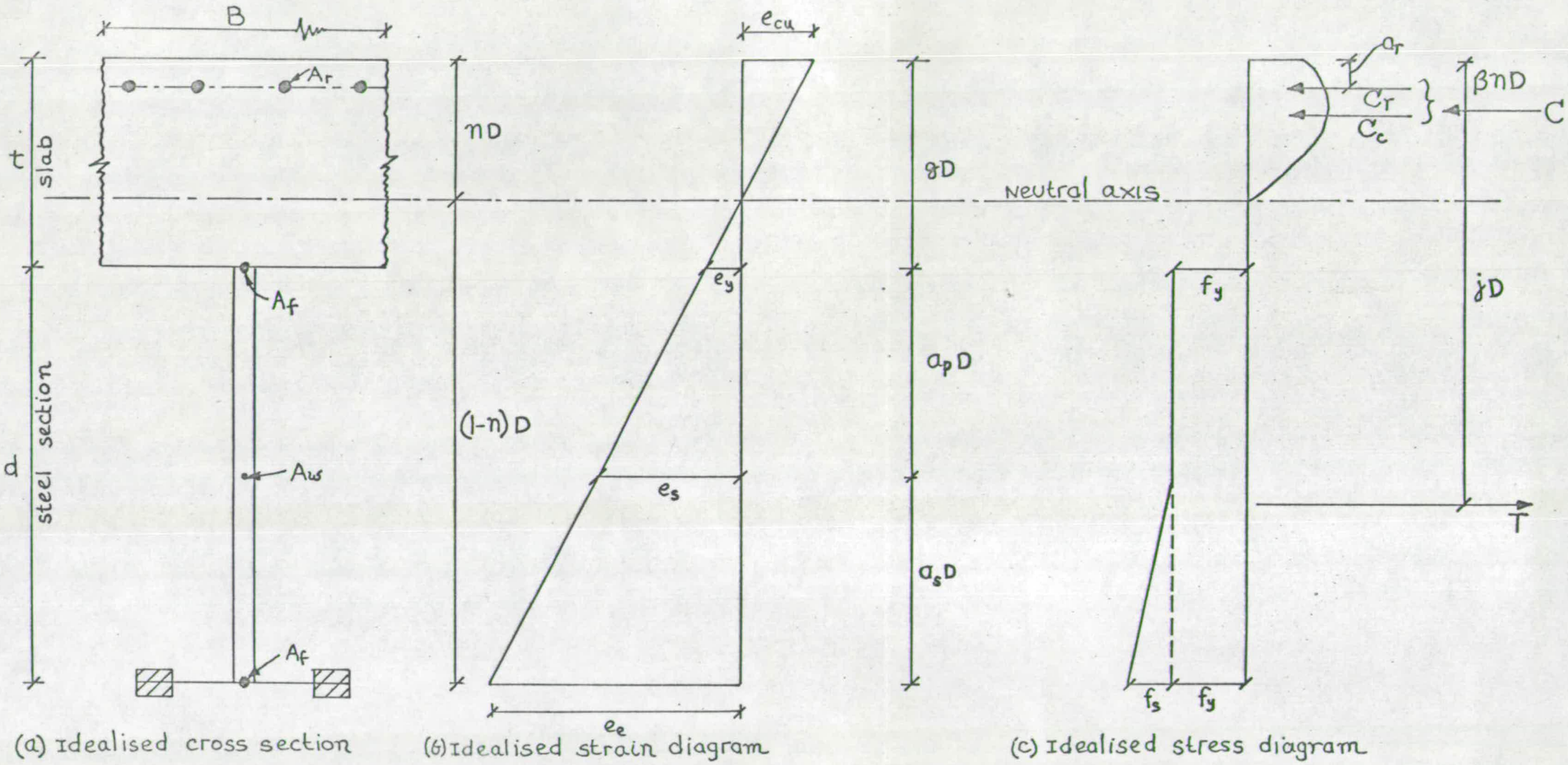

(a) Idealised cross section

A_f = Area of flange

A_w = Area of web

(b) Idealised strain diagram

(c) Idealised stress diagram

CASE(II) NEUTRAL AXIS WITHIN SLAB
steel section fully plastic
WITH STRAIN-HARDENING

FIG. 3·6

The neutral axis depth nD is given by

$$n^2 - P_1 n - P_2 = 0 \quad \ldots\ldots\ldots\ldots\ldots\ldots\ldots \quad (3.12)$$

where

$$P_1 = \frac{2uk\left[\left(1 - \frac{k_1}{k}\right)s - (a_f + a_w f)(u + r) - s(1 + u)(a_f - a_w f g)\right]}{2su - a_w f k\left[(u + r)^2 - s(1 + u)^2\right]} \quad \ldots\ldots\ldots \quad (3.13)$$

$$P_2 = \frac{ku^2\left[(2a_f + a_w f) + g s (2a_f - a_w f g)\right]}{2su - a_w f k\left[(u + r)^2 - s(1 + u)^2\right]} \quad \ldots\ldots\ldots \quad (3.14)$$

where

$$u = \frac{\epsilon_{cu}}{\epsilon_y} \qquad k = \frac{A_s f_y}{\alpha' B_e D f_c'} \qquad k_1 = \frac{A_r f_{yr}}{\alpha' B_e D f_c'}$$

$$f = D/d \qquad g = t/D \qquad a_f = A_f/A_g \qquad a_w = A_w/A_g$$

$$C_c = \alpha' B_e n D f_c' \qquad C_1 = A_r f_{yr} \qquad C = C_c + C_r$$

$$r = \epsilon_s/\epsilon_y \qquad s = E/E_{sh}$$

$$a_s = 1 - \frac{n(u + r)}{u} \qquad a_p = \frac{n(r - 1)}{u}$$

$$a_e = \frac{n}{u f_y}(f_y - f_y') \qquad f_s = \frac{f_y}{s}\left[\frac{u}{n} - (u + r)\right]$$

α' and β are obtained from Fig. 2.3 or from equations (2.2) and (2.3).

Case (ii) Neutral axis within the slab and steel fully plastic.

Vide Fig. 3.6(b) and 3.6(c)

$$M_c = A_s f_y (D - d/2) + a_f A_s f_s D + a_w a_s f \frac{A_s}{s} \frac{f_s}{2} D(1 - \frac{a_s}{3})$$

$$- \alpha' B_e nD f_c' \beta nD - A_r f_{yr} a_r \quad \ldots\ldots\ldots\ldots\ldots\ldots \quad (3.15)$$

The neutral axis depth nD is given by

$$n^2 - F_1 n - F_2 = 0 \quad \ldots\ldots\ldots\ldots\ldots\ldots \quad (3.16)$$

where

$$F_1 = \frac{2uk \left[(1 - \frac{k_1}{k})s - (a_w + a_w f)(u + r)\right]}{2su - a_w f k (u + r)^2} \quad \ldots\ldots\ldots \quad (3.17)$$

$$F_2 = \frac{ku^2 (2a_f + a_w f)}{2su - a_w f k (u + r)^2} \quad \ldots\ldots\ldots\ldots\ldots\ldots \quad (3.18)$$

Case (iii) Neutral axis in the steel beam.

This case is not considered here, as in such cases, the strain-hardening effect can be safely ignored.

3.4 Computer programme.

A "program" for K.D.F.9 Computer (Appendix 1 gives a copy of programme in Atlas Autocode) was prepared to calculate M_c and other quantities for the above two cases. When steel does not reach the strain-hardening stage at Maximum moment which develops when the maximum concrete edge strain reaches the value specified in assumption (iv), the programme automatically ignores the strain-hardening. This occurs when,

$$a_s \leq 0$$

or

$$n \geq \frac{u}{(u + r)} \quad \ldots\ldots\ldots\ldots\ldots\ldots \quad (3.19)$$

3.5 Comparison with test results.

In order to check the validity of above formulae, the programme was run using the test data published by Chapman and Balakrishnan(57). The theoretical and experimental results are compared in Table 3.1. There is a very close agreement. The ultimate moments for beams A_5 and A_6 are overestimated, the reason being that they are not provided with sufficient shear connection to develop full theoretical ultimate moment. The collapse of beam A_6, as a matter of fact, is caused by stud failure.

3.6 Derivation of formulae, without allowing for strain-hardening

Case (i) Neutral axis within the slab and steel partly elastic

substituting $s \longrightarrow \infty$ and $f_s = 0$ in equations (3.11) to (3.14),

$$M_c = A_s f_y (D - d/2) - a_f A_s (f_y - f'_y) t - a_w a_e f A_s \frac{(f_y - f'_y)}{2} \left(\frac{a_e D}{3} + t\right)$$

$$- \alpha' B_c \, nD \, f'_c \, \beta \, nD - Ar \, fyr \, a_r \quad \ldots\ldots\ldots\ldots\ldots\ldots \quad (3.20)$$

The neutral axis depth is given by

$$n^2 - P_1 \, n - P_2 = 0 \quad \ldots\ldots\ldots\ldots\ldots\ldots\ldots \quad (3.21)$$

where $$P_1 = \frac{2uk\left[\left(1 - \frac{k_1}{k}\right) - (1 + u)(a_f - a_w f g)\right]}{2u + a_w f k (1 + u)^2}$$

P_2 $$P_2 = \frac{ku^2 g (2a_f - a_w f g)}{2u + a_w f k (1 + u)^2}$$

Case (ii) Neutral axis within the slab and steel fully plastic (Fig. 3.7)

substituting $s \rightarrow \infty$ and $f_s = 0$ in equations (3.15) to (3.18),

$$M_c = A_s f_y (D - d/2) - \alpha' B_e \, nD \, f'_c \, \beta \, nD - A_r f_{yr} a_r \quad \ldots\ldots\ldots \quad (3.24)$$

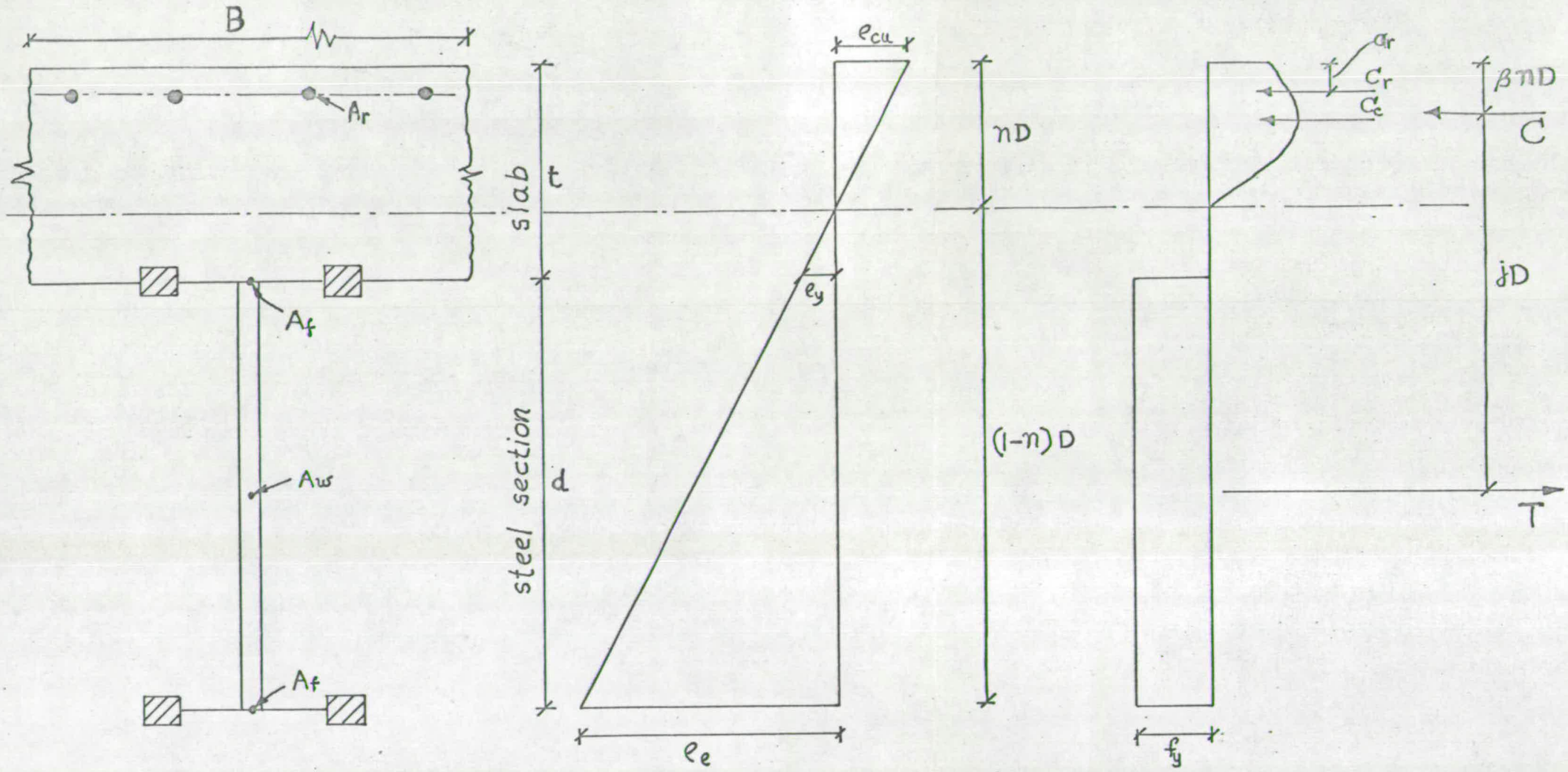

(a) Idealised cross section (b) Idealised strain diagram (c) Idealised stress diagram

CASE(iii) NEUTRAL AXIS IN THE SLAB
STEEL FULLY PLASTIC
NO STRAIN-HARDENING

FIG. 3·7

Table 3.1 Comparison of Test Results.

Chapman and Balakrishnan's Experiments.

Beam	A_1	A_2	A_3	A_4	A_5	A_6
Type of loading	point load at mid span					
Connector design % ge	38	42	47	57	72	99
Type of connectors			Headed studs			
6" cube strength PSI	4270	4960	3560	4560	5900	5930
yield stress T.S.I. of steel	15.35	14.74	16.95	16.36	15.34	14.87
r	11.3	4.6	1	1	1	2.4
s	2.1	17.7	21.15	10.66	10.66	17.7
observed concrete strain at spalling of concrete	.0038	.0041	.0043	.0040	.0040	.0045
observed concrete strain at or near collapse	.004913	.006863	.00413	.004756	.005175	.004262
Exptal ulti. load (tons)	43	45	45	52	47	42.5
Theoretical concrete strain- e_{cu} at maximum moment	.00344	.00335	.00353	.00340	.00323	.00322
Theoretical ultimate load, tons	40.53	44.25	45.20	53.81	56.71	49.62
$\frac{\text{Exptal ulti. load}}{\text{Theoretical load}}$	1.08	1.02	0.998	0.97	0.83	0.86
$\frac{\text{Exptal concrete strain at spalling of concrete}}{\text{Theoretical concrete edge strain}}$	1.1	1.22	1.22	1.18	1.24	1.40

The neutral axis depth nD is given by

$$nD = \frac{A_s f_y - A_r f_{yr}}{\alpha' B_e f_c'} \quad \ldots\ldots\ldots\ldots\ldots\ldots \quad (3.25)$$

The formula (3.24) can be re-written as

$$M_c = A_s f_y (d/2 + t - \beta\, nD) + A_r f_{yr} (\beta\, nD - a_r) \quad \ldots\ldots\ldots \quad (.24a)$$

If longitudinal reinforcement in slab is ignored ($A_r = 0$), the usual formula is obtained.

$$M_c = A_s f_y \left(d/2 + t - \frac{\beta A_s f_y}{\alpha' B_e f_c'} \right) \quad \ldots\ldots\ldots\ldots\ldots\ldots \quad (3.24b)$$

Barnard (54) assumes a minimum value of 0.54 for the coefficient β/α'

Slutter (59) and ACI-ASCE Committee (71) assume $\beta/\alpha' = 0.59$.

Viest (56) assumes $\beta/\alpha' = 0.5$.

If the cylinder strength $f_c' = 0.85\, c_u$ where c_u = cube strength, the formula (3.24b) can be re-written as,

$$M_c = A_s f_y \left[d/2 + t - \frac{\beta A_s f_y}{0.85\, \alpha' B_e C_u} \right] \quad \ldots\ldots\ldots\ldots\ldots \quad (3.24c)$$

In C.P.117 part 1 (73), the coefficient $\frac{\beta}{0.85\,\alpha'}$ is replaced by a conservative value of 0.75 i.e. $\beta/\alpha' = 0.6375$. In addition the cube strength is reduced by a further factor 2/3 and a nominal yield stress is assumed for steel.

In the present investigation, it is proposed to use the formula (3.24) obtaining the values of α' and β from the graph in Fig. 2.3 or from equations (3.5) and (3.6). In other words, α'/β is variable and takes the value from 0.54 to o,668 corresponding to the value of $f_c' = 2000$ to 8000 PSI.

Case (iii) Neutral axis in the steel beam.

This case is more complex than other cases and further assumptions have to be made. As suggested by Barnard (74), the maximum moment can be calculated with sufficient accuracy for practical purposes, if it is assumed that steel is plastic in tension and compression and the concrete force, with its line of action at $t/2$ from top of slab, is equal to

$$C_c = 0.8 B_e t f_c' \quad \ldots\ldots\ldots\ldots\ldots\ldots \quad (3.26)$$

The assumed distribution of stress is shown in Fig. 3.8.

Resolving longitudinally,

$$A_s f_y = 2 A_{sc} f_y + 0.8 B_e t f_c' + A_r f_{yr} \quad \ldots\ldots\ldots\ldots \quad (3.27)$$

This equation gives Asc, area of steel in compression and hence d_c and nD since the dimensions of steel are known.

Taking moments about the neutral axis,

$$M_c = A_s f_y (D - d/2 - nD) + A_{sc} f_y d_c + 0.8 B_e t f_c' (nD - t/2)$$

$$+ A_r f_{yr} (nD - a_r) \quad \ldots\ldots\ldots\ldots\ldots\ldots \quad (3.28)$$

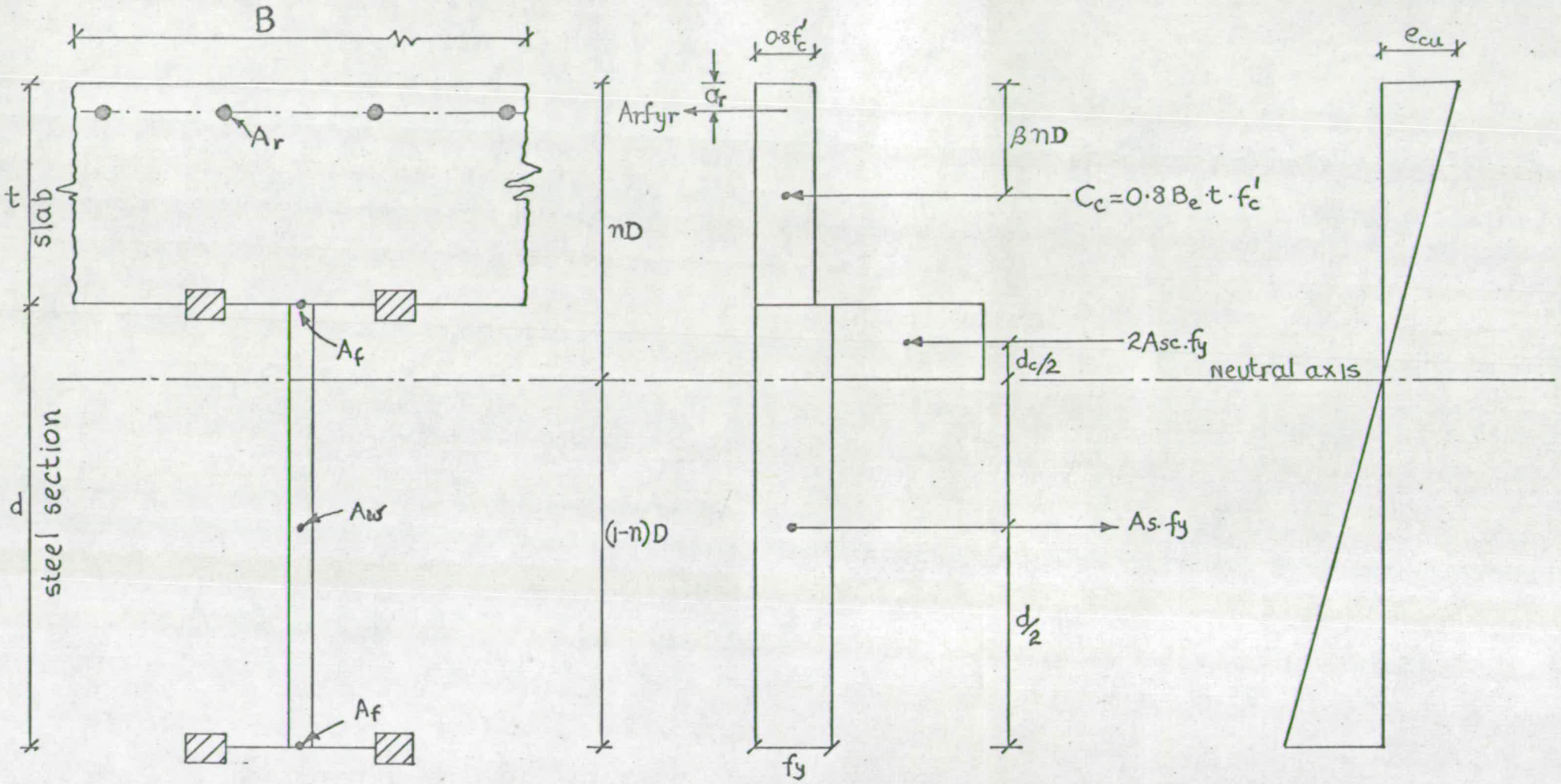

(a) Idealised cross section (b) Idealised stress diagram (c) Idealised strain diagram

CASE(iii) NEUTRAL AXIS IN STEEL BEAM

STEEL FULLY PLASTIC IN TENSION & COMPRESSION
NO STRAIN-HARDENING

FIG. 3·8

CHAPTER 4

UPPER-BOUND SOLUTIONS BY CONSIDERATION OF COLLAPSE MECHANISMS.

4.1 Introduction

An upper-bound solution provides either the correct collapse load or else predicts too high a collapse load. The basic conditions of an upper-bound solutions are:

(i) A valid mechanism which will satisfy the boundary conditions is presupposed.

(ii) The work done by external loads must equal the internal work dissipated.

(iii) The stress-strain relationship of material follows "Rigid-plastic" theory.

(iv) The deformations are defined such that the system must obey the yield criterion.

The condition (ii) does not allow constant collapse loads with strain-hardening steels or materials with no well-defined yield point, i.e. Limit Analysis (19) is then not applicable but the results are no doubt safe as long as the yield stress is well defined for the material.

Several alternative yield-line patterns are considered and the lowest value of collapse load obtained is taken as the "upper-bound" value. Using the Work Equation presented in the previous chapter, upper-bound solutions will now be derived for certain simply supported composite Beam and Slab Bridges, treating each of them as (a) Equivalent orthotropic slab and (b) Beam and slab system.

(a) Equivalent orthotropic slab method

The ultimate load analysis of a composite beam and slab system presents

problems which are far more complex than those of simple slabs. The failure mode is greatly influenced by the geometrical arrangement of beams. No exact method has yet been developed for its analysis. The Equivalent slab method is a great simplification of the behaviour of the structure and has been employed (75,76,77) successfully in the elastic analysis of bridge decks. Sawko and Saha (78) have extended the same to calculate collapse load on a grillage tested by Reynolds (79) and demonstrated the simplicity of this approach compared to the alternative plastic hinge analysis (79). They pointed out that an open grillage was an extreme case and an actual bridge deck would approach the behaviour of the orthotropic slab with smaller rib sizes and the above method would be even more justified.

The transformation of a Beam and Slab Bridge to an equivalent orthotropic slab for yield-line analysis is done as follows:

The total actual width **H** of a bridge deck is replaced by an equivalent width (Fig. 4.1) given by

$$H_e = (n - 2)h + \frac{2M_{ce}\, h}{M_c} \qquad \ldots\ldots\ldots\ldots\ldots\ldots \quad (4.1)$$

Where n = total number of composite beams including outer ones,

M_c = ultimate moment of an inner beam (T-beam),

M_{ce} = ultimate moment of an outer beam (L-beam),

h = spacing of beams

In the equivalent slab the end supports of beams are replaced by point supports (Fig. 4.2). The positive (sagging) ultimate moments of beams and slab are replaced by an equivalent ultimate moment $\mu_e m$ per unit width of slab as indicated by the moment key line in Fig. 4.2(b). The value of $\mu_e m$ for a bridge deck with L-beams at edges (Fig. 4.1) is given by

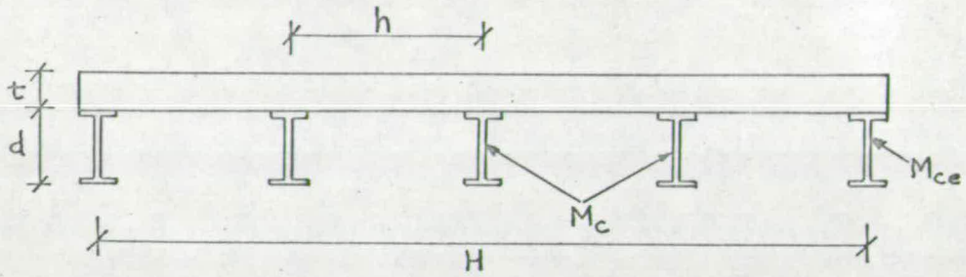

(a) Crosssection of actual bridge

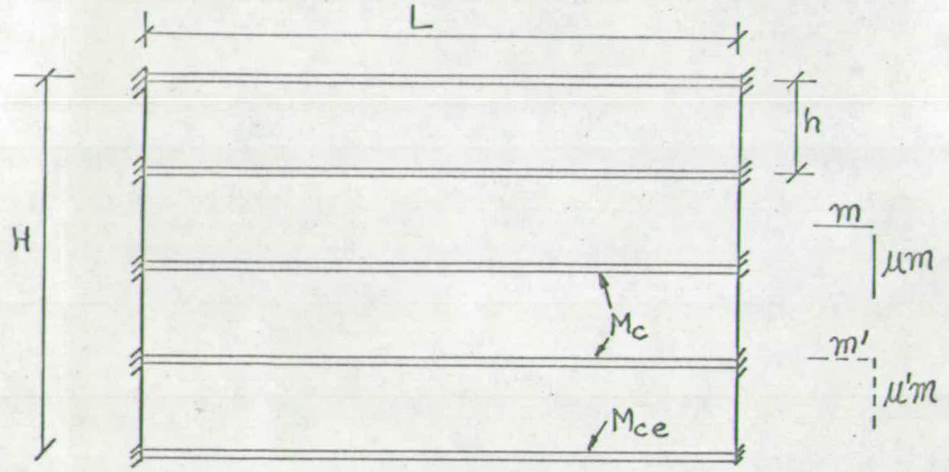

(a) Plan of actual bridge

FIG. 4·1

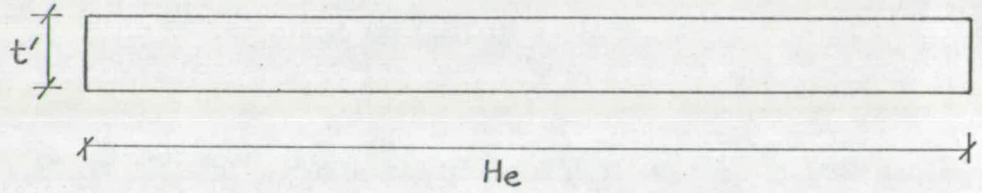

(b) Cross section of equivalent slab

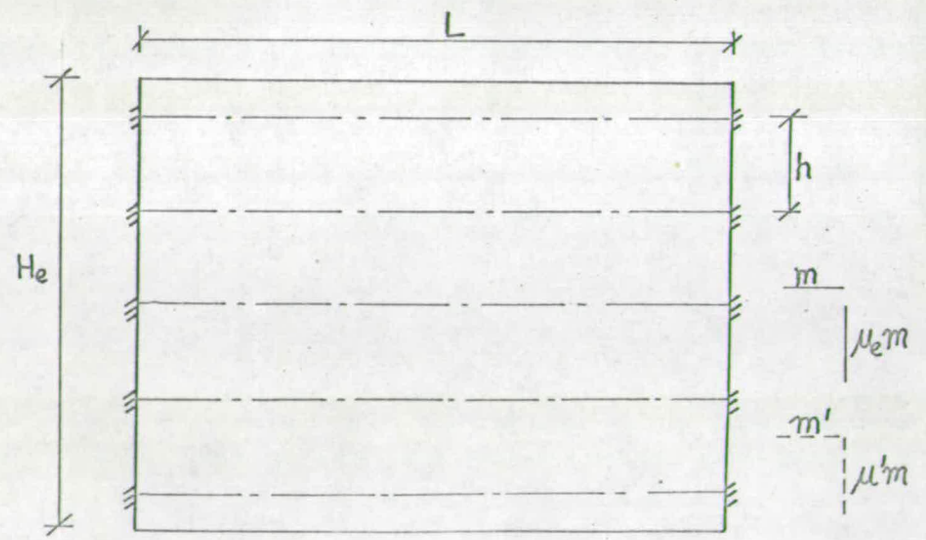

(b) Plan of equivalent slab

FIG. 4·2

$$\mu_e^m = \frac{(n-2)\, M_c + 2M_{ce} + (n-1)(h-B_c)\mu_m}{H_c} \quad \ldots\ldots\ldots\ldots \quad (4.2)$$

For a bridge deck with all identical T-beams,

$$\mu_c^m = \frac{M_c + (h-B_c)\mu^m}{h} \quad \ldots\ldots\ldots\ldots\ldots\ldots \quad (4.3)$$

The negative (hogging) ultimate moment of slab is unchanged which implies that there is no contribution from the steel section. If all the beams are identical T-beams, the equivalent width equals actual width (Fig. 4.3)

(b) Beam and slab Method

In this method the structure is divided into individual longitudinal members and transverse slab each possessing the appropriate ultimate strength. The longitudinal members consist of (i) composite Beam with an effective width of slab acting with it and (ii) longitudinal strip of slab in excess of the effective width (Fig. 4.3). The slab is assumed continuous over several line supports provided by the beams. The modes of collapse involve plastic hinges in the beams. When a plastic hinge develops in a beam, the beam is ignored except that its end supports still act as point supports to the slab which now spans between the adjacent beams (Fig. 4.4).

4.2 Punching Shear.

Before moment type failures based on yield-line theory are considered it is necessary to investigate punching shear failure which has been of frequent occurance in laboratory tests (80 to 84). Since the provision of shear reinforcement is not always practicable in slabs, the practice is to minimise the chances of punching shear failure by proper proportioning and detailing of members of a structure.

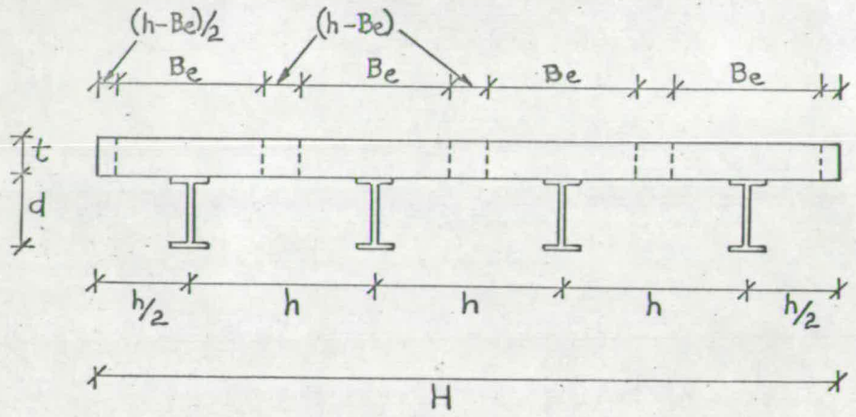

(a) Cross section of actual bridge

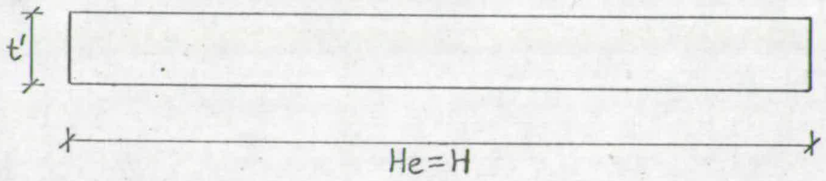

(b) Cross section of equivalent slab

FIG. 4·3

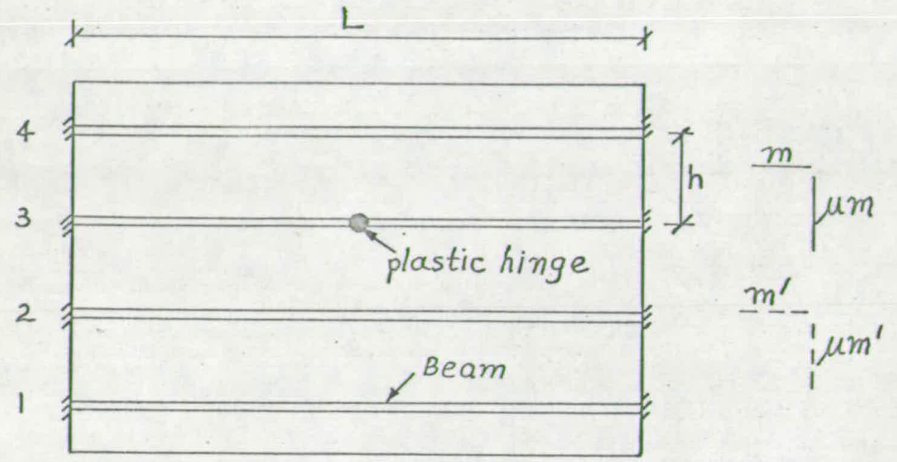

(a) Plan of bridge

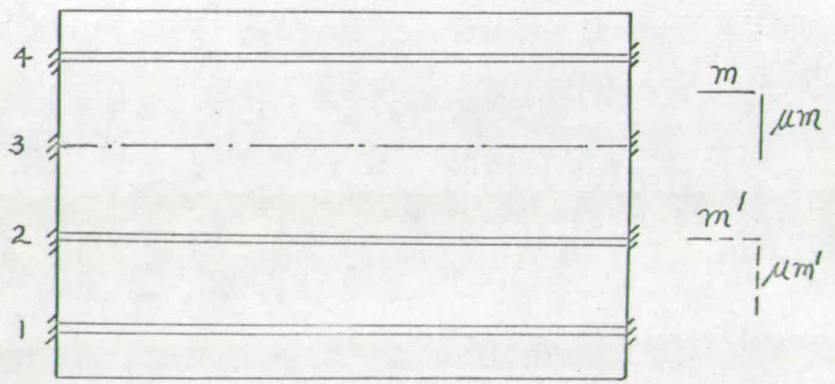

(b) Plan of bridge after failure of beam 3

FIG. 4·4

Punching shear is a complex phenomenon involving a three dimensional criterion of failure. Most of the formulae in use at present are empirical based on experiments.

Base (82) tested slabs 24" x 24" x 3" with a central punch 4" square. The ultimate shear stress v_c based on a critical section at a distance of half the slab thickness outside the loaded area was found to depend on the percentage of reinforcement. Thus, when the percentage of reinforcement varies from 0.54 to 2.46, it was observed that

$$v_c = 220 \text{ to } 300 \text{ lbs/in.}^2 \quad \ldots\ldots\ldots\ldots\ldots\ldots \quad (4.4)$$

Teychenne (85) gave a formula for the modulus of rupture for sand and gravel concretes as

$$v_o = 8.3 \sqrt{\text{cube strength}} \quad \ldots\ldots\ldots\ldots\ldots\ldots \quad (4.5)$$

where v_o = ultimate shear stress at zero distance from the punch.

The tests of Richart and Kluge (81) indicated that

$$\begin{aligned} v_1 &= 0.081 f_c' \text{ for 6" dia. disks} \\ &= 0.079 f_c' \text{ for 2" dia. disks} \quad \ldots\ldots\ldots\ldots \quad (4.6) \end{aligned}$$

where v_1 = ultimate shear stress at a critical section at a distance equal to the effective depth of the slab outside the loaded area.

Whitney (86) who investigated the ultimate shear strength of Flat slabs, Footings, Beams and Frame members, suggested a formula, which included the effect of the flexural strength of slab and which showed an excellent agreement with the results calculated from both the slab and footing tests.

His formula is

$$v_c = 100 + 0.75 \frac{m}{d_1^2} \sqrt{\frac{d_1}{l_s}} \quad \ldots\ldots\ldots\ldots\ldots\ldots \quad (4.7)$$

where m = Moment capacity per inch width of slab

d_1 = Effective depth of slab

l_s = Distance from the face of the column to load position.

v_c = ultimate shear stress at a distance $d_1/2$ from the loaded area.

Yitzhaki (87) developed a formula for evaluating the punching strength of reinforced concrete related to the flexural strength of slab.

$$v_1 = (149.3 + 0.164\, p\, f_y) \quad \ldots\ldots\ldots\ldots\ldots\ldots \quad (4.8)$$

$$P_{punch} = \frac{m v_1}{p\, f_y\, d_1} (4a + 8d_1) \quad \ldots\ldots\ldots\ldots\ldots\ldots \quad (4.9)$$

where $p = A_r/d_1$ = proportion of reinforcement.

a = side length of loaded area of square shape. For round and rectangular shapes, a is taken as the side length of a square shape having the same area.

v_1 = Ultimate shear stress at a critical section at a distance equal to d_1 from the loaded area.

P_{punch} = Punching load.

The punching failure can be avoided by satisfying the condition that $P_{flex} = P_{punch}$ in which case, the balanced reinforcement strength should be equal to

$$p_o f_y = \frac{149.3 \left(1 + 0.5 \frac{a}{d_1}\right)}{1 - 0.164\left(1 + 0.5 \frac{a}{d_1}\right)} \quad \ldots\ldots\ldots\ldots \quad (4.10)$$

where P_{flex} = collapse load at flexural failure

P_o = Balanced proportion of reinforcement.

Moe's (88) empirical formula for the ultimate shear stress is

$$v_o = \frac{15\sqrt{f_c'}\ (1 - 0.075\frac{a}{d_1})}{\frac{1 + 21ad_1\sqrt{f_c'}}{P_{flex}}} \quad \ldots\ldots\ldots\ldots \quad (4.11)$$

where $P_{punch} = 4\ ad_1\ v_o$ $\ldots\ldots\ldots\ldots\ldots\ldots\ldots$ (4.12)

a = side length of loaded area of square shape.

For rectangular shapes,

$$a_{nom} = l_1[1 - \frac{s_1}{l_1}(1 - \frac{s_1}{l_1})] \quad \ldots\ldots\ldots\ldots\ldots \quad (4.13)$$

Where l_1 and s_1 are respectively the lengths of the longest and shortest sides of the rectangular area.

For design purposes his recommendations are

$$\left.\begin{aligned} v_o &= (9.23 - 1.12\frac{a}{d_1})\sqrt{f_c'} \quad \text{for } \frac{a}{d_1} \leqslant 3 \\ v_o &= (2.5 + 10\frac{d_1}{a})\sqrt{f_c'} \quad \text{for } \frac{a}{d_1} > 3 \end{aligned}\right\} \quad \ldots\ldots\ldots \quad (4.14)$$

Strictly speaking the above formulae are applicable to the slabs which do not act compositely with the beams. Test (80) indicated that the punching load per panel is found to be 20 to 25% larger for the composite than for the non-composite bridges. This may be explained like this. When the slab is in direct compression, as it is at mid span of a composite beam bridge, the neutral axis for local bending under the load is at a lower level than normal

and there is a larger area available to resist shear; consequently the punching load is higher. These tests also indicate that the resistance to punching increases with restraint to rotation at the edges of the punched panel. Tests of short and Thomas (83) also confirm this increase of punching load, which varied from 40 to 50 percent. There is no satisfactory theory at present to account for the increases of punching load caused by the composite action.

In the present investigation, it is proposed to adopt Moe's (88) recommendations and increase the punching load by 20% to allow for the composite action.

4.3 Solutions by Equivalent Slab Method

4.3.1 Three-longitudinal composite Beam Bridge with point load at mid span of inner longitudinal (Fig. 4.5)

The outer beams are free to rotate about their own axis and their ends are not held down. Therefore it is assumed that no moment is developed along the negative yield lines on top of slab ($i_m = i_{\lambda m} = o$). The self weight of the bridge is ignored. The possible modes of collapse are considered below:

Mode A (Fig. 4.6)

In this mode, failure takes place across the whole width of the bridge deck. For a vertical displacement of unity along the yield line DE the Work Equation yields the following expression for collapse load:

$$P_A = 12\, \mu_e{}^m \rho \qquad \ldots\ldots\ldots\ldots\ldots\ldots\ldots\ldots \quad (4.15)$$

where $\rho = {}^h/_L$

Mode B (Fig. 4.7)

For a unit displacement under the load, the Work Equation yields,

$$P_{B/m} = 2\Big[2(1 + i_1)\tan \phi/2 + 2\sec(\psi - \phi/2)\{\mu_e \cos \phi/2 \sin\psi - \sin \phi/2 \cos\psi\}$$

$$+ 2i_2 \cos \phi/2 \sec(\psi - \phi/2)\operatorname{cosec}\psi \{\mu' \sin^2\psi + \cos^2\psi\} + 2\cot\psi\Big] \quad \ldots(4.16)$$

where ϕ and ψ are the parameters which define the yield-line pattern. μ_e, μ', i_1 and i_2 are the coefficients indicating the variation of ultimate moment m (reinforcement) as shown by the moment key lines.

From the geometry of the yield line pattern, it can be shown that

$$\cot\psi + \tan \phi/2 = \tfrac{1}{2\lambda} \qquad \ldots\ldots\ldots\ldots\ldots\ldots\ldots \quad (4.17)$$

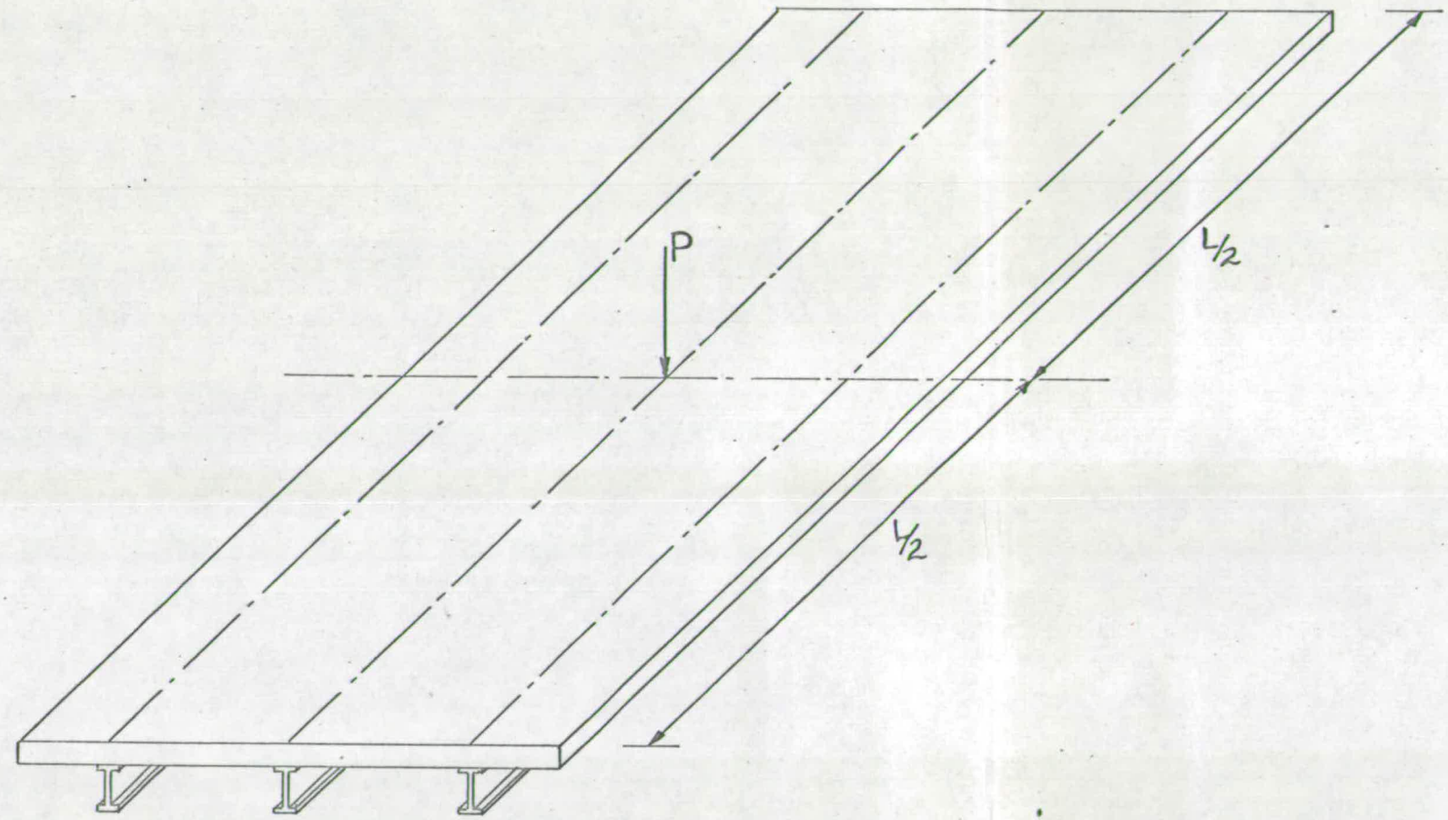

FIG.4.5

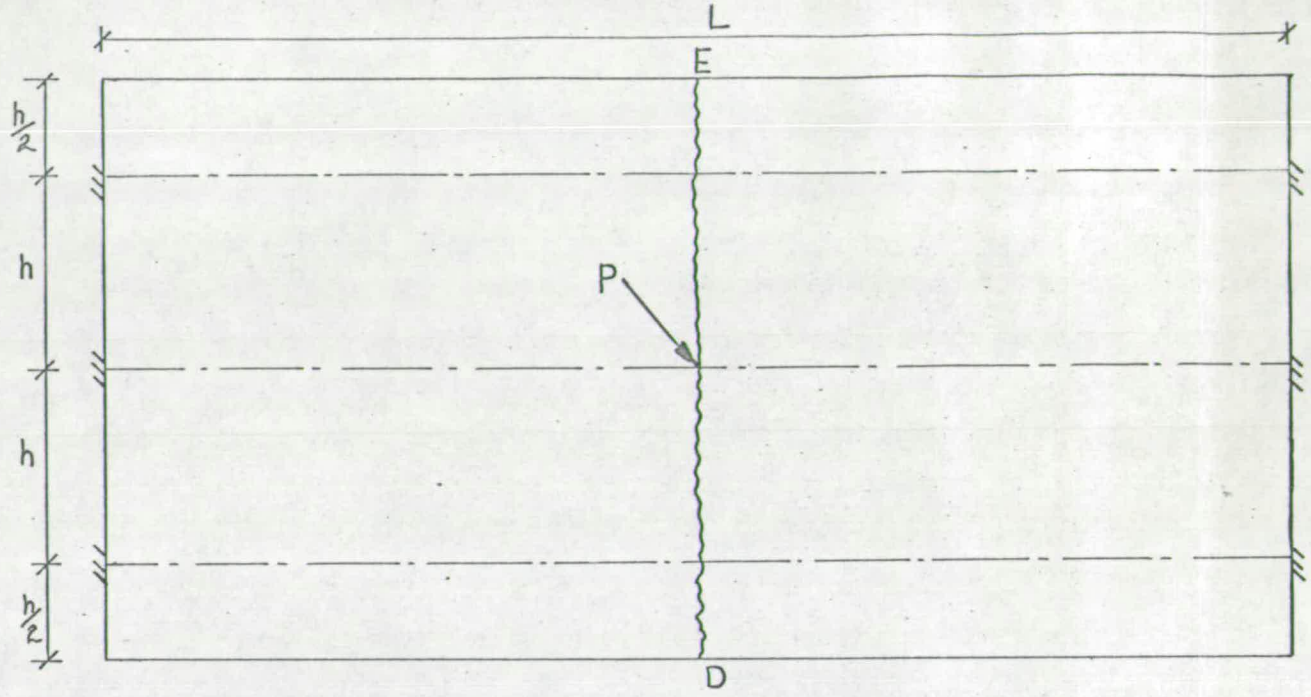

FIG.4·6 MODE A

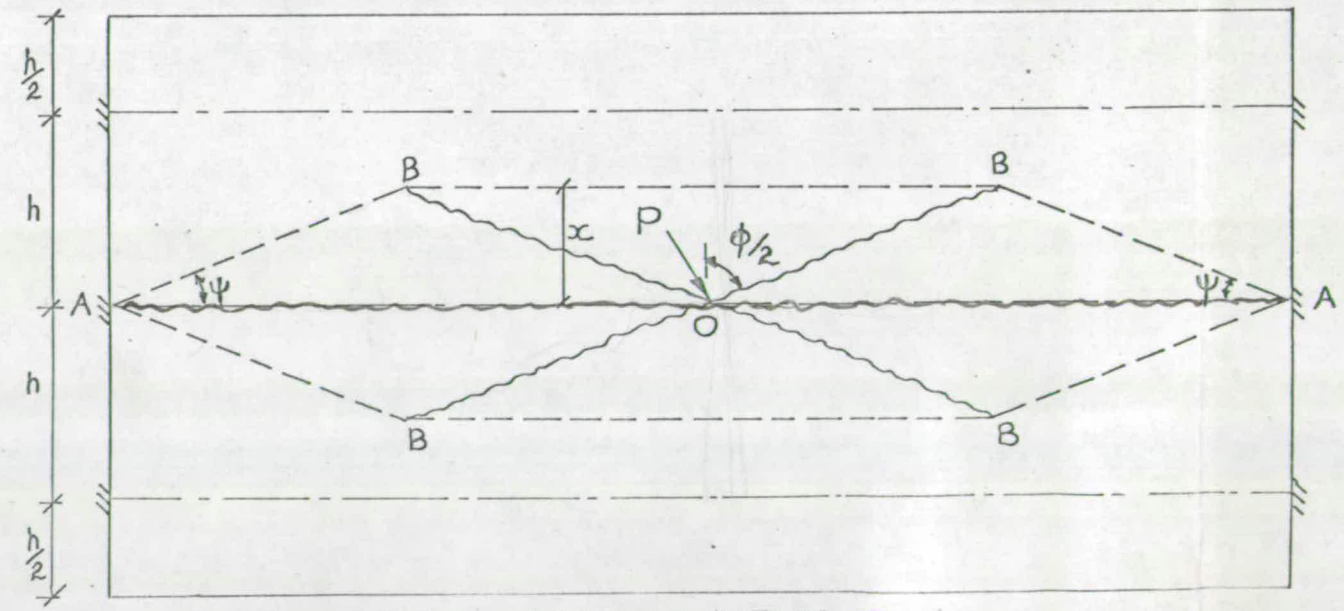

FIG.4·7 MODE B

yield line	moment
OB	m / $\mu_e m$
BB	$i_1 m$ / $i_1 \mu' m$
AB	$i_2 m$ / $i_2 \mu' m$

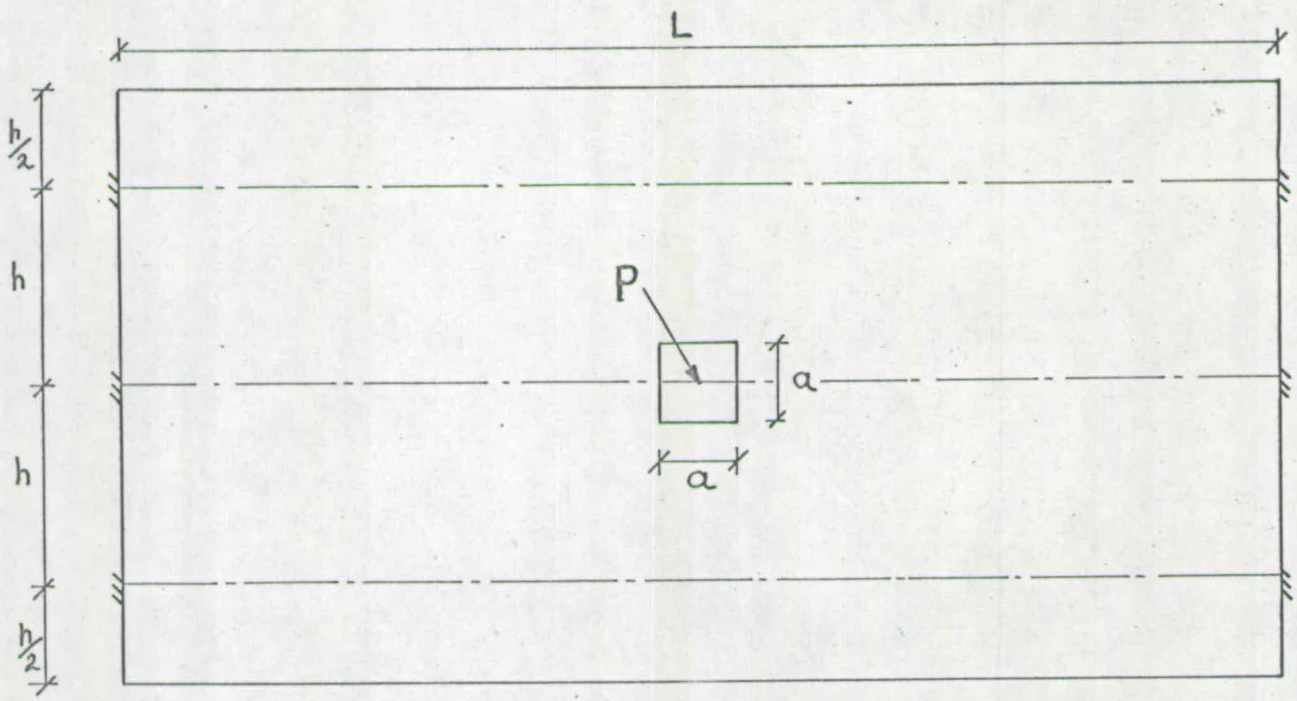

FIG. 4.8 MODEC

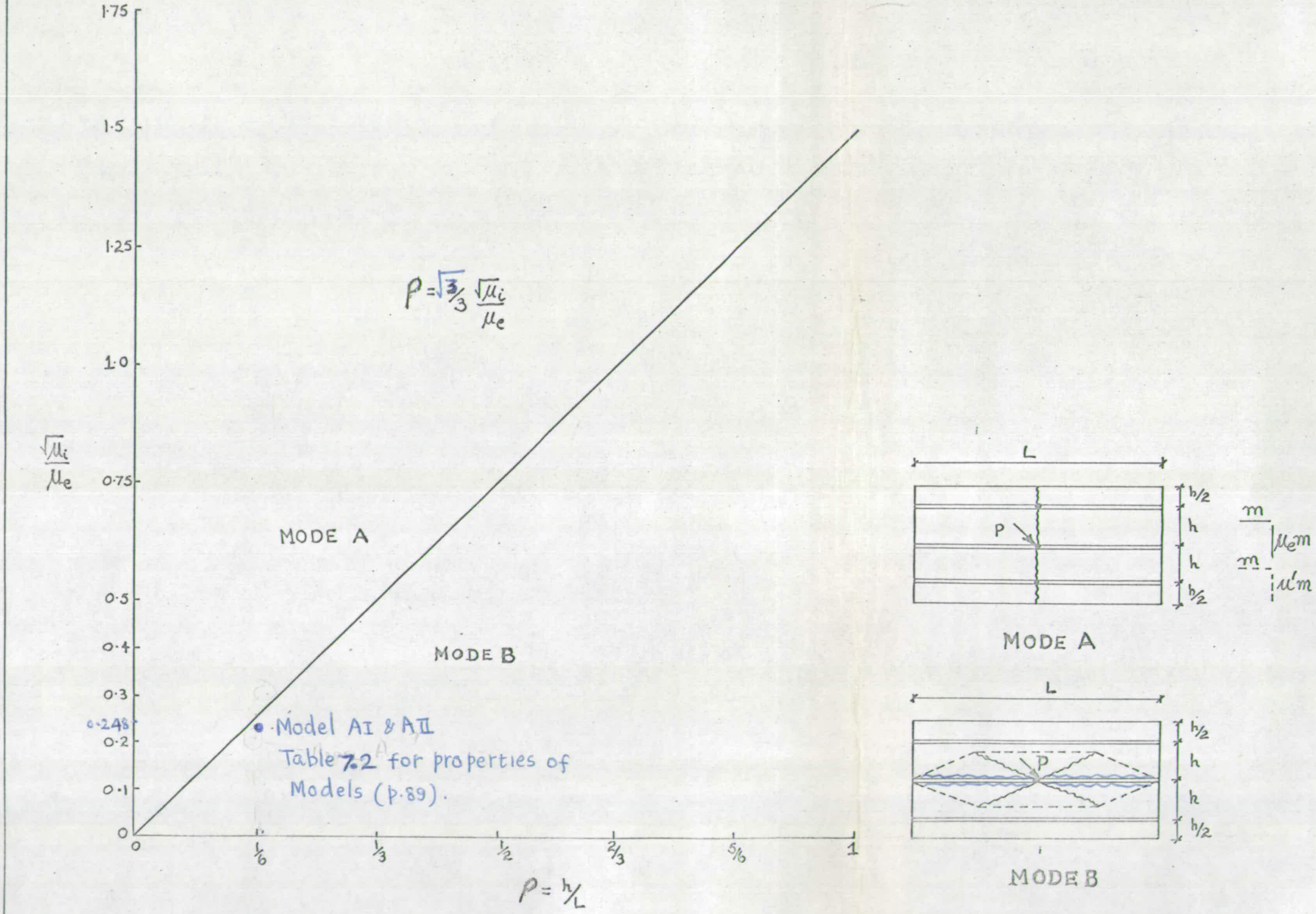
1·75
1·5
1·25
1·0
0·75
0·5
0·4
0·3
0·248
0·2
0·1
0
$\frac{\sqrt{\mu_i}}{\mu_e}$
$P = \frac{\sqrt{3}}{3} \frac{\sqrt{\mu_i}}{\mu_e}$
MODE A
MODE B
Model AI & AII
Table 7.2 for properties of Models (p.89).
0
1/6
1/3
1/2
2/3
5/6
1
$P = h/L$
L
P
h/2
h
h
h/2
m
$\mu_e m$
m
$\mu' m$
MODE A
L
P
h/2
h
h
h/2
MODE B

FIG. 4·9

where $\lambda = \frac{x}{L}$

x = Distance of yield line BB from the load.

L = span of the bridge.

substituting for ψ from Equation (4.17) in Equation (4.16) and simplifying,

$$P_{B/m} = 2[2(i_1 - 2i_2)\tan\phi/2 + 4(1 + i_2)\tan^2\phi/2 + 4(\mu_e + i_2\mu') + \frac{i_2}{\lambda} + \frac{1}{\lambda} - 2\tan\phi/2] \quad \ldots\ldots (4.18)$$

$\frac{d(P_{B/m})}{d\phi} = 0$ leads to

$$\tan\phi/2 = \frac{(2i_2 - i_1 + 1)}{4\lambda(1 + i_2)} \quad \ldots\ldots\ldots\ldots\ldots\ldots\ldots\ldots \quad (4.19)$$

$\frac{d(P_{B/m})}{d\lambda} = 0$ leads to

$$\frac{i_2}{\lambda^2} = 4(1 + i_2)\tan^2\phi/2 + 4(\mu_e + i_2\mu') \quad \ldots\ldots\ldots\ldots \quad (4.20)$$

substituting from Eq. (4.20) for in Eq. (4.19),

$$\tan\phi/2 = \frac{\sqrt{\mu_i}\,(2i_2 - i_1 + 1)}{\sqrt{4(1 + i_1)\,i_2 - i_1^2 + 3 + 2i}} \quad \ldots\ldots\ldots\ldots\ldots\ldots \quad (4.21)$$

where $\mu_i = \frac{\mu_e + i_2\mu'}{(1 + i_2)}$

Substituting from Equation (4.21) for $\tan\phi/2$ in Equation (4.20),

$$\lambda = \frac{\sqrt{4(1 + i_1)\,i_2 - i_1^2 + 3 + 2i}}{4(1 + i_2)\sqrt{\mu_i}} \quad \ldots\ldots\ldots\ldots\ldots\ldots\ldots\ldots \quad (4.22)$$

substituting for $\tan\phi/2$ and λ in Equation (4.18),

$$\frac{P_B}{m} = 4\sqrt{\mu_i \{4(1 + i_1) i_2 - i_1^2 + 3 + 2i\}} \quad \ldots\ldots\ldots\ldots\ldots \quad (4.23)$$

As per the assumption made in this particular bridge deck, the negative yield lines AB and BB do not develop any moment which means that $i_1 m = i_2 m = 0$

Substituting $i_1 = i_2 = 0$, the following equations applicable in this case are obtained:

$$\left.\begin{aligned} P_{B/m} &= 4\sqrt{\mu_i \times 3} \\ \tan \phi/2 &= \sqrt{\mu_i / 3} \\ \lambda &= \frac{\sqrt{3}}{4\sqrt{\mu_i}} \\ \text{where } \mu_i &= \frac{\mu_e + i_2 \mu'}{(1 + i_2)} \end{aligned}\right\} \quad \ldots\ldots\ldots\ldots\ldots\ldots\ldots \quad (4.24)$$

Mode C (Fig. 4.8)

This is a punching shear failure and should not occur if there is perfect interaction between the steel joist and the slab at ultimate load conditions and both of them fail simultaneously. If there is not sufficient shear connection to prevent slip and uplift between the steel joist and the slab at mid span the slab will get separated from the joist which would have failed near ultimate load and will span between the outer girders. Thus, there is a chance of the load punching through the slab.

From Moe's empirical formulae (4.12 to 4.14),

$$P_{punch} = 4 a d_1 v_o \quad \ldots\ldots\ldots\ldots\ldots\ldots\ldots\ldots \quad (4.24)$$

Increasing the punching load of slab by 20%

$$P_c = \frac{4M_c}{L} + 1.2\, P_{punch} \quad \ldots\ldots\ldots\ldots\ldots\ldots\ldots\ldots \quad (4.25)$$

Maximum efficiency of a deck is achieved when the failure of mode A takes place, provided mode C is prevented by proper design.

Mode A precedes mode B if

$$P_A < P_B$$

which gives

$$\rho < \frac{\sqrt{3}}{3} \frac{\sqrt{\mu_i}}{\mu_c} \quad \ldots\ldots\ldots\ldots\ldots\ldots\ldots\ldots \quad (4.26)$$

The equation (4.26) is plotted in Fig. 4.9 from which it is possible to predict the mode of failure for the given values of P and $\frac{\sqrt{\mu_i}}{\mu_c}$ or to choose their values for a failure mode which results in maximum efficiency of the deck.

4.3.2 Three-longitudinal composite beam bridge with a pair of point loads on outer longitudinal (Fig. 4.10)

The unloaded beams are free to rotate about their own axes but their ends are held down in order to prevent their lifting off the supports under the eccentric loading. It is assumed that moments are developed along the negative yield lines on the top of the slab.

Mode A. (Fig. 4.11)

For a vertual displacement of unity along the yield lines DE,

$$P_A = \frac{12 \mu_c\, m\, \rho}{(1-\beta)} \quad \ldots\ldots\ldots\ldots\ldots\ldots\ldots\ldots \quad (4.27)$$

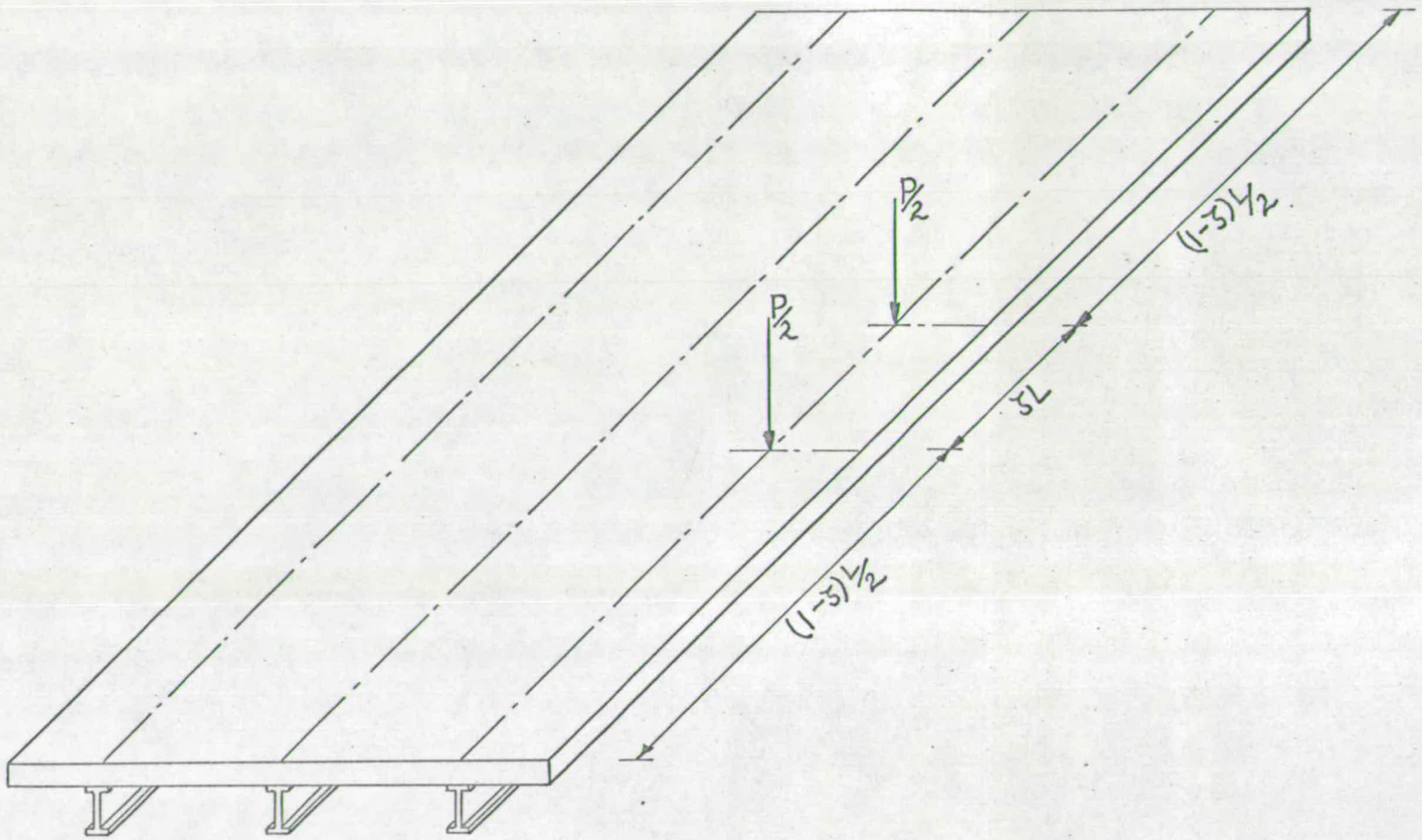

FIG. 4·10

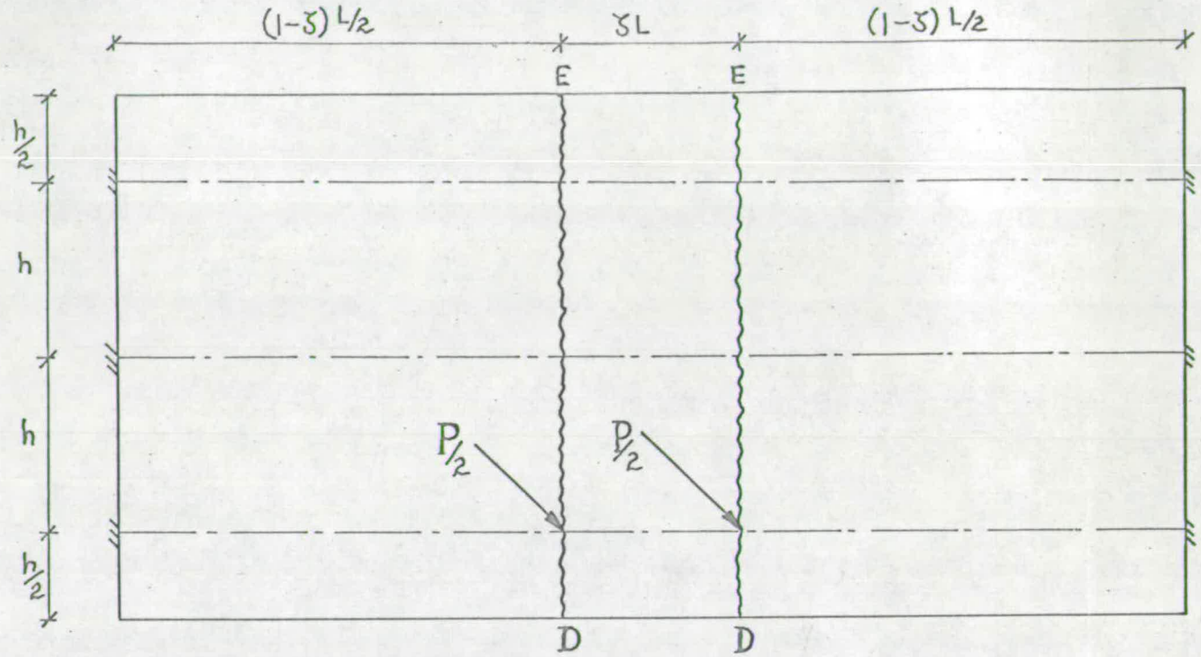

FIG. 4.11 MODE A

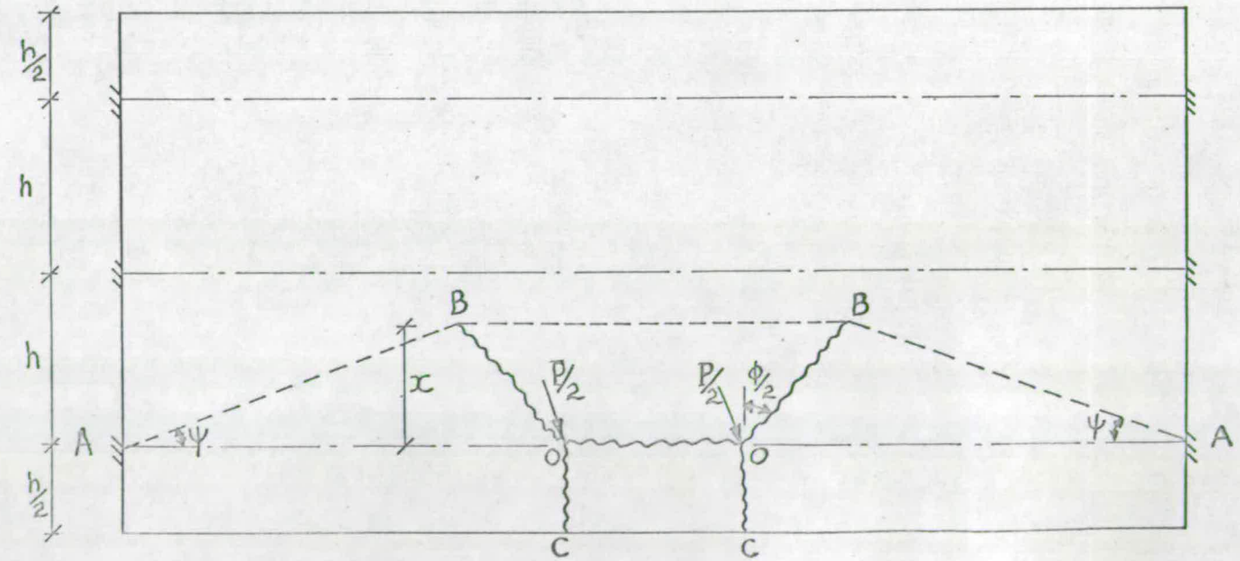

FIG. 4.12 MODE B

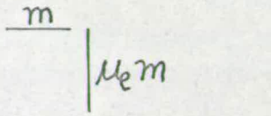

yield line	moment
OB	m
OC	μ'm
BB	i₁m
	i₁μ'm
AB	i₂m
	i₂μ'm

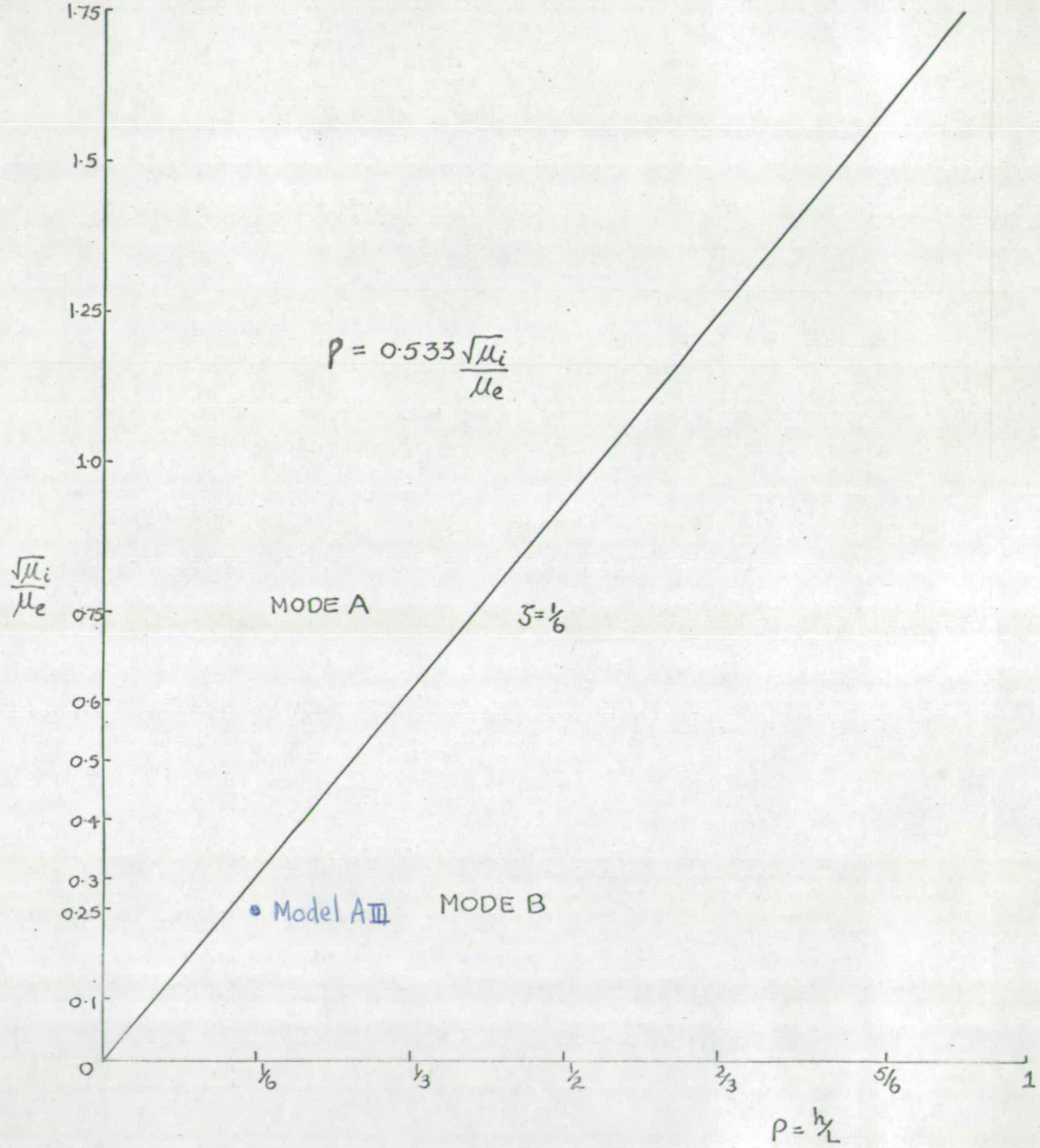

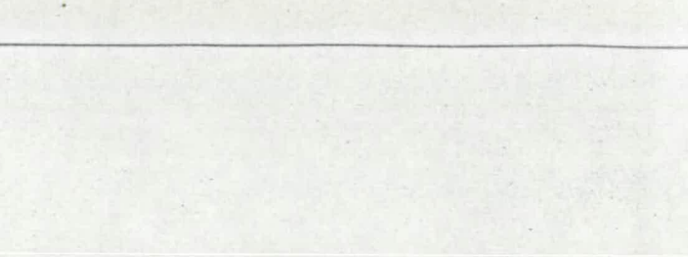

MODE A

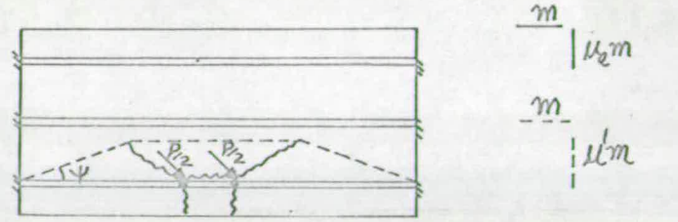

MODE B

FIG.4·13

Mode B (Fig. 4.12)

For a unit displacement along the yield lines OC,

$$P_{B/m} = \frac{2\mu_e P}{(1-\zeta)} + 2(1 + i_1)\tan\phi/2 + \frac{2(1 + i_1)}{(1-\zeta)} \sec\phi/2 \operatorname{cosec}\psi \cos(\psi - \phi/2)$$

$$+ 2\sec(\psi - \phi/2)\{\mu_e \cos\phi/2 \sin\psi - \sin\phi/2 \cos\psi\}$$

$$+ 2i_2 \cos\phi/2 \sec(\psi - \phi/2) \operatorname{cosec}\psi \{\mu' \sin^2\psi + \cos^2\psi\} \quad \ldots\ldots (4.28)$$

Noting that from the geometry of the yield line pattern,

$$\cot\psi + \tan\phi/2 = \frac{(1-\zeta)}{2\lambda} \quad \ldots\ldots\ldots\ldots\ldots\ldots (4.29)$$

Equation (4.28) can be rewritten in terms of parameters ϕ and λ,

$$P_{B/m} = \frac{2\mu_e P}{(1-\zeta)} - 2(2i_2 - i_1)\tan\phi/2 + \frac{(i_2 + \zeta) + \zeta(i_1 - i_2)}{\lambda}$$

$$+ \frac{4(\mu_e + i_2\mu')}{(1-\zeta)} + \frac{4\lambda}{(1-\zeta)}(1 + i_2)\tan^2\phi/2 \quad \ldots\ldots (4.30)$$

$$\frac{d(P_{B/m})}{d\phi} = 0 \text{ leads to } \tan\phi/2 = \frac{(2i_2 - i_1)(1-\zeta)}{4\lambda(1 + i_2)} \quad \ldots\ldots (4.31)$$

$$\frac{d(P_{B/m})}{d\lambda} = 0 \text{ leads to}$$

$$\frac{(i_2 + \zeta) + \zeta(i_1 - i_2)}{\lambda^2} = \frac{4(\mu_e + i_2\mu')}{(1-\zeta)} + \frac{4(1 + i_2)}{(1-\zeta)}\tan^2\phi/2 \quad \ldots (4.32)$$

$$\tan\phi/2 = \sqrt{\mu_i(1-\zeta)}(2i_2 - i_1) \Big/ \sqrt{4(1 + i_1)(i_2 + \zeta) - i_1^2(1-\zeta)} \quad \ldots\ldots (4.33)$$

substituting from Equation (4.33) for $\tan\phi/2$ in Equation (4.31),

$$\lambda = \frac{\sqrt{(1-\zeta)\ 4(1 + i_1)(i_2 + \zeta) - i_1^2(1-\zeta)}}{4\sqrt{\mu_i}(1 + i_2)} \quad \ldots\ldots\ldots (4.34)$$

substituting for tan $\phi/2$ and in Equation (4.30),

$$P_{B/m} = \frac{2\mu_e \rho}{(1-\zeta)} + \frac{2\sqrt{\mu_1}}{\sqrt{(1-\zeta)}} \left\{4(1 + i_1)(i_2 + \zeta) - i_1^2 (1-\zeta)\right\} \quad \ldots \quad (4.35)$$

Note:- Punching failure is not likely to occur for this type of loading. When the loaded beam fails, it will try to separate from the adjacent parts, resulting in Mode B or Mode A depending on the relative strengths of slab and beams.

Mode A precedes B if

$$P_A < P_B$$

which gives

$$\rho < \frac{\sqrt{\mu_i \ (1-\zeta)}}{5\mu_e} \left\{4(1 + i_1)(i_2 + \zeta) - i_1^2(1 - \zeta)\right\} m \quad \ldots \quad (4.36)$$

when $i_1 = i_2 = 1$ and $\zeta = 1/6$,

$$\frac{0.533\sqrt{\mu_i}}{\mu_e} \quad \ldots \quad (4.36a)$$

This equation is plotted in Fig. 4.13.

4.3.3 Four-longitudinal composite beam bridge with two pairs of central point loads on beams (Fig. 4.14).

The unloaded beams are free to rotate about their own axes and their ends are not held down. Therefore it is assumed that no moment is developed in negative yield lines on top of the slab ($i_1 m = i_2 m = 0$)

Mode A (Fig. 4.15)

For a vertual displacement of unity along the yield lines DE, the Work Equation yields,

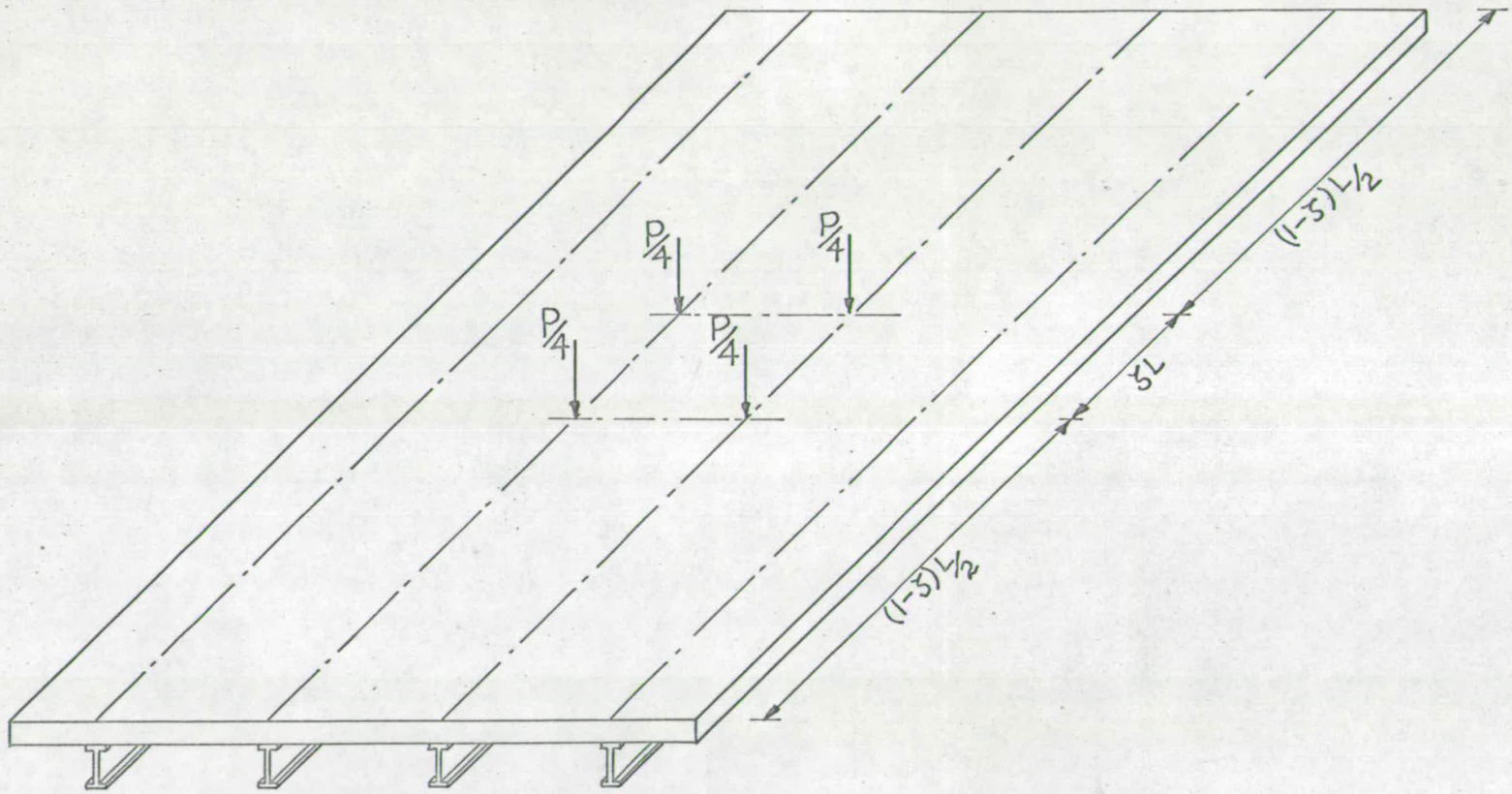

FIG. 4·14

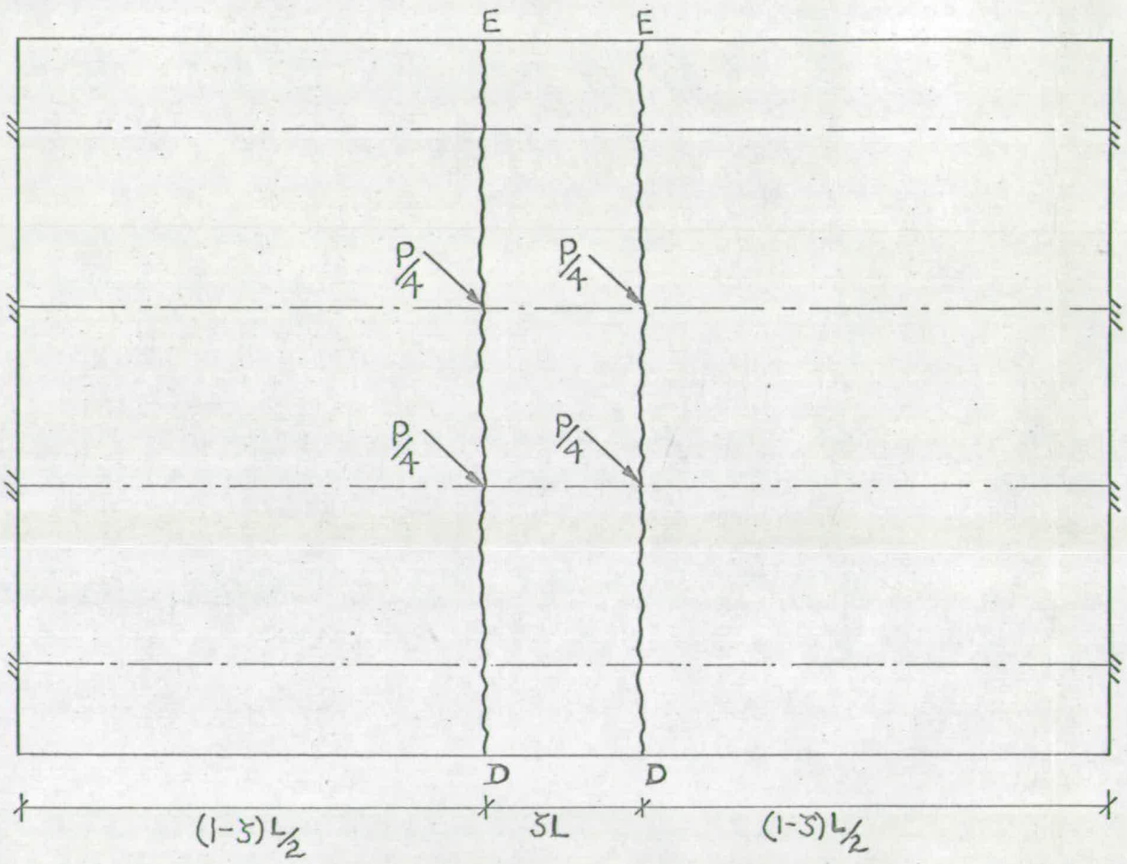

m

$\mu_e m$

FIG. 4.15 MODE A

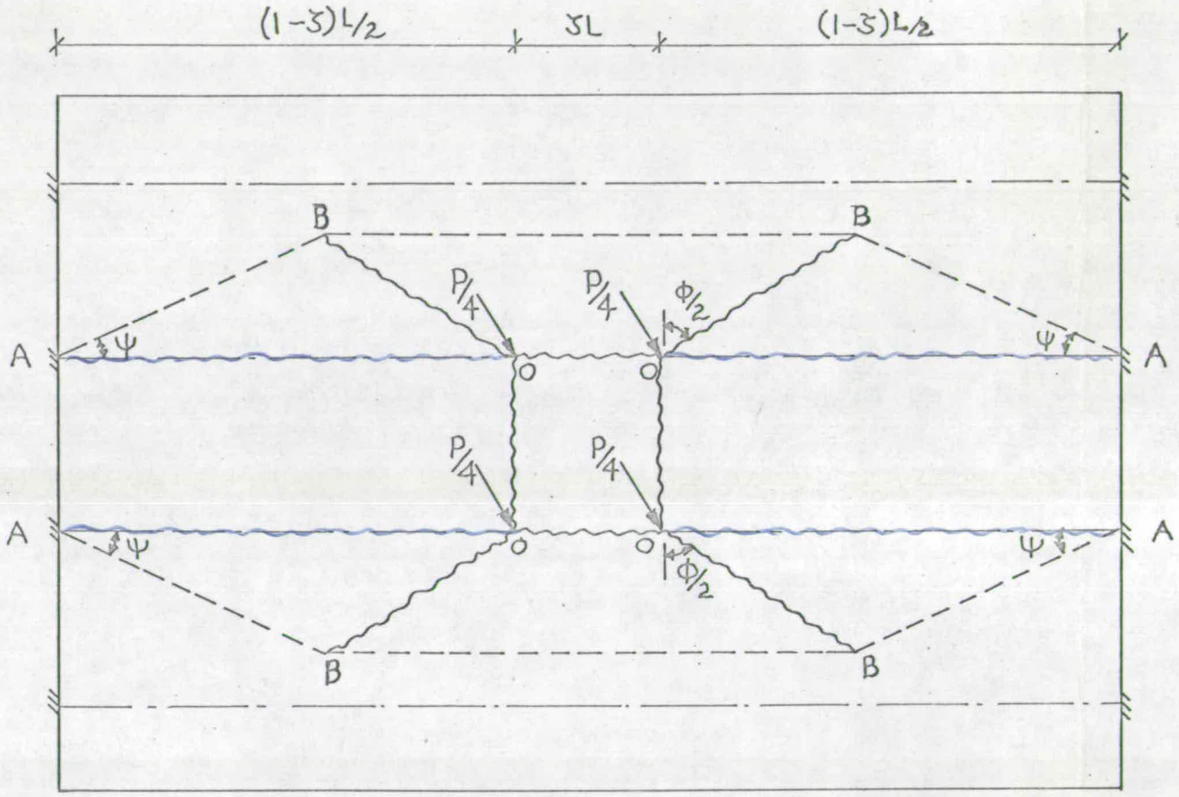

yield line	moment
OB	m
OO	$\mu_2 m$
BB	$i_1 m$
	$i_1 \mu' m$
AB	$i_2 m$
	$i_2 \mu' m$

FIG. 4·16 MODE B

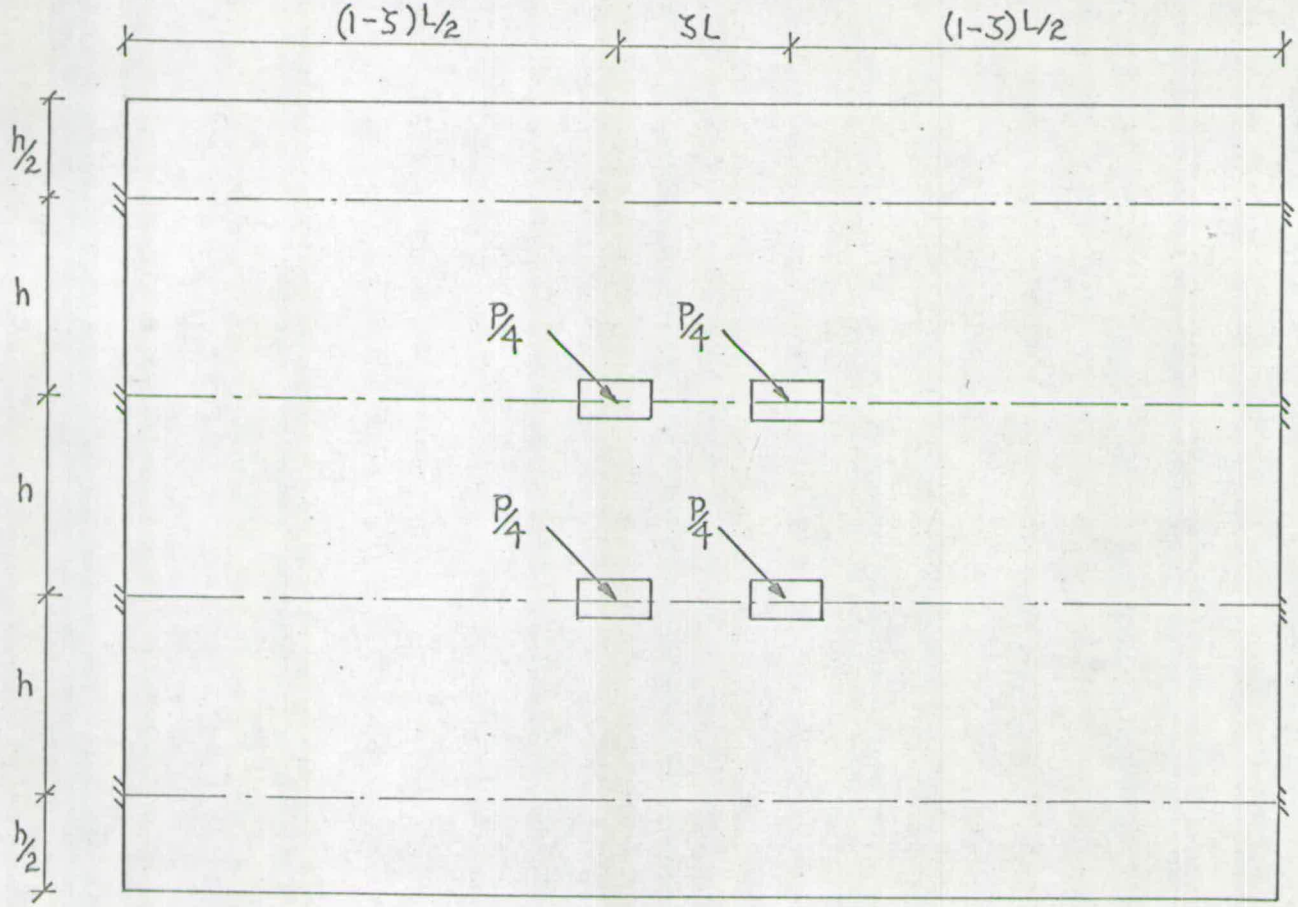

FIG. 4.17 MODE C

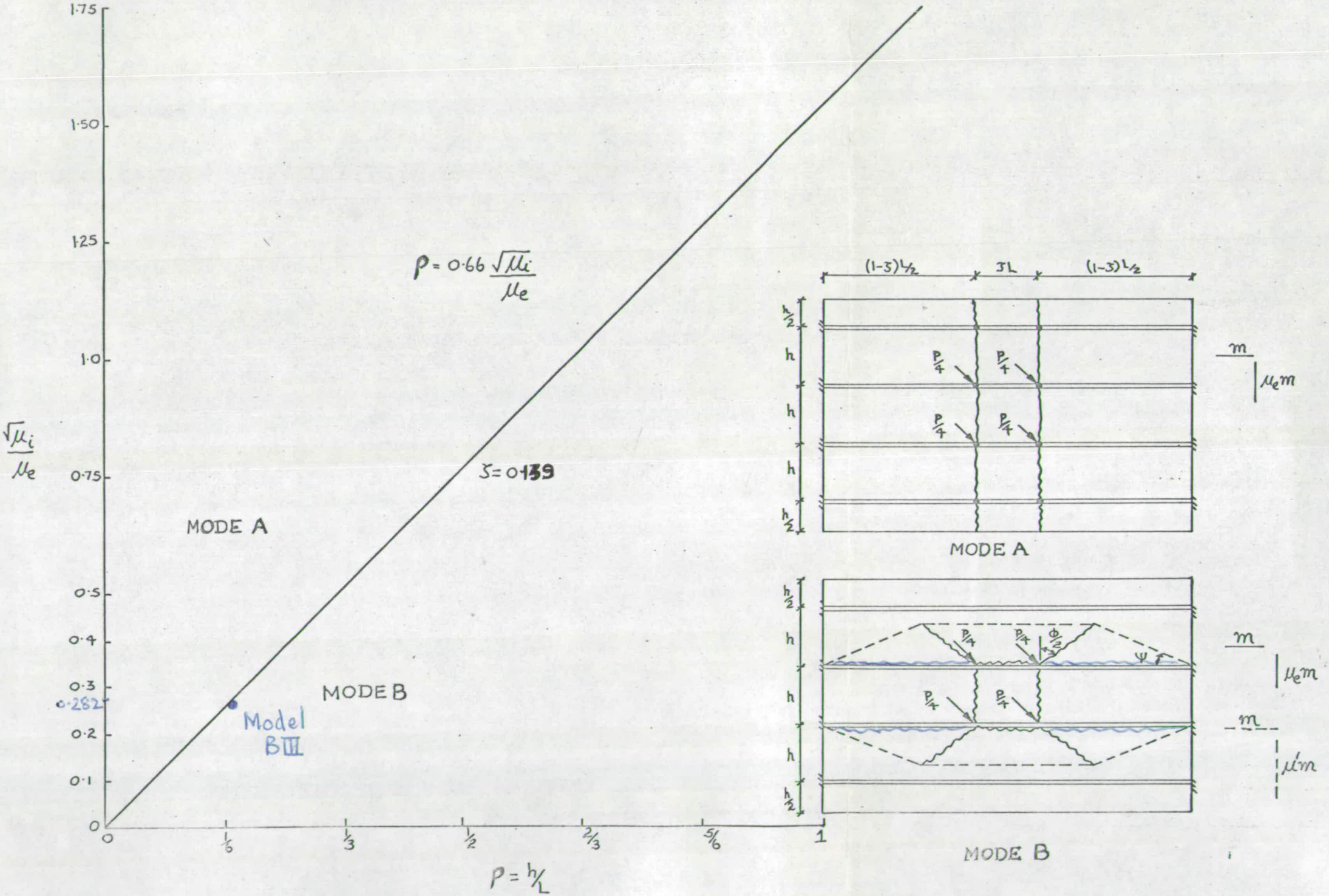
1·75
1·50
1·25
1·0
0·75
0·5
0·4
0·3
0·282
0·2
0·1
0
$\frac{\sqrt{\mu_i}}{\mu_e}$
$\rho = 0.66 \frac{\sqrt{\mu_i}}{\mu_e}$
$\zeta = 0.139$
MODE A
MODE B
Model BIII
0
1/6
1/3
1/2
2/3
5/6
1
$\rho = h/L$
(1-3)L/2
3L
(1-3)L/2
h/2
h
P/4
m
$\mu_e m$
MODE A
$\Phi/2$
Ψ
μm
MODE B

FIG. 4·18

$$P_A = \frac{16 \mu_e^m \rho}{(1-\zeta)} \qquad \ldots\ldots\ldots\ldots\ldots\ldots\ldots\ldots \quad (4.37)$$

Mode B (Fig. 4.16)

This mode is repetition of Mode B shown in Fig. 4.12 except that no moment is developed along the negative yield line BB.

substituting $i_1 = 0$ and multiplying Equation '4.35) by 2,

$$P_{B/m} = \frac{4 \mu_e \rho}{(1-\zeta)} + \frac{4\sqrt{\mu_i}(3-4\zeta)}{\sqrt{4(1-\zeta)^3-1}} \qquad \ldots\ldots\ldots\ldots\ldots\ldots \quad (4.38)$$

From Equation (4.33) and Equation (4.34),

$$\tan \phi/2 = \frac{\sqrt{\mu_i}}{\sqrt{4(1-\zeta)^3-1}} \qquad \ldots\ldots\ldots\ldots\ldots\ldots \quad (4.39)$$

$$\lambda = \frac{\sqrt{4(1-\zeta)^3-1}}{4(1-\zeta)\sqrt{\mu_i}} \qquad \ldots\ldots\ldots\ldots\ldots\ldots\ldots\ldots \quad (4.40)$$

$\tan \phi/2 = \frac{1}{4\lambda(1-\zeta)}$ and $\cot \psi = \frac{\sqrt{\mu_i}\,[2(1-\zeta)^2-1]}{\sqrt{4(1-\zeta)^3-1}}$ ..... (4.40a)

Mode C (Fig. 4.17)

The punching load is calculated using the formulae (4.12 to 4.14) noting that they are applied to each loaded area and the values are added up. Provided that Mode C is eliminated by proper design, Mode A precedes Mode B if

$$P_A < P_B$$

which gives

$$\frac{16 \mu_e^m \rho}{(1-\zeta)} < \frac{4 \mu_e^m \rho}{(1-\zeta)} + \frac{4\sqrt{\mu_i}\,(3-4\zeta)^m}{\sqrt{4(1-\zeta)^3-1}} \qquad \ldots\ldots\ldots\ldots \quad (4.41)$$

Noting that $\zeta = 0.139$, or $5/36$

$$\rho < 0.66 \frac{\sqrt{\mu_i}}{\mu_e} \qquad \ldots\ldots\ldots\ldots\ldots\ldots\ldots\ldots \quad (4.41a)$$

This equation is plotted in Fig. 4.18.

4.3.4 Four-longitudinal composite Beam Bridge with two pairs of eccentric point loads on beams (Fig. 4.19)

The unloaded beams are free to rotate about their own axes and their ends are not held down. Therefore it is assumed that no moment is developed along the negative lines on the top of the slab ($i_1 m = i_2 m = 0$)

Mode A (Fig. 4.20)

For unit displacement along the yield lines DE, the Work Equation yields,

$$P_A = \frac{16 \mu_c m \rho}{(1-\zeta)} \qquad \ldots\ldots\ldots\ldots\ldots\ldots\ldots\ldots \quad (4.42)$$

Mode B (Fig. 4.21)

This mode is similar to Mode B shown in Fig. 4.12 except that there is no moment developed along the yield lines AB and BB and the length of yield line OC now equals $\frac{3h}{2}$ and there are additional positive yield lines AO.

From the postulated yield pattern, it can be shown that,

$$\frac{P_B}{m} = \frac{6 \mu_e \rho}{(1-\zeta)} + \frac{2\sqrt{\mu_i}\,(3-4\zeta)}{\sqrt{4(1-\zeta)^3 - 1}} \qquad \ldots\ldots\ldots\ldots\ldots\ldots \quad (4.43)$$

The values of ϕ and λ are respectively determined from equations (4.39) and (4.40).

Note:- Punching failure is not likely to occur in this case for the reasons stated in section 4.3.2.

Mode A precedes Mode B if

$P_A < P_B$

which gives

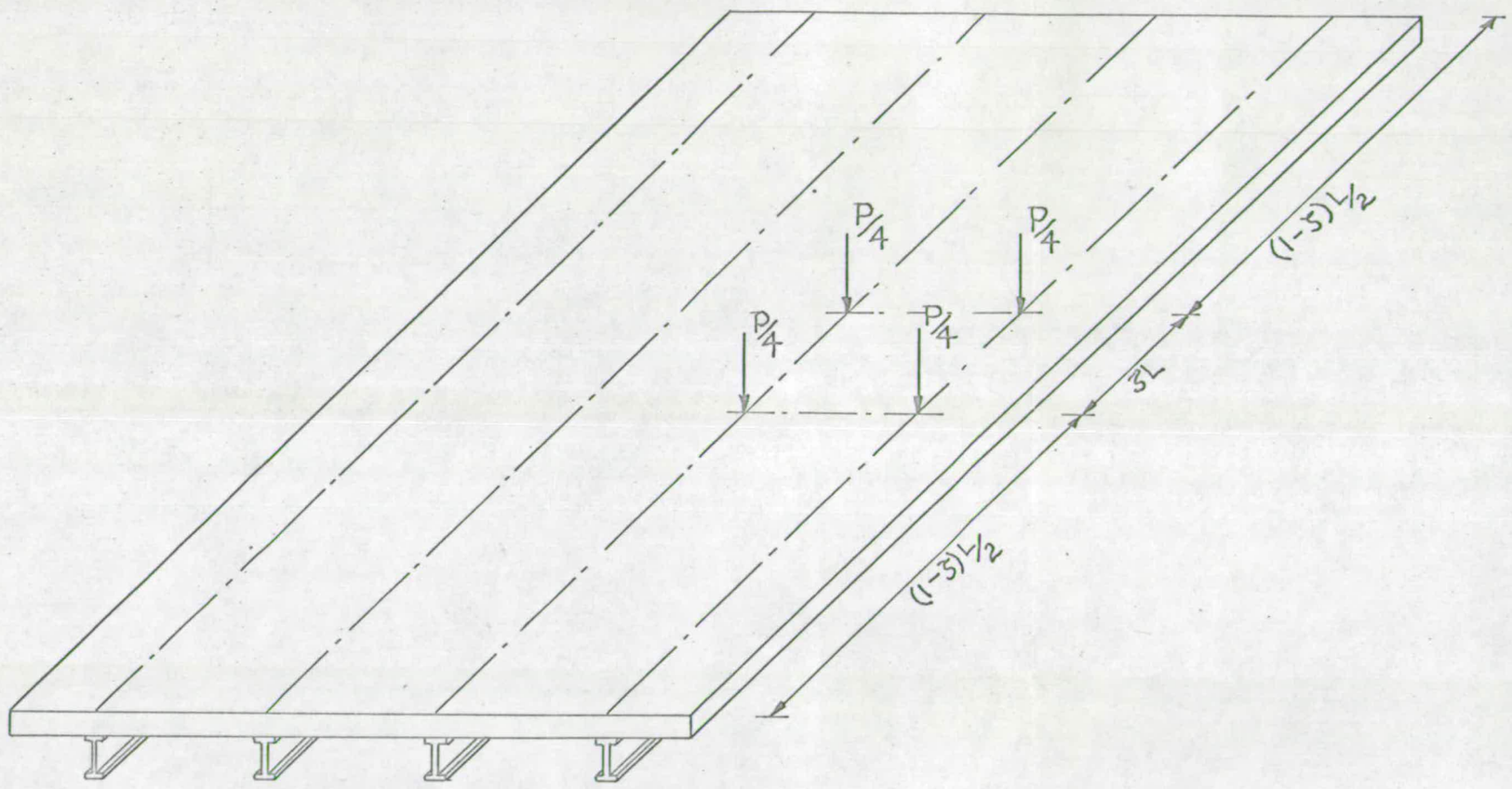

FIG. 4·19

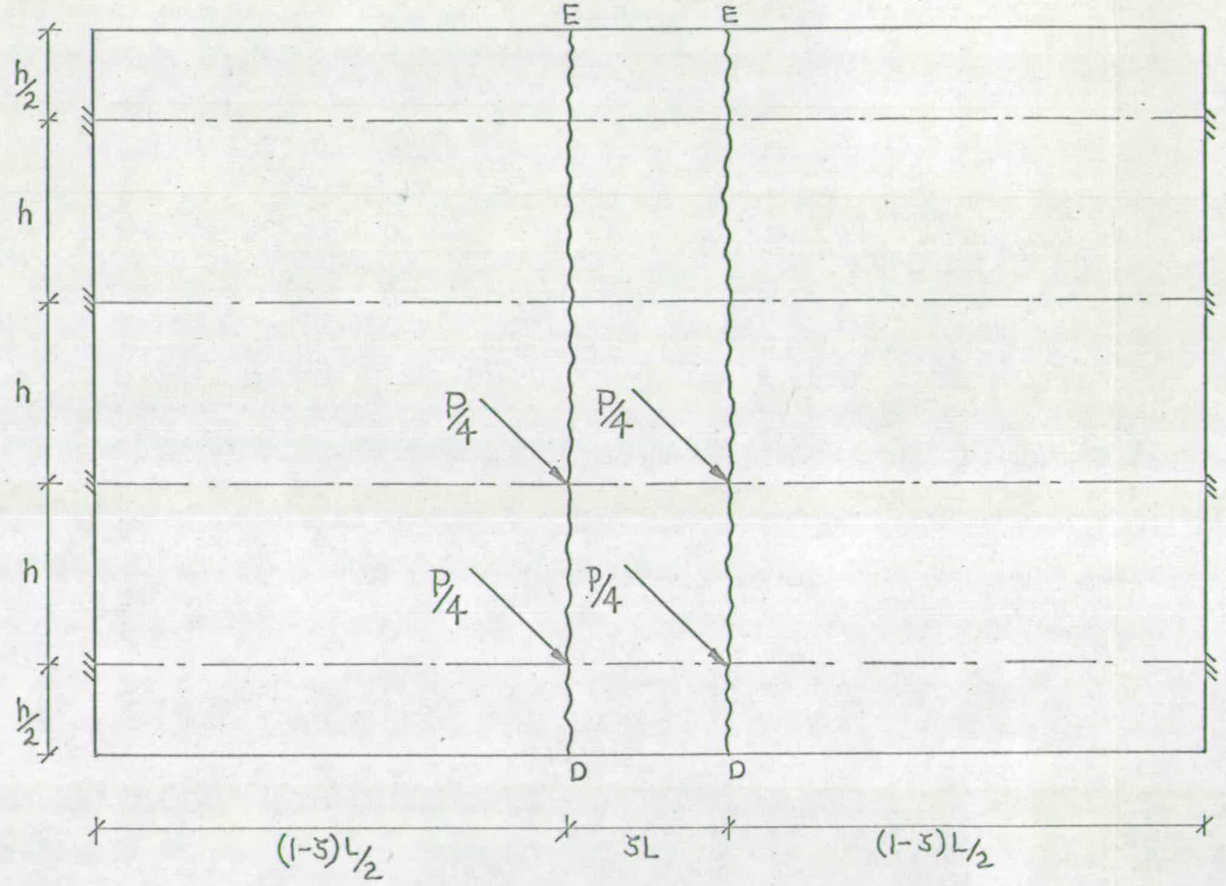

m

$\mu_e m$

FIG. 4.20 MODE A

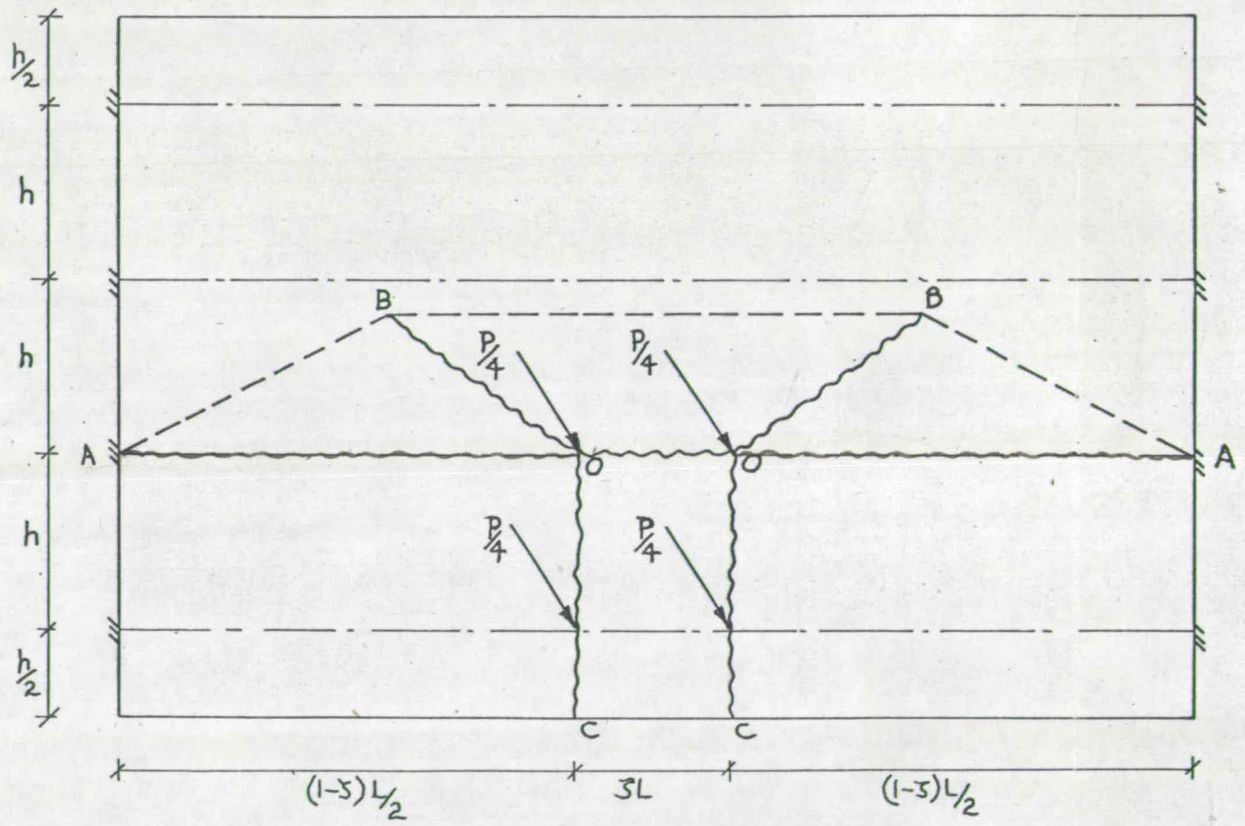

yield line	moment
OB, OC, OO	m, $\mu_2 m$
BB	$i_1 m$, $i_1 \mu' m$
AB	$i_2 m$, $i_2 \mu' m$

FIG. 4.21 MODE B

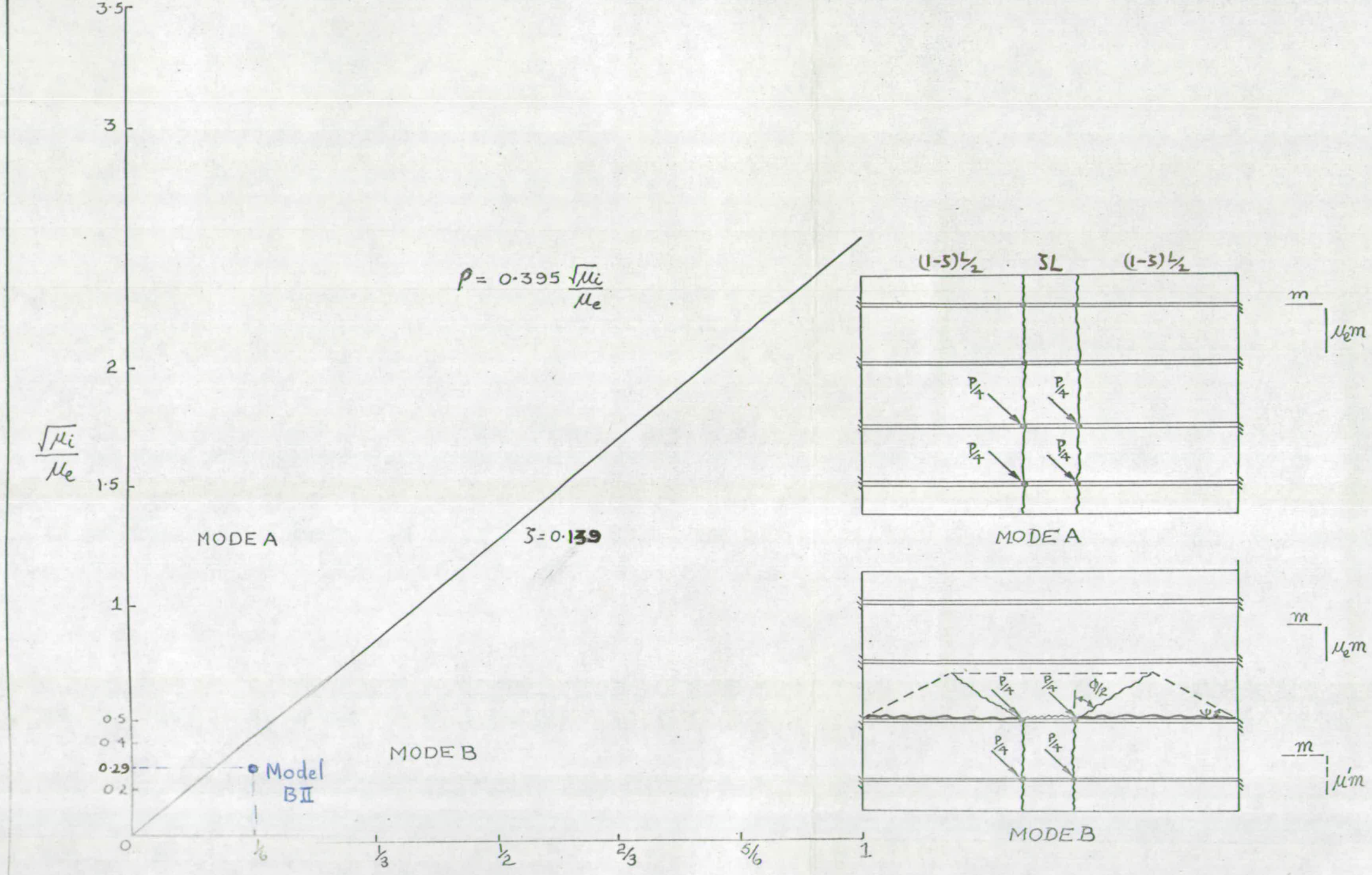
3·5
3
2
1·5
1
0·5
0·4
0·29
0·2
0
√μi/μe
ρ = 0·395 √μi/μe
ζ = 0·139
MODE A
MODE B
Model BII
1/6
1/3
1/2
2/3
5/6
1
ρ = h/L
(1-5)L/2
L
(1-5)L/2
m
μem
P/4
MODE A
m
μem
P/4
Q/2
m
μ'm
MODE B

FIG. 4·22

$$\rho < \frac{1}{5} \frac{\sqrt{\mu_i}}{\mu_c} \frac{(1-\zeta)(3-4\zeta)}{\sqrt{4(1-\zeta)^3 - 1}} \quad \ldots\ldots\ldots\ldots\ldots\ldots \quad (4.44)$$

When $\zeta = 0.139$,

$$\rho < 0.395 \frac{\sqrt{\mu_i}}{\mu_c} \quad \ldots\ldots\ldots\ldots\ldots\ldots\ldots\ldots \quad (4.44a)$$

This equation is plotted in Fig. 4.22.

4.3.5 Four-longitudinal Composite Beam Bridge with four pairs of eccentric point loads simulating the wheel loads of HB vehicle (Fig. 4.23).

The unloaded beams are free to rotate about their own axes and their ends are not held down implying that no moment is developed along the negative yield lines on top of the slab.

Only two lines of loads are considered. These correspond to the two axles of the abnormal vehicle crossing the bridge deck. For short spans this will produce the most adverse condition and for long spans the other axles can be treated in an identical way. The four pairs of loads are placed symmetrical to the mid span section but eccentric to the longitudinal central line of the bridge with the first pair on outer longitudinal.

Mode A (Fig. 4.24)

For unit displacement along the yield lines DE, the Work Equation yields

$$P_A = \frac{16 \mu_c m \rho}{(1-\zeta)} \quad \ldots\ldots\ldots\ldots\ldots\ldots\ldots\ldots \quad (4.45)$$

Mode B (Fig. 4.25)

This mode is the same as Mode B shown in Fig. (4.21) except that the displacement under the loads 7 and 8 is not unity and is equal to δ_1.

For unit displacement along the yield lines CO,

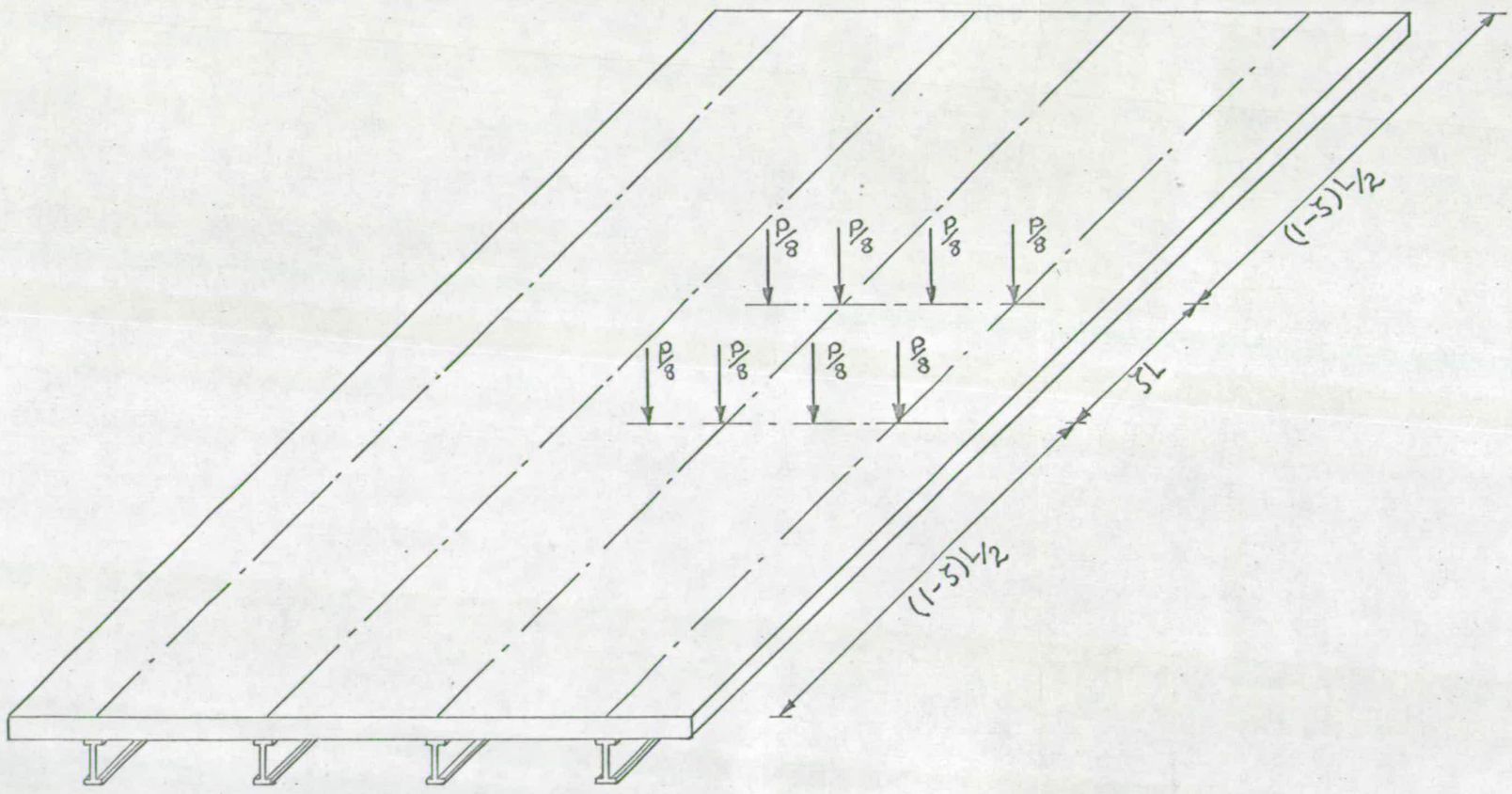

FIG. 4.23

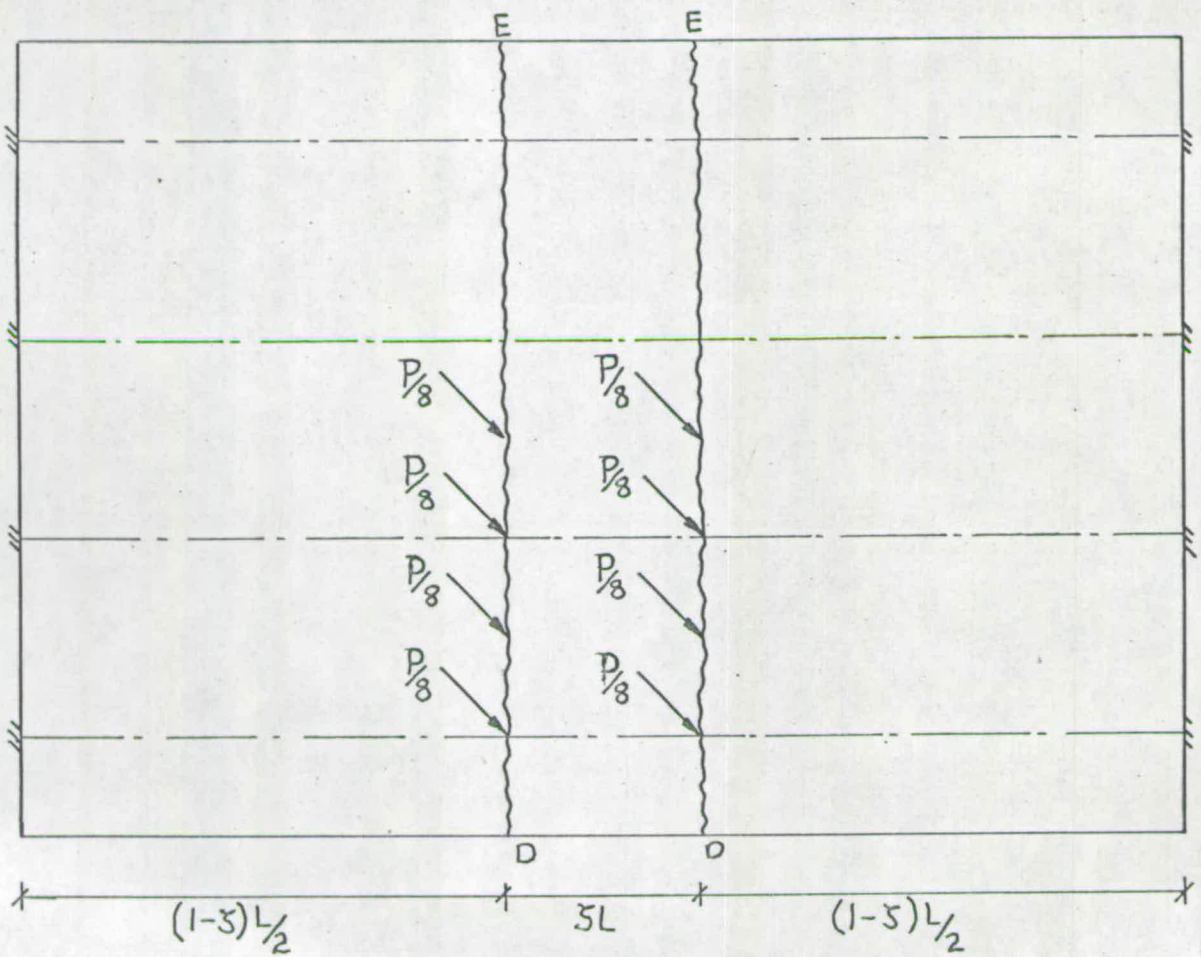

FIG.4.24 MODE A

m

$\mu_e m$

516

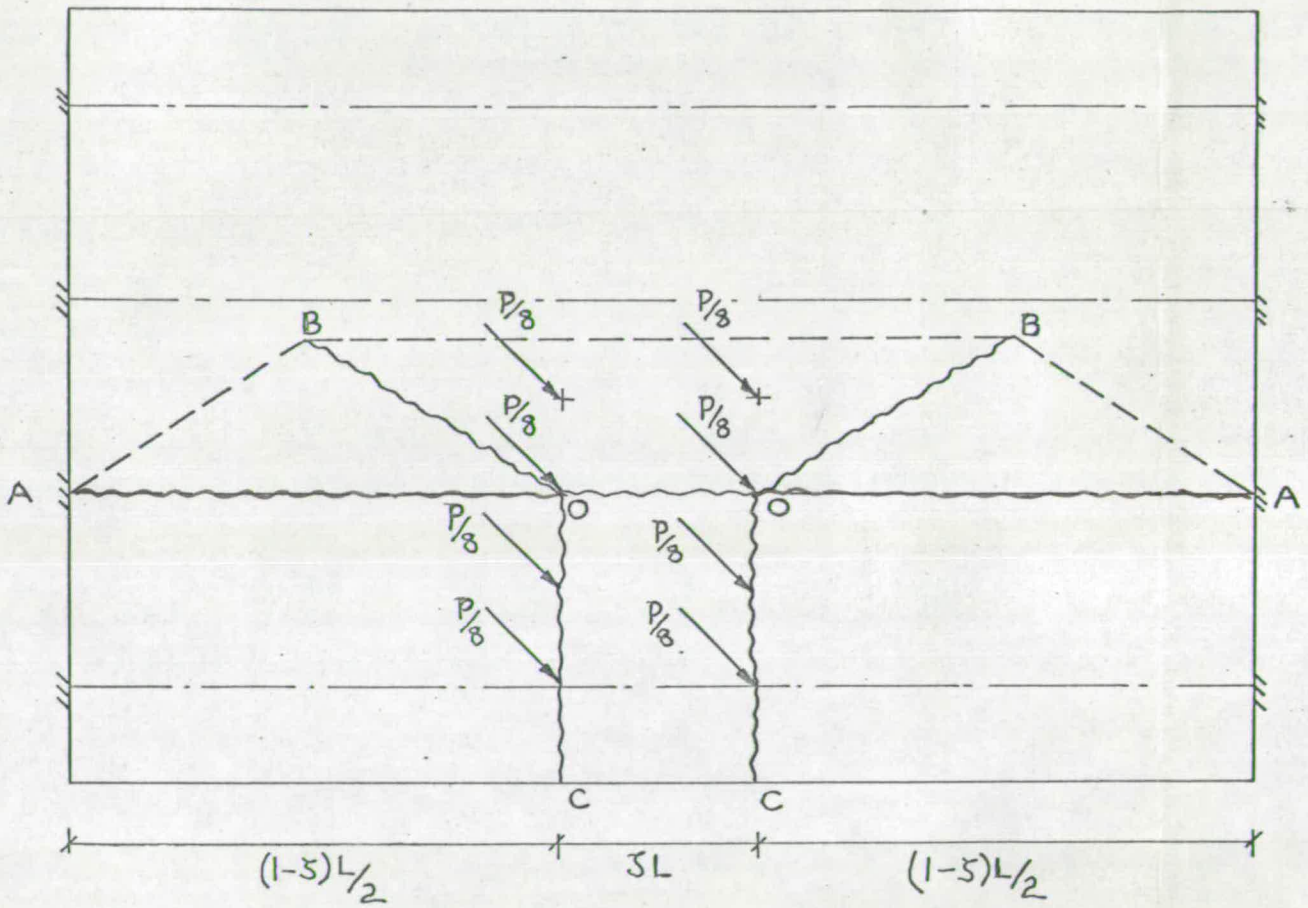

yield line	moment
OB	m
OC	$\mu_2 m$
OO	
BB	$i_1 m$
	$i_1 \mu' m$
AB	$i_2 m$
	$i_2 \mu' m$

FIG.4·25 MODE B

$$P_{B/m} = \frac{4}{(\delta_1 + 3)} \left[\frac{6\mu_c \rho}{(1-\xi)} + \frac{2\sqrt{\mu_i}}{\sqrt{4(1-\xi)^3 - 1}} (3 - 4\xi) \right] \quad \ldots\ldots \quad (4.46)$$

where $\delta_1 = (1 - \frac{\rho}{2\lambda})$

The values of ϕ and λ are determined respectively by the equations (4.39) and (4.40).

Note:- Punching failure is not likely to occur in this case for reasons explained in section 4.3.2.

Mode A precedes Mode B if,

$P_A < P_B$

which gives

$$\frac{16\mu_c \rho}{(1-\xi)} < \frac{4}{(\delta_1 + 3)} \left[\frac{6\mu_c \rho}{(1-\xi)} + \frac{2\sqrt{\mu_i}(3-4\xi)}{\sqrt{4(1-\xi)^3 - 1}} \right] \quad \ldots\ldots \quad (4.47)$$

4.4 Solutions by Beam and Slab Method

4.4.1 Three longitudinal composite Beam Bridge with point load at mid span. (Fig. 4.5)

The assumptions are the same as those made in section 4.3.1.

Mode A (Fig. 4.26)

$$P_A = \frac{12M_c}{L} + \frac{12\mu_m (h - B_e)}{L} \quad \ldots\ldots \quad (4.48)$$

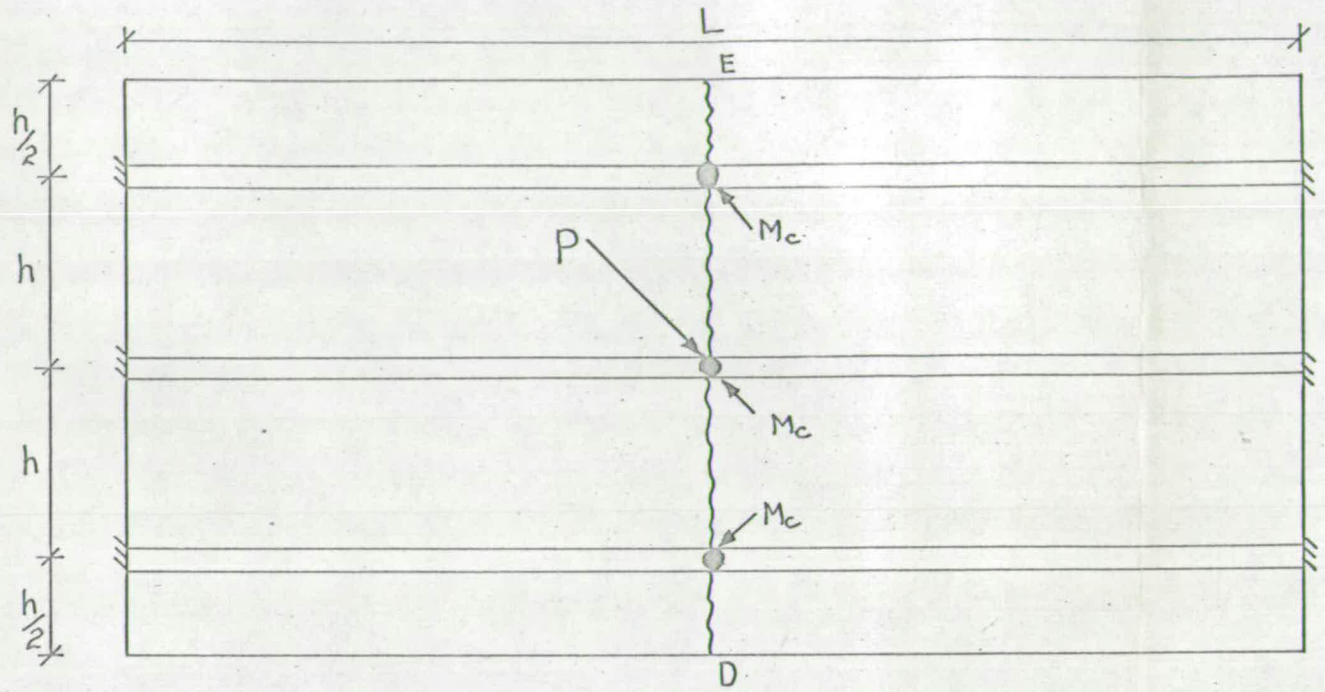

FIG 4·26 MODE A

m
μm

● Hinge in beam

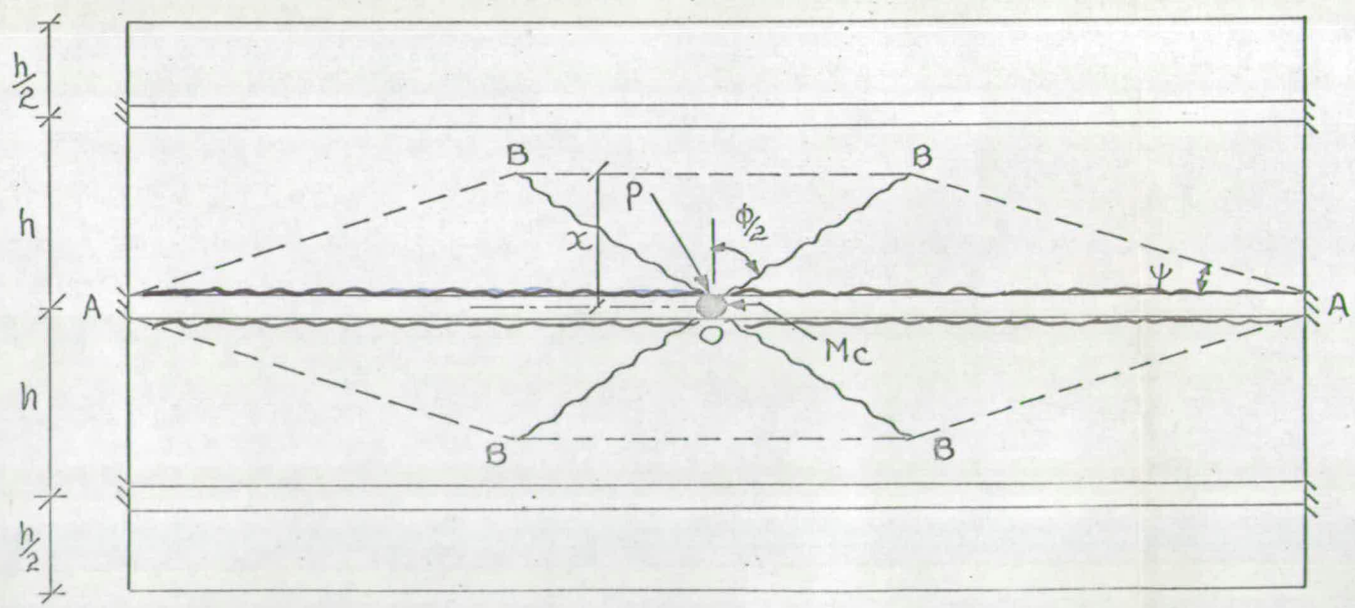

yield line	moment
OB	m / μm
BB	$i_1 m$ / $i_1 \mu' m$
AB	$i_2 m$ / $i_2 \mu' m$

FIG. 4·27 MODE B

or $P_A = 12 \mu_c m \rho$ . . . . . (4.48a)

Mode B (Fig. 4.27)

$$P_B = \frac{4M_c}{L} + 2\left[2(i_1 - 2i_2) \tan \phi/2 + \frac{i_2}{\lambda} + 4(\mu + i_2\mu')\lambda \right.$$

$$\left. + 4\lambda (1 + i_2) \tan^2 \phi/2 + \frac{1}{\lambda} - 2 \tan \phi/2 \right] m \quad \ldots (4.49)$$

$\frac{d(P_B)}{d\phi}$ = 0 leads to

$$\tan \phi/2 = \frac{(2i_2 - i_1 + 1)}{4\lambda(1 + i_2)} \quad \ldots (4.50)$$

$\frac{d(P_B)}{d\lambda}$ = 0 leads to

$$\frac{i_2}{\lambda^2} = 4(\mu + i_2\mu') + 4(1 + i_2) \tan^2 \phi/2 \quad \ldots (4.51)$$

subsituting from Equation (4.51) for in Equation (4.50),

$$\tan \phi/2 = \frac{\sqrt{\mu_s}\,(2i_2 - i_1 + 1)}{\sqrt{4(1 + i_1)\, i_2 - i_1^2 + 3 + 2i}} \quad \ldots (4.52)$$

where $\mu_s = \frac{\mu + i_2\mu'}{(1 + i_2)}$

substituting for $\tan \phi/2$ in Equation (4.50),

$$\lambda = \frac{\sqrt{4(1 + i_1)\, i_2 - i_1^2 + 3 + 2i}}{4(1 + i_2)\sqrt{\mu_s}} \quad \ldots (4.53)$$

where $0 \leqslant \lambda \leqslant \rho$

$$\therefore \quad P_B = \frac{4M_c}{L} + \sqrt{4\mu_s \{4(1 + i_1) i_2 - i_1^2 + 3 + 2i\} m} \quad \ldots\ldots \quad (4.54)$$

since $i_1 = i_2 = 0$,

$$P_B = \frac{4M_c}{L} + 4\sqrt{\mu_s}\sqrt{3m} \quad \ldots\ldots \quad (4.54a)$$

when $\lambda > \rho$ take $\lambda = \rho$ since λ can not exceed the value of ρ for the assumed yield pattern.

$$\therefore \quad \text{Tan } \phi_{/2} = \frac{1}{4\rho} \quad \ldots\ldots \quad (4.55)$$

substituting for λ and tan $\phi_{/2}$ in Equation (4.49) and putting $i_1 = 0$.

$$P_B = \frac{4M_c}{L} + \left[8\mu\rho + \frac{3}{2\rho}\right] m \quad \ldots\ldots \quad (4.56)$$

4.4.2 Three longitudinal composite Beam Bridge with point loads on outer longitudinal (Fig. 4.10)

The assumptions are the same as those made in section 4.3.2.

Mode A (Fig. 4.28)

$$P_A = \frac{12M_c}{(1-\zeta)L} + \frac{12\mu m (h - B_e)}{(1-\zeta)L} \quad \ldots\ldots \quad (4.57)$$

or $$P_A = \frac{12\mu_e \rho m}{(1-\zeta)} \quad \ldots\ldots \quad (4.57a)$$

Mode B (Fig. 4.29)

$$P_B = \frac{4M_c}{(1-\zeta)L} + \left[2(i_1 - 2i_2) \tan \phi_{/2} + \frac{i_2 + \zeta + \zeta(i_1 - i_2)}{\lambda} + \right.$$

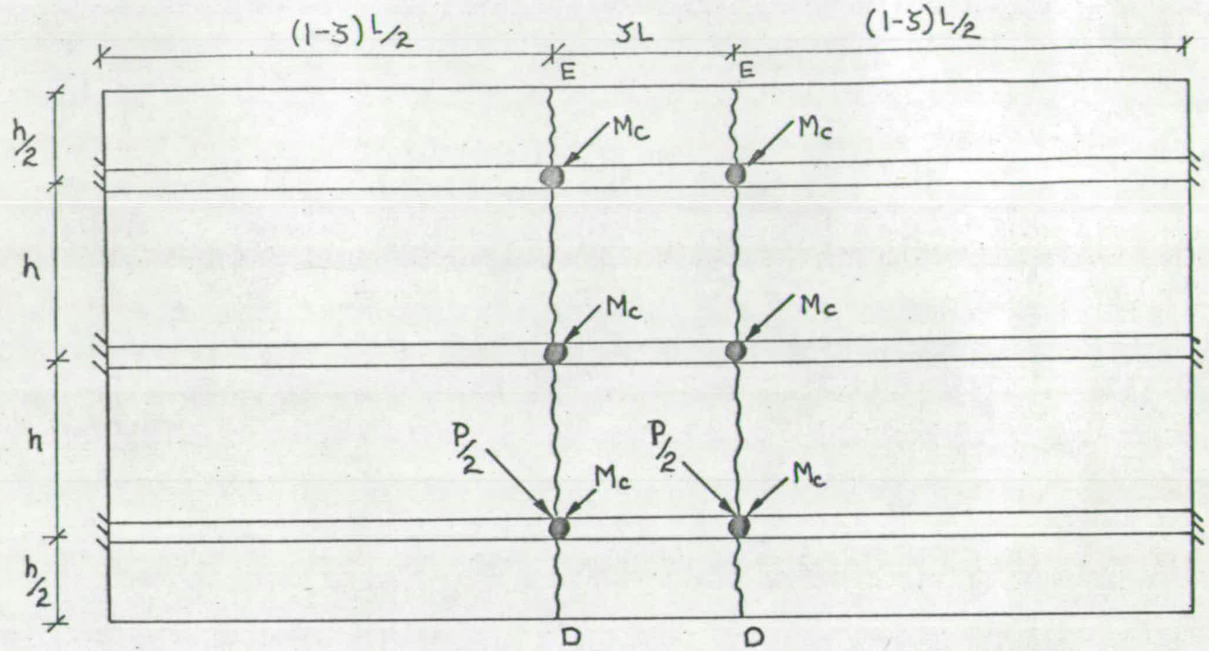

FIG.4.28 MODE A

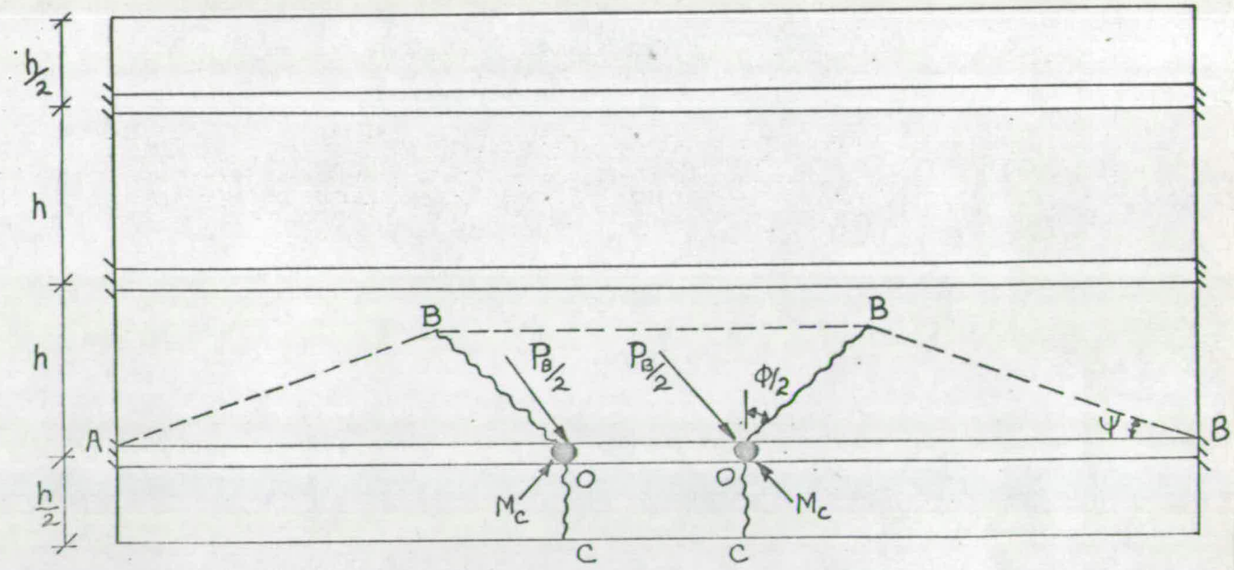

FIG.4.29 MODE B

m
μm

Hinge in beam

yield line	Moment
OB	m
OC	μm
BB	$i_1 m$
	$i_1 \mu' m$
AB	$i_2 m$
	$i_2 \mu' m$

$$+ \frac{4(\mu + i_2\mu')}{(1-\zeta)} + \frac{4\lambda}{(1-\zeta)}(1 + i_2)\tan^2 \phi/2 \Big] m \quad \ldots\ldots \quad (4.58)$$

$\frac{d(P_B/m)}{d\phi} = 0$ leads to

$$\tan \phi/2 = \frac{(2i_2 - i_1)(1-\zeta)}{4\lambda(1 + i_2)} \quad \ldots\ldots\ldots\ldots\ldots\ldots \quad (4.59)$$

$\frac{d(P_B/m)}{d\lambda} = 0$ leads to

$$\frac{(i_2 + \zeta) + \zeta(i_1 - i_2)}{\lambda^2} = \frac{4(\mu + i_2\mu')}{(1-\zeta)} + \frac{4(1 + i_2)}{(1-\zeta)} \tan^2 \phi/2 \quad .. \quad (4.60)$$

substituting from Equation (4.60) for in Equation (4.59),

$$\tan \phi/2 = \frac{\sqrt{\mu_s (1-\zeta)}(2i_2 - i_1)}{\sqrt{4(1 + i_1)(i_2 + \zeta) - i_1^2 (1-\zeta)}} \quad \ldots\ldots\ldots \quad (4.61)$$

substituting for $\tan \phi/2$ in Equation (4.59),

$$\lambda = \frac{\sqrt{(1-\zeta)}\sqrt{4(1 + i_1)(i_2 + \zeta) - i_1^2 (1-\zeta)}}{4\sqrt{\mu_s}(1 + i_2)} \quad \ldots\ldots \quad (4.62)$$

where $0 \leq \lambda \leq \rho$

$$P_B = \frac{4M_c}{(1-\zeta)L} + \frac{2\sqrt{\mu_s}}{\sqrt{(1-\zeta)}}\sqrt{4(1 + i_1)(i_2 + \zeta) - i_1^2 (1-\zeta)}\, m \quad .. \quad (4.63)$$

<u>when $\lambda > \rho$</u>, $\lambda = \rho$

From Equation (4.59),

$$\tan \phi/2 = \frac{(2i_2 - i_1)(1-\zeta)}{4\rho(1 + i_2)} \quad \ldots\ldots\ldots\ldots\ldots\ldots \quad (4.64)$$

$$P_B = \frac{4M_c}{(1-\zeta)L} + \left[\frac{(i_2 + \zeta) + \zeta(i_1 - i_2)}{} + \frac{4(\mu + i_2\mu)\rho}{(1-\zeta)} - \frac{(2i_2 - i_1)^2(1-\zeta)}{4(1 + i_2)\rho} \right] m \quad \ldots\ldots \quad (4.65)$$

or

$$P_B = \frac{4M_c}{(1-\zeta)L} + \left[\frac{(i_2 + \zeta) + \zeta(i_1 - i_2)}{\rho} + \frac{4(1 + i_2)\mu_s\rho}{(1-\zeta)} - \frac{(2i_2 - i_1)^2(1-\zeta)}{4(1 + i_2)\rho} \right] m \quad \ldots\ldots \quad (4.66)$$

4.4.3 Four longitudinal composite Beam Bridge with point loads at mid span of inner longitudinals (4.14).

The assumptions are the same as those made in section 4.3.3.

Mode A (Fig. 4.30)

$$P_A = \frac{16M_c}{(1-\zeta)L} + \frac{16\mu m(h-B_c)}{(1-\zeta)L} \quad \ldots\ldots\ldots\ldots\ldots\ldots \quad (4.66)$$

or $$P_A = \frac{16\mu_e m\rho}{(1-\zeta)} \quad \ldots\ldots\ldots\ldots\ldots\ldots \quad (4.66a)$$

Mode B (Fig. 4.31)

This mode is repetition of Mode B shown in Fig. 4.29 except that no moment is developed along the negative yield line AB and BB and there are additional positive yield lines AO. For unit displacement along oo,

$$P_B = \frac{8M_c}{(1-\zeta)L} + \frac{4\sqrt{\mu}\ (3-4\zeta)m}{\sqrt{4(1-\zeta)^3 - 1}} \quad \ldots\ldots\ldots\ldots\ldots \quad (4.67)$$

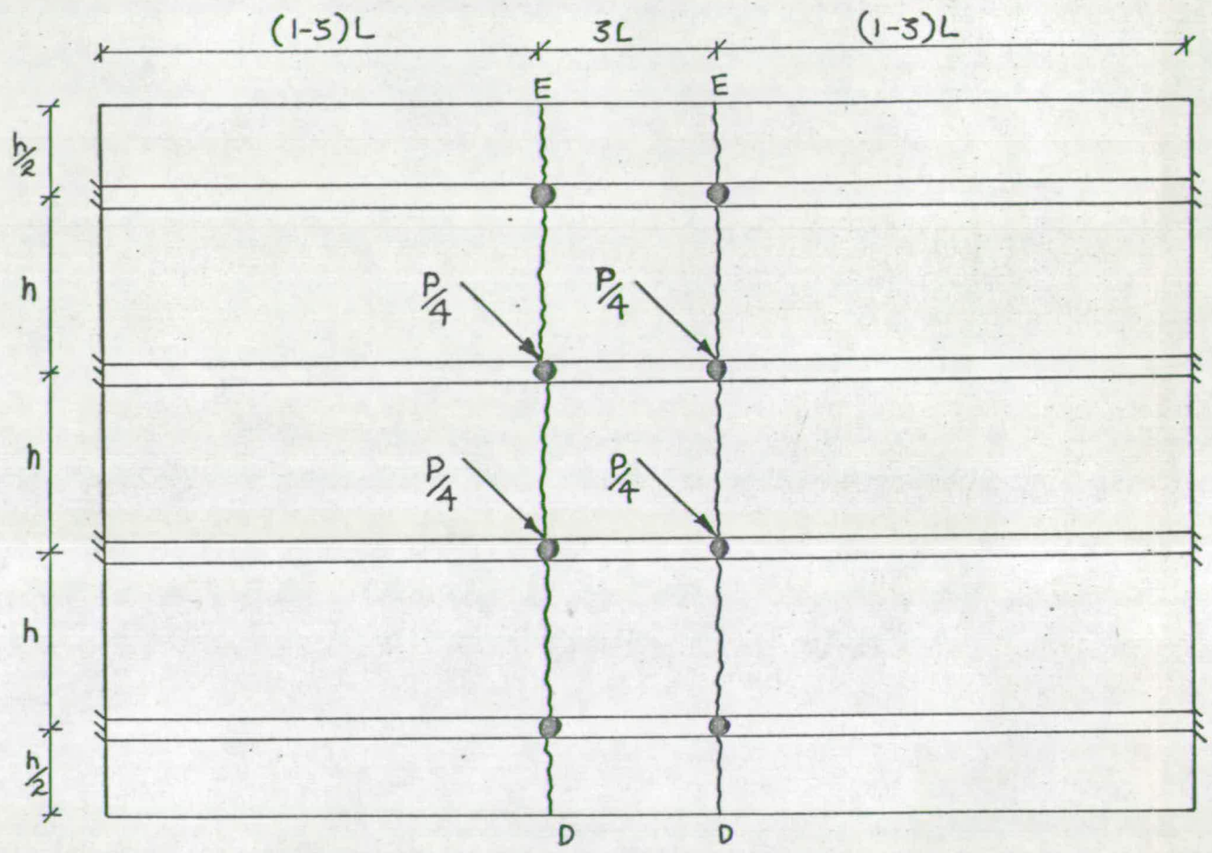

m
μm

● Hinge in beam

FIG.4.30 MODE A

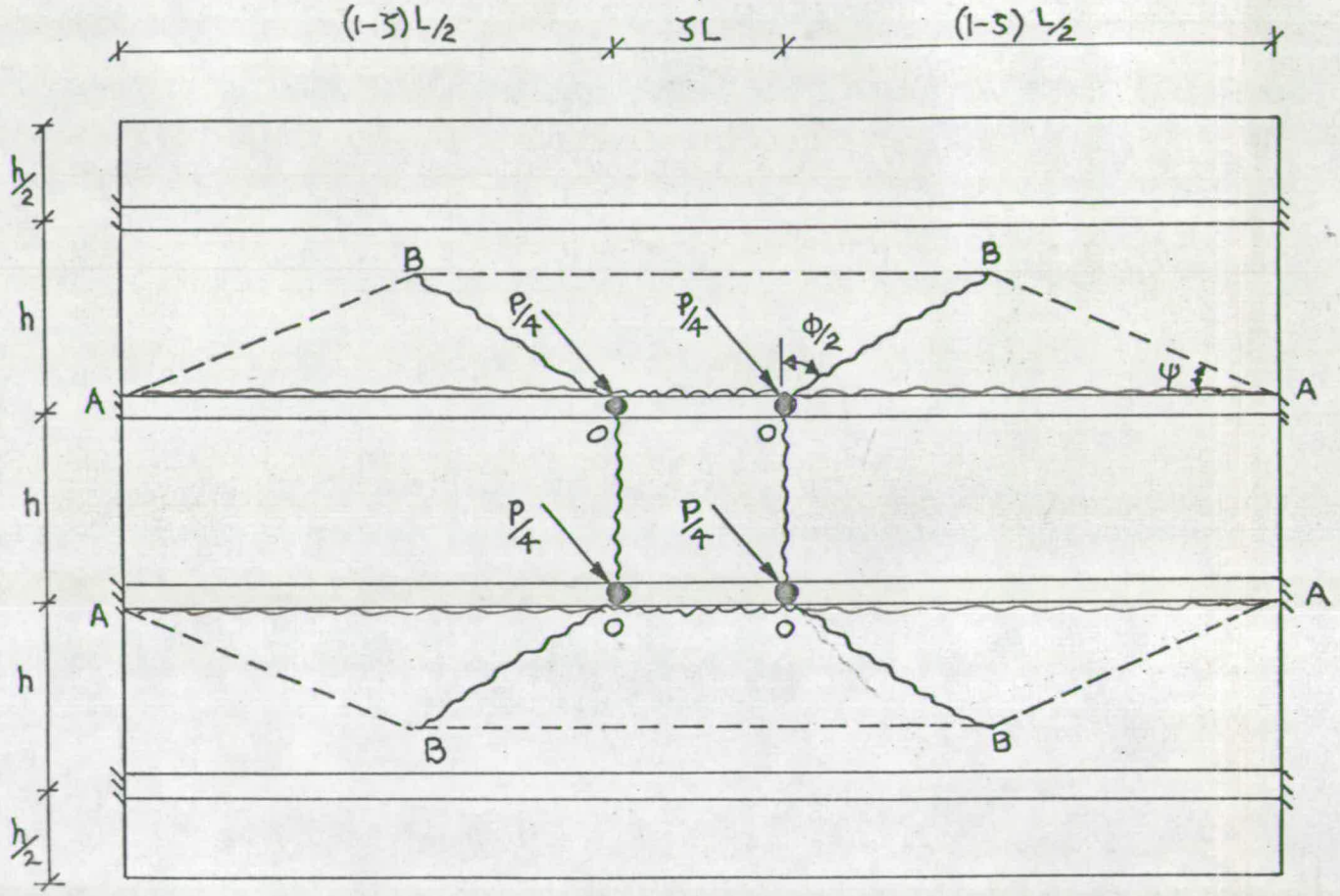

yield line	moment
OB	m
OO	μm
BB	i₁m, i₁μ'm
AB	i₂m, i₂μm

● Hinge in beam

FIG. 4.31 MODE B

From Equation (4.39) and Equation (4.40), replacing μ_i by μ,

$$\tan \phi/2 = \frac{\sqrt{\mu}}{\sqrt{4(1-\zeta)^3 - 1}} \quad \ldots\ldots\ldots\ldots\ldots\ldots \quad (4.68)$$

$$\lambda = \frac{\sqrt{4(1-\zeta)^3 - 1}}{4(1-\zeta)\sqrt{\mu_s}} \quad \ldots\ldots\ldots\ldots\ldots\ldots \quad (4.69)$$

where $0 \leq \lambda \leq \rho$

when $\lambda \geq \rho$, $\lambda = \rho$.

From Equation (4.40a) substituting $\lambda = \rho$,

$$\tan \phi/2 = \frac{1}{4\rho(1-\zeta)} \quad \ldots\ldots\ldots\ldots\ldots\ldots \quad (4.70)$$

Using the above values of λ and $\tan \phi/2$, it can be shown that,

$$P_B = \frac{8M_c}{(1-\zeta)L} + 2\left[\frac{4\mu\rho}{(1-\zeta)} + \frac{1}{\rho} - \frac{1}{2\rho(1-\zeta)} + \frac{1}{4\rho(1-\zeta)^3}\right] m \quad \ldots\ldots$$

$$\ldots\ldots\ldots \quad (4.71)$$

4.4.4 Four longitudinal composite Beam with eccentric loading (Fig. 4.19)

The assumptions are the same as those made in section 4.3.4.

Mode A (Fig. 4.32)

$$P_A = \frac{16M_c}{(1-\zeta)L} + \frac{16\mu m(h-B_e)}{(1-\zeta)L} \quad \ldots\ldots\ldots\ldots\ldots\ldots \quad (4.72)$$

or $$P_A = \frac{16\mu_e m}{(1-\zeta)L} \quad \ldots\ldots\ldots\ldots\ldots\ldots \quad (4.72a)$$

Mode B (Fig. 4.33)

This mode is similar to Mode B shown in Fig. 4.29 except that there is

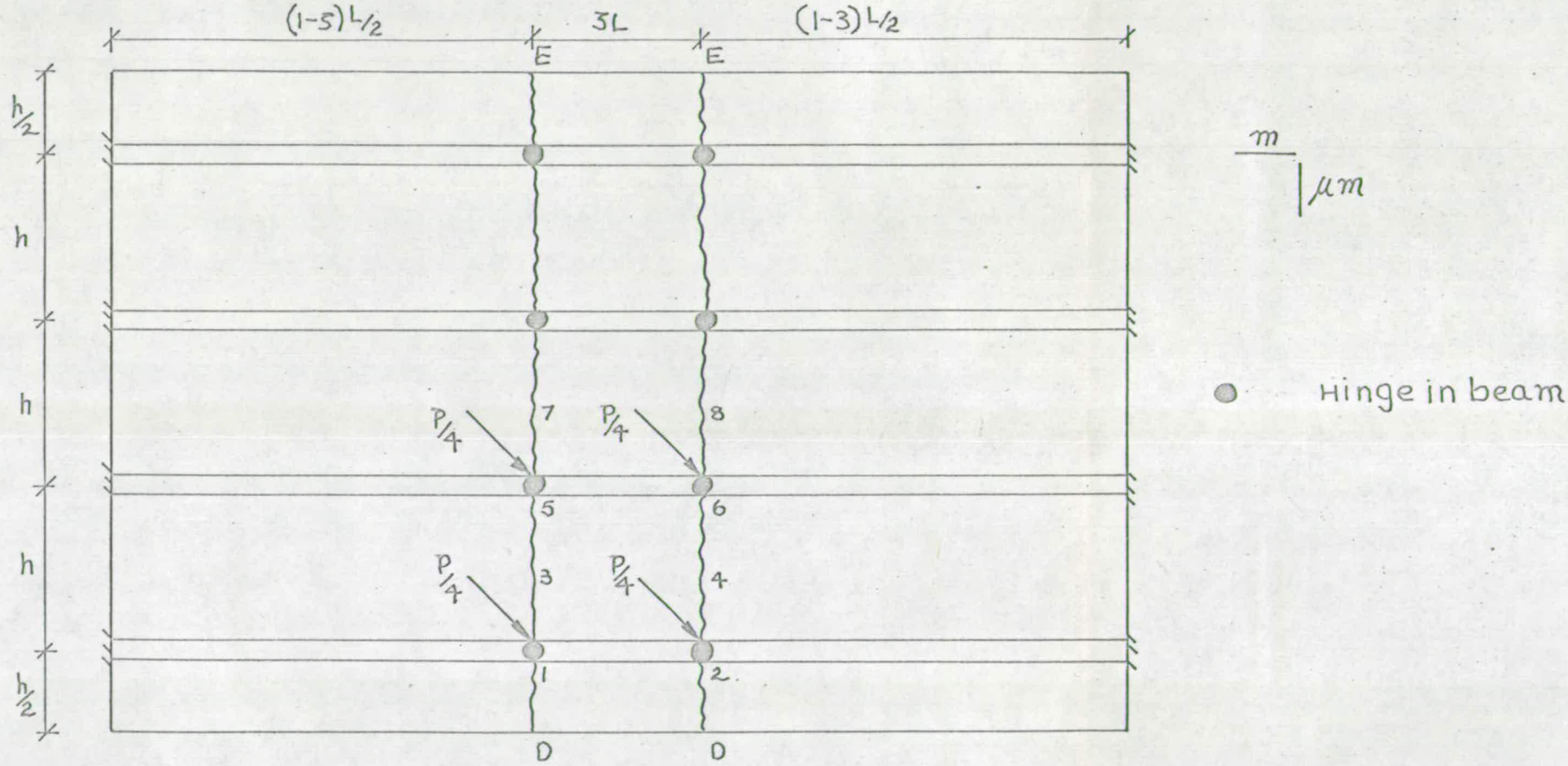

FIG. 4.32 MODE A

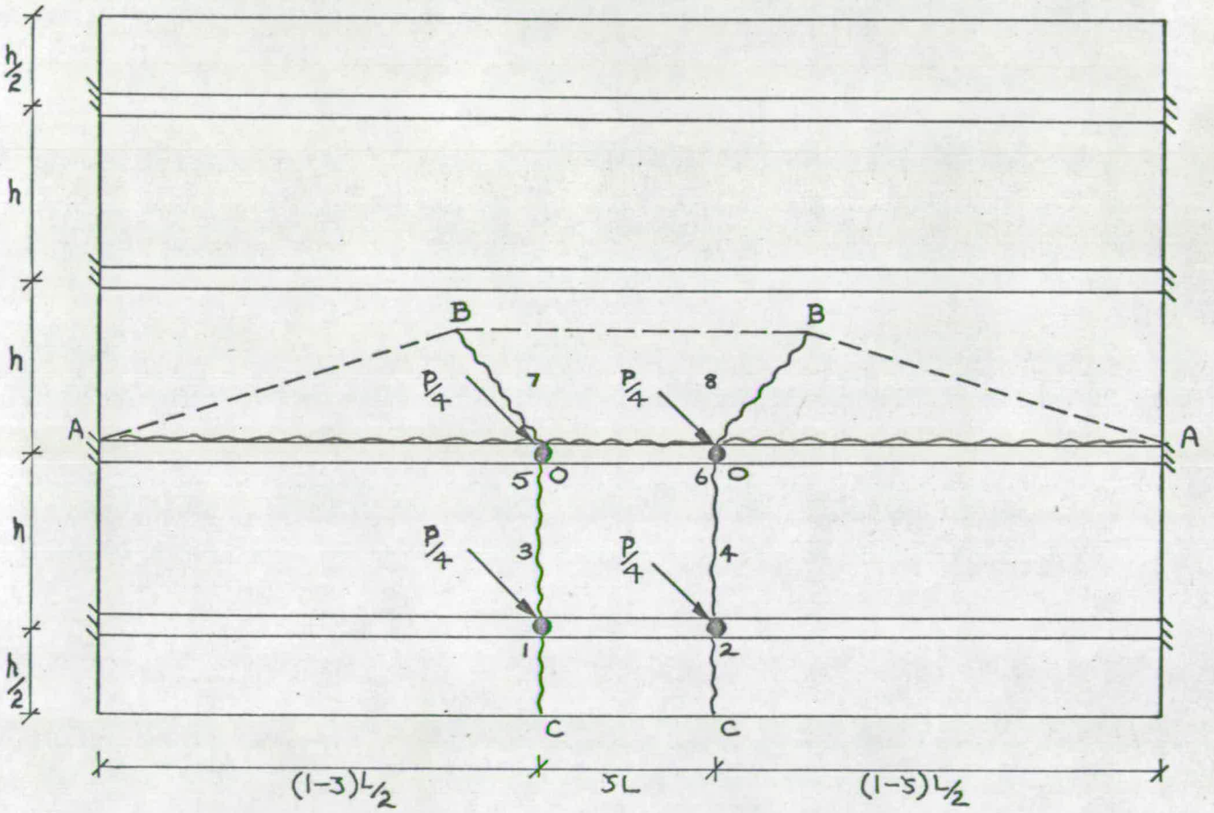

yield line	moment
OB	m
OC	μm
BB	$i_1 m$ / $i_1 \mu' m$
AB	$i_2 m$ / $i_2 \mu m$

● Hinge in beam

FIG. 4·33 MODE B

no moment developed along the yield lines BB and the length of yield line OC now equals $\frac{3h}{2}$ and there are additional positive yield lines AO.

Substituting $i_1 = 0$ and multiplying the first term of Equation (4.63) by 2,

$$P_B = \frac{8M_c}{(1-\beta)L} + \frac{2\sqrt{\mu_s}\,(3-4\beta)}{\sqrt{4(1-\beta)^3-1}} \qquad \ldots\ldots\ldots\ldots\ldots \quad (4.73)$$

From Equation (4.61) and Equation (4.62),

$$\tan \phi/2 = \frac{\sqrt{\mu_s}\,(1-\beta)\,i_2}{\sqrt{4(1-\beta)^3-1}} \qquad \ldots\ldots\ldots\ldots\ldots\ldots \quad (4.74)$$

$$\lambda = \frac{\sqrt{4(1-\beta)^3-1}}{4(1-\beta)\sqrt{\mu_s}} \qquad \ldots\ldots\ldots\ldots\ldots\ldots \quad (4.75)$$

where $0 \leq \lambda \leq \rho$

when $\lambda > \rho$, $\lambda = \rho$.

From Equation (4.40a)

$$\tan \phi/2 = \frac{1}{4\rho(1-\beta)} \qquad \ldots\ldots\ldots\ldots\ldots\ldots \quad (4.76)$$

Using the above values of λ and $\tan \phi/2$, it can be shown that,

$$P_B = \frac{8M_c}{(1-\beta)L} + \left[\frac{4\mu\rho}{(1-\beta)} + \frac{1}{\rho} - \frac{1}{2\rho(1-\beta)} + \frac{1}{4\rho(1-\beta)^3}\right] m$$

$\ldots\ldots\ldots$ (4.77)

4.4.5 Four longitudinal Composite Beam with point loads simulating HB vehicle (Fig. 4.23)

The assumptions and conditions are the same as described in section 4.3.5.

Mode A (Fig. 4.32 with additional point loads at points 3, 4, 7 and 8).

$$P_A = \frac{16M_c}{(1-\zeta)L} + \frac{16\mu m\,(h-B_e)}{(1-\zeta)L} \qquad \ldots\ldots\ldots\ldots\ldots\ldots \quad (4.78)$$

$$\text{or} \quad P_A = \frac{16\mu_e m}{(1-\zeta)} \qquad \ldots\ldots\ldots\ldots\ldots\ldots\ldots\ldots \quad (4.78a)$$

Mode B (Fig. 4.33 with additional point loads at points 3, 4, 7 and 8)

In this case, the displacement under the loads 7 and 8 is not unity and is equal to δ_1.

For unit displacement along the yield lines CO, the total collapse load is given by

$$P_B = \frac{4}{(\delta_1 + 3)}\left[\frac{8M_c}{(1-\zeta)L} + \frac{2\sqrt{\mu}\,(3-4\zeta)m}{\sqrt{4(1-\zeta)^3-1}}\right] \qquad \ldots\ldots\ldots \quad (4.79)$$

when $0 \leq \lambda \leq \rho$, the values of $\tan \phi/2$ and λ are calculated from the equations (4.74) and (4.75) respectively.

when $\lambda > \rho$, $\lambda = \rho$ and $\tan \phi/2$ is given by Equation (4.76).

$$P_B = \frac{4}{(\delta_1+3)}\left\{\frac{8M_c}{(1-\zeta)L} + \left[\frac{1}{\rho} - \frac{1}{2\rho(1-\zeta)} + \frac{1}{4\rho(1-\zeta)^3}\right]m\right\} \qquad \ldots\ldots\ldots\ldots \quad (4.80).$$

CHAPTER 5

TEST PROGRAMME

5.1 Object of tests

Any new application of simplified yield-line theory has to be supported by experiment. Because of the complexity of a composite beam bridge structure, the applicability of the analysis can be determined only by comparing the behaviour of actual structure with that predicted by the analysis. The object of tests in this investigation was twofold (i) to determine the ultimate capacity of the bridges and their manner of failure and (ii) to provide further information on the behaviour of the composite beam and the slab which constituted the bridge.

5.2 Outline of Test Programme

Laboratory tests were made on eight composite beam bridges. All of them were small-scale models of simple span right bridges. The variable in each group of the tests was only the type of loading which consisted of concentrated loads. Preceding the test on each model were Control Tests.

The tests were divided into two groups designated here as A-series and B- series. The specimens of A-series had a span of 72" and a slab width of 36". In the specimens of B-series, the span was kept the same but the slab width was 48". The loading for each model was as described below:

5.2.1 A-series with three longitudinals

Model A I and Model A II : single point load at mid span of inner beam (Fig. 4.5).

Model A III : A pair of point loads on outer beam (Fig. 4.10)

Model A IV : A pair of point loads on inner beam (Fig. 6.15c)

5.2.2 B-series with four longitudinals

Model B I : Four pairs of eccentric point loads simulating the wheel loads of HB vehicle (Fig. 4.23)

Model B II : Two pairs of eccentric point loads on beams (Fig. 4.19)

Model B III : Two pairs of central point loads on beams (Fig. 4.14)

Model B IV : A pair of point loads on inner beam (Fig. 4.30)

5.2.3 Control Tests

Along with each model a single composite beam which was identical in properties and six strips of slab, three representing the slab in transverse direction and three in longitudinal direction, were also cast. Also three 4" cubes and three 6" cubes were cast.

The Control Beams were tested under similar loading as the model. The slab strips were tested under central point loading.

5.3 Definition of terms

The transverse reinforcement of the slab is in the direction perpendicular to the beams.

The longitudinal reinforcement of the slab is in the direction parallel to the beams.

The value of $^{h}/_{L}$ expresses the ratio of the transverse spacing of the beams, h, to the span of the bridge, L.

A shear connector is a device which acts to transfer horizontal shear across the plane between the beam and the slab. In these tests, the shear connectors consisted of headed studs welded to the top flange of the beam.

Composite action is the interaction between the beam and slab. In the models tested, complete composite action was assumed to exist upto failure.

5.4 Design criteria for test speciemens

The models were designed with the object of keeping their size within practical limits and the cost minimum. The smallest structural steel sections available namely 3" x $1\frac{1}{2}$" x 4 lbs I-sections were used for the longitudinals.

5.4.1 Spacing of beams

The ratio of transverse spacing of beams to span was chosen to be one-sixth of the span for the following reasons:

(i) to keep it close enough to the usual value adopted in bridge design, and (ii) to minimise the effect of shear lag (63) so that the effective compressive flange width provided by the slab would be nearly equal to the actual width available.

5.4.2 Thickness of slab and reinforcement

The main consideration in deciding the thickness of the slab is to see that the maximum efficiency of the deck is achieved. The slab performs the dual function of distributing the loads transversely and acting as the compression flange of the beam. In the former function it should be made as stiff as possible but in the latter function its thickness has to be proportioned to suit the dimensions of the beam.

The yield-line pattern and the collapse load of a bridge deck are largely influenced by the ratio of ultimate moments in longitudinal and transverse directions. By choosing a critical ratio of these moments, a desired mode of failure for given geometry and loading can be obtained.

For a chosen value of $^{h}/_{L}$, the graphs shown in Figs. 4.9, 4.13, 4.18 and 4.22 can be used to obtain the optimum ratio of $\sqrt{\mu_i}/\mu_e$ based on the Equivalent slab Method, from which a suitable value of m for any

given value of M_c can be adopted. Similarly the Beam and slab Method, can be used to obtain the above values, if the latter method is chosen for the analysis,

5.4.3 Shear Connectors

The spacing of shear connectors worked out to be 2·6" centre to centre as per C.P.117, part1(73). But a spacing of 2" was adopted to prevent fouling with the spacing of welded mesh reinforcement of slab. The ultimate capacity of one shear connector was determined from push-out tests. A typical push-out Test Arrangement is shown in Fig. 5.1. The results of the test and the load-slip curve are given in Table 5.1 and Fig. 5.2 respectively. Assuming that steel section is fully plastic at maximum moment, the number of shear connectors is computed from the formula

$$N_c = \frac{T}{Q_c} \qquad \ldots\ldots\ldots\ldots\ldots\ldots\ldots\ldots\ldots \quad (5.1)$$

where N_c = Number of shear connectors between the points of maximum and zero moments,

$T = A_s f_y$ = Tensile force in steel section,

Q_c = Design value of one shear connector which is taken as 80 per cent of its ultimate capacity in push-out test.

5.5 Description of Models

The test speciemens may be considered as one-sixth models of short span composite beam bridges. All the beams were equally spaced. The models were not scaled down from full-sized bridges but were themselves designed. The design details are given in Table 5.2 and the typical sections are shown in Fig. 5.3.

5.6 Materials

The physical properties of the steel used in the beams were obtainedfrom

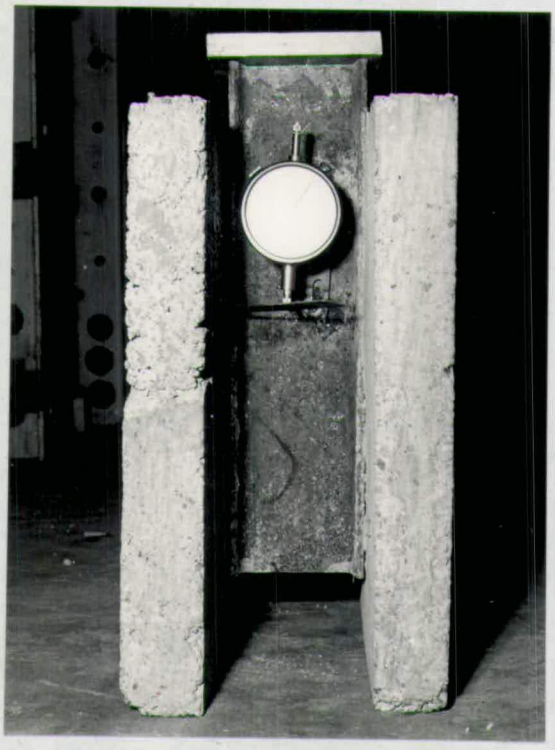

Fig.5.1 View of Push-out Test Arrangement

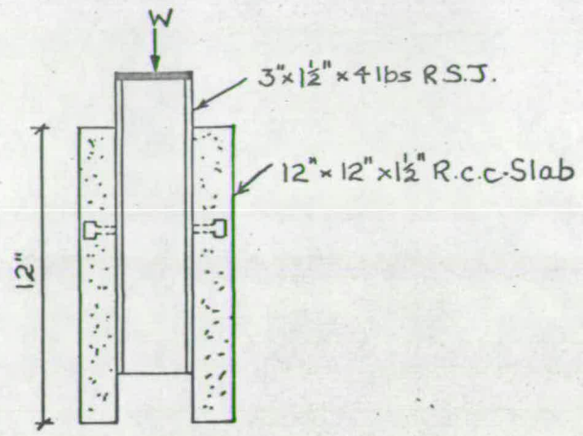

PUSH-OUT TEST
Specimen

AVERAGE FAILURE LOAD = 2·05 TONS

A TYPICAL
FIG. 5·2 LOAD-SLIP CURVE FROM PUSH-OUT TEST

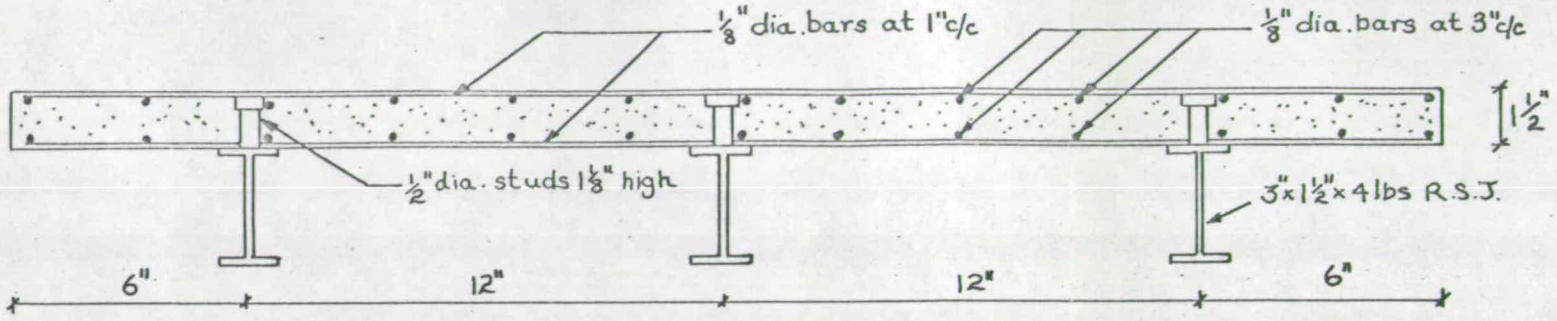

(a) TRANSVERSE SECTION
A-SERIES
SPAN=72"

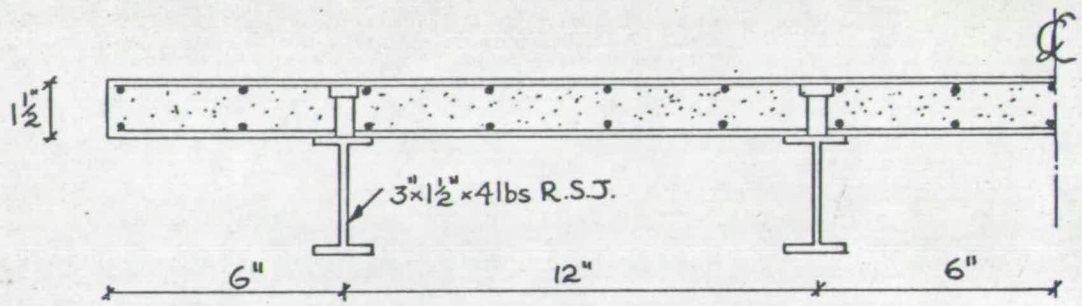

(b) HALF TRANSVERSE SECTION
B-SERIES
SPAN=72"

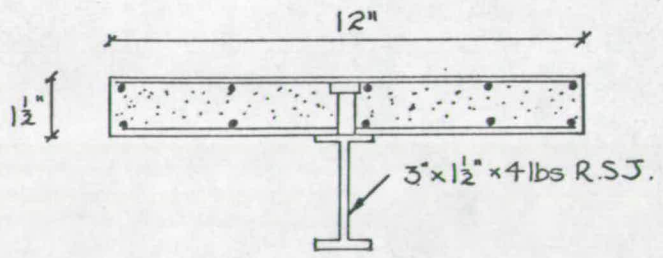

(c) TRANVERSE SECTION
OF
CONTROL BEAM
span=72"

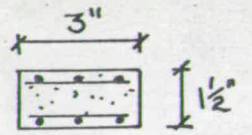

(d) Cross Section of
Slab strip S1 (3"x1½"x14")
span=12"

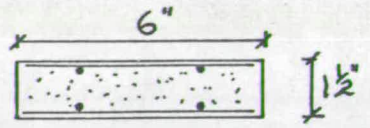

(e) Cross Section of
slab strip S2 (6"x1½"x14")
span=12"

NOTE: The reinforcement and shear connection are the same in all models

FIG. 5.3 SECTIONS OF MODELS

tension tests on coupons $^{3}/_{8}$" x $^{3}/_{16}$" in cross section cut from the flanges. The coupons were 8" long and were tested on 2" gauge length using "INSTRON" machine which has built-in Electrical Resistance Gauges to measure the strains. The results are given in Table 5.3 and the typical stress-strain diagrams are shown in Fig. 5.4(a).

Also bending test to destruction were conducted on 3" x $1\frac{1}{2}$" x 4 lbs R.S. joists with two-point loading. The load-strain curves are given in Fig. 5.5.

The slab reinforcement consisted of welded mesh of $\frac{1}{2}$" dia. bars. These bars had a high yield strength and low elongation. The properties obtained from tests are given in Table 5.4. A typical stress-strain diagram is given in Fig. 5.4(b).

The slabs were made from a concrete mix of proportions 1 cement, 2 fine sand and 3 coarse sand by weight with a water-cement ratio of 0.60 by weight. The properties of concrete used in the various specimens are given in Table 5.5.

TABLE 5.1

A typical push-out Test on $\frac{1}{2}$" dia. studs

Load per stud Tons	slip (in. x 10^{-4})
0.25	2.0
0.50	4.5
0.75	7.5
1.00	19.0
1.25	25.0
1.50	57.0
1.75	130.0
2.00	326.0
2.10	550.0

Average failure load = 2.05 tons per stud.

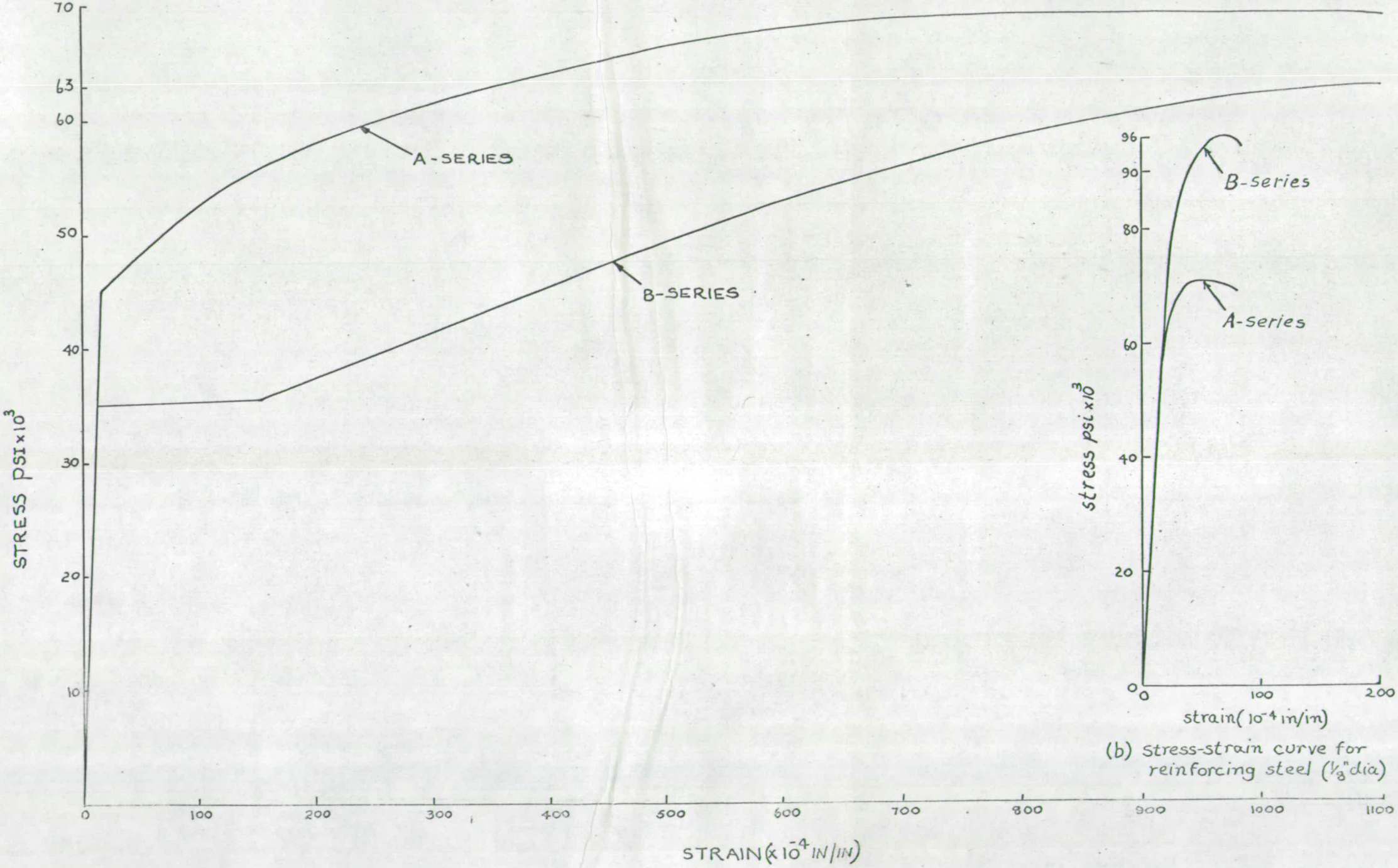

(b) Stress-strain curve for reinforcing steel (⅛" dia)

FIG. 5·4 (a) TYPICAL STRESS-STRAIN CURVES FOR STEEL IN BEAMS

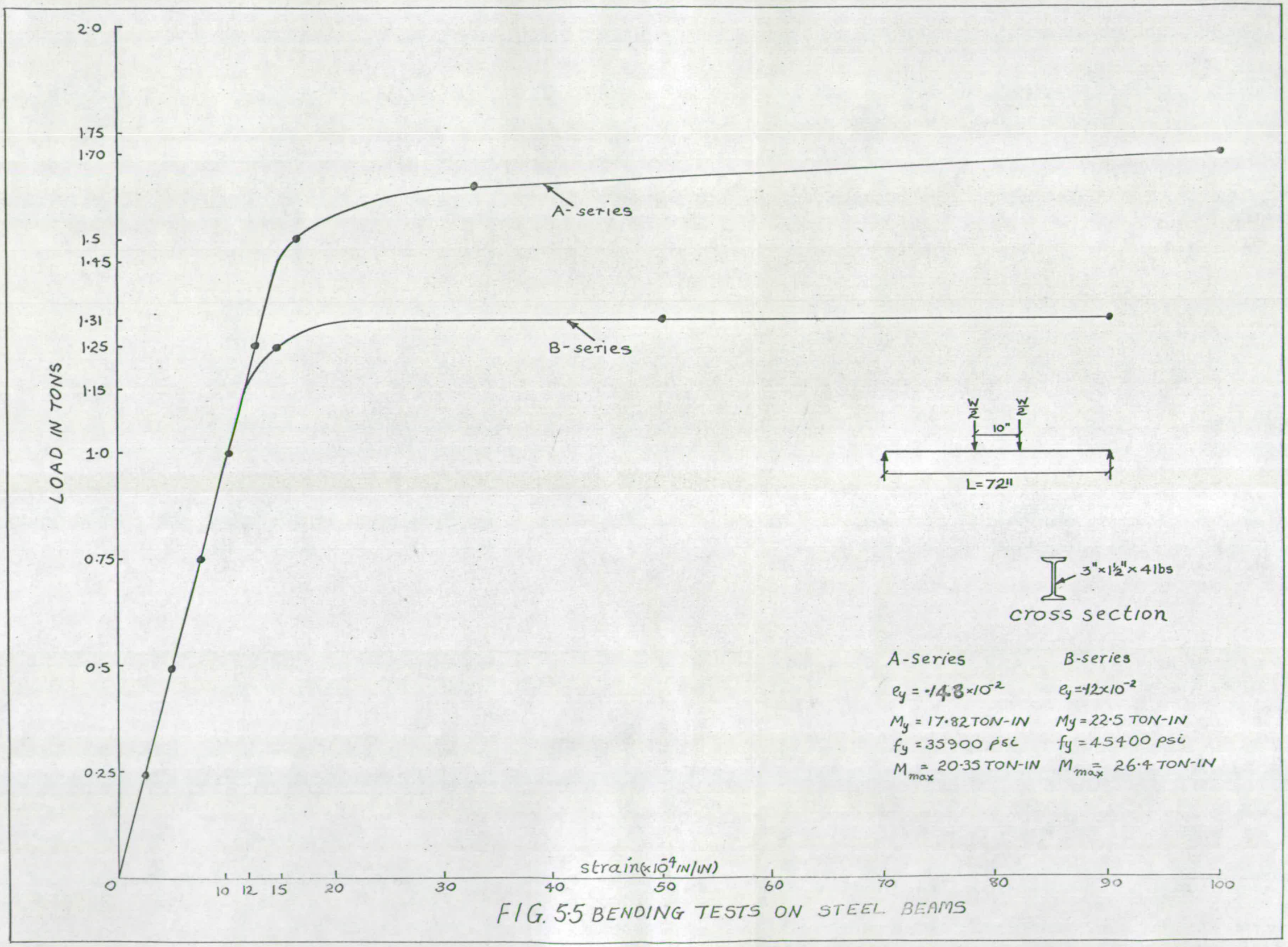

FIG. 5·5 BENDING TESTS ON STEEL BEAMS

TABLE 5.2

Design Details for all Model Bridges

	span, in.		72
	spacing of beams, in.		12
steel joist	size, in.		3 x $1\frac{1}{2}$
	weight, lbs/Ft.		4
	cross sectional area, sq. in.		1.18
	Modulus of section, in^3		1.11
shear connector	Type		Headed stud
	Diameter, in.		$\frac{1}{2}$
	Height, in.		$1\ ^1/8$
	spacing, in.		2
	Total number in span		36
Depth of slab, in.			$1\frac{1}{2}$
slab reinforcement			All bars 1/8" diameter
Transverse	Bottom	spacing, in.	1
		percent	0.94
	Top	spacing, in.	1
		percent	0.94
Longitudinal	Bottom	spacing, in.	3
		percent	0.34
	Top	spacing, in.	3
		percent	0.34

Table 5.3

Physical Properties of steel in beams

series	size of beam	No. of tests	yield point p.s.i. f_y	ultimate strength p.s.i. f_u	percent strain at first yield e_y	percent strain at strain hardening e_s	E p.s.i.	E_{sh} p.s.i.	s	r
A	3" x $1\frac{1}{2}$" x 4 lbs	6	45000	69000	0.15	0.15	30×10^6	1×10^6	30	1
B	3" x $1\frac{1}{2}$" x 4 lbs	6	35000	6[illegible]000	0.118	1.53	29.5×10^6	0.473×10^6	62.5	13

TABLE 5.4

Properties of 1/8" dia. reinforcing bars obtained from Tensile Tests on 2" G.L. specimens

series	No. of tests	yield point p.s.i. (approx.)	ultimate strength p.s.i.
A	3	63000	71000
B	3	65900	95700

TABLE 5.5

Properties of concrete obtained from tests on 4" and 6" cubes

Model	Age at Test days	No. of tests on		Average cube strength p.s.i.
		4" cube	6" cube	
AII	40	3	3	5227
A II	47	3	3	5096
A III	54	3	3	6290
A IV	56	3	3	3280
B I	30	3	3	5130
B II	37	3	3	6270
B III	44	3	3	5600
B IV	44	3	3	5600

5.7 Construction of Test specimens

Plywood forms for the bottom and sides of the slab were constructed around the steel beams after the shear connectors were welded to their upper flanges. The top and bottom layers of reinforcement for the slab of each model were cut to the required size out of a welded mesh of 3" x 1" openings. The two layers were spaced at the proper distance by a number of 1/4" square steel spacer bars containing two notches to receive the reinforcing bars of the two layers. The notches were spaced so as to provide a depth of cover equal to 1/8" between the transverse bars and the surface of the slab. The views of the form work for control beams, models of A-series and B-series with steel joists and reinforcement arranged in them are shown in Fig. 5.6, Fig. 5.7 and Fig. 5.8 respectively. The form work of each model was supported on two rigid supports 72" apart. The concrete was placed in and vibrated. During the operation, the entire weight of the forms and of the slab was carried by the I-beams. The curing of the slab in the forms carried out with wet sacking. The forms were removed after 12 days.

5.8 Loading Apparatus

A preliminary examination of the test programme indicated the need for a loading frame with an arrangement to vary the position of the point of application of the load. With this object in view, the frame shown in Fig. 5.9 was built for a capacity of 20 tons. The frame consisted of three portals placed parallel to each other at 3'-0" intervals and bolted down to the strong floor by 1½" dia. bolts. Each portal was made up of 12" x 4" channels bolted together by 7/8" dia. bolts and braced by 4" x 4" angles. The models were supported on end portals which were 6'-0" apart and 5'-0" high to permit access

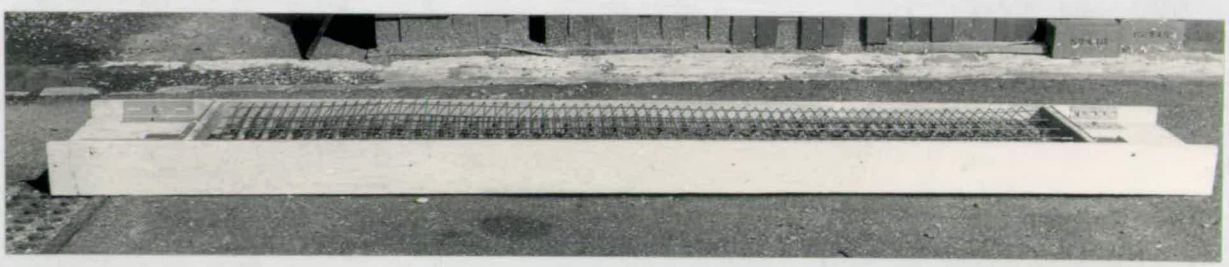

FIG.5.6 Form work for a Control Beam

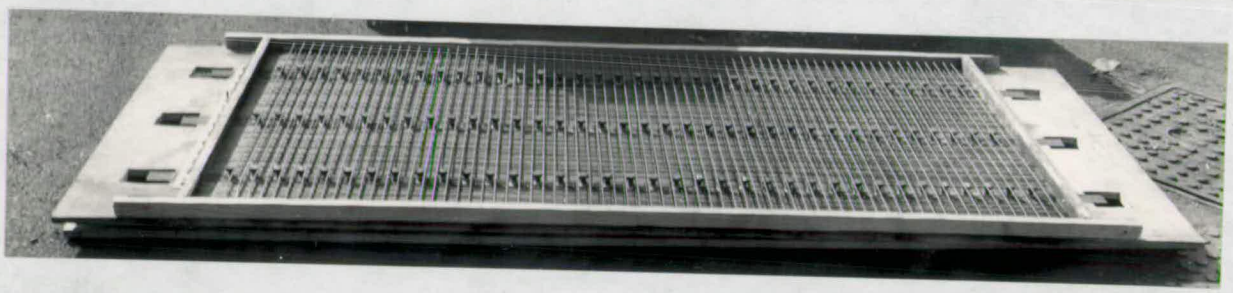

FIG.5.7 Form work for a 3-Longitudinal Bridge

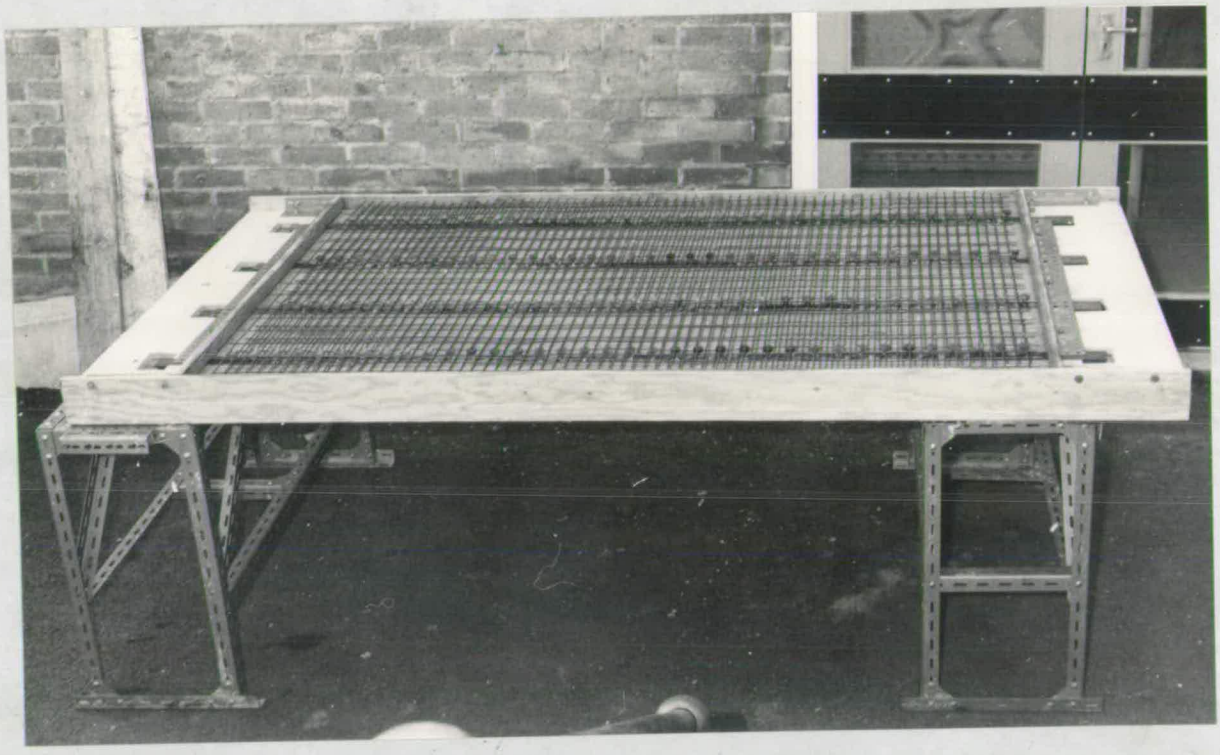

FIG.5.8 Form work for a 4-Longitudinal Bridge

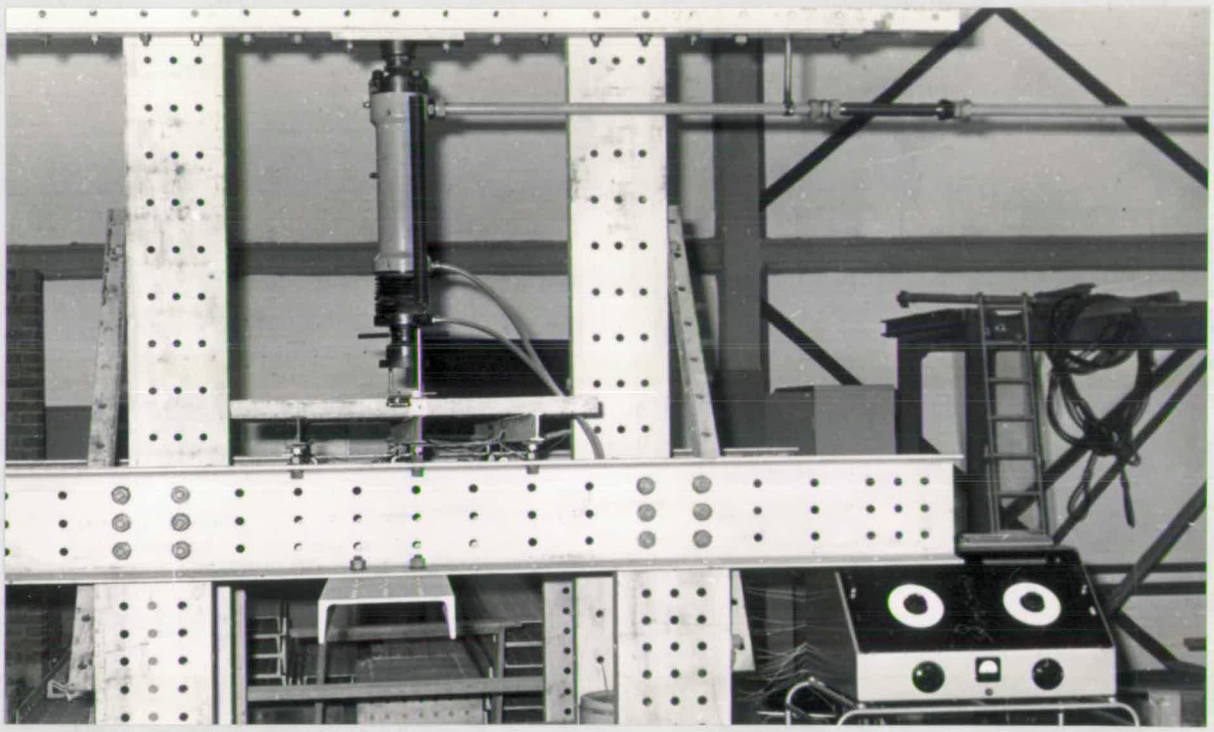

FIG.5.9 View of Loading Frame
with Model AI ready for test

to the underside for strain measurements and for observing the development of crack patterns. The horizontal channel of the central portal, which was at 9'-0" height and which provided the reaction to the loading jack (of Losenhausenwerk) was strengthened by another channel of the same dimensions bolted to it. The jack could be moved and fixed along the channel at 6" intervals. The jack was connected to the Losenhausenwerk Testing Machine with a maximum loading capacity of 20 tons.

Point loading was applied by the jack through mild steel distribution plates 4" x 4" x $\frac{1}{2}$" size on model A I and A II and 4" x 3" x $\frac{1}{2}$" on other models. They were bedded on rubber pads. When more than one load was applied simultaneously a distributing beam was used to transmit the load from the jack to the other loading plates. The bearings were designed to satisfy the requirement that the models should be freely supported. The beams were supported on steel rollers at one end and on hexagonal bars at the other. The experiments were limited to short-term loading tests with concentrated loads.

The control beams and slab strips were tested on Avery Testing Machine of 50 tons capacity in bending tests and of 100 tons capacity in tension and comparison tests (Fig. 5.10). The concrete cubes were tested on Denison Machine of 250 tons capacity.

5.9 Strain Measurements and Equipment

The strains were measured across the depth of the composite beams at mid span and quarter span using $\frac{1}{2}$" gauge length Sanders Roe Foil type Electrical Resistance Gauges and 10 mm. gauge length Y.L.10 type Japanese made Resistance Gauges, both of 120 ohms resistance. The latter gauges were capable of recording strain in steel up to 7 per cent well into the stage of strain-hardening, which was found in some of the steel beams. The usual

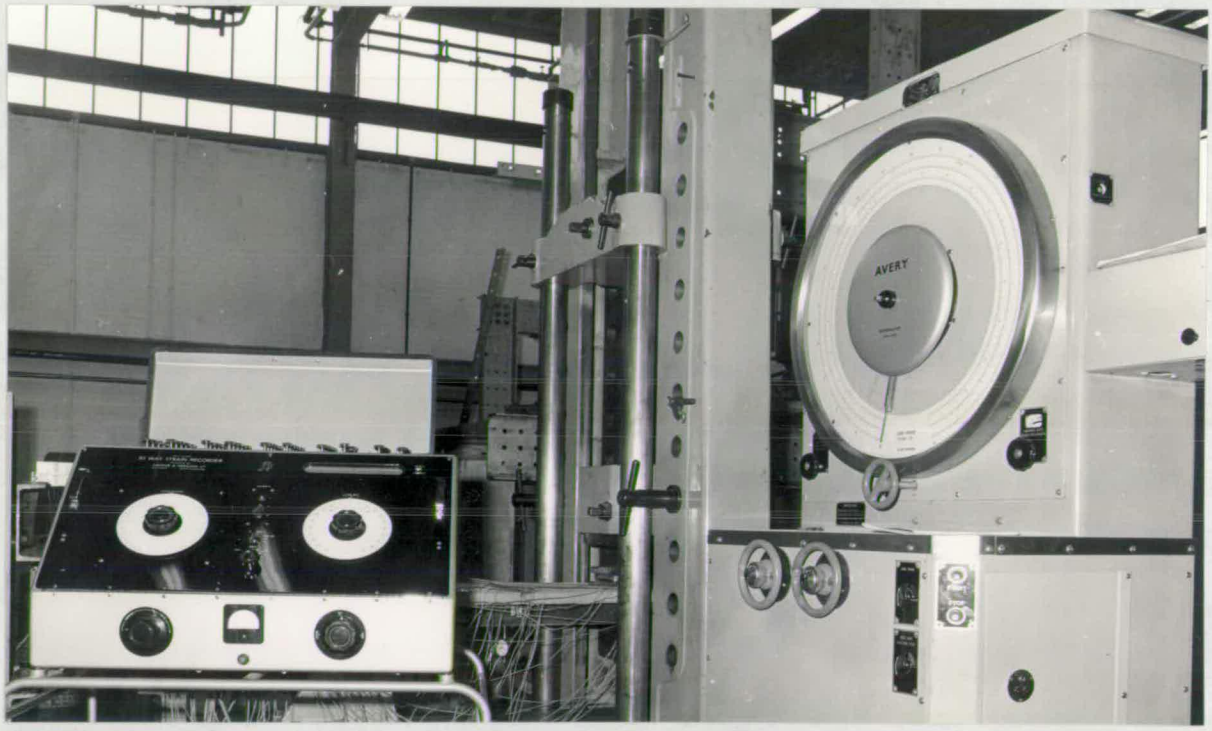

FIG.5.10 View of Savage&Parsons Ltd
50-way strain Recorder and
Avery Testing Machine

procedure for sticking the strain gauges was followed. In polishing the metal surfaces, care was taken to keep the amount of material removed to a minimum. Araldite was used to stick the Sanders Roe Gauges and C.N. Adhesive for Y.L.10 gauges.

The strain measurements on concrete surface at mid span and quarter span were carried out with 20 mm. gauge length PC-20 Japanese made Resistance Gauges. The P.S. Adhesive was first coated on the concrete surface to obtain a level surface. After it has set, P-2 Adhesive was used to stick these gauges.

The strains in some of the tests were recorded by "Savage and Parsons" 50-way strain Recorder (Fig. 5.10) and in some by "Data Logger" (Fig. 5.11). The working of Savage and Parsons Recorder (89) is as follows:

The active and dummy Resistance Gauges are connected in a Multiple Strain Gauge Bridge Circuit with a gauge selector switch as shown in Fig. 5.12. The Bridge is initially balanced by using the potentiameter known as Apex Resistance since it is impossible to manufacture strain gauge elements to have exactly the same resistance to within, say, 0.001 ohm.

The change in resistance of an active strain gauge caused by its elongation or contraction deflects the Galvanometer. Measurements are obtained by rebalancing the bridge as in ordinary Wheatstone Bridge practice by using the Slider Wire calibrated in terms of strain. The quantity measured is

$$G = n\,100\,\frac{\Delta R}{R} \qquad \ldots\ldots\ldots\ldots\ldots\ldots\ldots\ldots \quad (5.2)$$

and the strain e is related to the change in resistance by the expression

$$e = \frac{1}{K}\,\frac{\Delta R}{R} \qquad \ldots\ldots\ldots\ldots\ldots\ldots\ldots\ldots \quad (5.3)$$

where n = sensitivity Factor which can be given the values 10, 2 and 1, the maximum sensitivity being obtained when n = 10,

ΔR = change in resistance of the strain gauge,

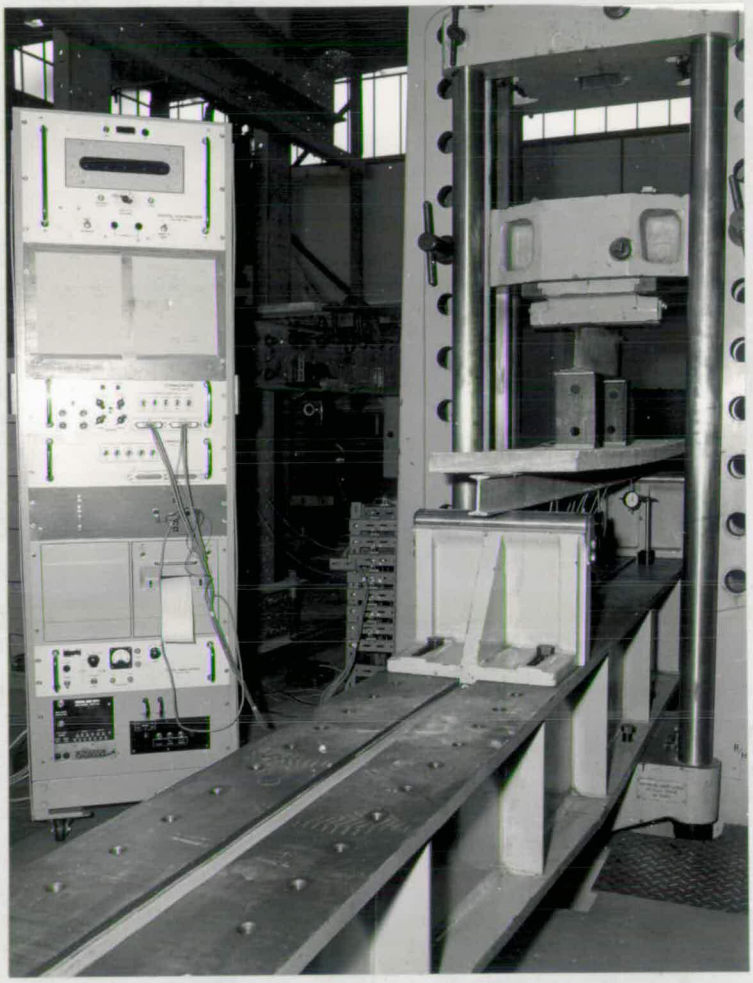

FIG.5.11 View of Data Logger and a Control Beam ready for loading on Avery Testing Machine

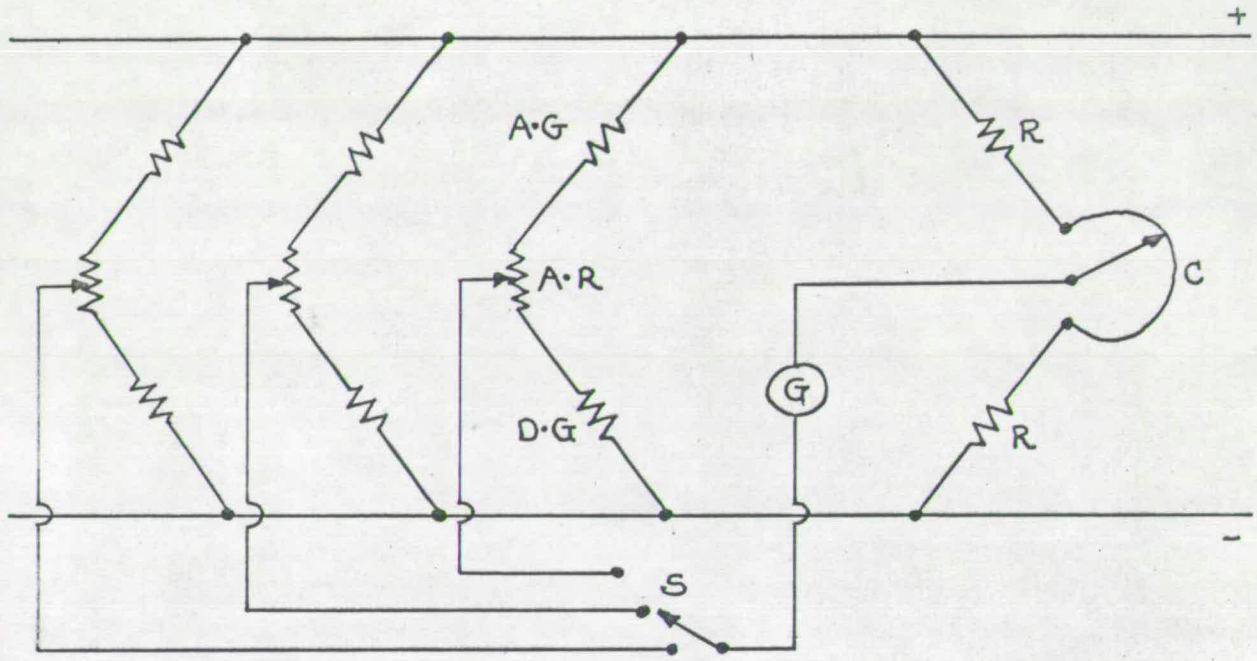

G : Galvanometer
A·R : Apex Resistance
C : Calibrated Slide Wire
A·G : Active Gauge
D·G : Dummy Gauge
S : Selector Switch
R : Built-in Resistance

FIG·5·12 MULTIPLE STRAIN GAUGE BRIDGE CIRCUIT

R = Resistance of the strain gauge,

and K = Gauge Factor.

The measurement of strain with K = 2 can be made to an accuracy of 5×10^{-6}, though it can be increased by interpolation. The principle on which the DataLogger works (90) is different. Instead of change in resistance, change in voltage caused by the change in resistance of an active strain gauge is read or printed out. This equipment provides the quickest means of recording a number of strain readings. The Data Logger that was fabricated in the Laboratory could record the strains from 100 channels at a time. The strain is calculated using the relation

$$e = \frac{4\Delta V}{KUn} \qquad \ldots\ldots\ldots\ldots\ldots\ldots\ldots\ldots\ldots\ldots \quad (5.4)$$

where ΔV = change in voltage

U = Input voltage

n = Sensitivity Factor, which can take a maximum value of 1000.

The measurement of strain to an accuracy of one-third microstrain is possible on this apparatus.

8" and 2" gauge length "Demec" Gauges were also used to measure the concrete surface strain at some points in order to check the reliability of P.C.20 Resistance Gauges.

The deflections at midspan and quarter span of the beams were measured using Baty Dial Gauges reading to 0.001" and 0.0001". These were mounted on magnetic bases for easy adjustment and were supported on a "Dexion" frame, which spanned between the two end portals supporting the model (Fig. 5.13).

The actual locations of strain and deflection measurements are given in each test set-up described later.

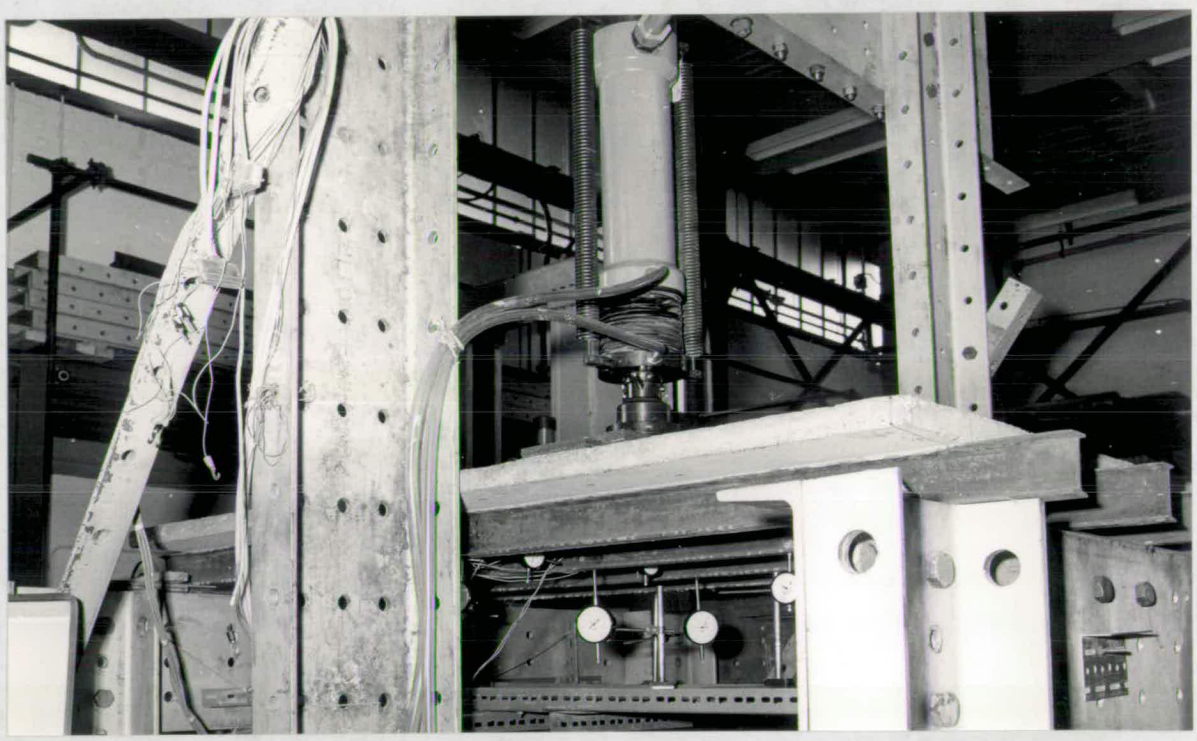

FIG.5.13 View of Loading Frame showing Deflection Dial Gauges

CHAPTER 6

DESCRIPTION OF TESTS

6.1 Test Procedure

The sequence of the testing operation was first to test the control beam, the slab strips and the concrete cubes belonging to each model which was tested last. The results of Control Tests enabled to have an estimate of the ultimate capacity and the deformations at corresponding points of bridge models. The entire testing operation of any one model and its control specimens was completed in two days.

6.2 Tests on Control Beams

Each Control Beam with its cross section as shown in Fig. 5.3(c) was tested by Avery Testing Machine on a span of 72". A typical test set-up is shown in Fig. 5.11. The usual procedure was to apply the load in increments of 0.5 tons and to measure the strains and deflections for each increment of load until the ultimate load was reached. A compression failure on the top of the slab at mid span or between the load points occurred in all the beams. There were no signs of longitudinal tension cracks on top of the slab. Some of the Control Beams were cut into two halves and each half was tested under a central load on a reduced span of 30". Longitudinal tension cracks were observed on the top of the slab before a compression crack formed across the width under the load when it finally collapsed (Fig. 3.2).

The test results and curves of each control beam are presented with the of the corresponding Bridge Model.

6.3 Tests on slab strips

The slab strips s_1 and s_2 with their cross sections as shown in Fig. 5.3(d) and 5.3(e) respectively were tested under a central point load on a span of 12".

A typical slab strip s_1 after failure is shown in Fig. 6.1(a). A typical Load-Deflection curve is given in Fig. 6.1 (b). The ultimate moments per unit width obtained from the tests are presented in Table 6.1.

TABLE 6.1

Ultimate moments obtained from tests on slab strips s_1 and s_2

Model	Average moment per unit width, Ton.in.	
	m	$\mu m = \mu' m$
A I	0.57	0.33
A II	0.58	0.31
A III	0.64	0.32
A IV	0.45	0.24
B I	0.58	0.315
B II	0.63	0.35
B III	0.63	0.35

6.4 Tests on Model Bridges

Each model bridge was placed on the loading frame and centered so that the hydraulic jack could apply the load where required. The jack was connected to the Losenhausenwerk Testing Machine which could be operated to apply the load gradually and hold it where necessary. A test set-up of Model A I is shown in Fig. 5.9. The range of loading was decided after computing the ultimate load by yield-line theory using the theoretical as well as experimental ultimate moments of Slab and Beam elements. To overcome any initial effects due to bedding of packing plates etc., a load approximately equal to $^2/_3$ of the

Fig.6.1a Slab strip S_1 after failure

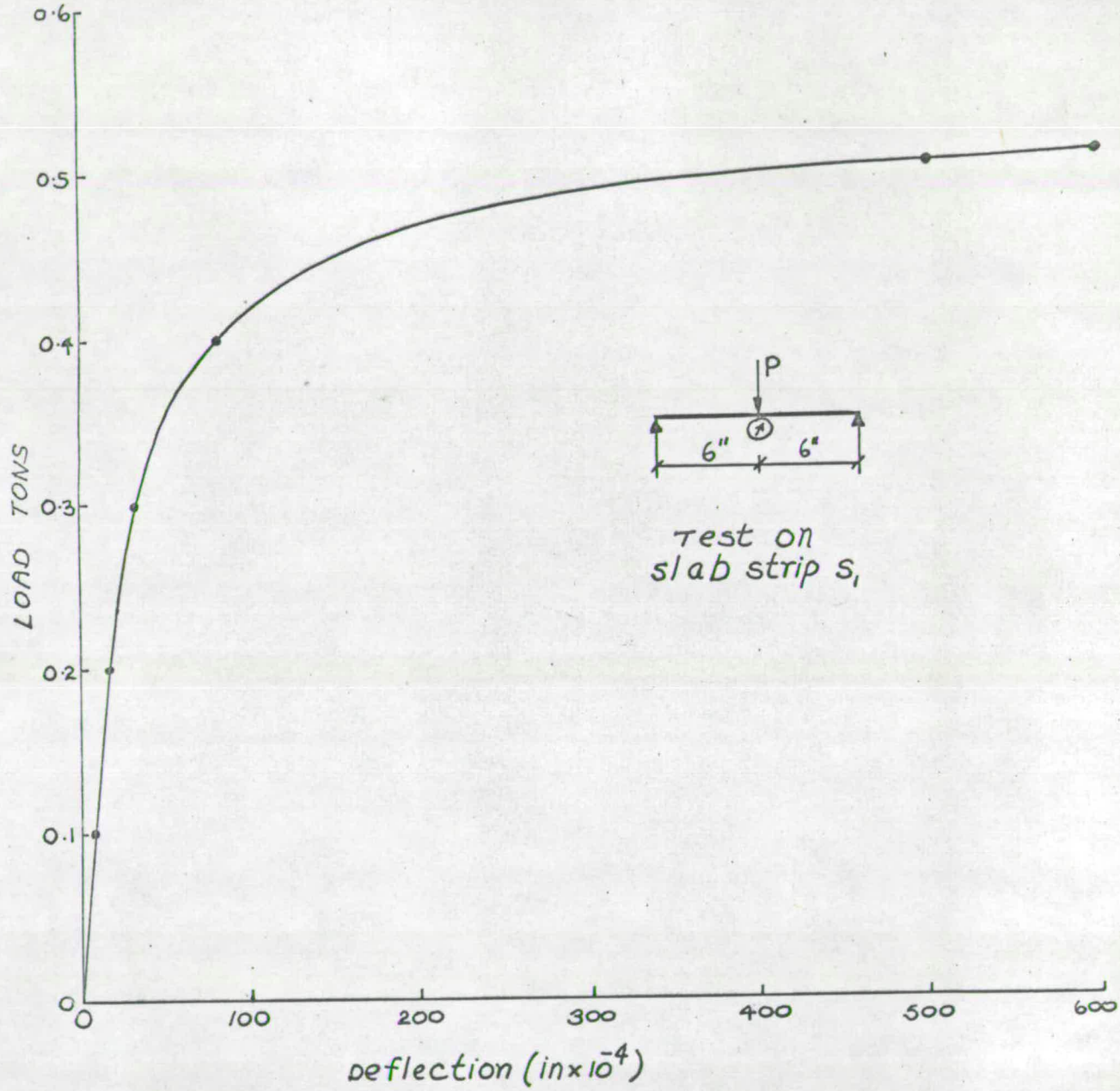

A typical Load-deflection curve for slab strip of Model AII

FIG. 6·1 (b)

load that would cause first yield was applied and removed thrice.

6.4.1 Model A I

Load position : Fig. 6.3(a)

cross section : Fig. 5.3(a)

Control Beam AICB : Moment-Deflection curve Fig. 6.1(c)

Moment-strain curve Fig. 6.2

View after failure Fig. 3.3

Load-Deflection curve : Fig. 6.3(b)

Load-Strain curve : Fig. 6.4(a)

Strain Distribution : Fig. 6.4(b) and 6.2(b)

Crack patterns : Fig. 6.10(a) & 6.10(b)
(same as model A II)

A point load was applied at mid span on the central beam. Yielding of the loaded I-beam occurred in the lower flange at mid span at a load of about 4.8 tons. The deflection had strated to increase non-linearly after this load. There were tension cracks at the bottom of the slab parallel to and at about 4" from the centre line of the loaded beam on either side at mid span. As the load was increased, these cracks became wider and deeper and spread towards the ends gradually taking a turn towards the ends of outer beams.

At 8 tons, the yielding had penetrated to about $^{3}/_{4}$ of the depth of the steel section of the loaded beam while strain-hardening was taking place in its lower flange. The tension cracks at the bottom of the slab formed closer to the loaded beam. Its curvature at mid span began increasing at a much faster rate than that of the slab indicating their imminent separation.

Yielding had commenced in the bottom flanges of outer beams at mid span and their deflections there had begun to show slight non-linearity. They had

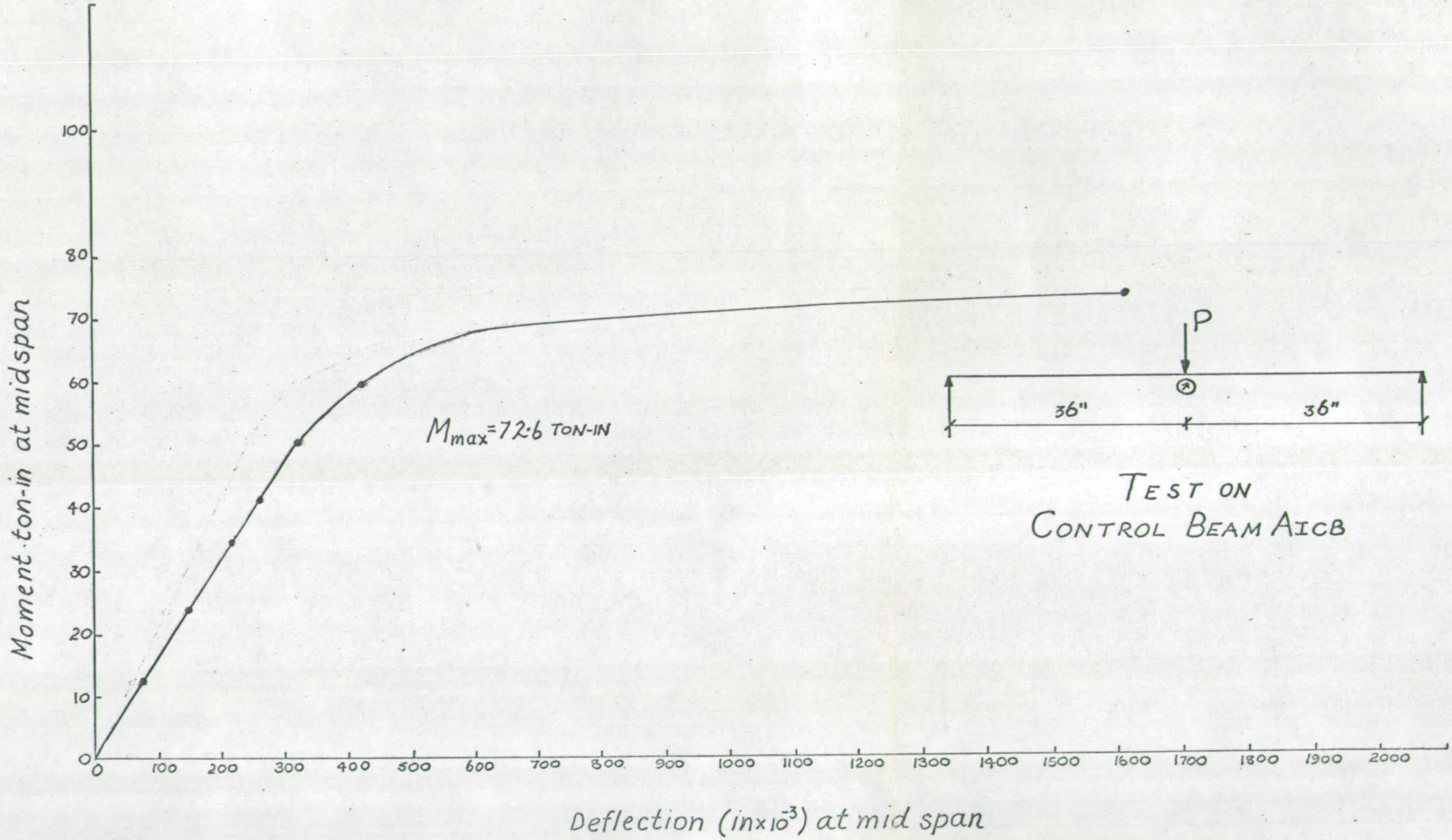
Moment-ton-in at midspan
0
10
20
30
40
50
60
70
80
100
0
100
200
300
400
500
600
700
800
900
1000
1100
1200
1300
1400
1500
1600
1700
1800
1900
2000
Deflection (in×10⁻³) at mid span
M_{max}=72.6 TON-IN
P
36"
36"
TEST ON
CONTROL BEAM AICB

FIG. 6·1(c)

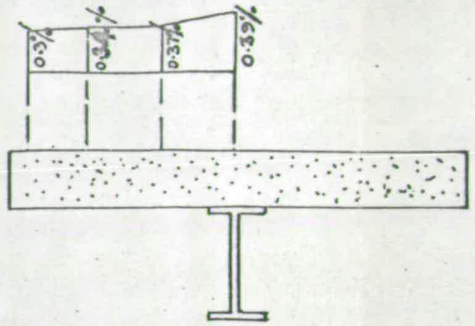

(b) compressive strain distribution across width

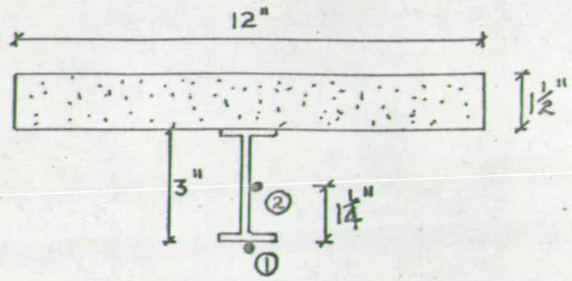

• Location of "DEMEC" gauge points (8" gauge length) at mid span of CONTROL BEAM AICB

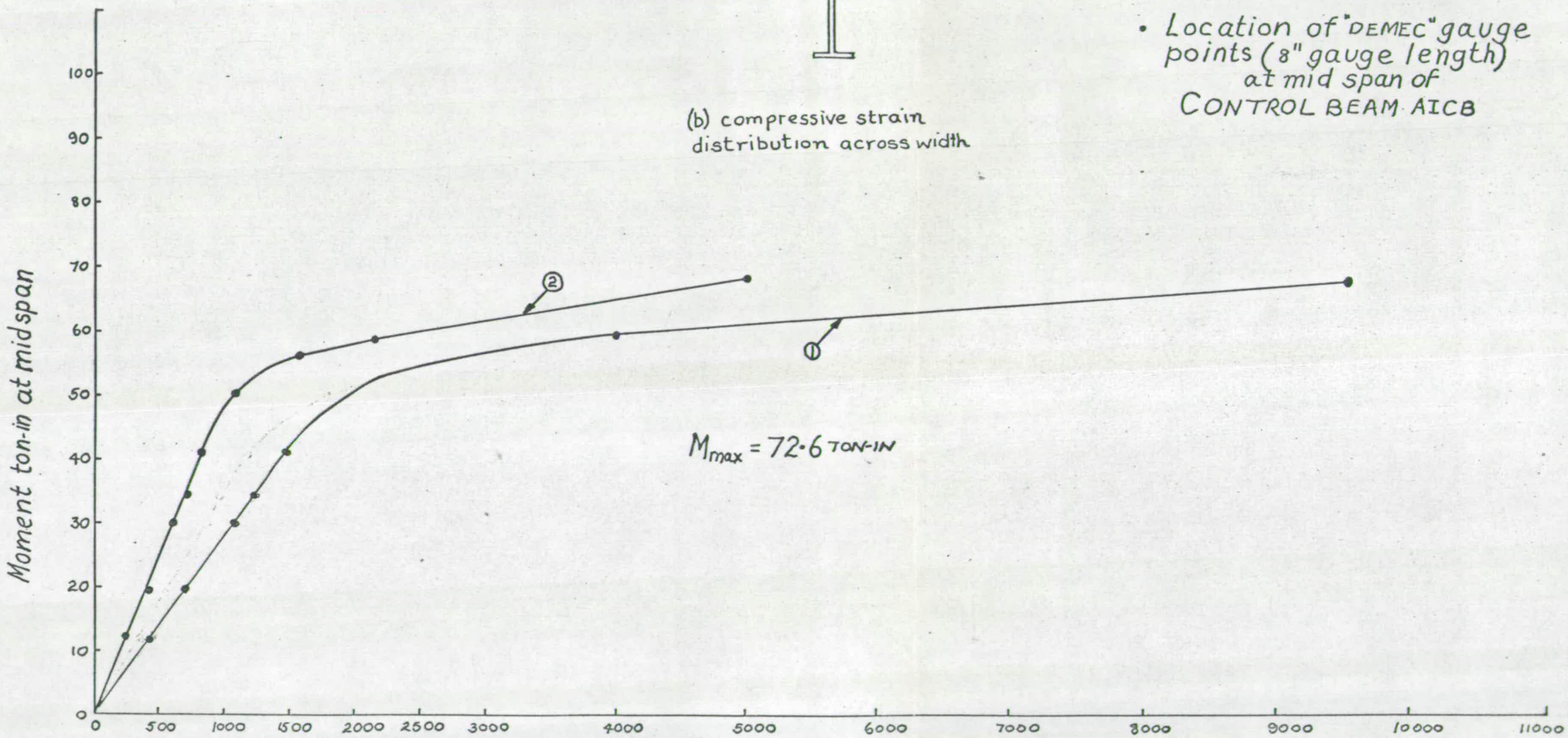

FIG. 6·2

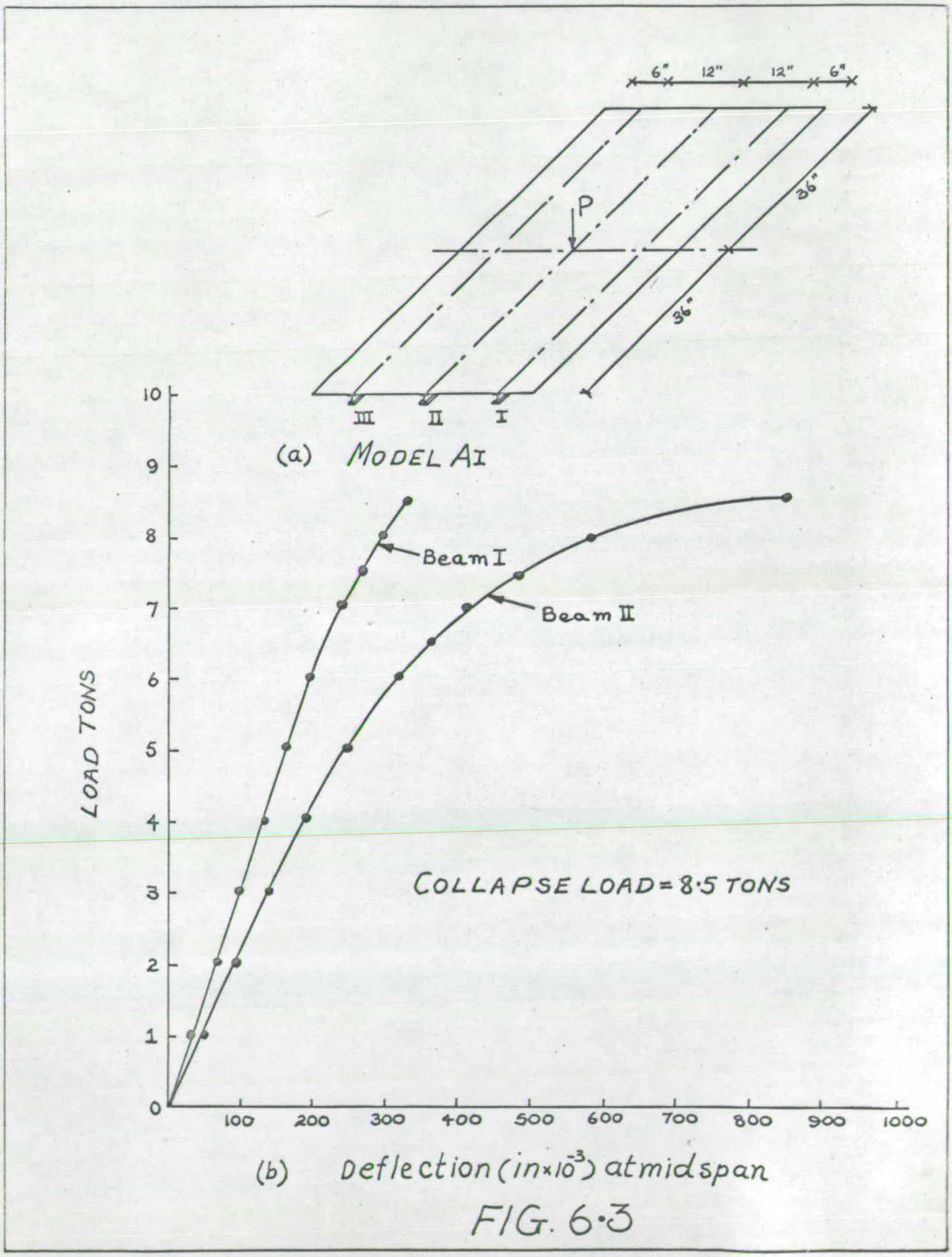
6"
12"
12"
6"
P
36"
36"
III
II
I
(a) MODEL AI
LOAD TONS
0
1
2
3
4
5
6
7
8
9
10
Beam I
Beam II
COLLAPSE LOAD = 8·5 TONS
100
200
300
400
500
600
700
800
900
1000
(b) Deflection (in×10⁻³) at mid span

FIG. 6·3

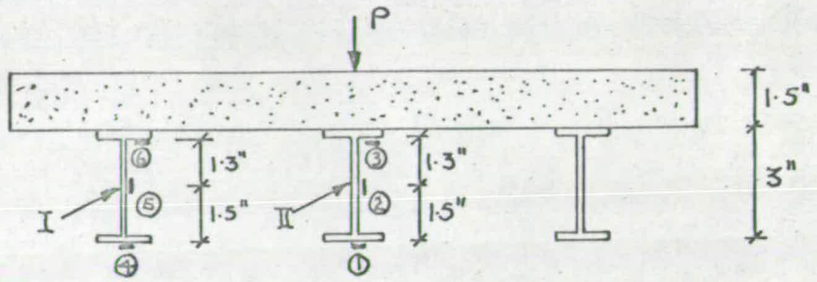

- Location of resistance gauges at mid span of Model AI

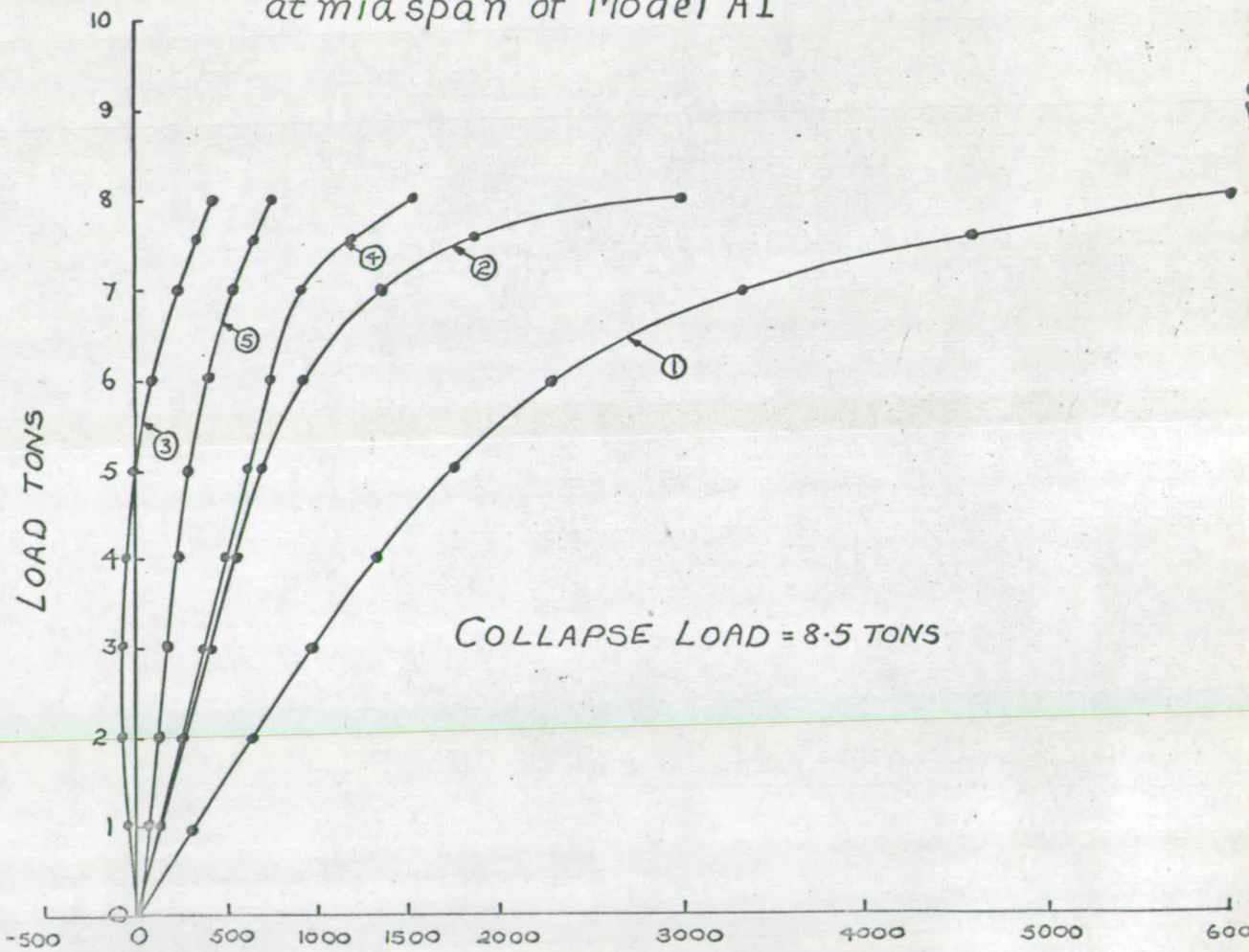

(a) Strain (10^{-6} in/in)

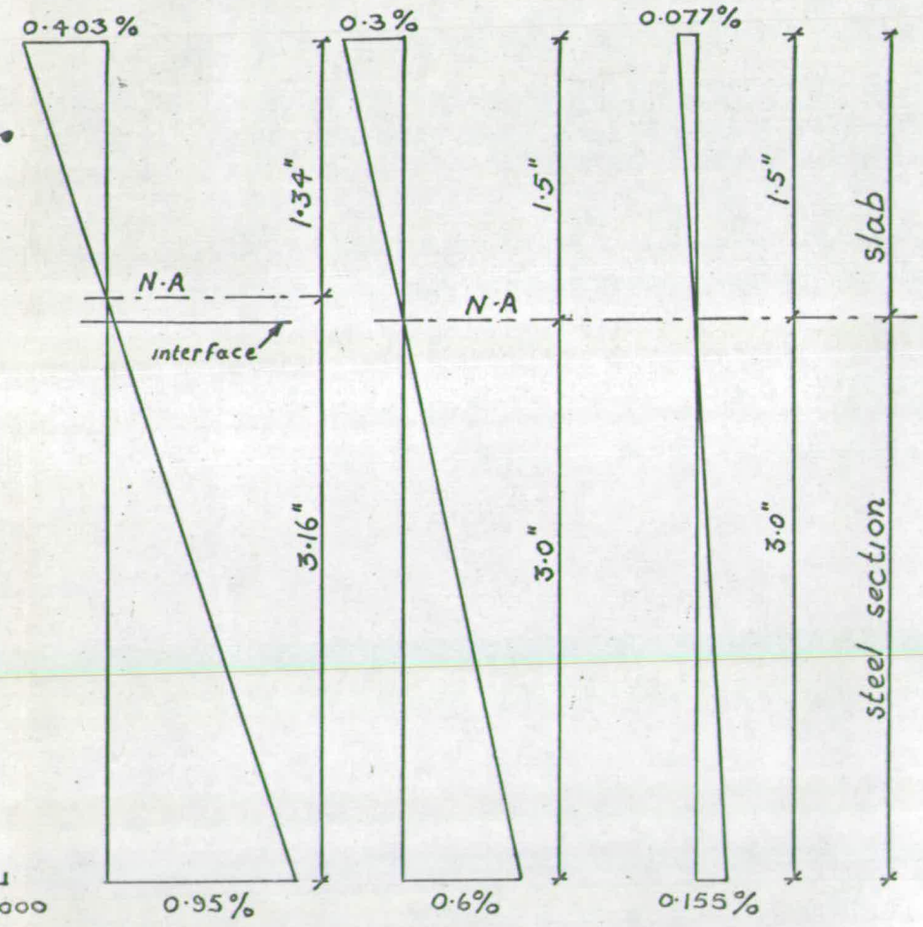

(b) Strain distribution near collapse

FIG. 6·4

rotated slightly towards the central beam. On the top of the slab tension cracks appeared roughly in the form of an ellipse with its minor axis nearly equal to two panel widths and major axis equal to the span of the beam, (Fig. 6.10a). At 8.5 tons the outer beams were still strong engough to act as supports to the slab. The bridge deck took the shape of a pyramid with its vertex at the load point, when the distribution plate punched through the slab and the load had fallen. The maximum load recorded was 8.5 tons.

6.4.2 Model A II

Load position : Fig. 6.7(a)

cross section : Fig. 5.3(a)

Control Beam AIICB : Moment-Deflection curve Fig. 6.5

Moment-Strain curve Fig. 6.6

View after failure Fig. 6.6(a)

Load-Deflection curves : Fig. 6.7(b), 6.8 and 6.9

Load-Strain curve : Fig. 6.10

Strain Distribution : Fig. 6.7(c)

Crack pattern : Fig. 6.10(a) and 6.10(b)

Model A II was a Companion Specimen to Model A I and was subjected to the same type of loading. The behaviour observed was similar and the final failure was by punching of the slab as in Model A I. The maximum load recorded was 9.15 tons. The strain-hardening of steel in the bottom flange of the loaded beam was more pronounced in this case and the strains well into this stage were recorded.

6.4.3 Model A III

Load positions : Fig. 6.1(a)

Cross section : Fig. 5.3(a)

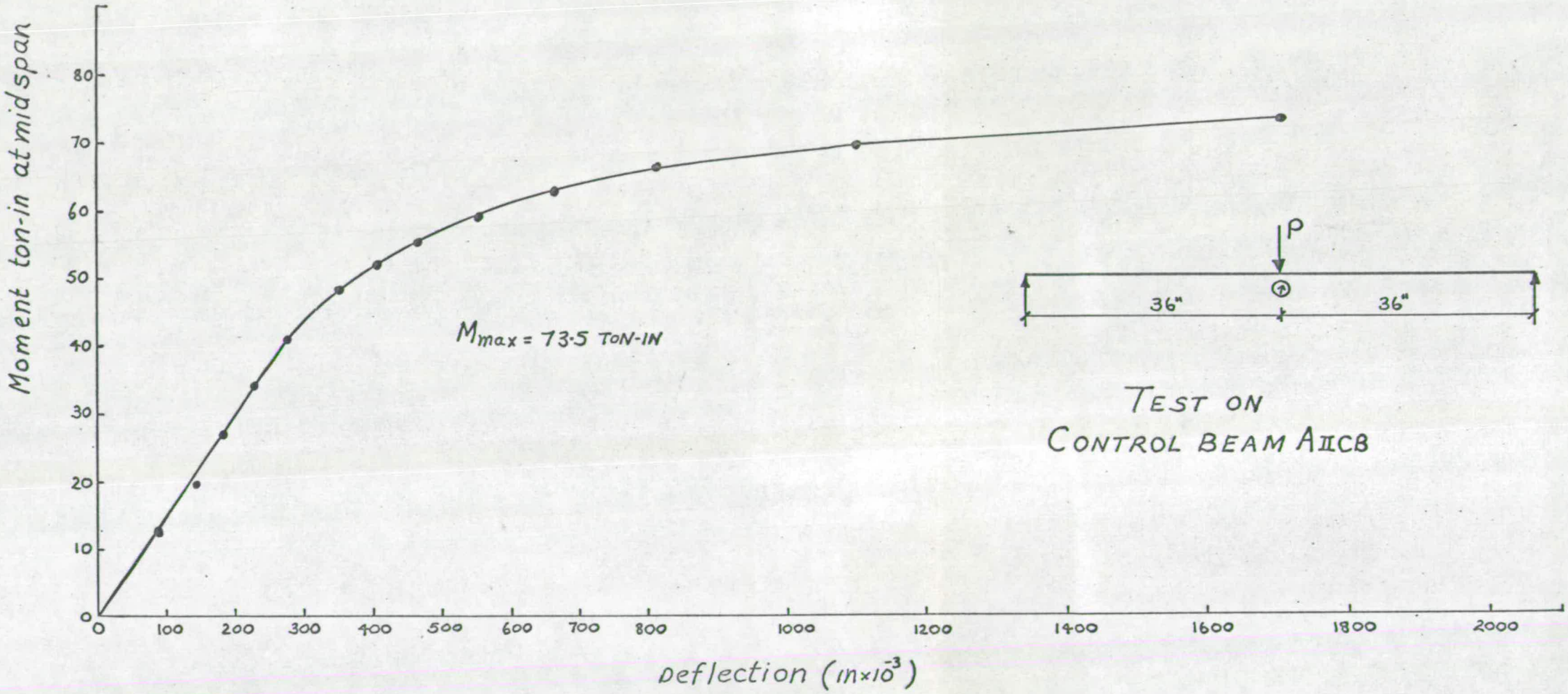
Moment ton-in at mid span
80
70
60
50
40
30
20
10
0
0
100
200
300
400
500
600
700
800
1000
1200
1400
1600
1800
2000
Deflection (in×10⁻³)
M max = 73·5 TON-IN
P
36"
36"
TEST ON
CONTROL BEAM AIICB

FIG. 6·5

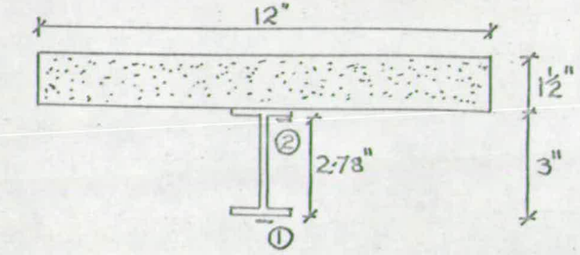

– Location of Resistance gauges at mid span of Control Beam A II CB

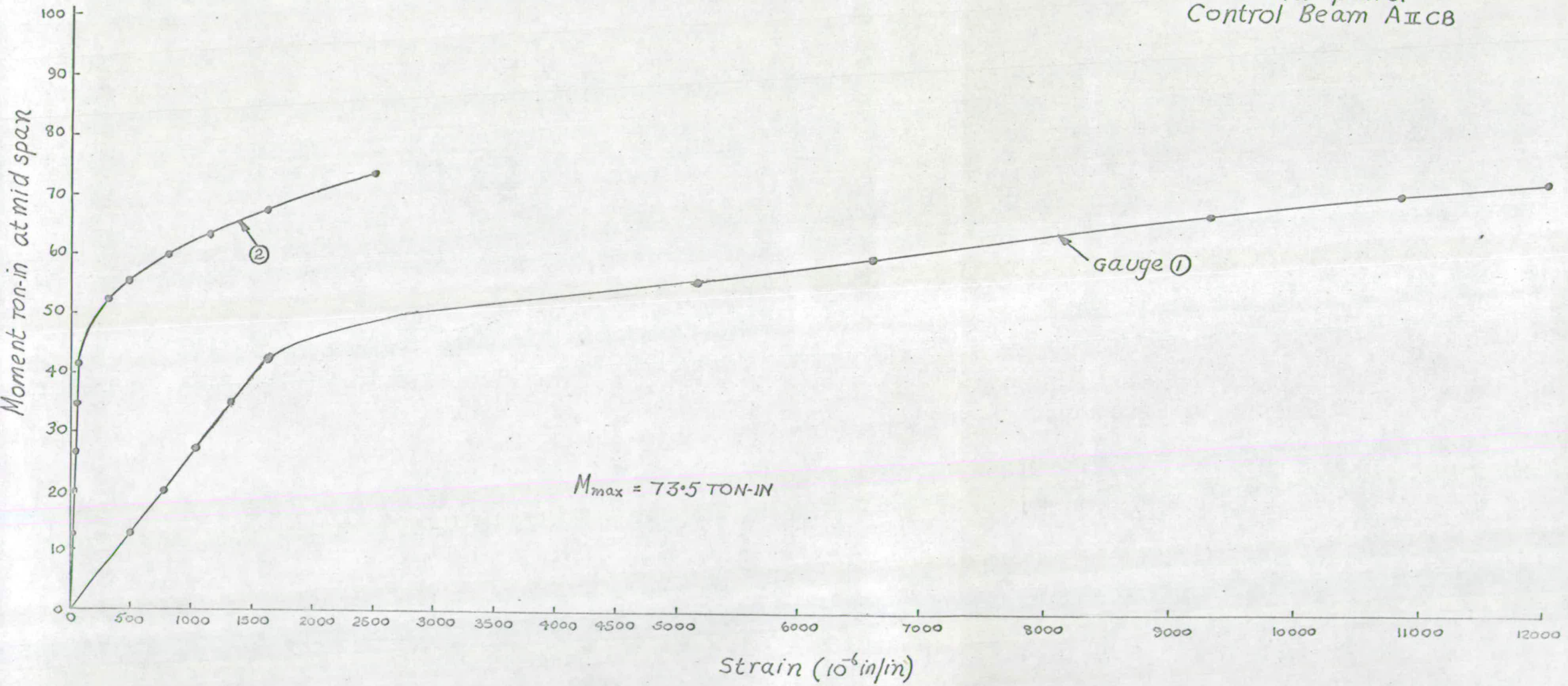

FIG. 6·6

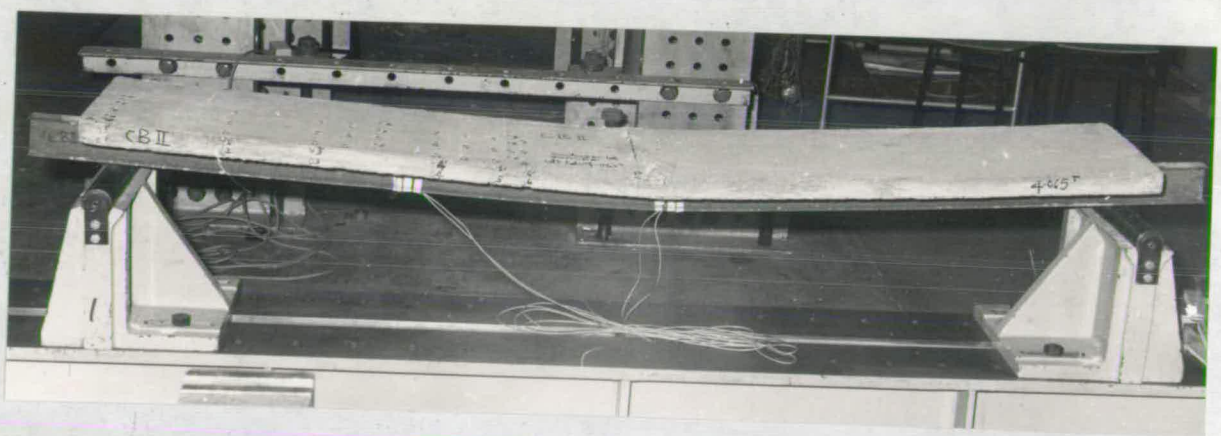

FIG.6.6(a) Control Beam AIICB after failure

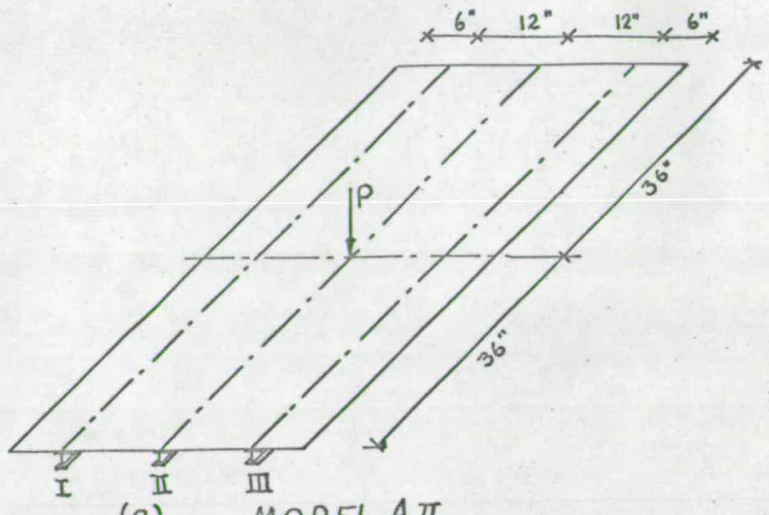

(a) MODEL AII

(b) deflection ($in \times 10^{-3}$) at midspan

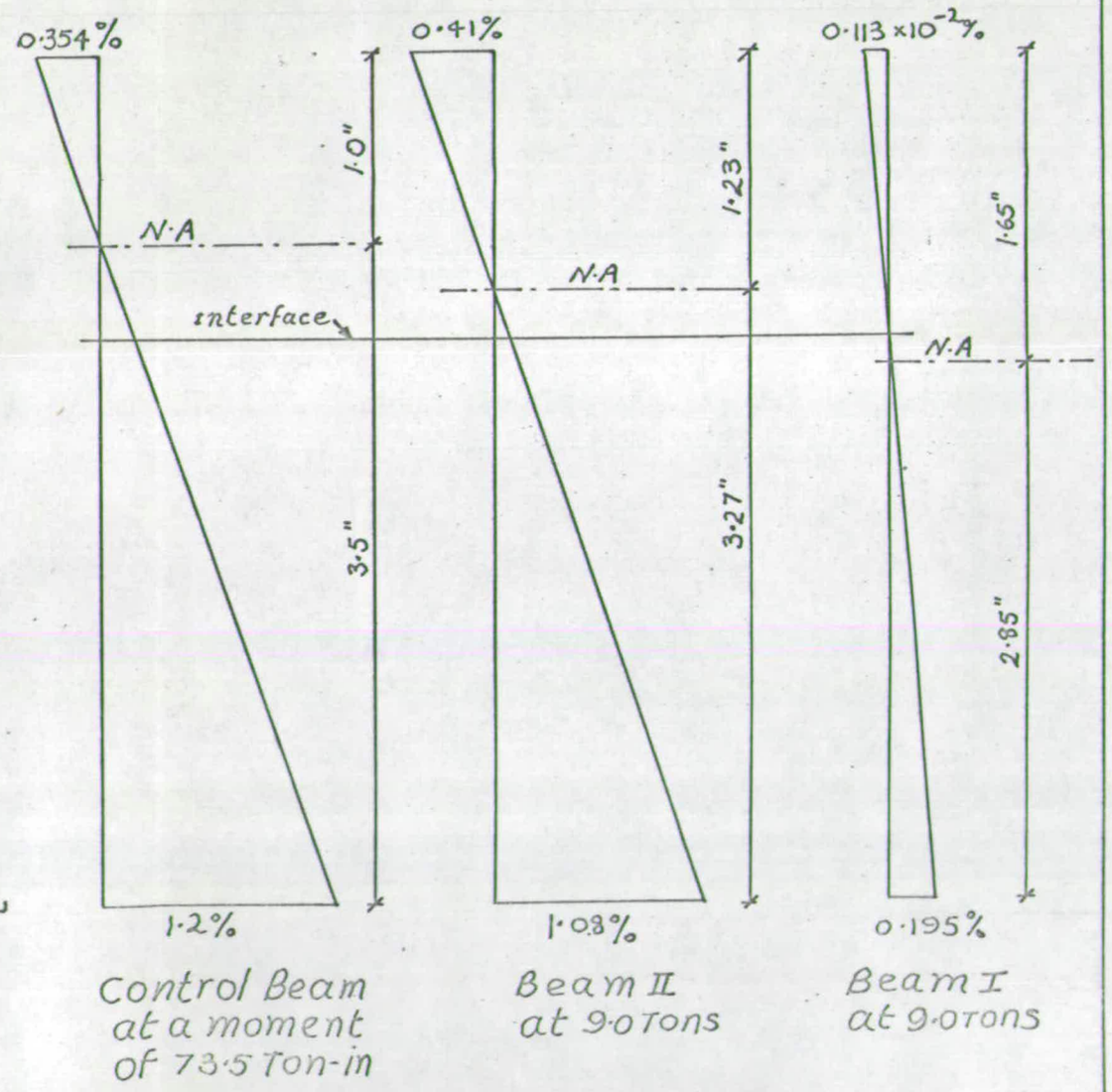

(c) strain distribution near collapse

FIG. 6·7

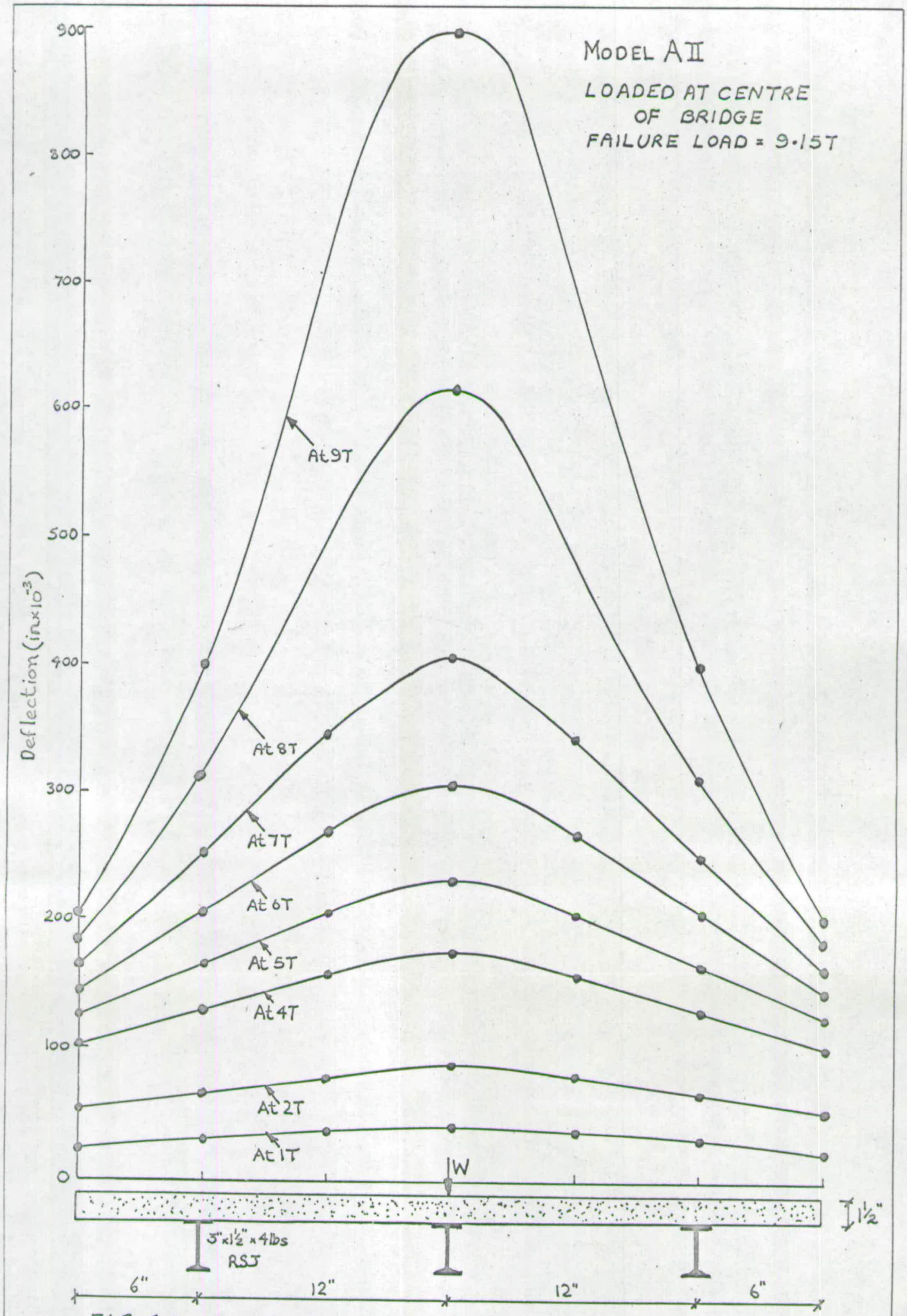

FIG.6.8 Deflection at mid span section

MODEL AII

LOAD AT CENTRE OF BRIDGE
FAILURE LOAD = 9·15^{T}

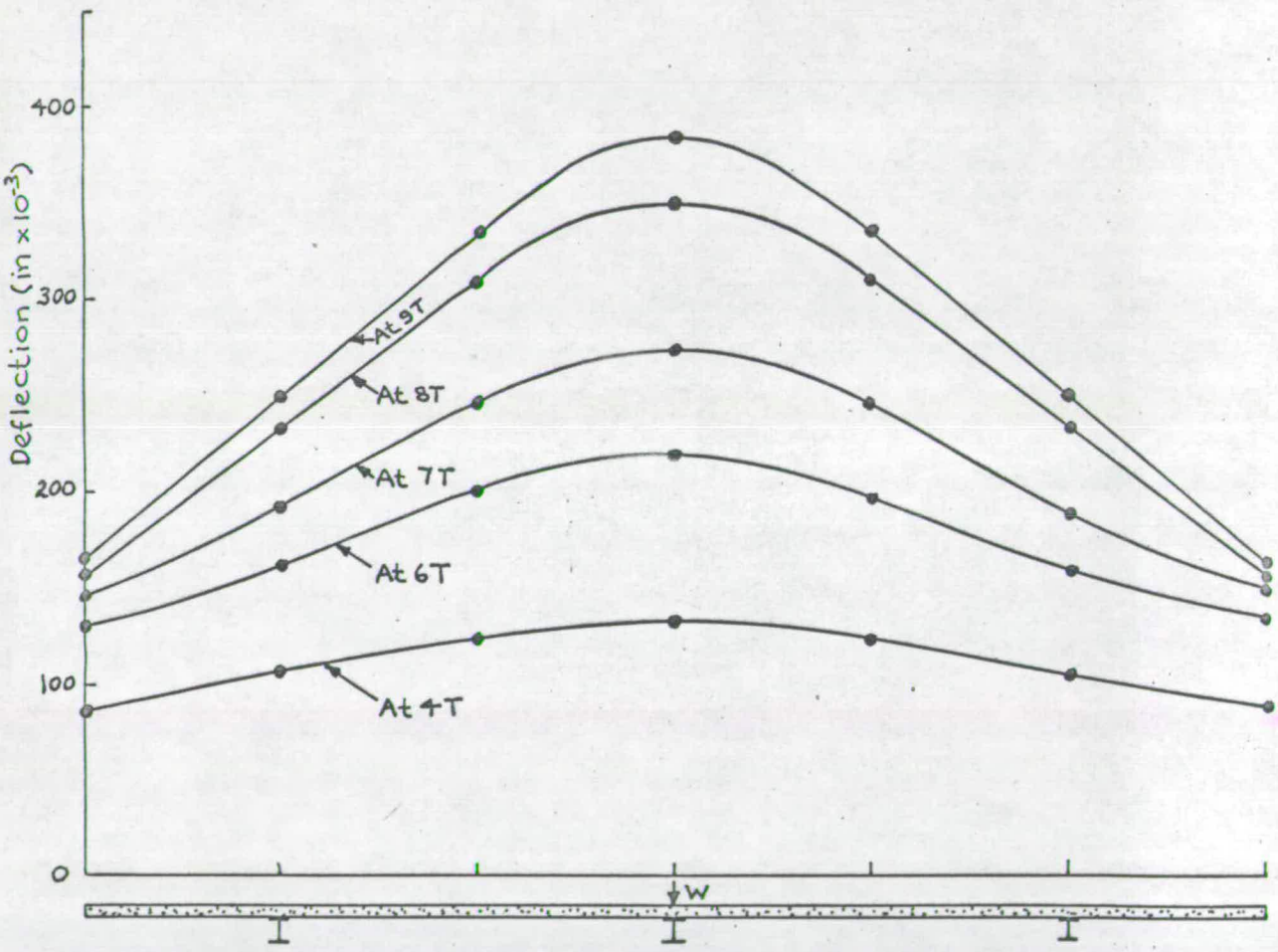

Deflection at ¼ span section

FIG. 6·9

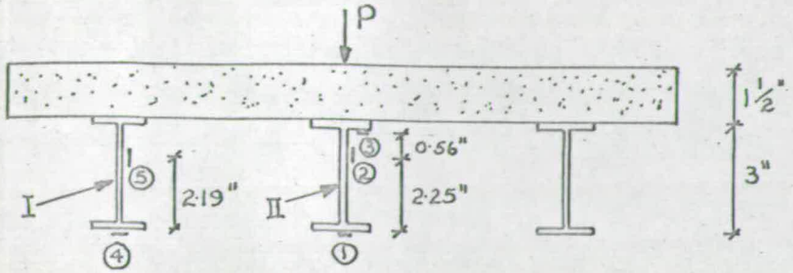

- Location of resistance gauges at midspan of Model AII

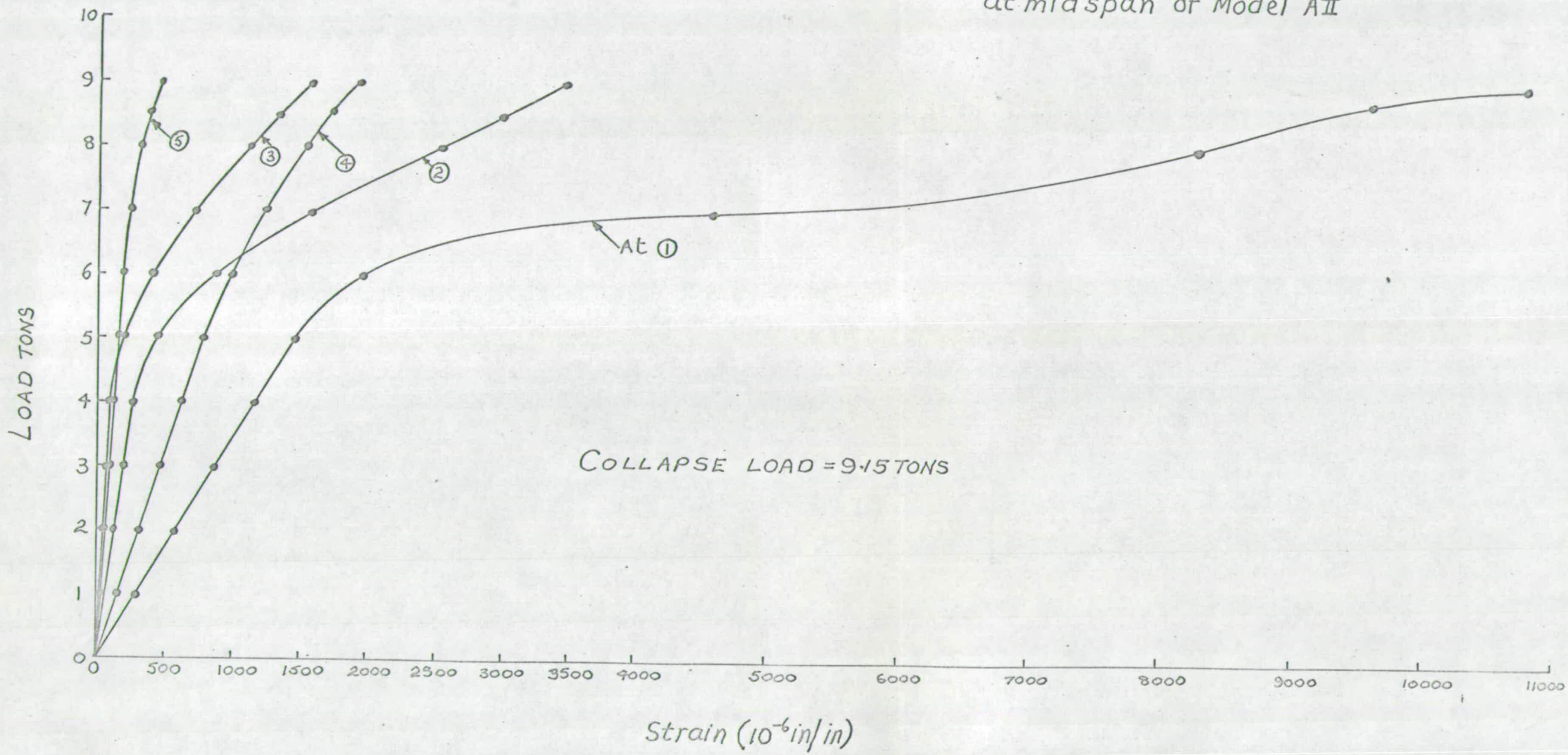

FIG. 6·10

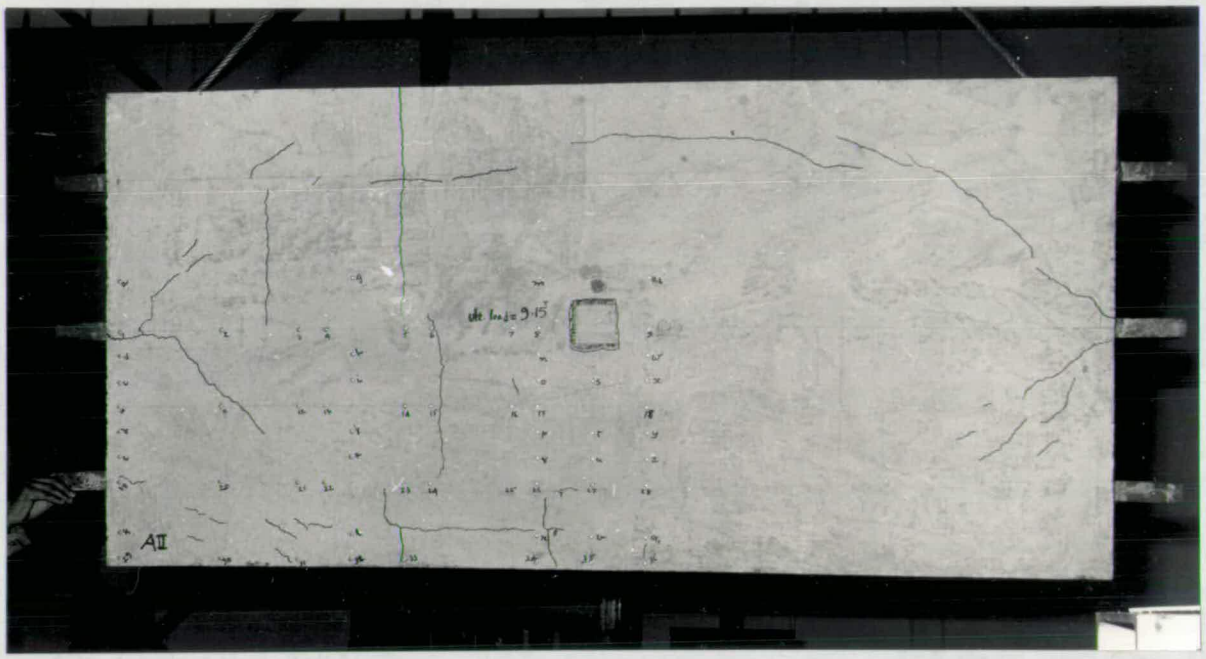

(i) Top

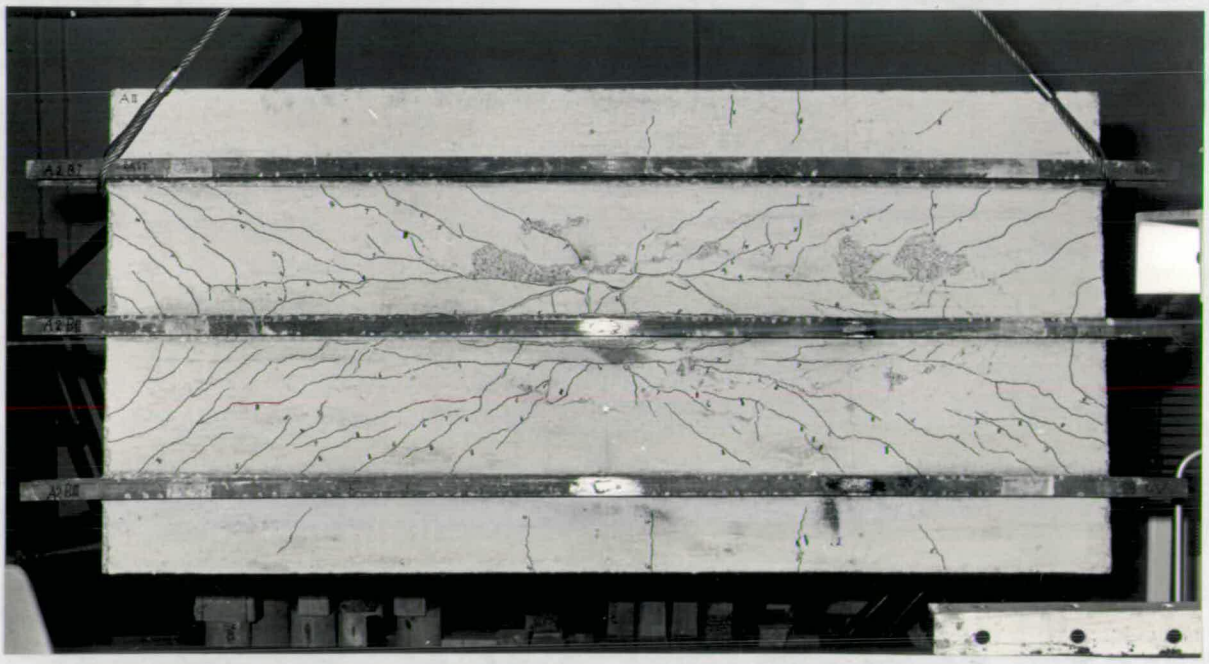

(ii) Bottom

FIG.6.10(a) Crack Pattern of Model AII after failure. compare with FIG.6.10(b).

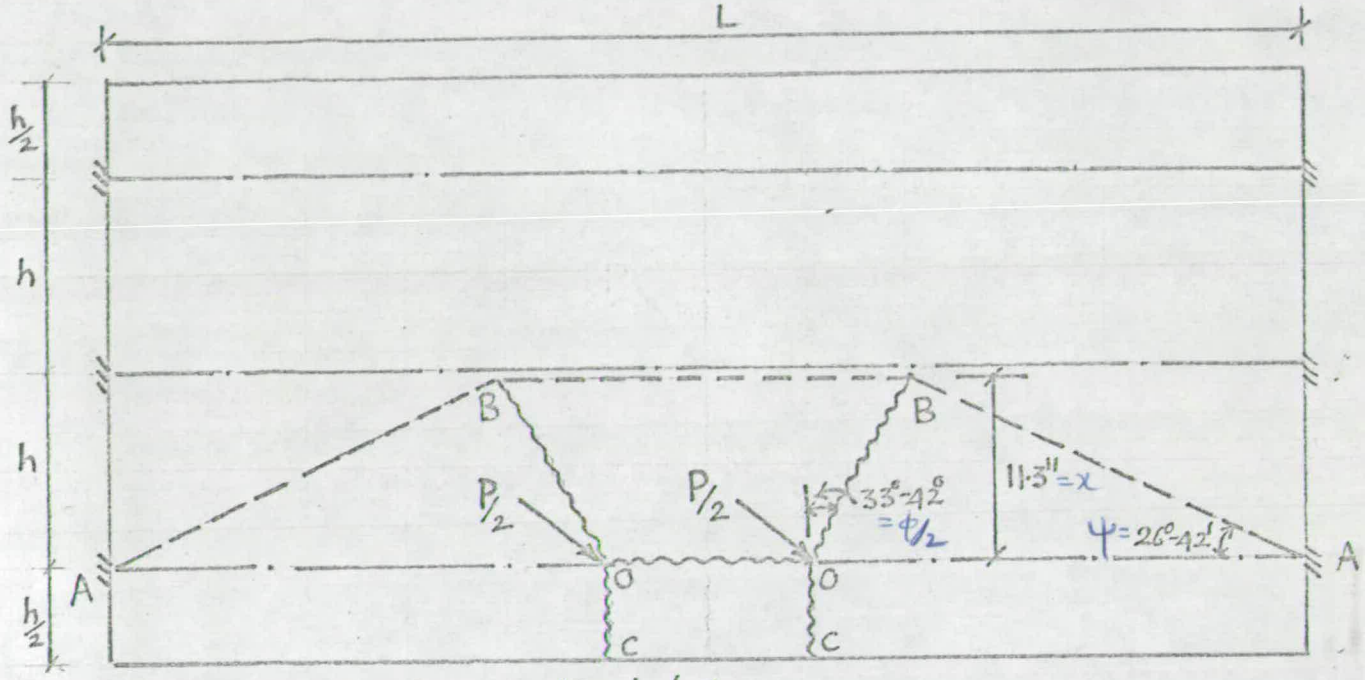

Model A III
Theoretical yield pattern

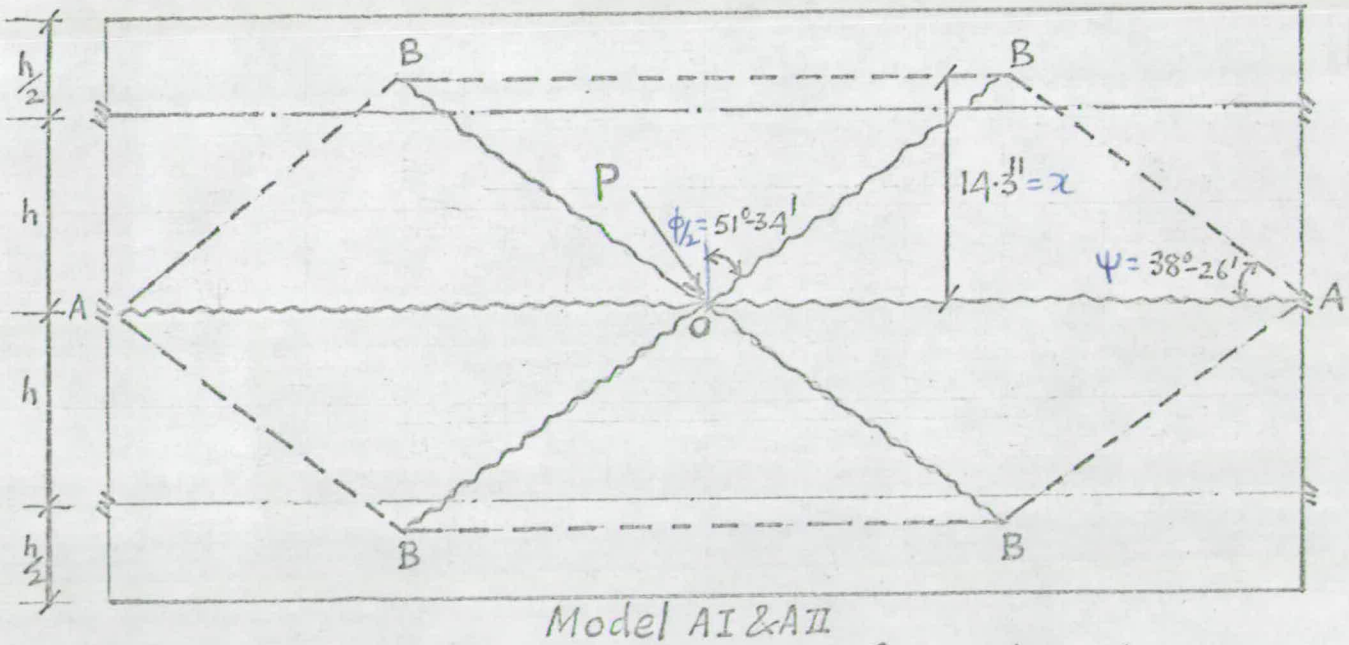

Model A I & A II

FIG 6·10(b) Theoretical yield pattern (Equivalent slab Method)

Control Beam AIIICB : Moment-Deflection curve Fig. 6.11

Moment-Strain curve Fig. 6.12

View after failure Fig. 6.12(a)

Load-Deflection curve : Fig. 6.13(b)

Load-Strain curve : Fig. 6.14

Strain Distribution : Fig. 6.15

Crack patterns : Fig. 6.15(a) and 6.15(b) & 6.10(b)

The model was subjected to two-point loading on outer beam. The ends of other two beams were anchored down in order to prevent their lifting up due to eccentricity of the loading.

The non-linearity of strain had commenced at 5.2 tons in the bottom flange of the loaded beam and at 7 tons in the central beam. Tension cracks at the bottom of the slab emanated from the load points and spread at an inclination of about 45° to the axis of the beam. At about 9.5 tons, they had penetrated deep into the slab and crushing of concrete had taken place on the top of slab along these lines. Also on the top of slab, a large tension crack accompanied by smaller cracks on either side developed roughly in the form of a parabola with its vertex touching the central beam at its mid span and passing through the ends of the loaded beam. As the failure load was approached, the deflections at mid span of the two unloaded beams have started decreasing. At collapse, the outer (unloaded) beam had actually deflected upwards to a considerable extent. The failure load was 9.85 tons. Strain-hardening of steel was also observed in this case.

6.4.4 Model A IV

Cross section : Fig. 5.3(a)

Crack pattern : Fig. 6.15(c)

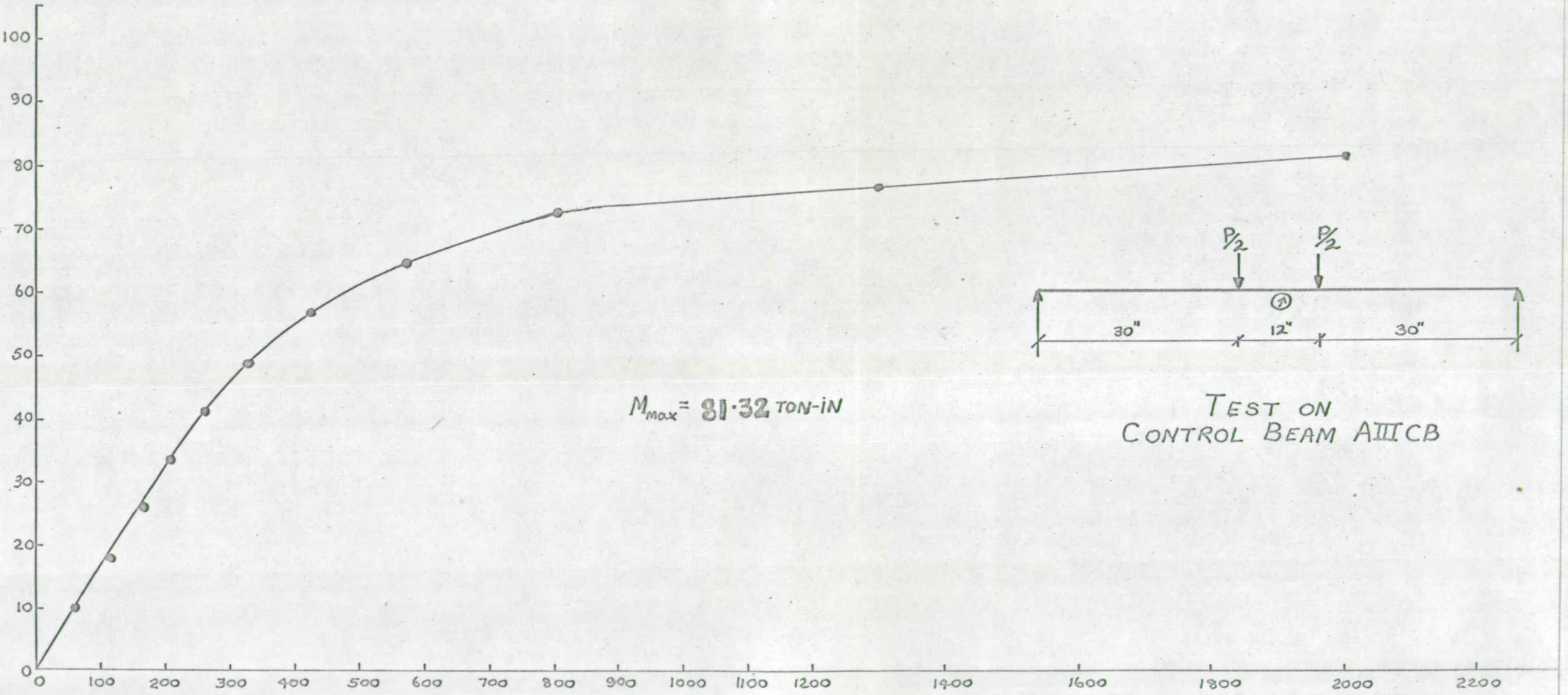
Moment (ton-in) at mid span
100
90
80
70
60
50
40
30
20
10
0
0
100
200
300
400
500
600
700
800
900
1000
1100
1200
1400
1600
1800
2000
2200
Deflection (in x 10⁻³) at midspan
M max = 31·32 TON-IN
P/2
P/2
30"
12"
30"
TEST ON
CONTROL BEAM AIIICB

FIG. 6·11

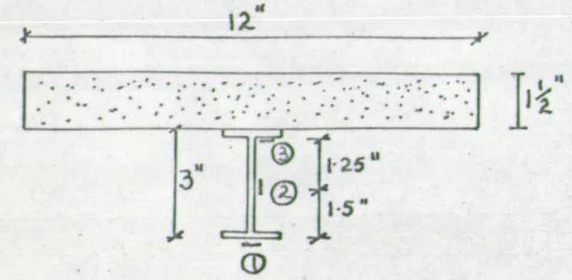

– Location of resistance gauges at midspan of CONTROL BEAM AIIICB

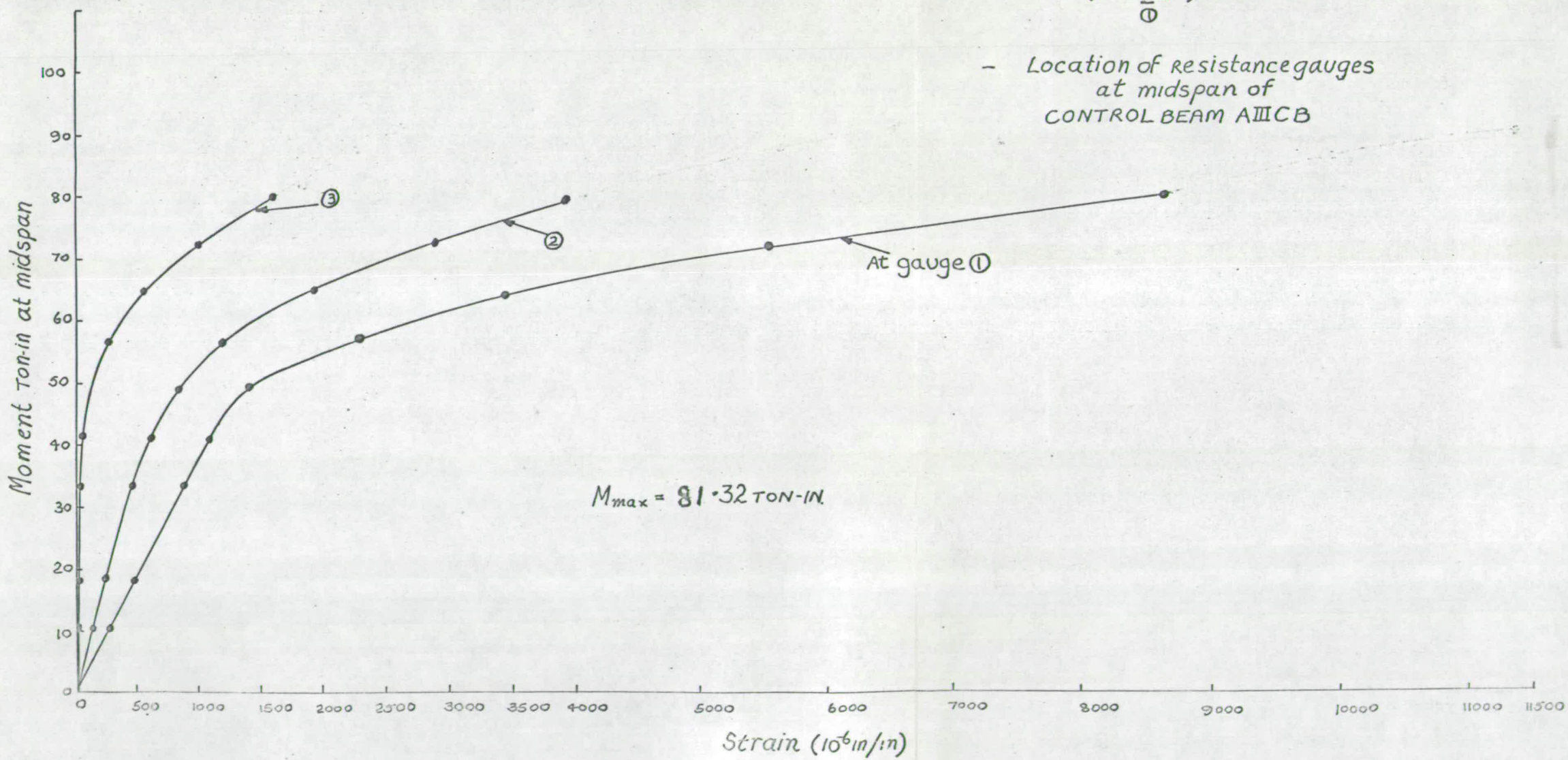

FIG. 6·12

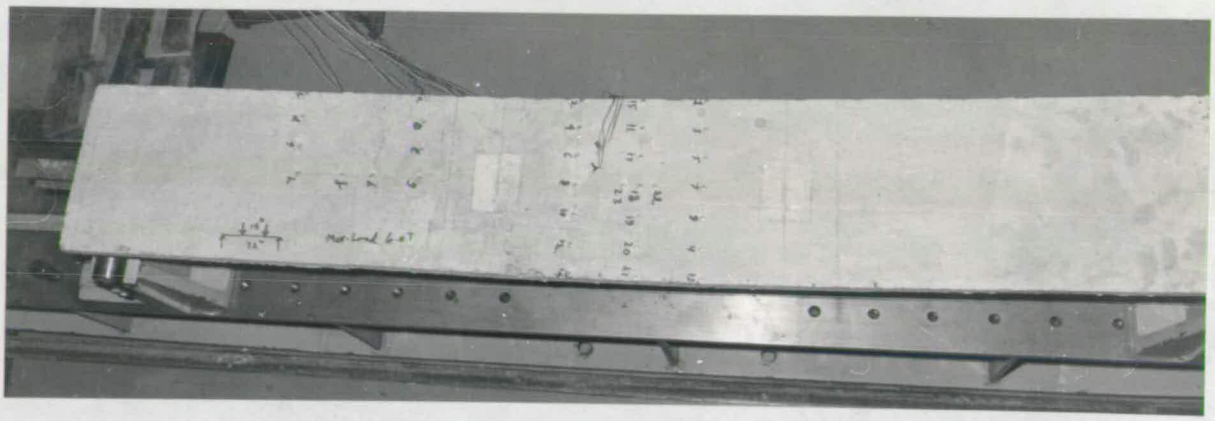

FIG.6.12(a) Control Beam AIIICB after failure

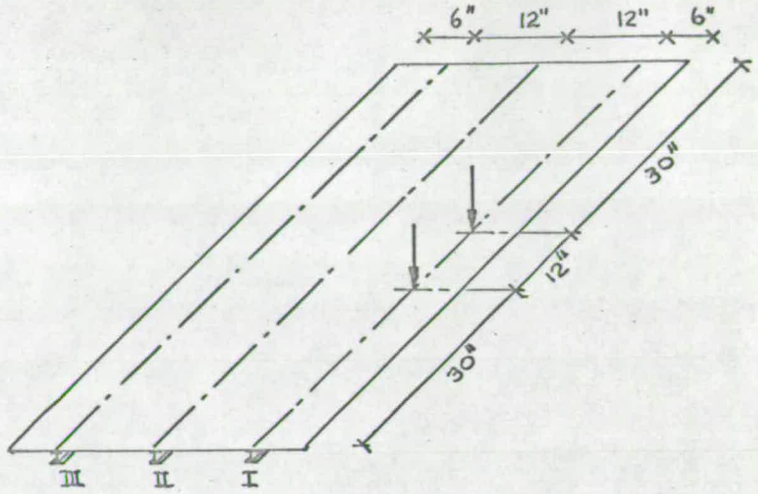

(a) MODEL AIII

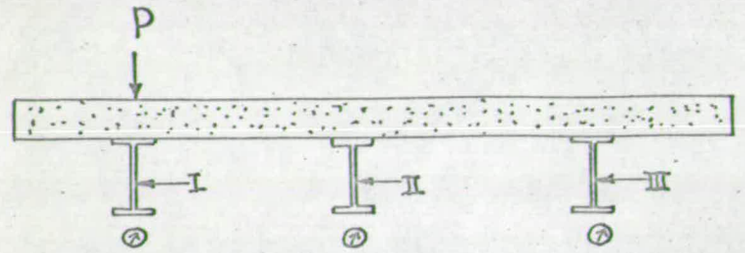

Cross Section of Model AIII at mid span

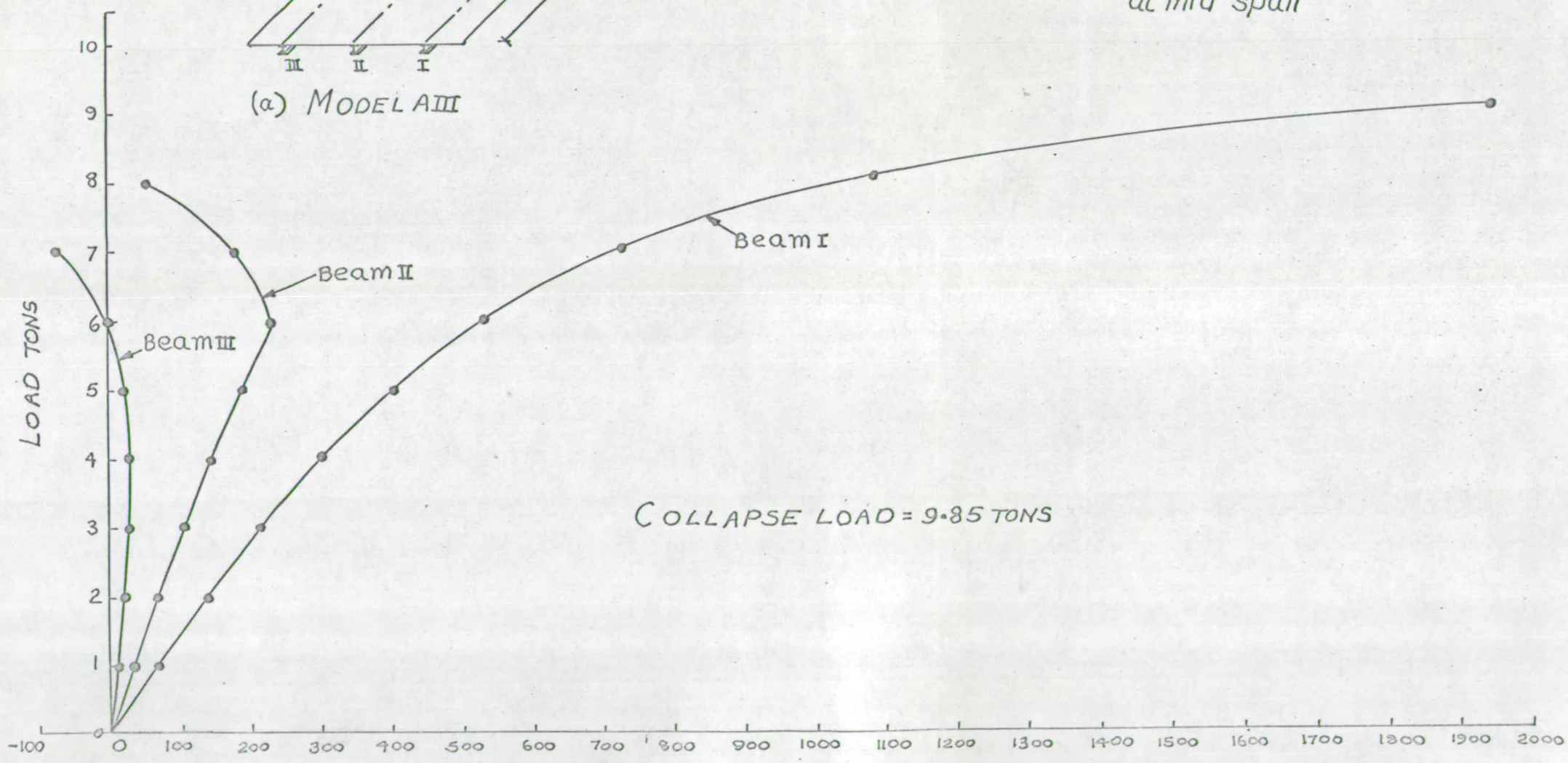

COLLAPSE LOAD = 9·85 TONS

(b) deflection ($in \times 10^{-3}$) at mid span

FIG. 6·13

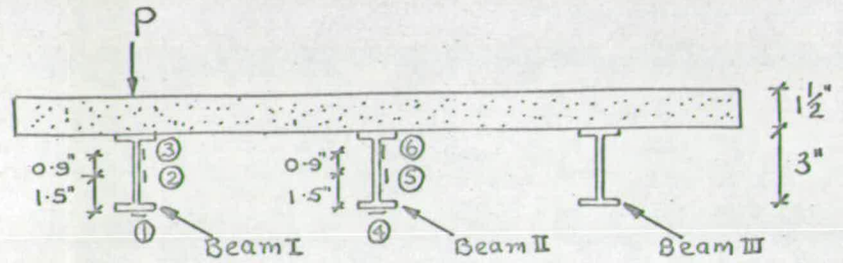

– Location of resistance gauges at mid span of Model A III

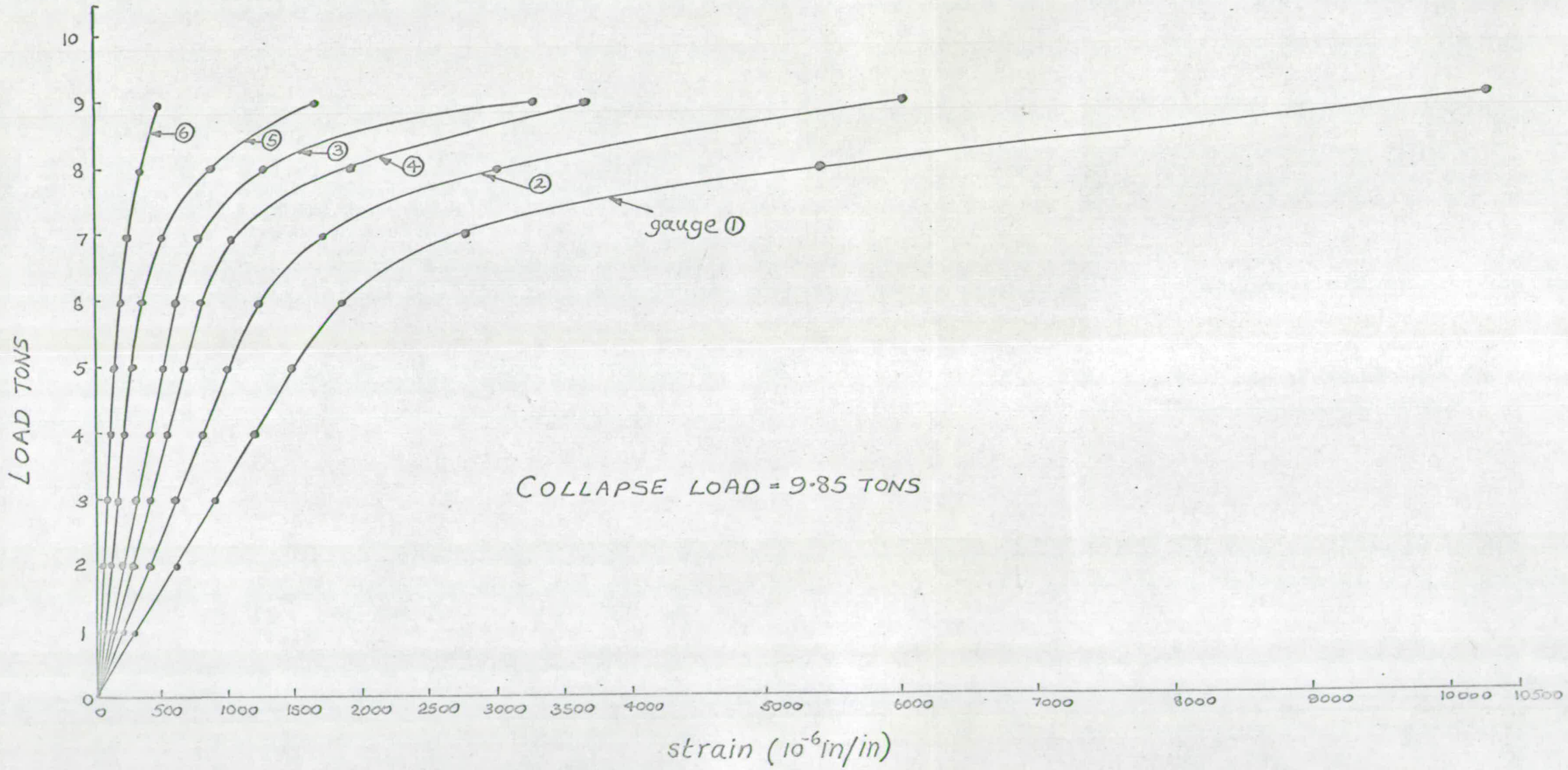

COLLAPSE LOAD = 9·85 TONS

FIG. 6·14

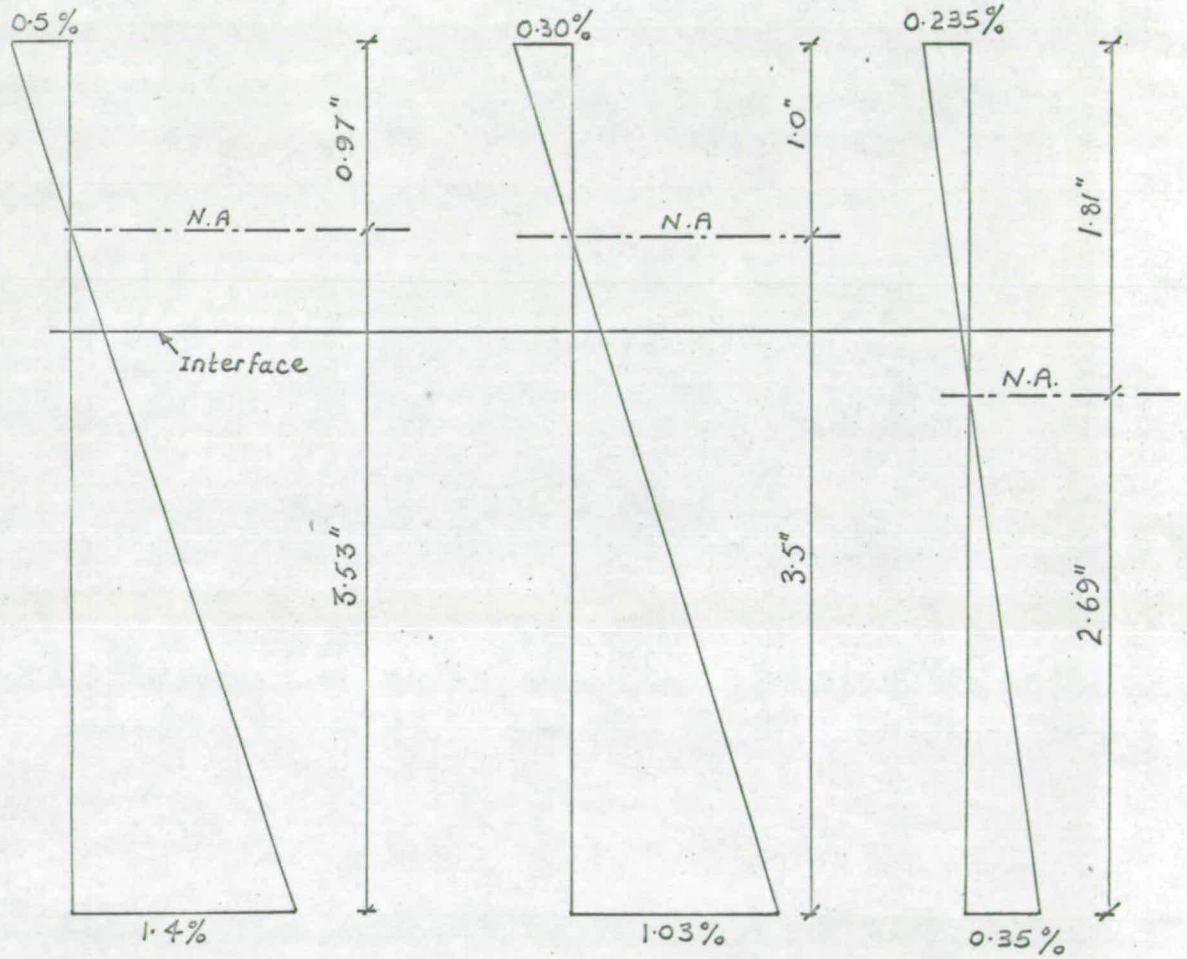

Strain distribution near collapse
in Model A III

FIG. 6·15

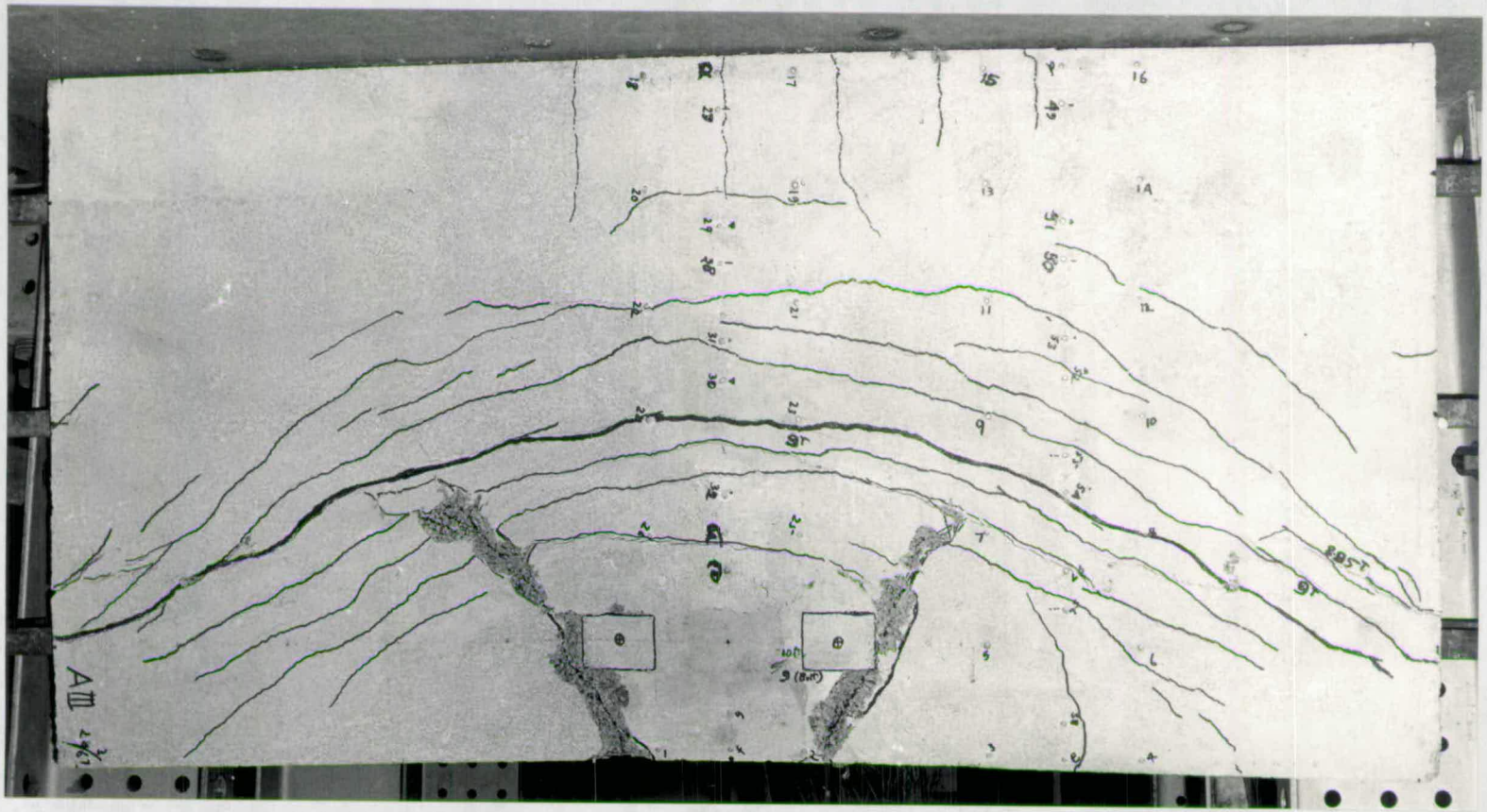

(i) Top

FIG.6.15(a) Crack Pattern of Model AIII after failure. compare with FIG·6·10(b).

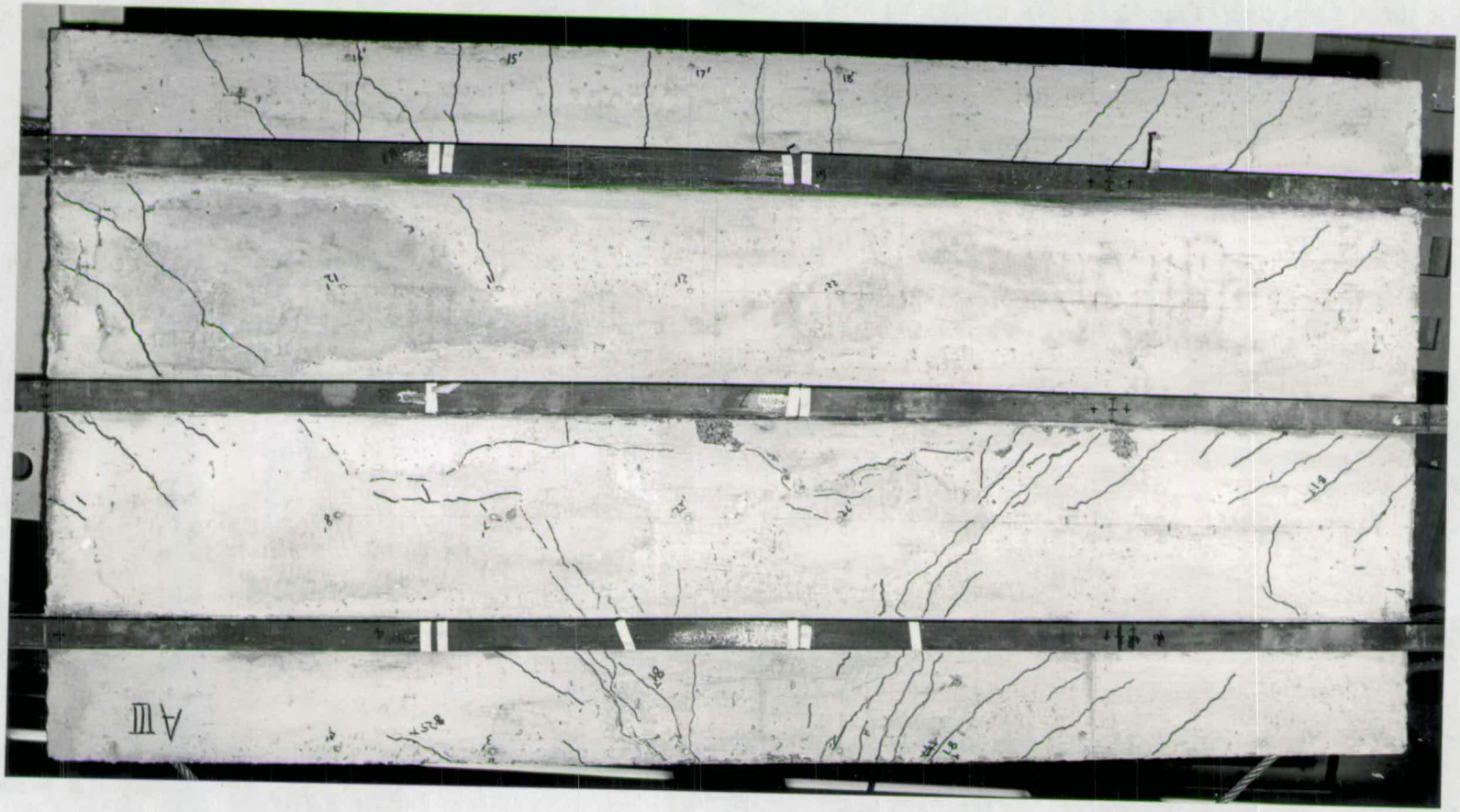

(ii) Bottom

FIG.6.15(a) Crack Pattern of Model AIII after failure

FIG.6.15(b) Top of Model AIII after failure

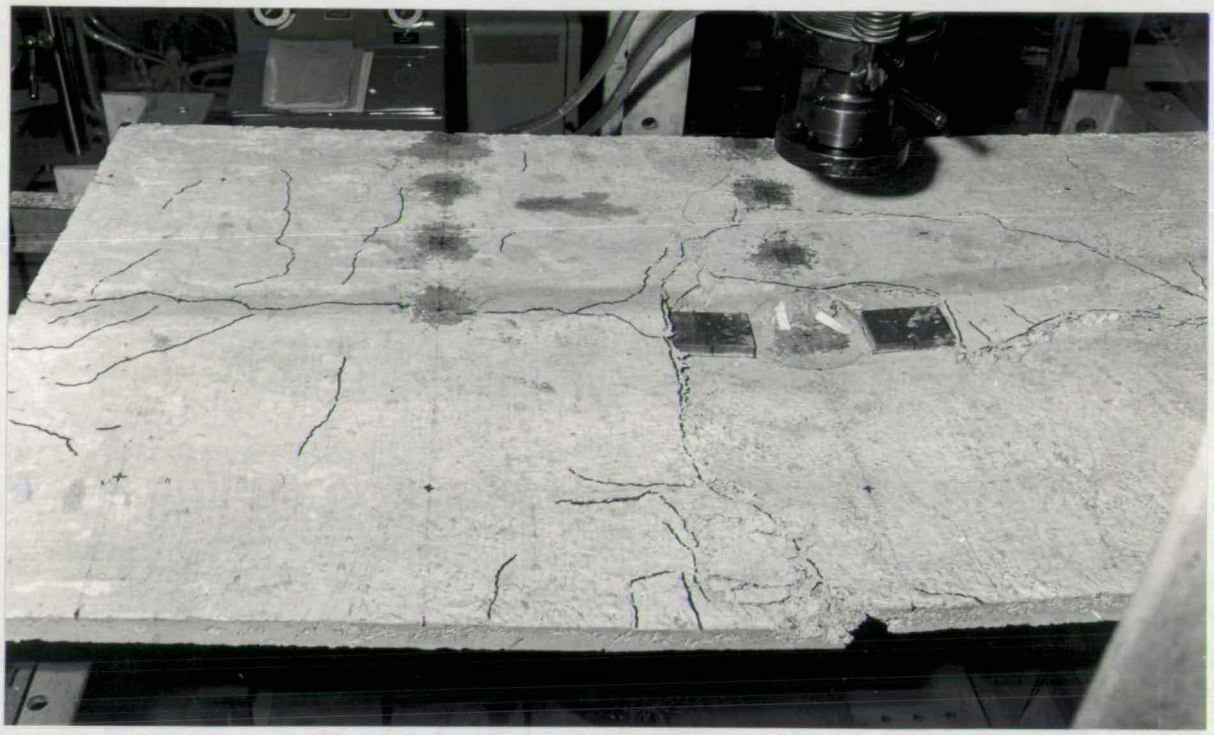

(i) Top

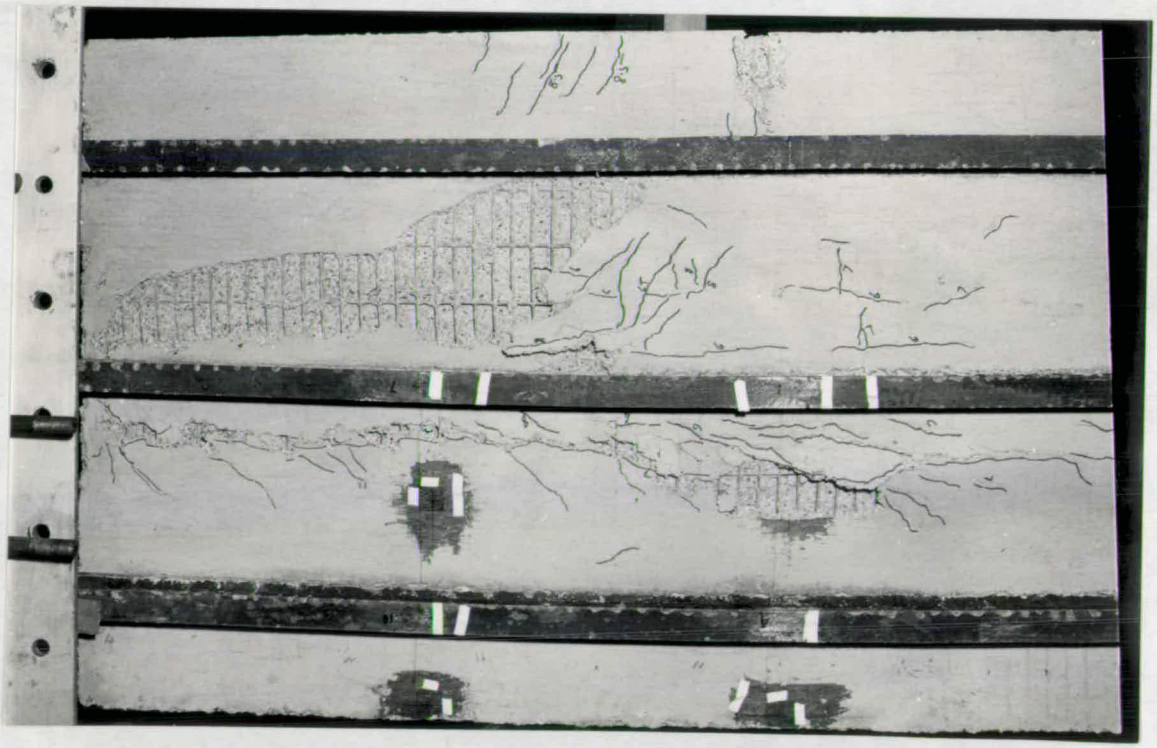

(ii) Bottom

FIG.6.15(c) Model AIV after failure

It was another companion specimen to Model A I but was subjected to two point loads 10 " apart in place of a single point load at mid span. Since the quality of concrete used was poor, it failed by developing a longitudinal tension crack along the loaded beam. There was extensive spalling of concrete at the bottom of the slab before failure occurred. These was no punching of the distribution plates through the slab. At mid span, a compression crack almost across the whole width of the bridge had formed. The failure load was 8.5 tons.

6.4.5 Model B I

Load position : Fig. 6.18(a)

Cross section : Fig. 5.3(b)

Control Beam BICB : Moment-Deflection curve Fig. 6.16

Moment-strain curve Fig. 6.17

View after failure Fig. 6.17(a)

Load-Deflection curve : Fig. 6.18(b)

Load-Strain surve : Fig. 6.19

Strain Distribution : Fig. 6.20

Crack pattern : Fig. 6.20(a) & 6.20(b).

This test was planned to simulate the wheel loads of HB vehicle on bridge decks. The eight-point loading was applied by distributing the jack load by means of rigid steel blocks resting on rollers at load points. Non-linearity of load-deflection and load-strain behaviour was noticed in the bottom flange of loaded beams I and II, when the total load reached a value of 4.5 tons. the bottom of the slab, tension cracks which originated at the load positions spread towards the ends of the beams III and IV. On the top of slab, tension cracks appeared along the beam III at mid span. They extended on either side to a length equal to about one-third span and turned towards the ends of the

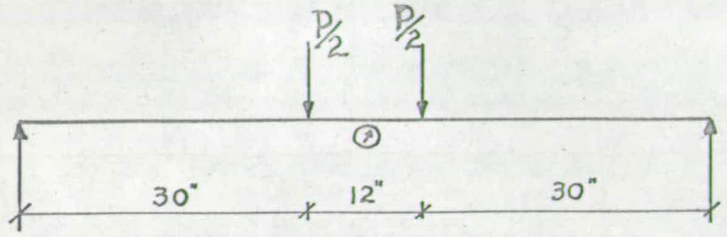

TEST ON
CONTROL BEAM BICB

$M_{max} = 44.5$ TON-IN

FIG. 6·16

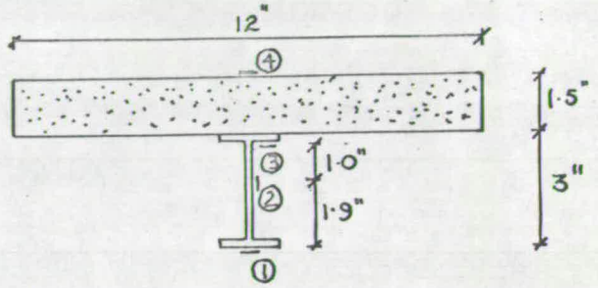

- Location of resistance gauges at mid span of CONTROL BEAM BICB

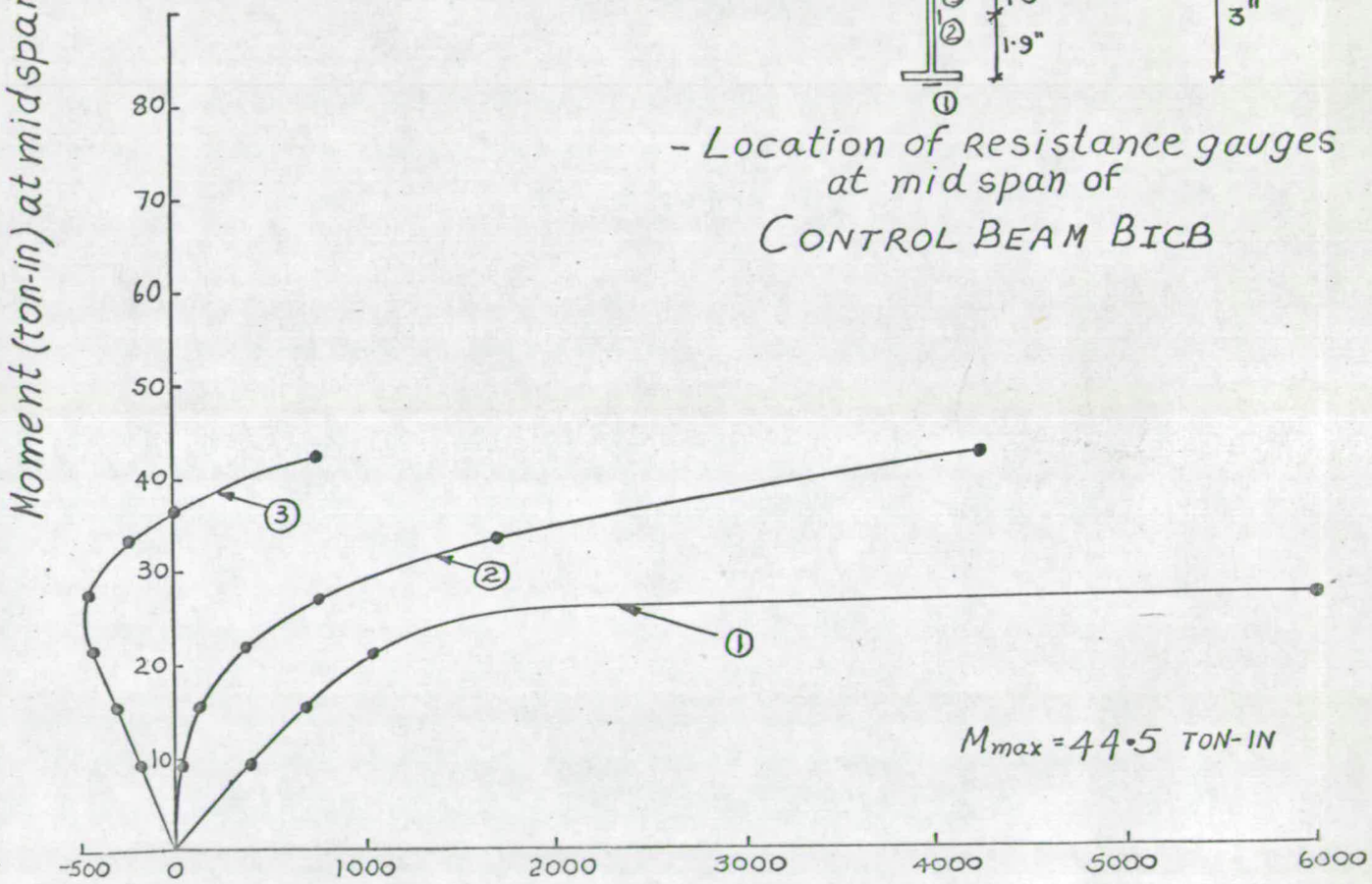

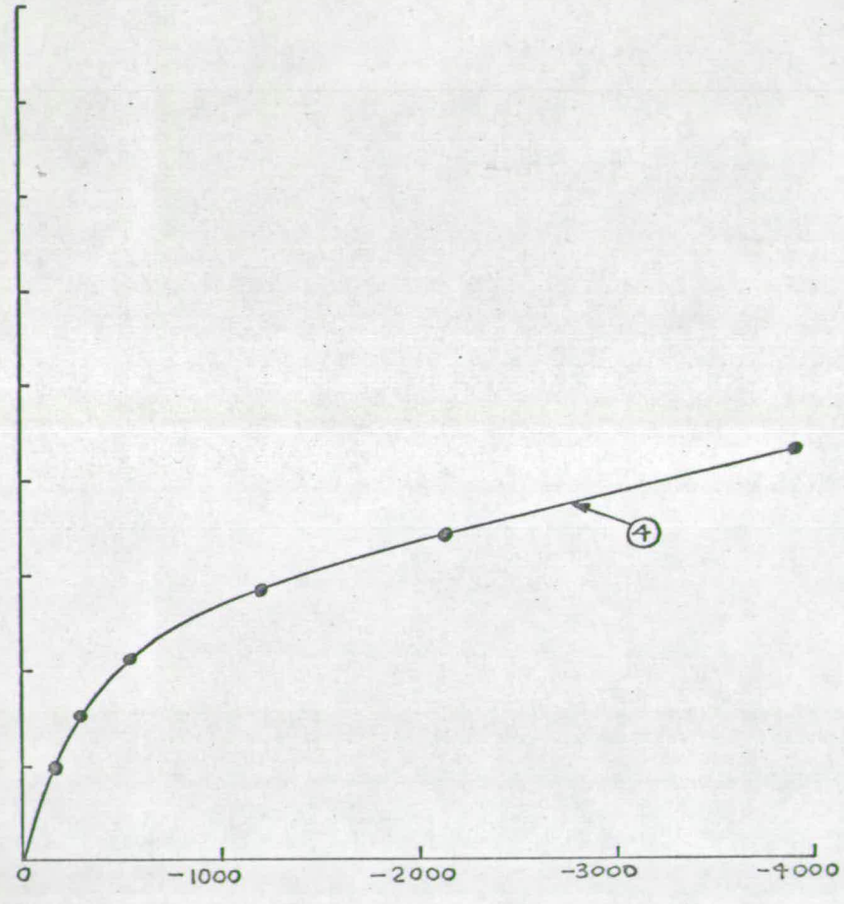

FIG. 6·17

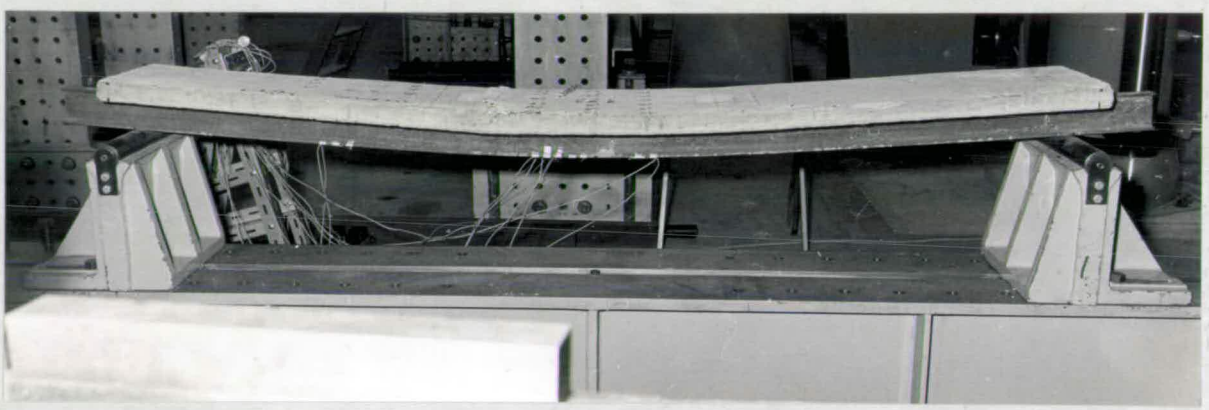

FIG.6.17(a) Control Beam BICB after failure

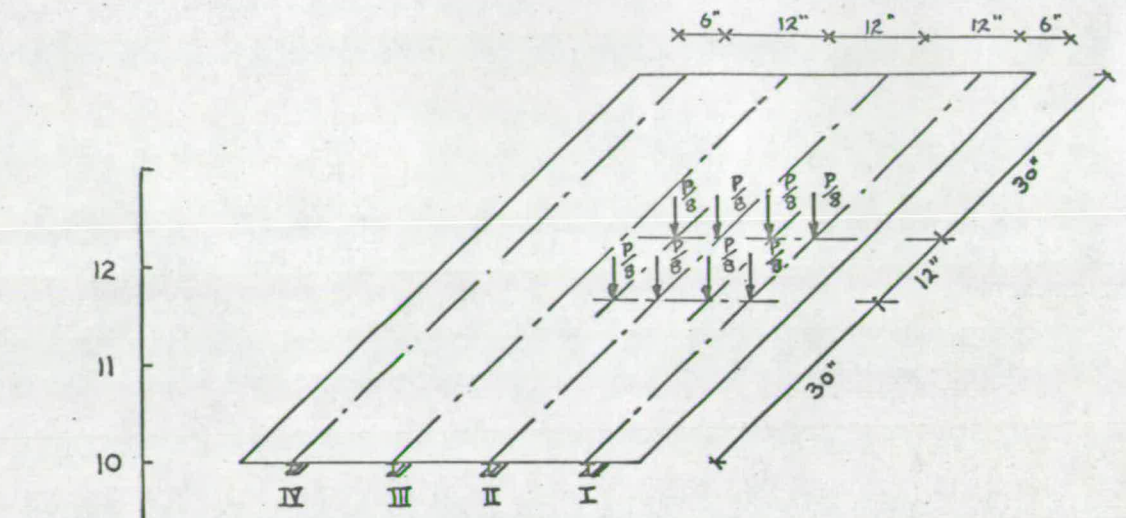

(a) MODEL BI
(LOADS SIMULATING HB VEHICLE)

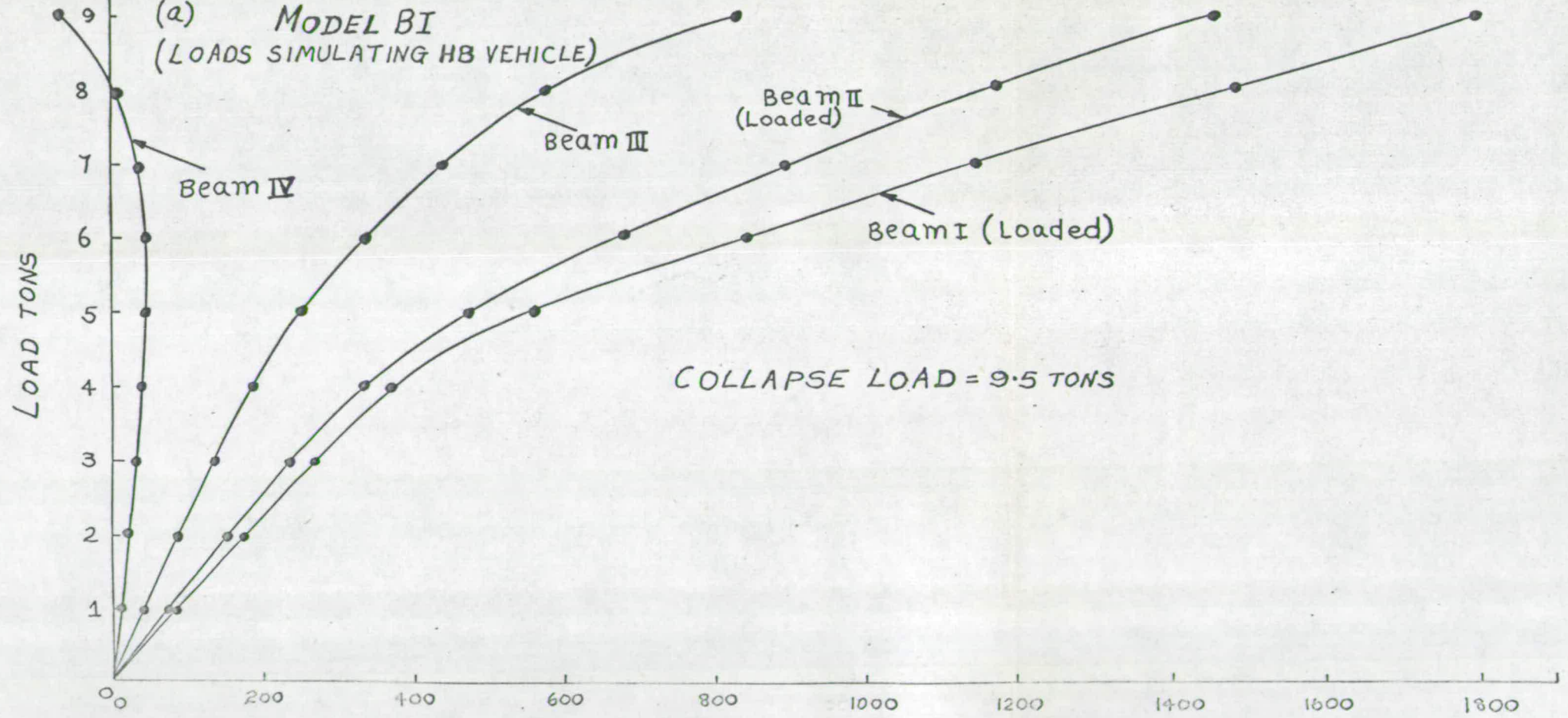

(b) Deflection ($in \times 10^{-3}$) at mid span

FIG. 6·18

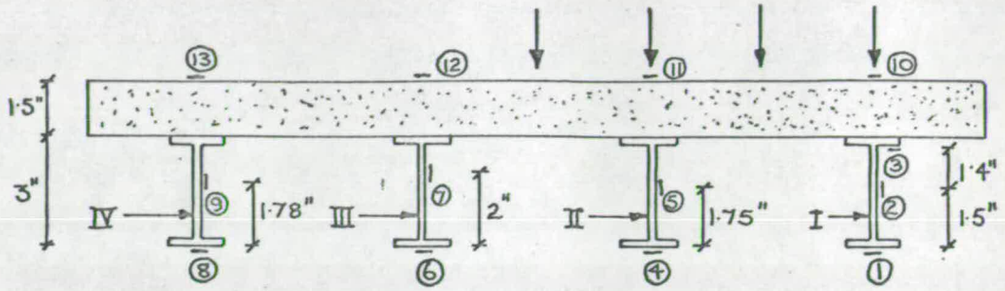

– Location of Resistance gauges at mid span of Model BI

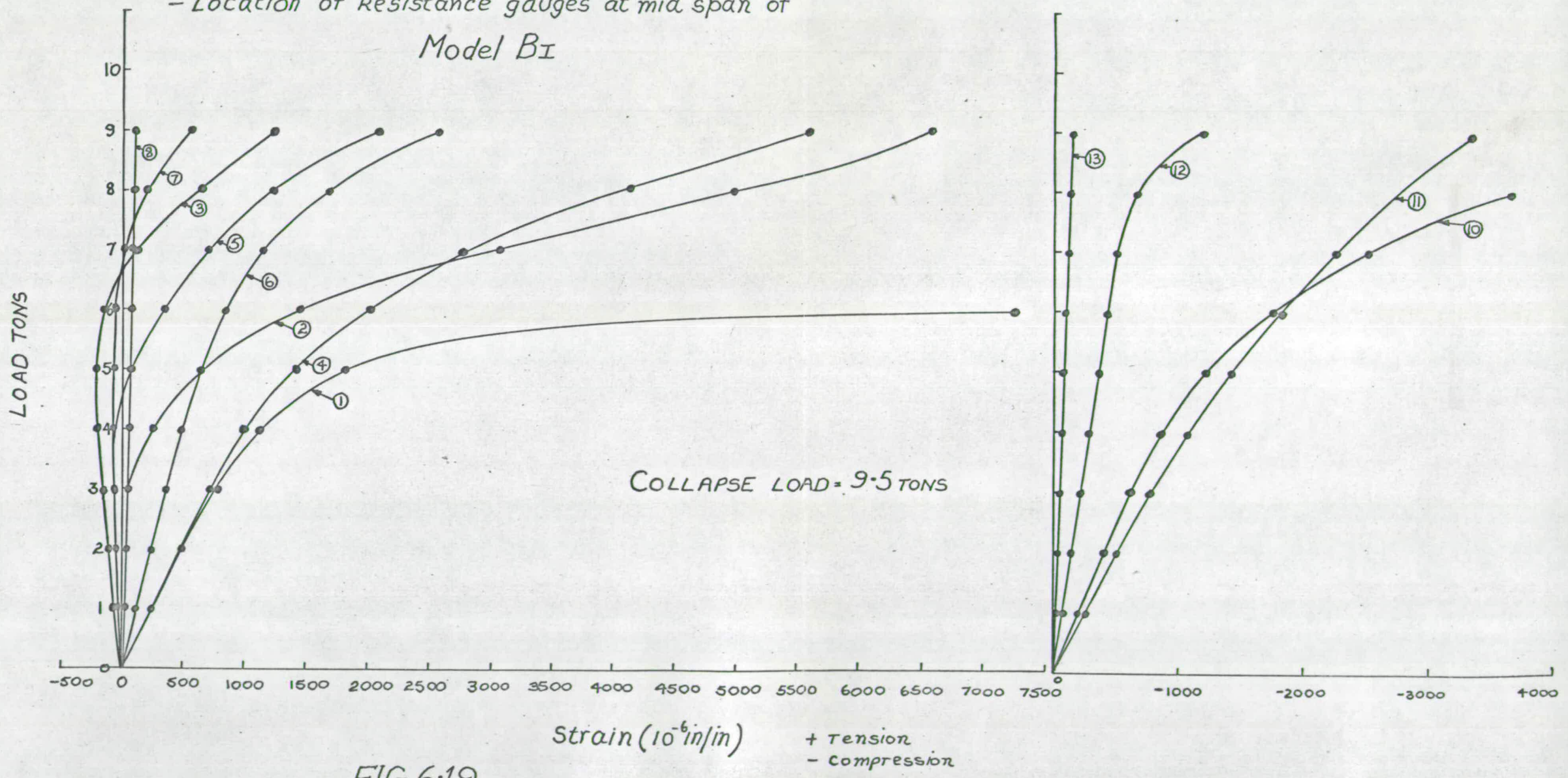

FIG. 6·19

AB – Deduced from strains on steel section assuming full interaction

AB′ – Measured on surface of concrete

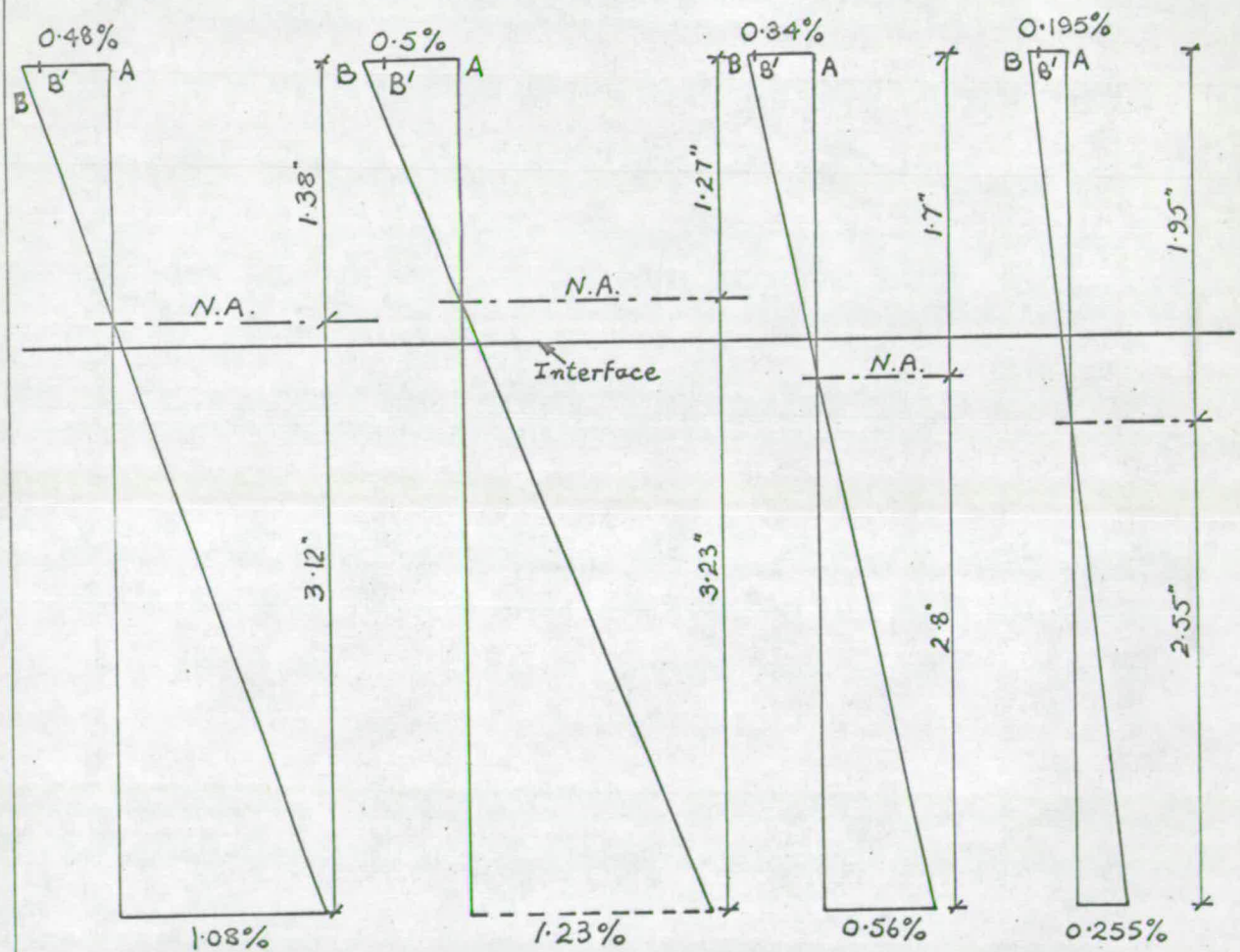

strain distribution near collapse in Model BI

FIG. 6·20

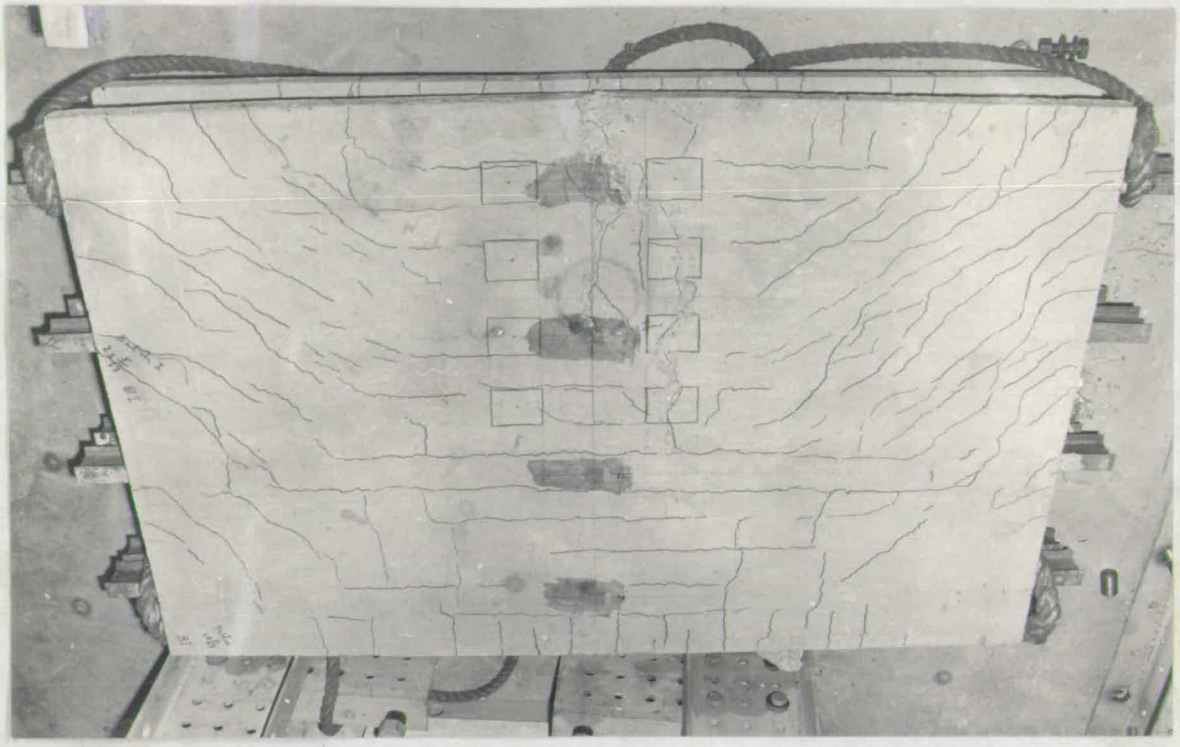

(i) Top

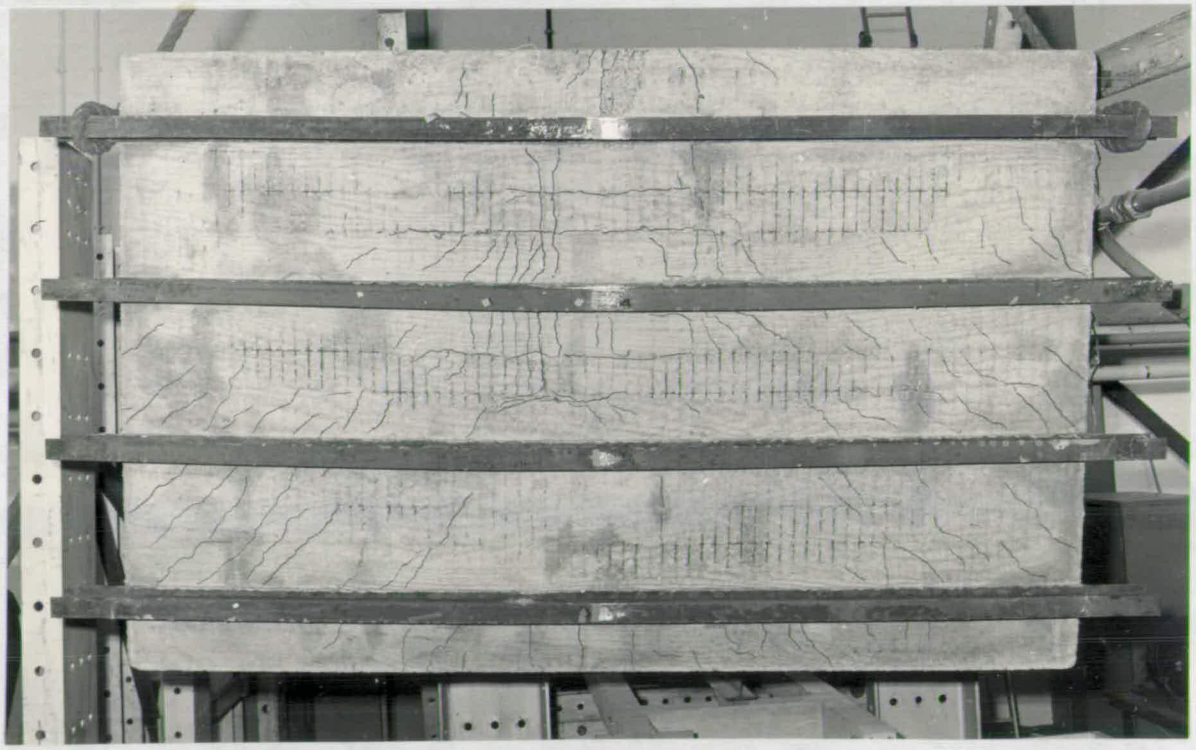

(ii) Bottom

FIG.6.20(a)Crack Pattern of Model BI after failure. compare with FIG·6·20(b)

TABLE 7·7a

Values of $\phi/2$, ψ and x for yield patterns

Model	Equivalent slab Method			Beam and slab Method			Experimental (Average)		
	$\phi/2$	ψ	x in	$\phi/2$	ψ	x in	$\phi/2$	ψ	x in
AI & AII	51°-34′	38°-26′	14·3	56°-18′	38°-42′	12	57°-0	34°-0′	12 to 15
AIII	33°-42′	26°-42′	11·3	32°-0′	23°-6′	"	32°-30′	25°-0′	10 to 12
BI	59°-24′	56°-30′	12·8	61°-0′	55°-0′	"	50°-0′	48°-0′	12 to 18
BII	58°-12′	54°-24′	14·0	60°-6′	53°-30′	"	50°-0′	50°-0′	12 to 18
BIII	56°-54′	53°-30′	13·7	60°-6′	53°-30′	"	51°-0′	50°-0′	12 to 14

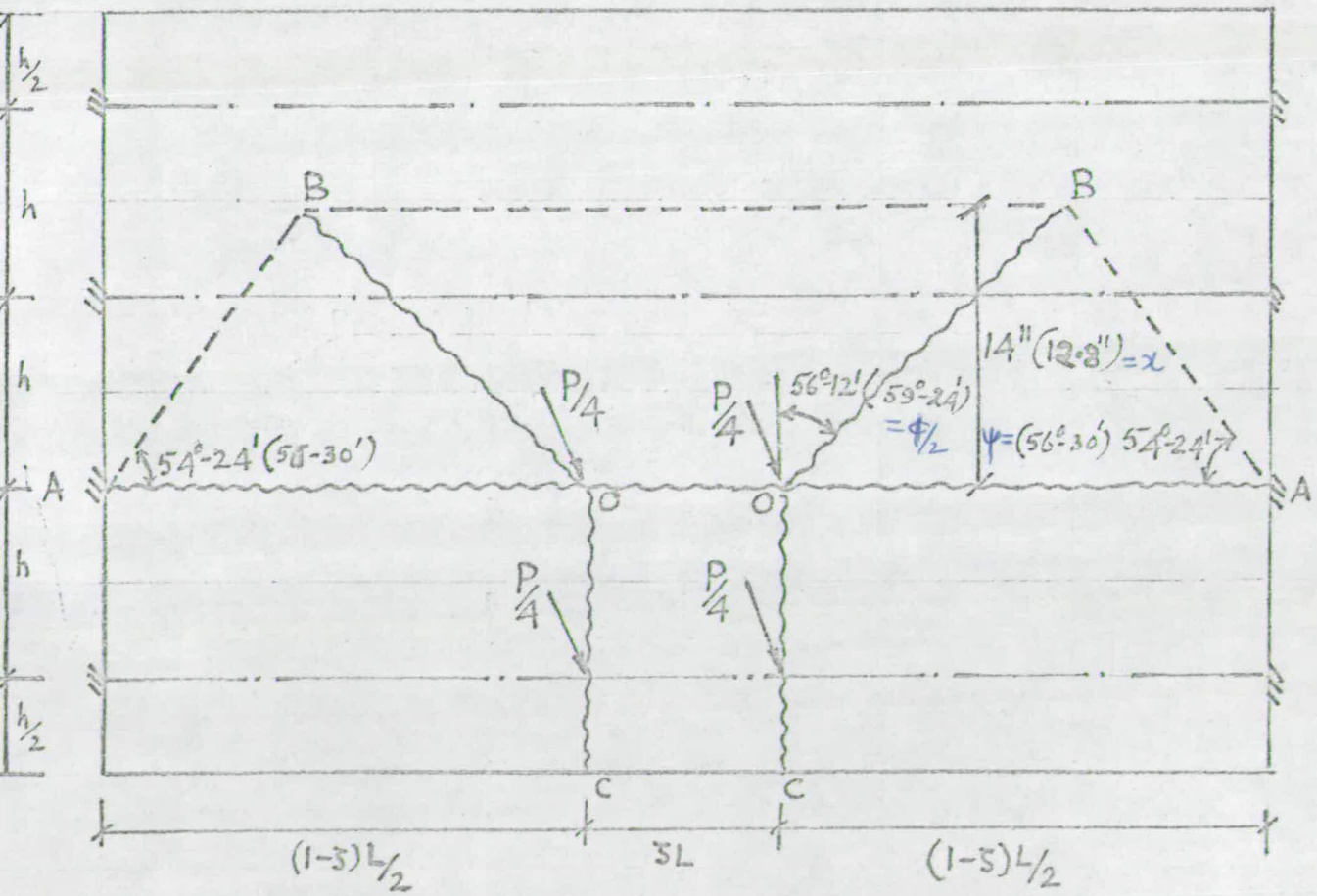

Model BII &(BI)

Theoretical yield pattern (Equivalent slab Method)

FIG·6·20(b)

loaded beams I and II. On the top of slab, crushing of concrete took place parallel to the line of loads. As the load was increased, the separation of the two loaded beams from the rest of the system became more evident as shown by the tension crack lines on the top of the slab. The bridge failed at 9.5 tons. The strain gauge readings indicated strain-hardening in the web of the beam and the bottom flange of the beam II.

The strain readings in the control beam as well as in the beams of the model (Fig. 6.17 and 6.19) show that there was compression in the top flanges of the beams in elastic range indicating less composite action perhaps caused by slip greater than expected at interface. This has slightly reduced the ultimate capacity of the control beam as well as the model.

6.4.6 Model B II

Load positions	:	Fig. 6.23(a)
cross section	:	Fig. 5.3(b)
Control Beam BIICB	:	Moment-Deflection curve Fig. 6.21
		Moment-Strain curve Fig. 6.22(a)
		View after failure Fig. 6.22(c)
Load-Deflection curve	:	Fig. 6.23(b)
Load-Strain curve	:	Fig. 6.24
Strain Distribution	:	Fig. 6.22(b)
Crack patterns	:	Fig. 6.24(a) & 6.20(b)

The loading is similar to that of Model B I except that the point loads over panels are omitted. The deformations and the manner of failure near ultimate load were almost identical to those of Model B I, though in the elastic range, its behaviour as revealed by the Load-Strain curves (Fig.6.24)

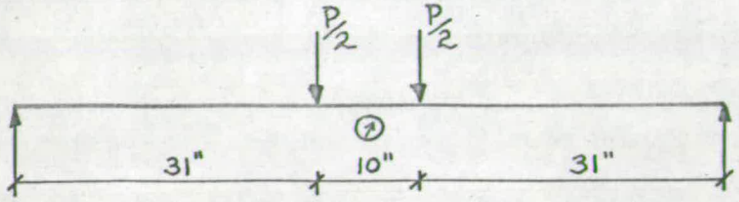

TEST ON
CONTROL BEAM BIICB

FIG. 6·21

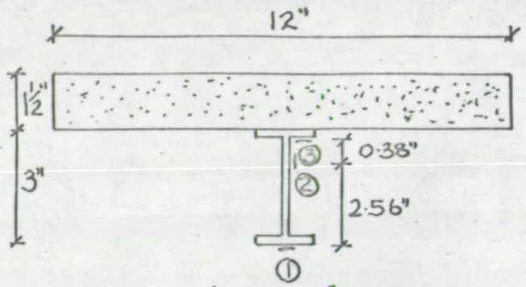

– Location of resistance gauges at mid span of CONTROL BEAM BIICB

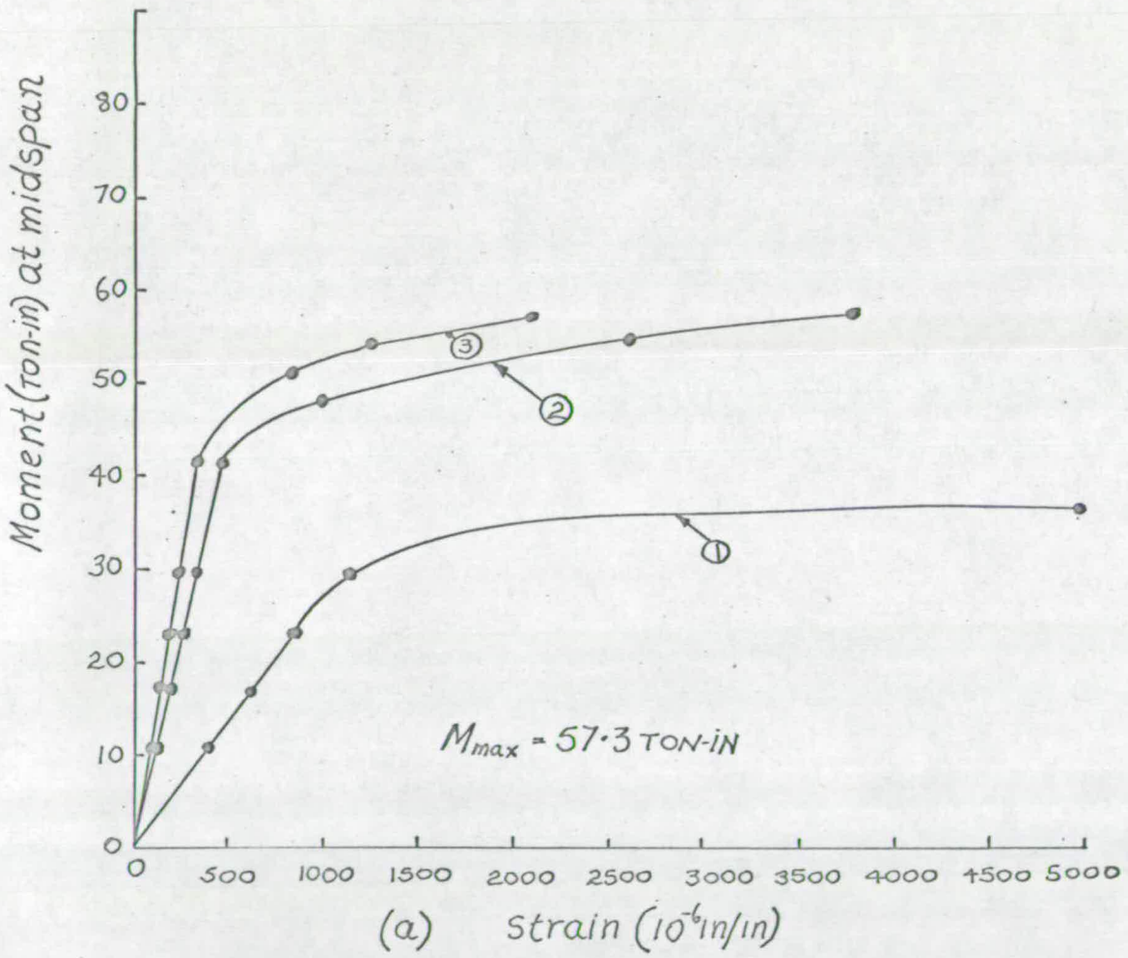

(a) Strain (10^{-6} in/in)

FIG. 6·22

AB- Deduced from strains on steel section assuming full interaction
AB'- Measured on surface of concrete

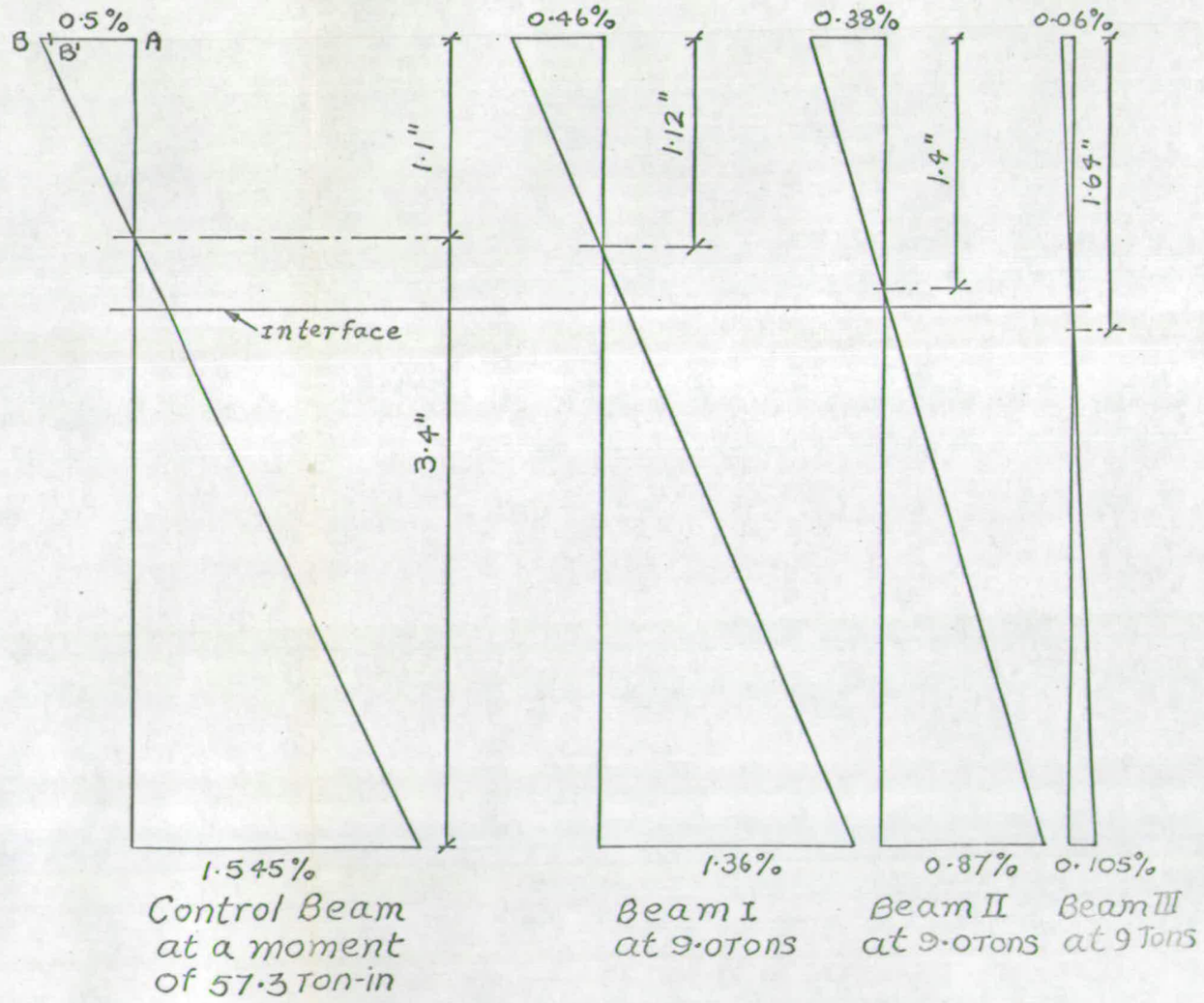

(b) strain distribution near collapse in Model BII

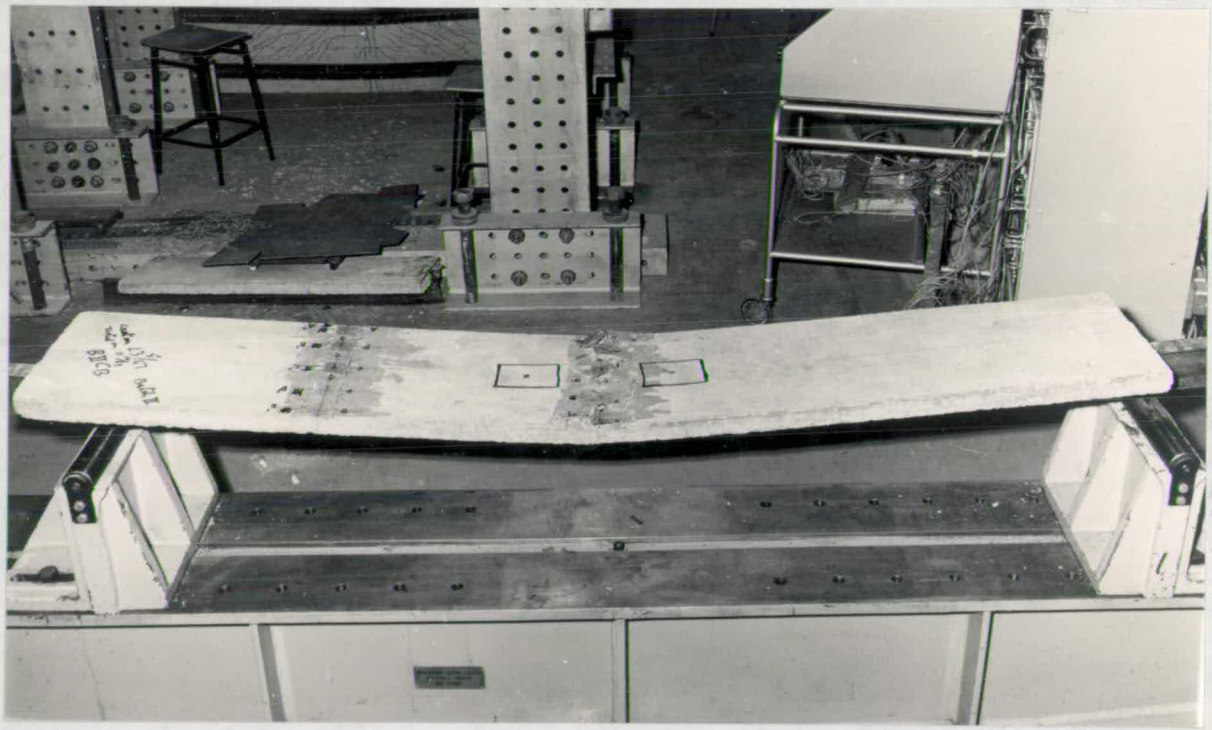

BIICB
FIG.6.22(c) Control Beam after failure

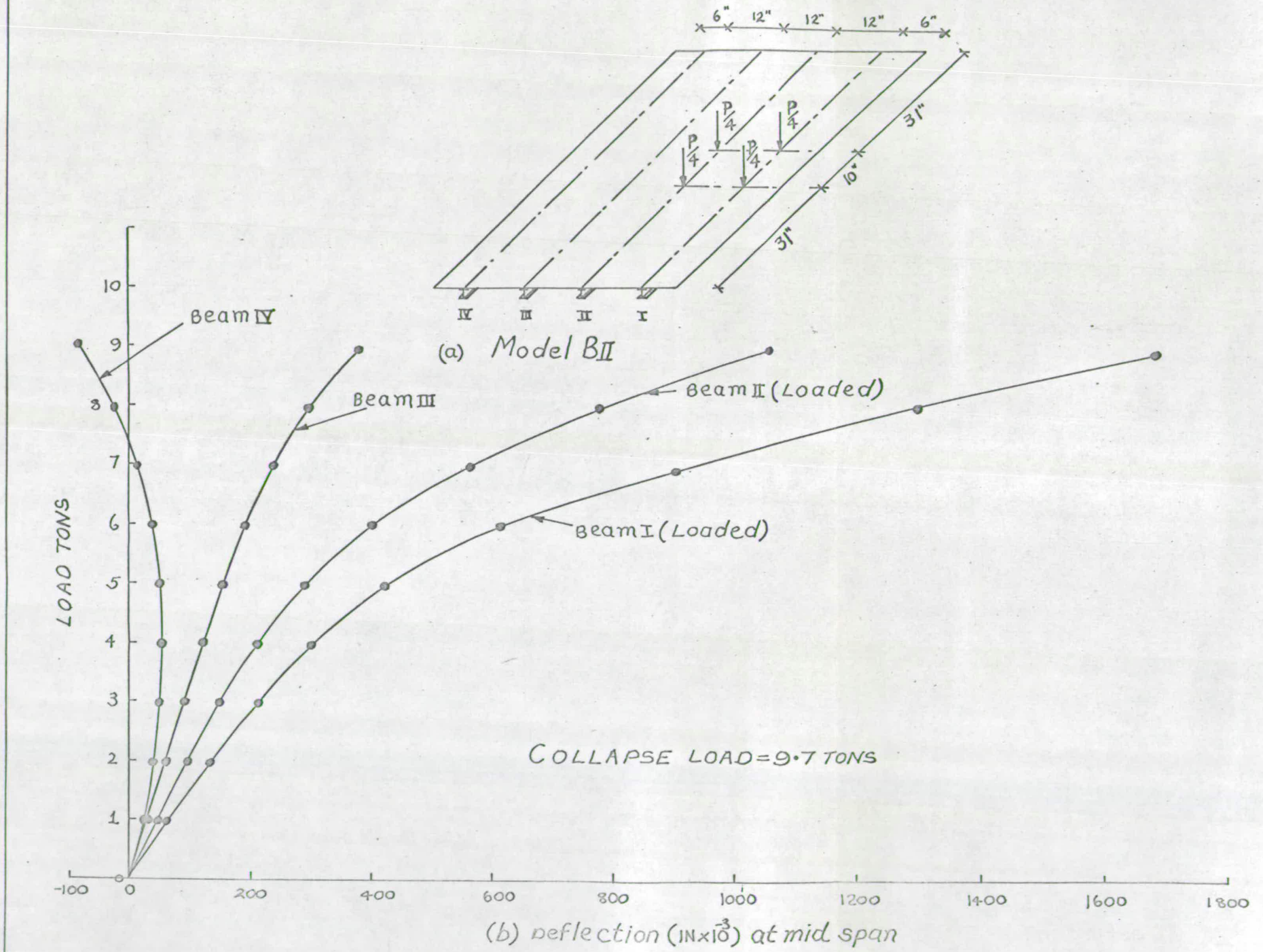
6"
12"
12"
12"
6"
P/4
P/4
P/4
P/4
31"
10"
31"
IV
III
II
I
(a) Model BII
LOAD TONS
Beam IV
Beam III
Beam II (Loaded)
Beam I (Loaded)
COLLAPSE LOAD = 9·7 TONS
-100
0
200
400
600
800
1000
1200
1400
1600
1800
(b) deflection (IN×10⁻³) at mid span

FIG. 6·23

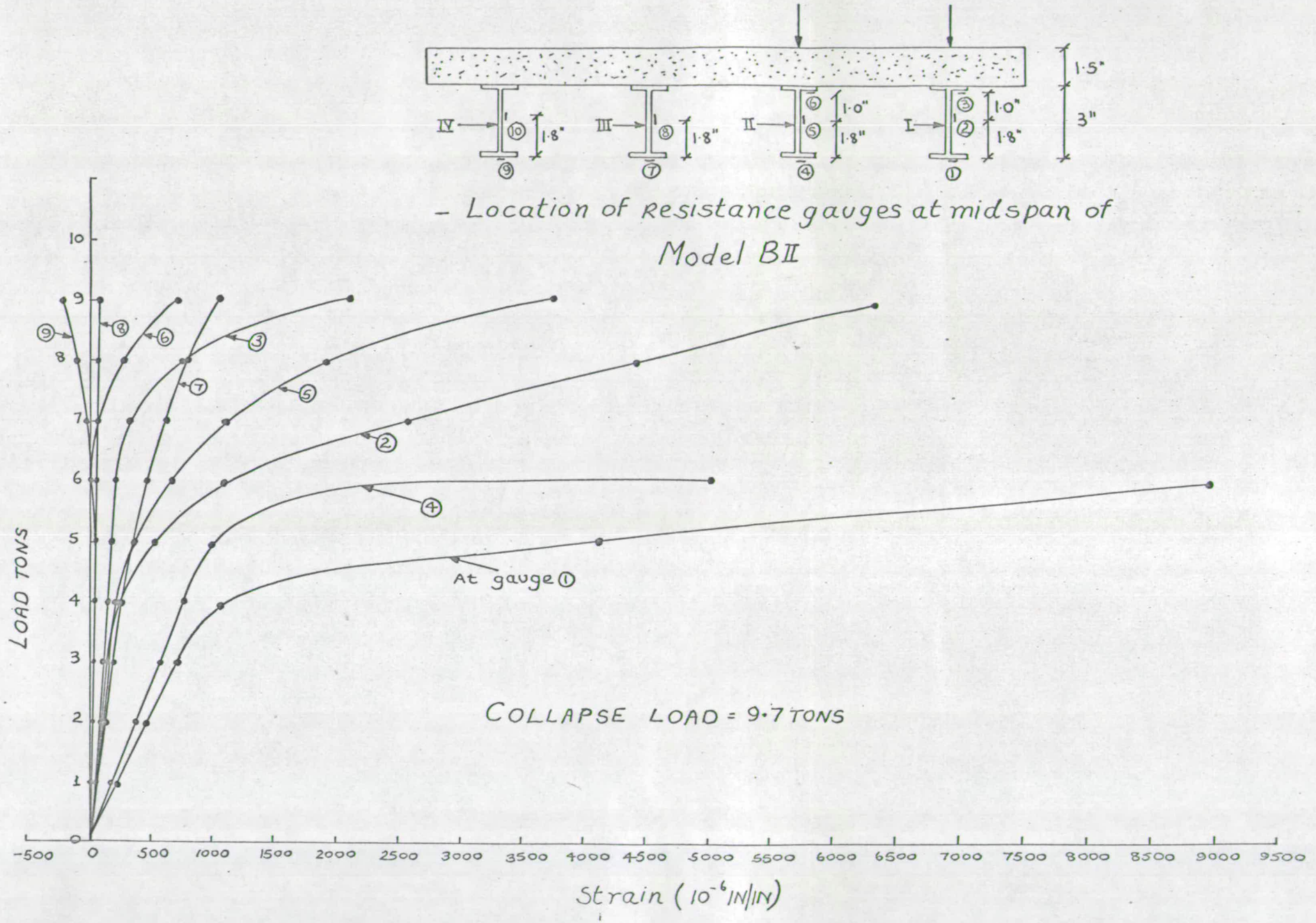

– Location of resistance gauges at midspan of Model BII

FIG. 6·24

(i) Top

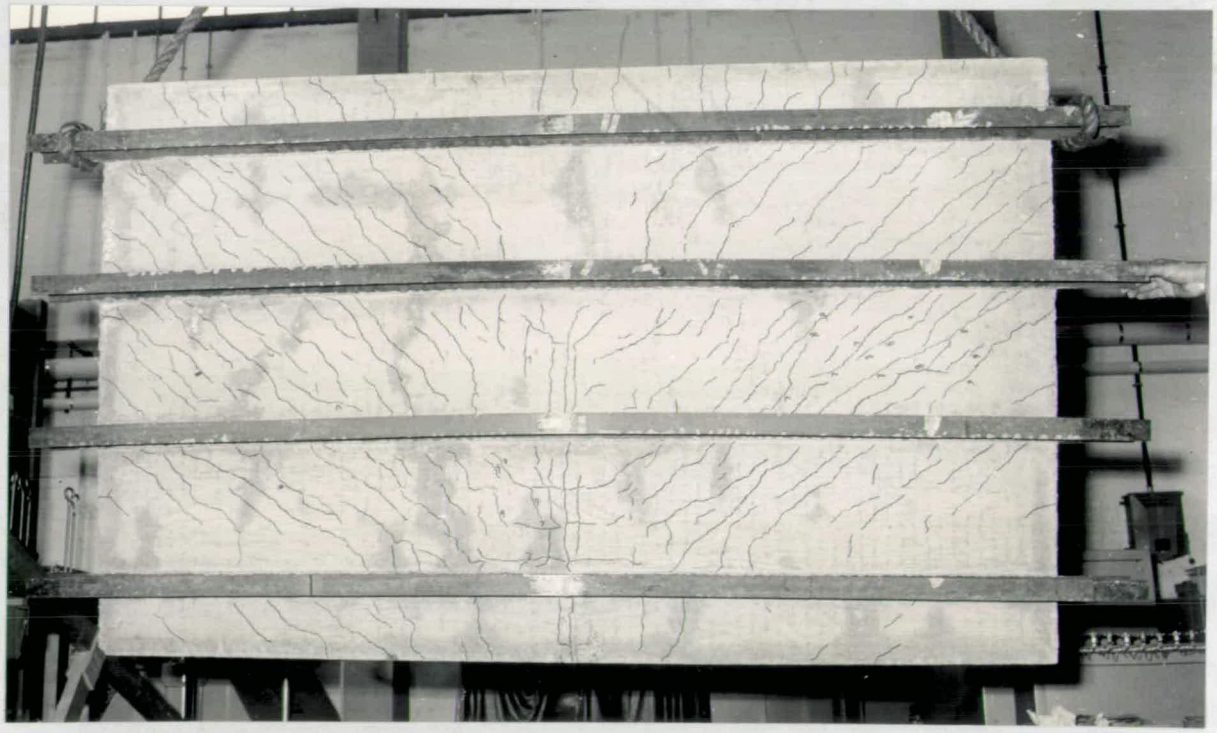

(ii) Bottom

FIG.6.24(a) Crack Pattern of Model BII after failure. compare with FIG.6.20(b).

was slightly different. In the absense of slip measurements, this might be attributed to the different amounts of slip that might have occurred in the two models.

6.4.7 Model B III

Load positions	:	Fig. 6.27(a)
Cross section	:	Fig. 5.3(b)
Control Beam BIIICB	:	Moment-Deflection curve Fig. 6.25
		Moment-Strain curve Fig. 6.26
		View after failure Fig. 6.26(a)
Load-Deflection curve	:	Fig. 6.27(b)
Load-Strain curve	:	Fig. 6.28(a)
Strain Distribution	:	Fig. 6.28(b) and 6.29
Crack pattern	:	Fig. 6.29(a) and Fig. 6.29(b) & 6.29(c)

The four-point loading was symmetrically applied over the central beams. The crack pattern is partly comparable with that of Model A I or A II. Punching through the slab did not occur in this case due to increased area provided by four distribution plates under the point loads. The loaded (inner) beams failed first transferring more load to the outer ones, which have also failed as the load was increased. A compression crack formed almost across the whole width of the bridge as seen in Fig. 6.29(b). Crushing of concrete was more pronounced on one side of the bridge than the other.

This might have been caused by loss of symmetry due to

(i) slight error in positioning the loads,

(ii) small variations found in the dimensions of the steel beams used in this model.

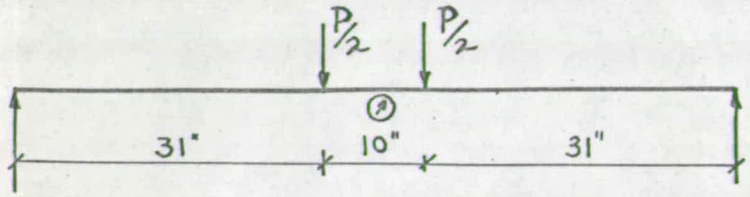

TEST ON
CONTROL BEAM BIII CB

FIG 6·25

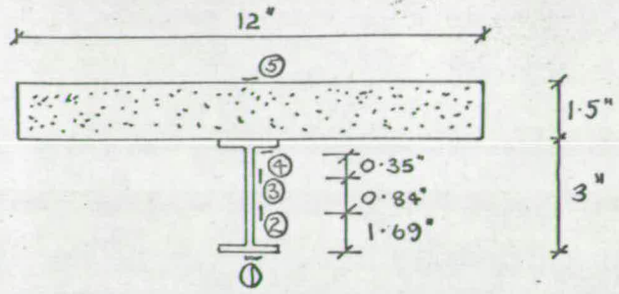

-Location of resistance gauges at mid span of CONTROL BEAM BIII CB

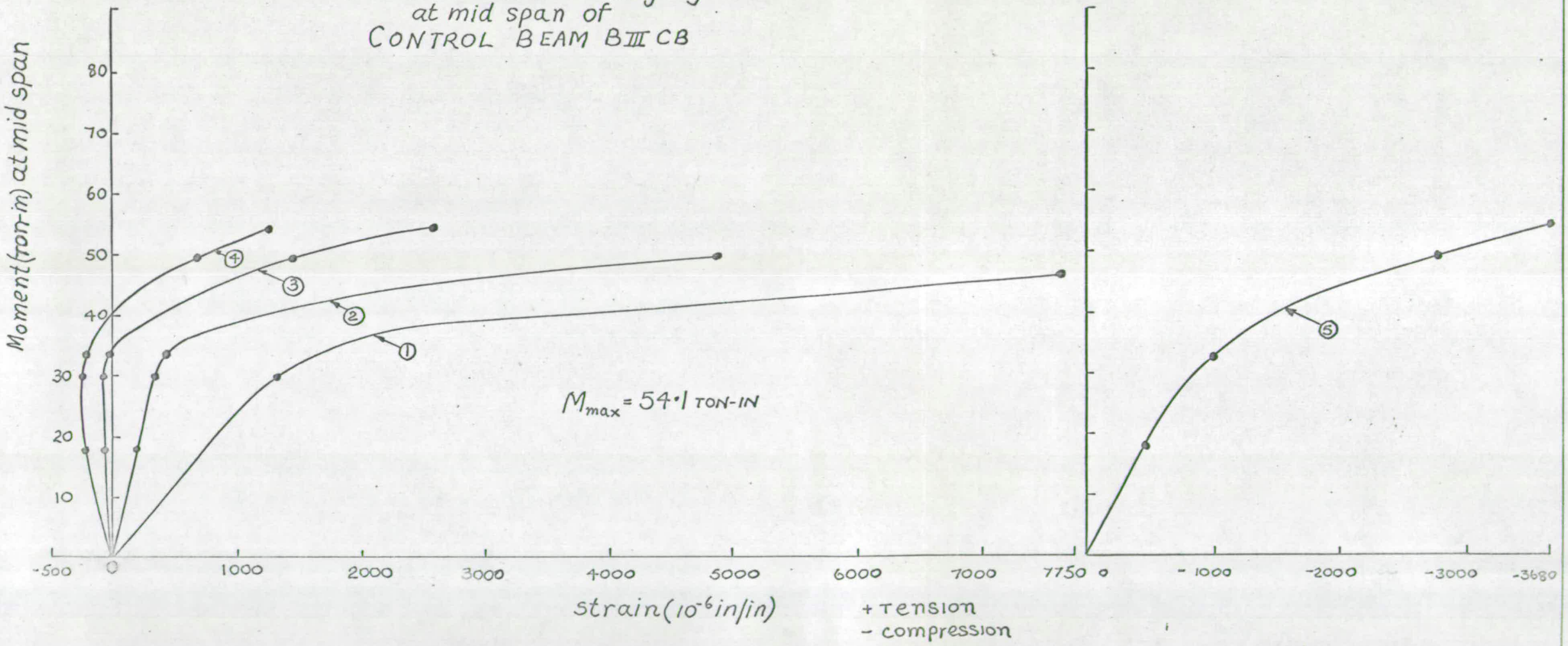

FIG 6·26

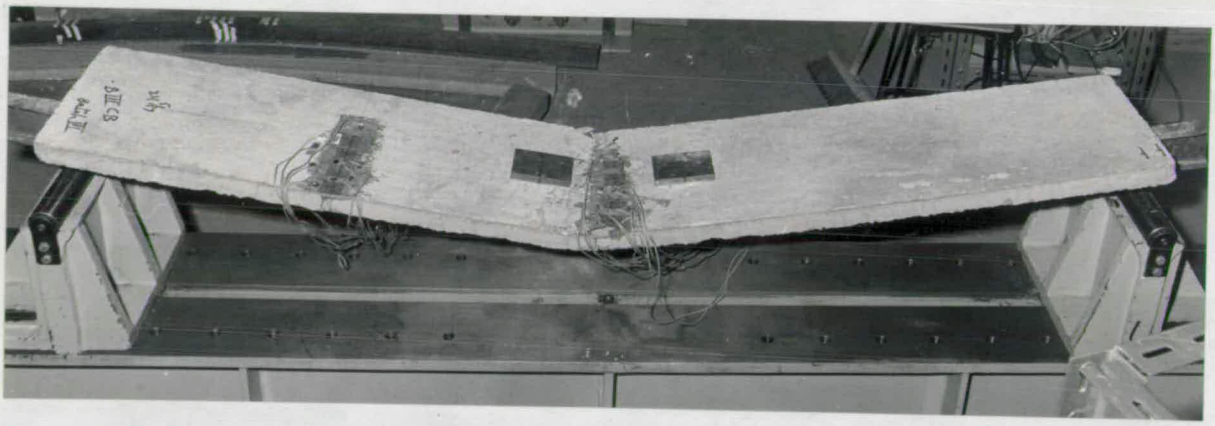

FIG.6.26(a) Control Beam BIIICB after failure

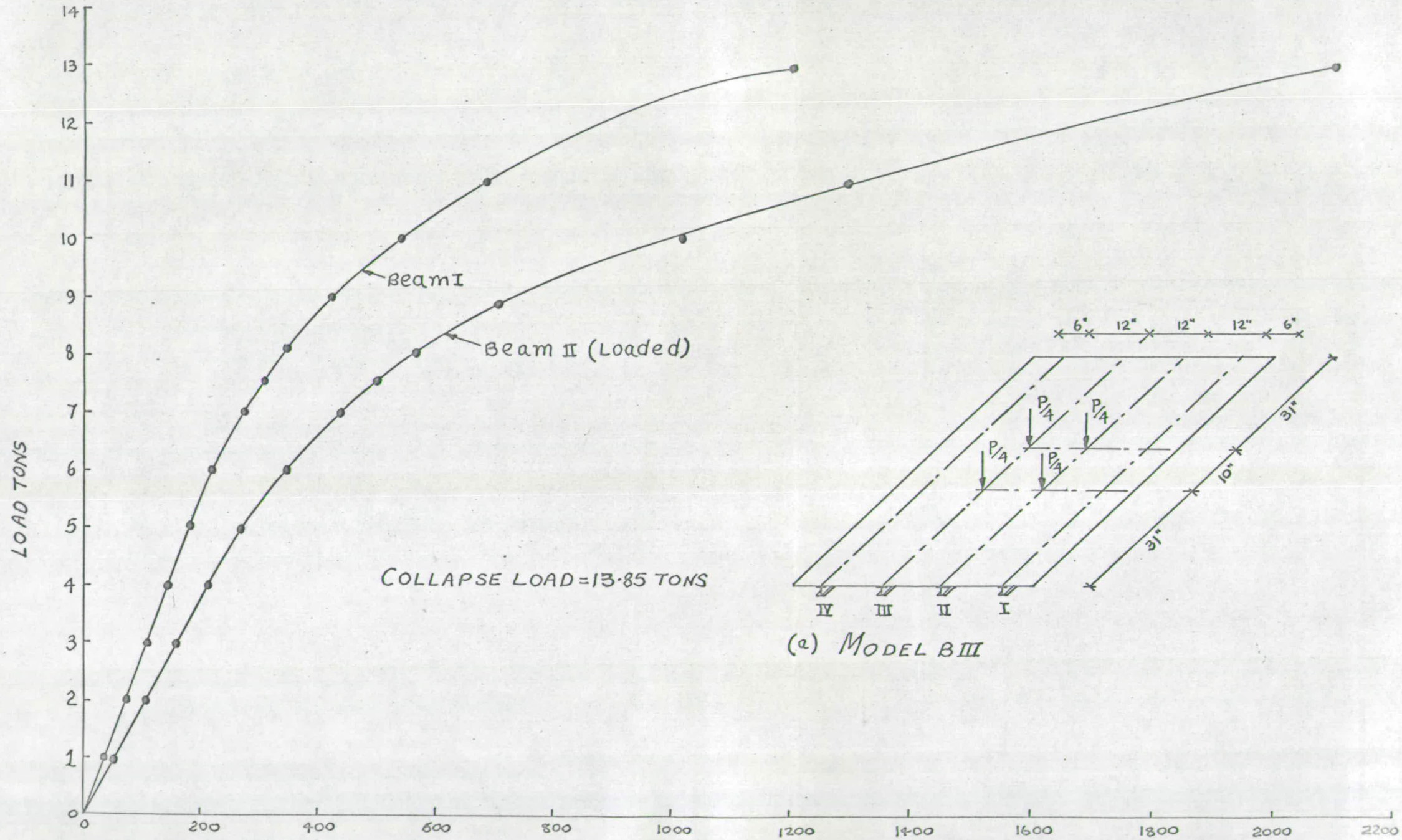

(a) MODEL B III

(b) Deflection ($in \times 10^{-3}$) at mid span

FIG. 6·27

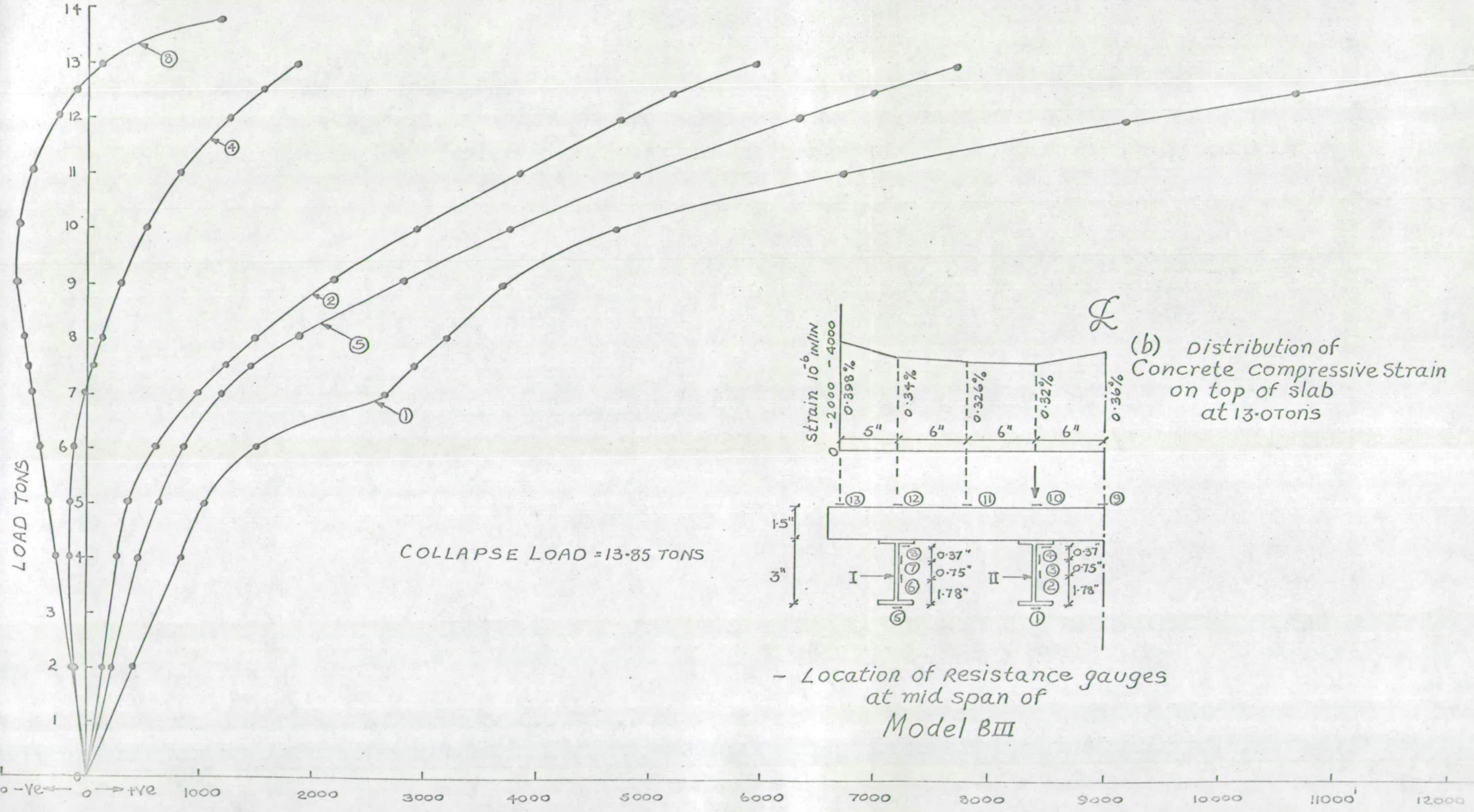

(a) Strain (10^{-6} in/in)

(b) Distribution of Concrete compressive Strain on top of slab at 13·0 tons

– Location of Resistance gauges at mid span of Model BIII

FIG. 6·28

AB - Deduced from strains on steel section assuming full interaction

AB' - Measured on surface of concrete

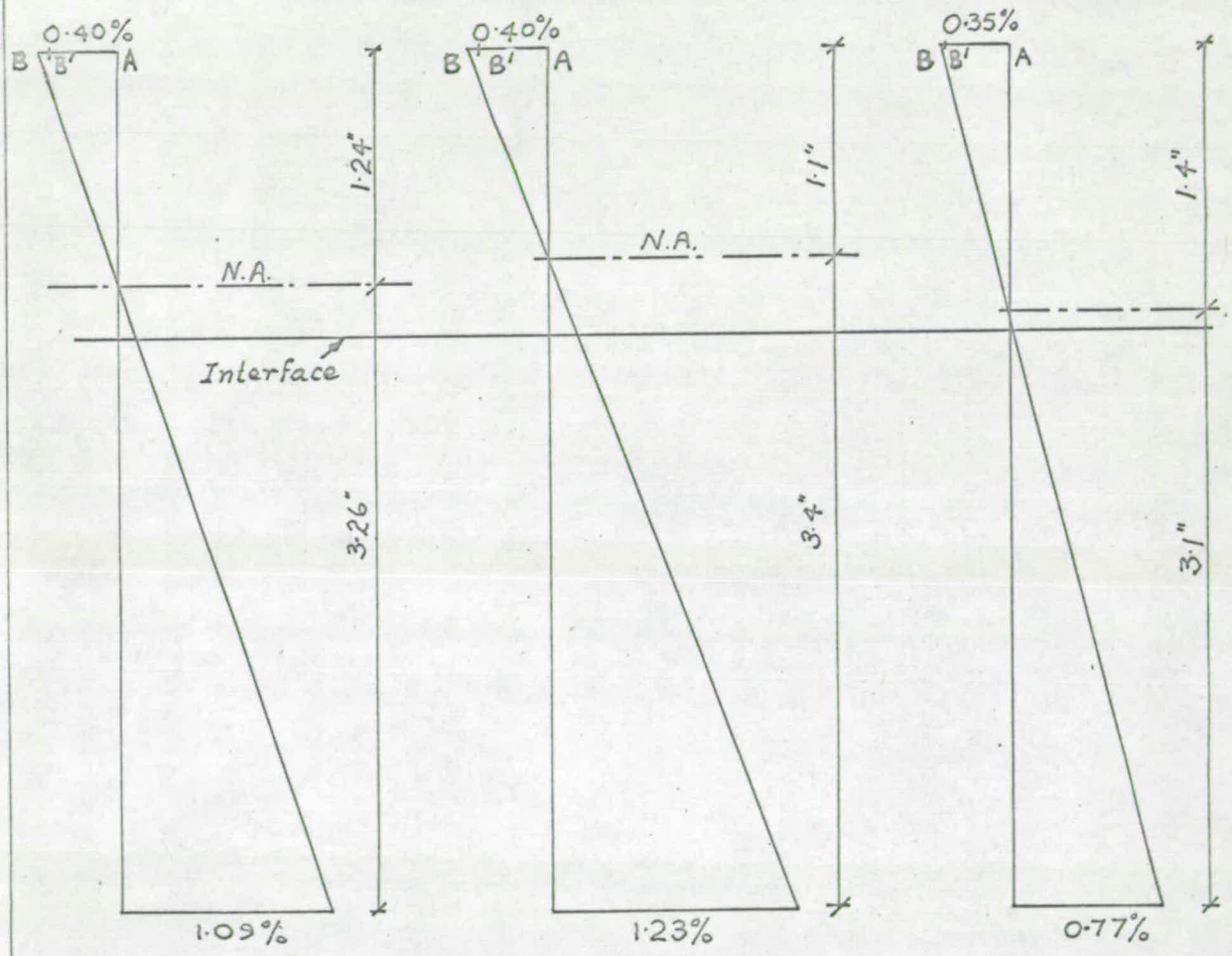

strain distribution near collape in Model BIII

FIG. 6·29

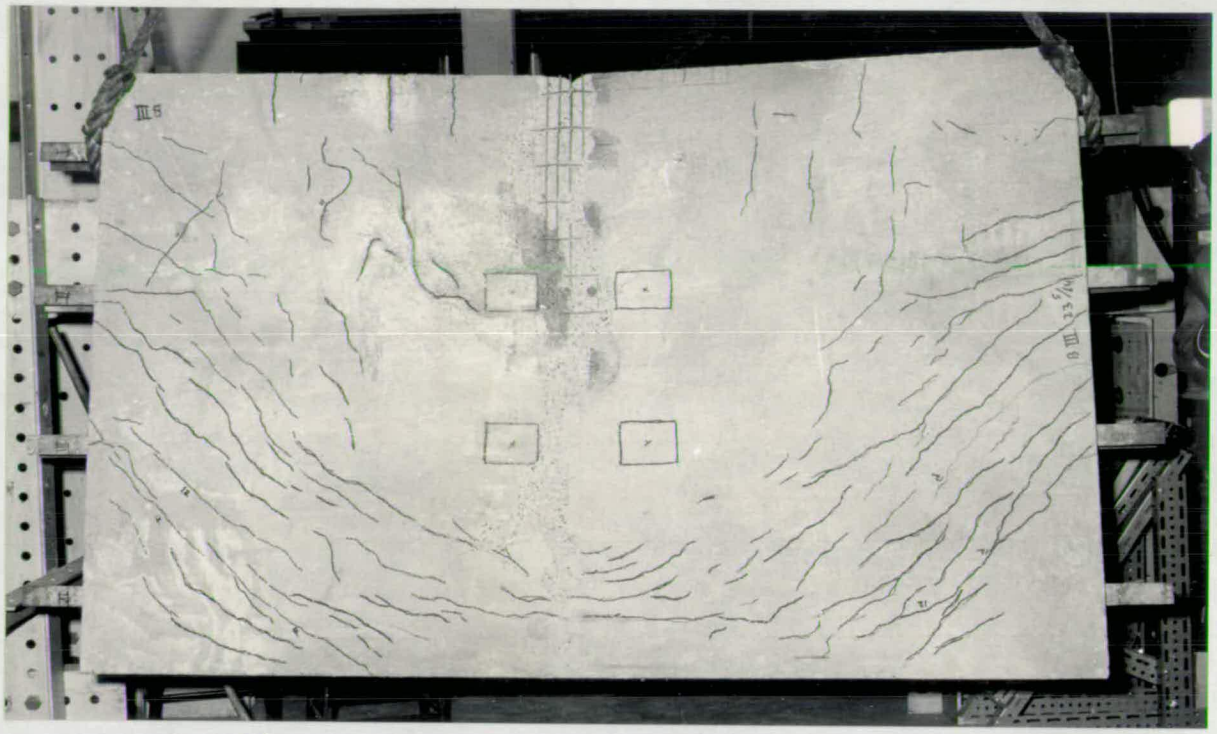

(i) Top

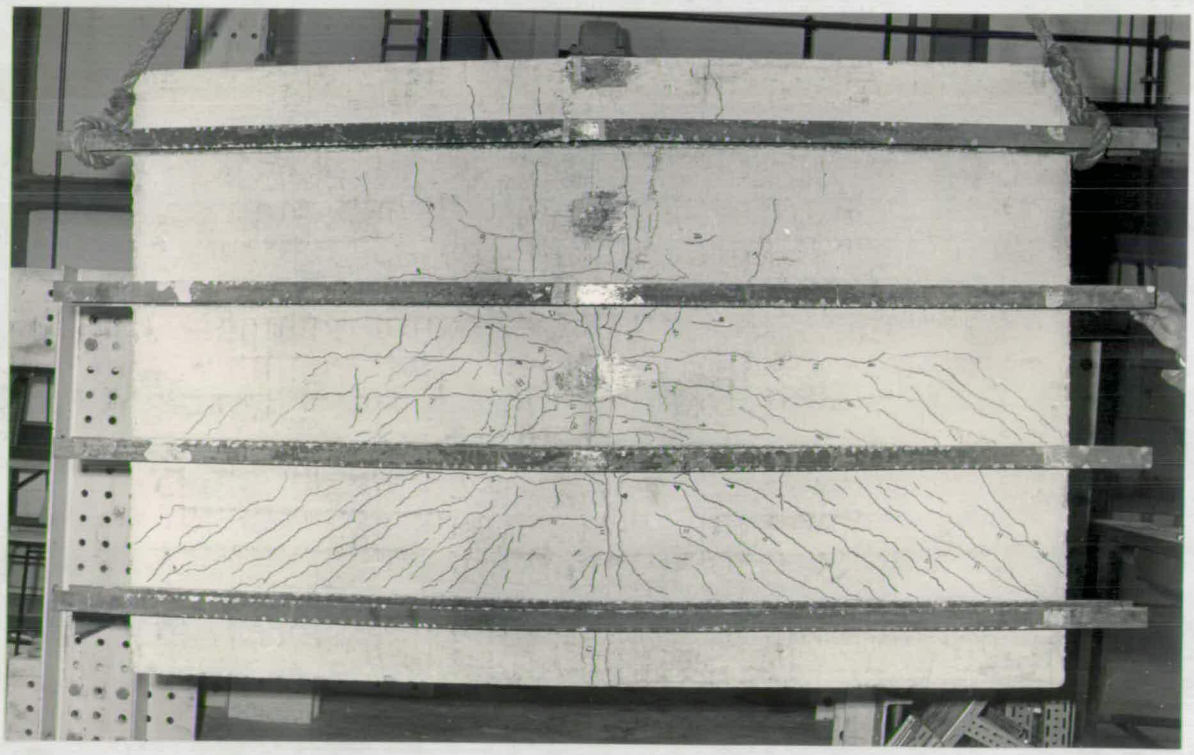

(ii) Bottom

FIG.6.29(a) Crack Pattern of Model BIII after failure. compare w
FIG·6·29(c

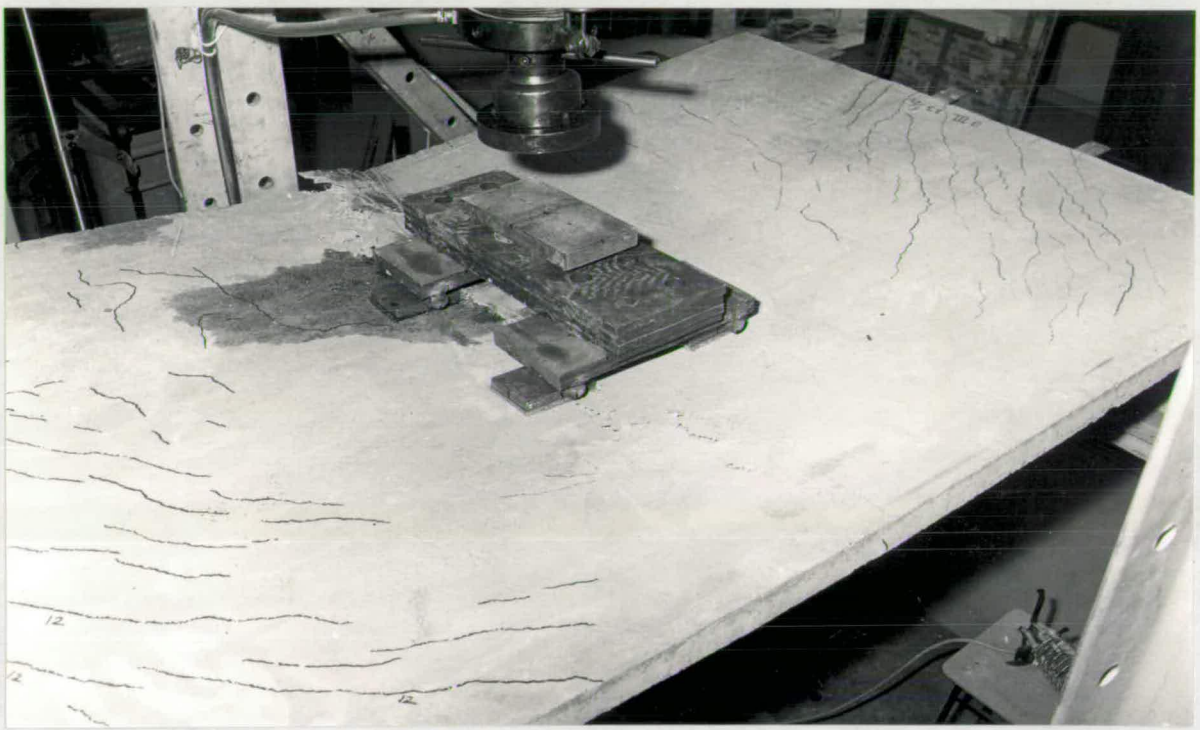

FIG.6.29(b) Top of Model BIII after failure

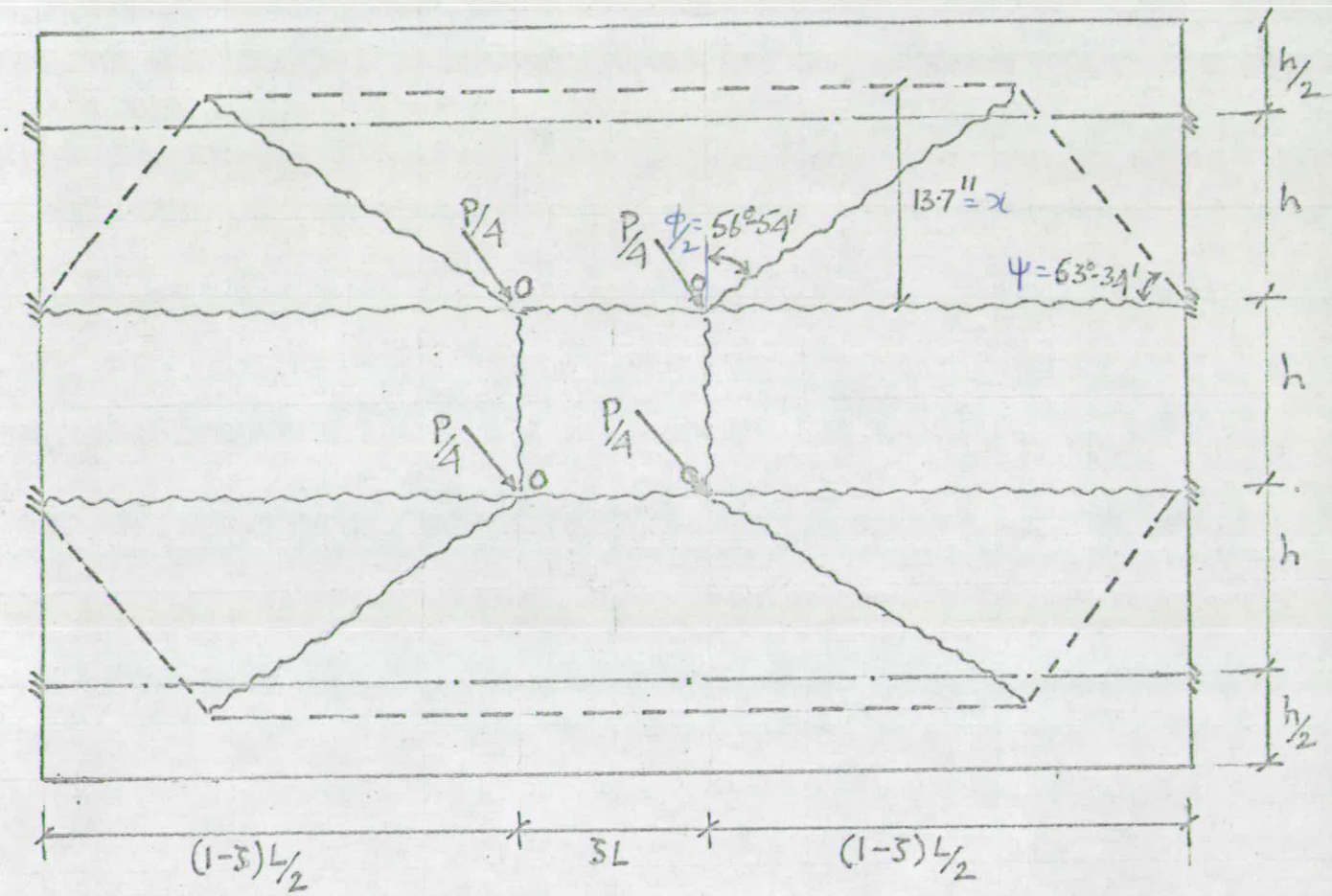

Model BIII
Theoretical yield pattern (Equivalent slab Method)

FIG·6·29(c)

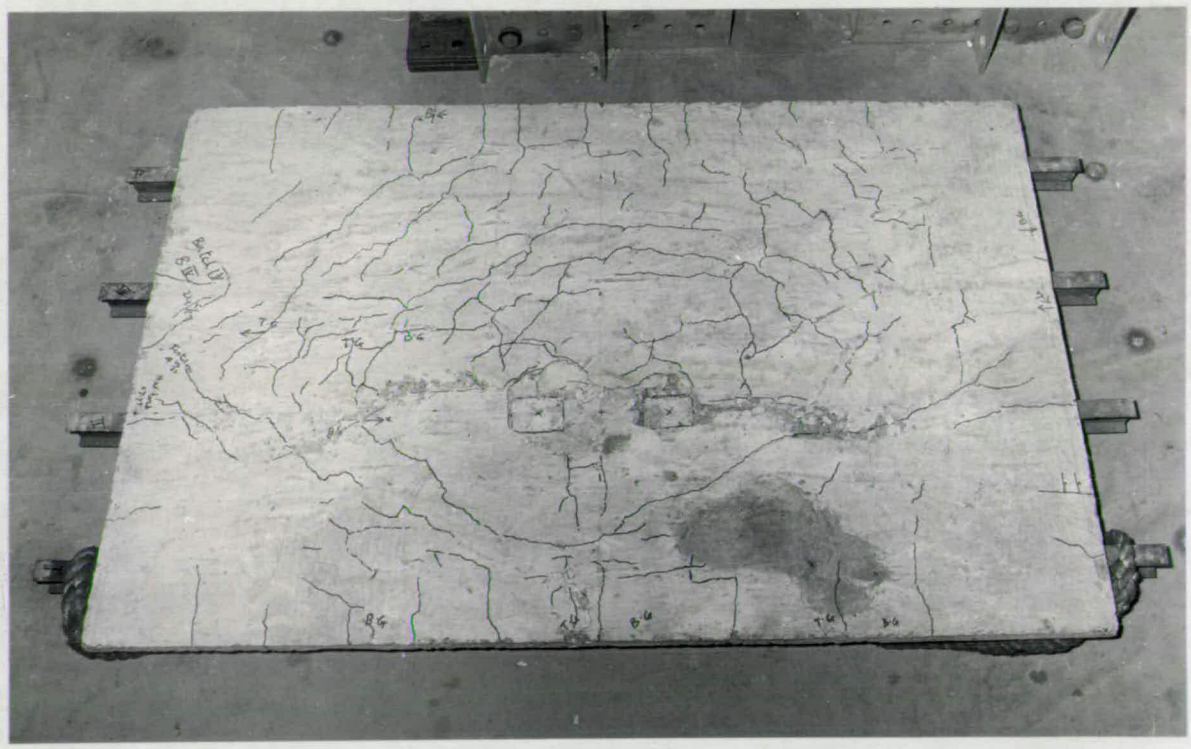

TOP

FIH.6.30 Crack Pattern of Model BIV after failure

(iii) strain-hardening of steel that had developed to different degrees in different beams.

However, for practical purposes it can be assumed that the bridge deck had failed across its whole width, resulting in Mode A, which is the desired one for maximum efficiency of a bridge deck. The failure load was 13.85 tons, the highest for all models tested.

6.4.8 Model B IV

cross section : Fig. 5.3(b)

crack pattern : Fig. 6.30

This test was planned to investigate if the punching of slab that had been observed in the tests on Models AI and A II could be prevented by two-point loading. Two point loads 10" apart were applied symmetrically at mid span of the inner beam as marked in Fig. 6.30. The crack pattern developed at failure was similar to that observed in Model A I and A II. The failure load was 8.6 tons.

This model was cast using the concrete from the same batch as Model BIII. Therefore the sectional properties of Model B III are used in calculating the ultimate load of Model B IV.

CHAPTER 7

DISCUSSION OF TEST RESULTS

7.1 Introduction

The applicability of yield-line theory to a composite steel-concrete structure mainly depends on the quality of steel used. The quality of the concrete has no measurable effect since the slabs have to be lightly reinforced so that only the yield point of the steel is the decisive factor. However, it should be kept in view that the concrete should not be too weak to affect the load-slip characteristics of the shear connectors (89), which may result in splitting along the line of the connectors. This had been observed in Model A IV which was cast in concrete of lower strength.

The steel used in beams of Models of A-series, had developed strain-hardening to a considerable extent as shown in Fig. 5.4(a). Tests indicate that strain-hardening has a beneficial effect on the ultimate capacity of a structure, though it complicates the analysis.

For high strength steel without a marked yield point, the stress-strain curve as seen in Fig. 5.4(b) has relatively shorter horizontal portion than ordinary mild steel. This curve, of course, represents an extreme case because steel, which is more work-hardened than the steel mesh used in the tests, is not used in practice. In such cases, an ultimate load analysis for simple structures is, no doubt, permissible, though this is not on a par with the response of steel structures to idealised plastic theory (21).

6 The pattern of yield lines that may develop in a beam and slab system largely depends on

(i) System of reinforcement,

(ii) Spacing of beams,

(iii) Support conditions,

and (iv) type of loading.

In the present tests, the system of reinforcement, spacing of beams and support conditions are kept the same in every model, the only variable being the type of loading. Therefore the whole discussion now centres round the behaviour of the test specimens under different loading conditions.

7.2 Degree of composite action

In the present investigation, it is assumed that complete interaction between the beam and slab up to failure is achieved by the provision of adequate number of mechanical shear connectors. It is important at the outset to verify how far this assumption is realised in the tests since the entire theory for predicting the maximum ultimate moment of a composite beam is simplified by this basic assumption.

The useful ultimate capacity of a stud shear connector (56) can also be computed from the following formula:

For $h_s/d_s \geq 4.2$,

$$Q_{uc} = 330\, d_s^2 \sqrt{f'_c} \qquad \ldots\ldots\ldots\ldots\ldots\ldots \quad (7.1)$$

For $h_s/d_s \leq 4.2$,

where Q_{uc} = useful ultimate capacity of one stud, lbs.

d_s = stud diameter, in.

h_s = stud height, in.

For a stud connector used in the Test Specimens, the minimum value of useful ultimate capacity works out to be 3200 lbs or 1.43 tons.

The design value of one shear connector as per C.P.117, part 1 (73)

works out 1.64 tons, for the ultimate capacity of 2.05 tons found from the tests (Table 5.1). Using the formula (5.1) and the details given in Tables 5.2 and 5.3, the actual maximum shear force to which a shear connector is likely to be subjected works out to be 1.32 tons. The slip corresponding to this load from the graph given in Fig. 5.2 is 26 x 10^{-4} in. This is much less than the suggested safe value (91) at which full interaction could be assumed without introducing any appreciable error in the calculation of maximum moment.

7.3 Behaviour of Control Beams and Slab Strips

Tests of all the Control Beams, except the Control Beam B I CB, gave the values of ultimate moments higher than the theoretical ones. The gap between theory and test was as high as 30 per cent in the beams of A-series and 20 per cent in B-series, even after allowance was made for the effect of strain-hardening in the theory. This was expected because of the limit put on the maximum value of concrete edge strain e_{cu} at maximum moment (Equation 3.10) The theoretical values of e_{cu} varied from 0.318 to 0.334 per cent for different strengths of concrete used against the experimental values which varied from 0.35 to 0.50 per cent.

Permitting higher values of e_{cu} observed in tests, this gap could be made as small as possible, but how far this is justified is in doubt because of many uncertainties inherent in the strain-hardening nature of steel and the strain-softening nature of concrete.

In the case of control beam B I CB, the experimental value is slightly less than the theoretical one. This might be attributed to the presence of slip greater than expected, possibly caused by defective welding of shear connectors in this particular beam.

The ultimate moments of slab strips obtained from tests generally agree with theoretical values which were on safe side.

7.4 Behaviour of beams in models

First yielding of the beams was characterised by an abrupt change in the slope of load-strain curves. Yielding occurred first in the loaded beam and was shortly followed by large deflections. With further increase of the load, yielding penetrated deeper into the steel section of the loaded beam and spread to the adjacent beams.

In the case of Model A I and Model A II, yielding did not reach through the entire cross-section of the loaded beam, though strain-hardening had commenced in the bottom flange and deflections were increasing fast. Yielding occurred in the bottom flanges of outer beams but did not penetrate deeper into the steel sections. Their deflections at mid span were just beginning to increase non-linearly. In other words, the outer beams were still acting as strong supports to the slab, when the failure of the bridge occurred.

In the case of Model A III, yielding reached through the entire cross-section of the loaded (outer) beam while strain-hardening was taking place in the bottom flange and web. Yielding had penetrated nearly half the depth of the steel section of central beam. The outer (unloaded) beam was far from yielding stage and deflected upwards at mid span, hinging on supports which were anchored down.

The behaviour of individual beams in B-series was similar to that in A-series, under similar loading but the behaviour of the Models was, to some extent, different in some cases.

In the Models B I and B II which are comparable to the Model A III in

the type of loading, the outer beams (unloaded) were far from yielding stage and deflected upwards as in Model A III. In the Model B I, which is comparable to the Models A I and A II in the type of loading, there was no punching of slab and the beams (unloaded) have also failed at ultimate load which was not the case with the Models A I and A II. This will be further discussed in section 7.6.

The notable feature in all the models tested was that the outer beams, when loaded, produced relatively larger strains and deflections than the loaded central beams at their corresponding sections at failure. The loaded beams, whether inner or outer, had tended to separate from the rest of the bridge deck near ultimate load. In all the tests, the loaded beams had failed first and the beams immediately next to them had failed or nearly failed. The beams, two spacings away from the loaded ones, were not much affected.

7.5 Behaviour of Slab in Flexure

The cracks in the slabs in majority of the tests, were not wide open since the reinforcement in the slab consisted of steel with high yield strength and low elongation. There were many small cracks by the side of larger ones. The assumption that full moment of resistance is developed along the yield lines was not realised in some tests namely on the models where the ends of unloaded beams were not anchored down to prevent their lifting up due to eccentricity of the load applied. Even where the ends of a beam were anchored down, there was rotation of its cross section at mid span as the I-section is torsionally weak. Only in Model A III, where the two unloaded beams were firmly anchored down, there was a negative yield line along which full moment could be assumed to have been developed. The positive yield lines were also

well formed in this case as seen in Fig. 6.15(a).

7.6 Punching of slab

The load distribution plate 4" x 4" x $\frac{1}{2}$" size had punched through the slab in Model A I and A II, where the loading consisted of a point load applied at mid span over the central beam. The probable causes for this punching are:

(i) inadequate size of distribution plate under the point load,

(ii) stress concentration under the loaded area subjected to high vertical shear,

and (iii) any vertical separation of the slab from the steel joist.

In later tests, the causes (i) and (ii) were removed by applying two-point loading, which was distributed over a relatively larger area and provided a region of no shear between the load points. There was no punching of slab in Models A IV and B IV, which were subjected to similar loading.

The size of the distribution plate was determined from the condition that the punching load computed using the formula (4.25) was not less than the maximum ultimate load of the bridge deck in flexure.

Laboratory tests (81, 83) indicate that when a single load was placed over a panel, failure occurred as a result of punching shear, i.e. by separation from the slab of a truncated conical section. In Model B I, the loads over the panels were accompanied by loads over the joists and there was no punching of slab.

7.7 Sectional Properties

7.7.1 Control beams

The sectional properties of control beams calculated using the formulae

derived in Chapter 3 are presented in Table 7.1.

7.7.2 Model bridges tested by the author

The properties of model bridges calculated using the theoretical ultimate moments of beams and slab elements are presented in Table 7.2. The values of m and μ m are computed from the formula (2.1b).

7.7.3 Model bridge tested by others (Model SG_5)

The properties of a composite beam bridge tested by Short and Thomas (83) are calculated assuming a cube strength of 5000 p.s.i. for the concrete and yield point of 40000 p.s.i. for the steel. They are presented in Table 7.3.

7.8 Calculation of ultimate loads of Bridge models

The Figures showing the módes of collapse considered for each model and the appropriate formulae derived in Chapter 4 are presented in Table 7.4 for ready reference.

7.8.1 Formulae for Model A IV and B IV

For Model A IV and B IV, the formulae for ultimate loads are obtained by modifying the expressions derived for Model B III to suit the loading conditions and the number of longitudinals.

Model A IV $\quad i_1 = 0, \quad i_2 = 0$ and $\beta = 5/36$.

(a) Equivalent slab Method

$$P_A = \frac{12\mu_e m}{(1-\beta)} \qquad \ldots\ldots\ldots\ldots\ldots\ldots\ldots\ldots \quad (7.1)$$

$$P_B = \frac{4\sqrt{\mu_i (3-4\beta)}\, m}{\sqrt{4(1-\beta)^3 - 1}} \qquad \ldots\ldots\ldots\ldots\ldots\ldots\ldots\ldots \quad (7.2)$$

(b) Beam and slab Method

TABLE 7.1

Sectional Properties of Control Beams

Control Beam	A I CB	A II CB	A III CB	B I CB	B II CB	B III CB
Cube strength C_u, p.s.i.	5227	5096	6290	5130	6270	5600
cylinder strength, f'_c p.s.i.	4450	4320	5340	4370	5310	4750
Effective width, B_e, inches	10.32	10.31	10.36	10.31	10.36	10.33
Neutral axis depth from top of slab, inches	1.29	1.30	1.21	1.31	1.01	1.10
concrete edge strain, e_{cu} (10^{-2} in/in)	0.332	0.334	0.318	0.333	0.318	0.327
steel edge strain e_e (10^{-2} in/in)	0.828	0.822	0.865	0.992	1.097	1.016
Curvature at mid span (in^{-1} x 10^{-4})	25.77	25.68	26.29	29.45	31.46	29.85
Lever arm, inches	2.94	2.96	2.87	2.55	2.57	2.53
strain-hardening stress, f_s, Tsi	3.03	3.00	3.19	0	0	0
steel force, T, Tons.	20.12	19.89	21.49	17.93	18.41	18.41
Ultimate moment M_c, Ton-in.	59.22	58.81	61.75	45.89	47.32	46.57
condition of steel section at failure	partly elastic	partly elastic	partly elastic	partly elastic	Fully plastic	Fully plastic
Experimental ultimate load P_{max}, tons	4.04	4.07	5.41	2.96	3.7	3.5

TABLE 7.2

Properties of Model bridges

Model	M_c Ton-in.	m Ton-in/in	$\mu m = \mu' m$ Ton-in/in	$\mu = \mu'$	μ_e (Eq. 4.3)	$\mu_s = \frac{\mu + \mu'}{2}$	$\mu_i = \frac{\mu_e + \mu'}{2}$	$\sqrt{\mu_i}$	$\frac{\sqrt{\mu_i}}{\mu_e}$
A I	59.22	0.557	0.315	0.566	8.969	0.566	4.77	2.18	0.243
A II	58.81	0.555	0.309	0.557	8.878	0.557	4.72	2.17	0.245
A III	61.75	0.61	0.328	0.539	8.474	0.539	4.51	2.12	0.25
A IV	48.69	0.445	0.252	0.567	9.18	0.567	4.87	2.20	0.239
B I	45.89	0.556	0.313	0.563	6.95	0.563	3.76	1.94	0.278
B II	47.32	0.624	0.335	0.535	6.38	0.535	3.46	1.86	0.29
B III	46.57	0.580	0.319	0.55	6.77	0.55	3.66	1.91	0.282
B IV	46.57	0.580	0.319	0.55	6.77	0.55	3.66	1.91	0.282

TABLE 7.3

Properties of Model bridge tested by Short and Thomas

Model	C_u p.s.i.	M_c Ton-in.	M_{ce} Ton-in.	m Ton-in/in	μm Ton-in/in	$\mu' m$ Ton-in/in	$\mu_s = \frac{\mu + \mu'}{2}$	μ_e	$\sqrt{\mu_i}$
S G_s	5000	582	435	1.2	0.54	0.22	0.317	13.6	2.62

TABLE 7.4

Modes of collapse and formulae for ultimate loads

Model	i_1	i_2	ζ	Equivalent slab Method		Beam and slab Method	
				Modes shown in Figures	Formulae given in section	Modes shown in Figures	Formulae given in sections
A I	0	0	0	4.6 to 4.9	4.3.1	4.26, 4.27	4.4.1
A II	0	1	0	4.6 to 4.9	4.3.1	4.26, 4.27	4.4.1
A III	1	0	1/6	4.11 to 4.13	4.3.2	4.28, 4.29	4.4.2
B I	0	0	1/6	4.24 to 4.25	4.3.5	4.32, 4.33	4.4.5
B II	0	0	5/36	4.20 to 4.22	4.3.4	4.32, 4.33	4.4.4
B III	0	0	5/36	4.15 to 4.18	4.3.3	4.30, 4.31	4.4.3

$$P_A = \frac{12 M_e \, m}{(1-\zeta)} \qquad \ldots\ldots\ldots\ldots\ldots\ldots\ldots\ldots\ldots\ldots \quad (7.3)$$

$$P_B = \frac{4M_c}{(1-\zeta)L} + 2\left[\frac{4M_s \rho}{(1-\zeta)} + \frac{1}{\rho} - \frac{1}{2\rho(1-\zeta)} + \frac{1}{4\rho(1-\zeta)^3}\right] m \quad \ldots (7.4)$$

Model B IV $\quad i_1 = 0, \quad i_2 = 0, \quad \zeta = 5/36$

(a) Equivalent slab Method

$$P_A = \frac{16 M_e \, m}{(1-\zeta)} \qquad \ldots\ldots\ldots\ldots\ldots\ldots\ldots\ldots\ldots\ldots \quad (7.5)$$

$$P_B = \frac{4\sqrt{M_i (3-4\zeta)}}{\sqrt{4(1-\zeta)^3 - 1}} \, m \qquad \ldots\ldots\ldots\ldots\ldots\ldots\ldots\ldots \quad (7.6)$$

(b) Beams and slab Method

$$P_A = \frac{16 M_e \, m}{(1-\zeta)} \qquad \ldots\ldots\ldots\ldots\ldots\ldots\ldots\ldots\ldots\ldots \quad (7.7)$$

$$P_B = \frac{4M_c}{(1-\zeta)L} + 2\left[\frac{4M_s \rho}{(1-\zeta)} + \frac{1}{\rho} - \frac{1}{2\rho(1-\zeta)} + \frac{1}{4\rho(1-\zeta)^3}\right] m \quad \ldots (7.8)$$

7.9 Comparison of theory and tests

7.9.1 Control Beams

The ultimate moments and the corresponding concrete edge strains and Shape Factors of Control Beams obtained from theory and tests are compared in Tables 7.5 and 7.6 respecively.

7.9.2 Model bridges

The theoretical and experimental ultimate loads of Model Bridges are compared in Table 7.7. The values of $\phi/2$, ψ and x for yield patterns are compared in Table 7.7(a) (P.77h)

7.10 Ratios of yield load to ultimate load of Model bridges

The ratios of yield load to ultimate load of Model bridges for the given loading conditions are calculated from theory using Harmonic Analysis (92)

determine the load at first yield. In applying the above analysis, zero torsional rigidity for all models except Model A III was assumed and the parameter "α" for the transformed section was evaluated using the modular ratio equal to $500/\sqrt{C_u}$ (70). The average value of "α" for all the models was found to be 12. For model A III, torsional rigidity was considered ("β" = 1.22) since the two unloaded beams were firmly anchored down at the supports.

The above ratios obtained from the tests are presented along with the theoretical ones in Table 7.8 for ready comparison.

TABLE 7.5

Comparison of theory and tests on control beams

Control Beam	ultimate moments, M_c, Ton-in.			Maximum concrete edge strain, e_{cu}, (10^{-2} in/in.)		
	Theory	Test	$\frac{\text{Test}}{\text{Theory}}$	Theory	Test	$\frac{\text{Test}}{\text{Theory}}$
A I CB	59.22	72.6	1.22	0.332	0.403	1.22
A II CB	58.81	73.5	1.25	0.334	0.354	1.06
A III CB	61.75	81.32	1.32	0.318	0.50	1.57
B I CB	45.89	44.5	0.97	0.333	0.48	1.44
B II CB	47.32	57.3	1.22	0.318	0.50	1.57
B III CB	46.57	54.1	1.16	0.327	0.40	1.22

TABLE 7.6

Comparison of theoretical and experimental shape factors

Control Beam	Theoretical		Experimental	
	M_y Ton-in.	Shape Factor M_c/M_y	M_y Ton-in.	Shape Factor M_c/M_y
A I CB	40.0	1.48	41.0	1.76
A II CB	41.4	1.42	41.0	1.79
A III CB	42.0	1.47	43.0	1.87
B I CB	31.1	1.48	23.0	1.94
B II CB	32.5	1.46	31.0	1.85
B III CB	32.5	1.44	32.0	1.69

TABLE 7.7

Comparison of Theory and Tests on Model bridges

Model	Equivalent slab Method				Beam and slab method		
	P_A (tons)	P_B (tons)	P_{test}	$\frac{P_{test}}{P_{min}}$	P_A (tons)	P_B (tons)	$\frac{P_{test}}{P_{min}}$
A I	9.98	8.4	8.5	1.01	9.98	8.72	0.97
A II	9.85	7.95	9,15	1.16	9.85	8.69	1.05
A III	12.40	10.31	9.85	0.96	12.40	8.54	1.15
A IV	9.45	7.63	8.5	1.12	9.45	7.78	1.10
L I	12.33	10.10	9.5	0.94	12.33	10.40	0.92
B II	12.36	9.14	9.7	1.06	12.36	9.23	1.05
B III	12.10	11.68	13.85	1.18	12.10	12.15	1.14
B IV	9.45	8.65	8.6	0.99	9.45	9.13	0.94
S G_s	-	27.5	35.0	1.27	-	34.15	1.01

TABLE 7.8

Ratios of yield load to ultimate load of model bridges

Model	Theory			Experiment		
	yield load, P_y, tons	ultimate Load P_u, tons	P_u/P_y	yield load P_y, tons	Ultimate Load P_u, tons.	P_u/P_y
A I	5.57	7.48	1.31	4.8	8.5	1.77
A II	5.57	7.34	1.29	5.0	9.15	1.83
A III	4.85	8.54	1.76	5.2	9.85	1.89
B I	4.58	9.87	2.15	4.5	9.5	2.11
B II	4.00	8.83	2.20	4.5	9.7	2.15
B III	6.38	11.05	1.73	5.6	13.85	2.47
B IV	5.24	7.99	1.52	4.2	8.6	2.02

CHAPTER 8

CONCLUSIONS

8.1 Preliminary Remarks

The following conclusions drawn from the results of tests on eight small-scale models may be considered in general as qualitative. Even the few quantitative statements should be considered as tentative in view of the character and limitations of the test programme. It was not expected that the tests would yield definite answers to the many questions regarding the behaviour of Composite Beam and slab structures near collapse. It was hoped that the small-scale models could more conveniently be fabricated and tested within the limits of time and would provide further insight into the nature of the problem, though full-size tests of bridges are desirable for many reasons For one thing, the stress-strain properties of steel used in small-size reinforcement and joists are not the same as those of steel used in large-size sections of a full-size structure. The self weight in a small-scale model is small and is often ignored in the analysis whereas in a full-size bridge it is considerable and may influence the mode of failure. Obviously, tests of full-size bridges would provide more conclusive evidence regarding the validity of the theoretical analysis. However, it is believed that the test programme reported herein has yielded much useful information. It may be mentioned here that in postulating different collapse mechanisms, only straight line yield patterns are considered in order to simplify the theory. Experience shows (21) that curved yield line patterns do not change the ultimate load to any great extent and any small gain of accuracy is not worth the labour involved in solving the complicated algebraic expressions especially in the analysis of orthotropic slabs.

8.2 Composite Beams and slab

(i) Where strain-hardening of steel is negligibly small, the theory based on the assumption that concrete attains 2/3 cube strength or the value given by Hognestad's stress block (Fig. 2.3) at maximum moment, predicts a sufficiently accurate value of moment compared with test results. The ultimate moment calculated on the basis of 4/9 cube strength (C.P.117, part 1, 1965) is conservative.

(ii) where strain-hardening of steel is present, a theory is developed in Chapter 3 to predict the ultimate moment of a composite beam This prediction is in close agreement with the test results (Tab 3.1), provided the correct values of r and s are well ascertained by tensile tests on steel specimens. The control tests in the present investigation indicate that there is wide variation in the value r and s for the specimens cut from the same steel section.

(iii) The strains measured show that the strain distribution is more or less linear across the depth of the composite section implying that any slip present at interface can be ignored.

(iv) The longitudinal strain distribution across the width of the slab shown in Fig. 6.2(b) agrees well with the theory behind the concept of effective width of slabs.

(v) In the tests the extreme fibre strain in concrete at maximum moment varied from 0.0033 to 0.005. The formula (3.10) gives a safe estimate of the value of this strain.

(vi) In all the beams tested, the neutral axis moved upwards after the bottom flange of the beam yielded and was in the slab at maximum moment. The strain distribution shows that the longitudinal rein-

forcement at the top of the slab has yielded, as assumed, at maximum moment. It also shows that at maximum moment the section was fully plastic in beams where strain-hardening of steel was not appreciable. In beams where strain-hardening of steel was appreciable, the steel section was not fully plastic, the neutral axis being relatively nearer the top flange of the steel joist.

(vii) The Shape Factor determined from the tests varied from 1.69 to 1.94. The theoretical shape factor varied from 1.42 to 1.48.

8.3 Bridge models

(i) The test results show ample evidence of the real nature of the yield lines and the validity of the theory.

(ii) The differences between the theory and test results were of minor importance and on the conservative side, with a few exceptions. The tendency of the tests to give greater ultimate loads than the yield line theory may be attributed mainly to

(a) membrane effect inherent in T-beam action.

(b) strain-hardening of steel, where it occurred.

(iii) Of the two methods of analysis, (i) Equivalent slab Method and (ii) Beam and slab Method, the former generally gave lower values of collapse load for all the models under investigation. The patterns of yield lines calculated from both the methods did not differ much. Though more experimental evidence is needed before the relative merits of the two methods are decided, it can be stated that the former method is more suited to the analysis of a bridge deck with smaller rib sizes which would approach the behaviour of an orthotropic slab, and the

latter method to a bridge deck with larger rib sizes. The steel beams in this case would obviously act as strong supports to the slab.

(iv) The observed yield patterns generally corresponded to the theoretical patterns. When two patterns gave more or less the same ultimate load, both the yield patterns were observed as in Model B III (Fig. 6.29b).

(v) The strains and the deflections measured in the beams of the model bridges were similar to those of control beams, although slightly smaller in magnitude. It is therefore sufficiently accurate to use the sectional properties of the separate elements in analysing the complete system.

(vi) The ratios of yield to ultimate load obtained from test results varied from 1.77 to 1.89 in models of A-series and from 2.11 to 2.47 in those of B-series. The steel used in beams of A-series had higher strength at first yield than the steel used in beams of B-series. The theoretical values of the above ratios varied from 1.29 to 1.76 in models of A-series and from 1.20 to 2.20 in those of B-series (Table 7.8). It is therefore suggested that due consideration should be given to the yield strength of steel in choosing a load factor.

8.4 Punching Failure

(i) The chances of failure of a bridge deck due to punching of the slab are less if the point loads over a panel of panels are accompanied by other point loads over the beams as in a multi.point loading simulating the wheel loads of a HB vehicle.

(ii) Under a multi-point loading, mentioned above, it is possible to prevent altogether, a punching failure if the relative strengths of beam and slab and the geometry of their arrangement are properly designed.

Bibliography

(1) Baker, J.F. "The design of steel frames" Structional Engineer. Vol. 27 (1949).

(2) Baker, J.F., Horne, M.R., and Heyman, J., "The Steel Skeleton Vol. 2". Cambridge University Press 1956.

(3) Neal B.G., "The plastic methods of structural Analysis" Chapman and Hall.

(4) Beedle, L.S. Plastic Design of Steel Frames " John Wiley (N.Y.), 1958.

(5) Johansen, K.W. Brudlinietiorier, I Kommission Los Teknisk Forlag, Copenhagen, 1952. Originally a doctor's thesis in Danish.

(6) Johansen, K.W. "Yield-line theory". English translation published by Cement and Concrete Association, London, 1962.

(7) Greenberg, H.J., and Prager, W. "On limit design of beams and frames" Trans.ASCE No 117, 1952.

(8) Horne, M.R., "Fundamental Propositions in the Plastic Theory of Structures Journal of I.C.E. 34, 1950.

(9) Siess, C.P., "Review of research on ultimate strength of reinforced concrete members" Journal of A.C.I. June 1952.

(10) Baker, A.L.L., "The ultimate load theory applied to the design of reinforced and prestressed concrete frames. London. Concrete Publications Ltd, 1956.

(11) Ernst, G.C., Moment and shear redistribution in two span continuous reinforced concrete beams. A.C.I. Journal Vol. 30, No. 5, Nov. 1958.

(12) Corley, W.G. "Rotational capacity of Reinforced Concrete Beams" Journal of the Struct. Div. Proc. ASCE Oct. 1965. Vol. 92. No. ST5

(13) Jones, L.L. and Wood, R.H., "Yield-line analysis of slabs" Thames and Hudson. Chatto and Windus 1967.

(14) Bach, "Elasticität und Restigkeit ". Berlin, Springer Verlog, 1914.

(15) Svenson, "Ingeniören" 1916 and Laerebog i Jaernbeton, 1918, 1931.

(16) Ingerslav, A. "Strength of rectangular slabs" Journal Inst. Struct. Engineers. Vol. 1 Jan. 1923.

(17) Hognestad, E. "Yield-line theory for the ultimate flexural strength of Reinforced concrete slabs."

(18) Mansfield, E.H., "Studies in Collapse analysis of rigid-plastic plates with a square yield diagram". Proc. Roy. Soc. (A) Vol. 241, 1957.

(19) Prager, W., and Hodge, P.G., "Theory of perfectly plastic solids" Wiley.

(20) Prager, W., "Discontinuous fields of plastic stress and flow" Proc. 2nd U.S. National Congress of App. Mech. 1954. Published by A.S.M.E.

(21) Wood, R.H. "Plastic and elastic design of slabs and plates, London. Thames and Hudson, 1961.

(22) Kemp, K.O., "The evaluation of nodal and edge forces in the yield-line theory" in Recent Developments in yield-line theory. M.C.R. Special publications May 1965. Cement and Concrete Association.

(23) Morley, C.T., "Equilibrium methods for exact upper bounds of rigid plastic plates" Publication same as (22).

(24) Wood, R.H., "New Techniques in nodal force theory for slabs". Publication same as (22).

(25) Zones, L.L. "The use of nodal forces in yield line analysis". Publication same as (22).

(26) Hillerborg, S., "A plastic theory for the design of reinforced concrete

slabs". Prel. publications, 6th congress, Int. Ass. Bn. & Struct. Eng. Stockholm, 1960.

(27) Sawezuk, A., and Jaeger, T., Grenstrag fahigkeits-Theorie der Platten, Springen-Verlag.

(28) Baus, R. and Tolaccia, S., Calcul a la rupture des dalles en beton arme et etude experimentale du batiment et des travaux publics, September, 1963.

(29) Kemp, K.O., "The Yield criterion for orthotropically Reinforced slabs". International Journal of Mechanical Sciences, V. 7, No. 11. Nov. 1965.

(30) Lenshow, Rolf and Mite A. Sozen., "A Yield criterion for Reinforced Concrete Slabs" Journal of A.C.I. No. 5. Proc. V. 64 May 1967.

(31) Nielsen, M.P., "Vridnings for og med Jernbetonplader" Academy of Engineering, Copenhagen, 1965.

(32) Kwiecinski, M.W., "Yield criterion for Initially Isotropic Reinforced slab". Magazine of Concrete Research (London), V. 17, no. 51, June 1965.

(33) Kwiecinski, M.W. "Some tests on the yield criterion for a Reinforced concrete slab". Magazine of Concrete Research (London), V. 17, no. 52, September, 1965.

(34) Hillerborg, A., "Armering av elasticitetsteoretiskt beraknade platten, Skivor och skel" Betong (Stockholm), 1953.

(35) Lenkei, P., "Some Problems of Yield Conditions for Reinforced Concrete slabs," Bulletin No. 2, Scientific Institute for Building (ETI), Budapest, 1966.

(36) Park, R., "Ultimate strength of rectangular concrete slabs under short term uniform loading with edges restrained against lateral movement" Proc. I.C.E. London, June 1964.

(37) Ockleston, A.J., "Loading test on reinforced concrete slabs spanning in two directions. Paper no. 6, Portland Cement Institute, Richmond, Johannesburg.

(38) Nylander, H., "Korsarmerade betongplatter". Bull. 5. Roy. Inst. Tech. Stockholm.

(39) Reports 26A, B, C, of the Commissic voor vitroering van Research ingelsteld door de betonvereinigung-Betonverenigung, Nassau Dillenburg Stras, 42, Den Haag.

(40) Nylander, H., Punching of Reinforced concrete slabs, Bulletin d' information No. 44. Commite Europeen du Beton, 8 Avenue de l'Arsenal Luxembourg.

(41) Hognestad, E., Hanson, N.W., and McHenry, D. "Concrete stress distribution in ultimate strength design", Journal of A.C.I. Vol. 27, No. 4. Dec. 1955.

(42) Mattock, A.H., "The strength of singly reinforced beams in bending". Proc. of a symposium on the strength of concrete structures." Cement and concrete Association, London, May, 1956.

(43) Morice, P.B., "The strength of simply supported slab bridges subjected to concentrated loads". Proc. of a Symposium on the strength of concrete structures. Cement and Concrete Association, London, May, 1956.

(44) Roderick, J.W., and Heyman, J., "Extension of the simple plastic theory to take account of the strain-hardening range". Proc. Inst. Mech. Engrs. W.E.P. nos. 63-69, 1951. Vol. 165 p. 189.

(45) Medland, I.C., "Strain-hardening and the collapse of steel frame works" Ph.D. Thesis, 1963, Victoria University of Manchester.

(46) Sawko, F. "Effect of strain-hardening on the elasto-plastic behaviour

(47) Discussion on (46), Proc. Instn. Civ. Engrs, Vol. 32, pp 294-307, October 1965.

(48) Sawko, F., "Collapse load of structures allowing for strain-hardening." Proc. Inst. Civ. Engrs. Vol. 31, pp. 147-153.

(49) Maxwell, G. Lay., "A new approach to inelastic structural design". Proc. Instn. Civ. Engrs., Vol. 34, pp 1-24. May 1966.

(50) Horned, M.R., and Chin, M.W., "Plastic design of portal frames allowing for frame instability and strain-hardening effects" Proc. I.C.E., Vol. 37, May 1967.

(51) Sawko, F., and Wilde, A.M.B., "Automatic analysis of strain-hardening structures (with particular reference to steel B.S. 986). Proc. I.C.E. Vol. 37, May 1967.

(52) Davies, J.M., "Frame instability and strain hardening in plastic theory" Jl. of struct. Div., ASCE, Vol. 92, no. ST3, Proc. paper 4836, June 1966, pp. 1-15.

(53) Adekola, A.O., "Interaction between steel beams and a concrete floor slab." Ph.D. Thesis, Nov. 1959. Imperial College of Science and Technology, London.

(54) Barnard, P.R., and Johnson, R.P., "Ultimate strength of Composite Beams" Proc. I.C.E., Vol. 32, Oct. 1965.

(55) Siess, C.P., Viest, I.M., and Newmark, N.M. "Studies of slab and highway bridges, part III. "Small scale tests of shear connectors and composite T-beams" University of Illinois Engineering Experimental station Bulletin 396.

(56) Viest, I.M., Fountain, R.S., and Singleton, R.C., "Composite construction in steel and concrete." McGraw Hill Book Co. New York, 1958.

(57) Chapman, J.C., and Balakrishnan, S., "Experiments on composite beams". Structural Engineer, Vol. 42, Nov. 1964.

(58) Chapman, J.C., "Composite Construction in steel and concrete. The behaviour of composite beams" Structural Engineer, Vol. 42. Apr . 1964.

(59) Slutter, R.G., and Driscoll Jr., Flexural strength of steel-concrete composite beams". Jl. of struct. Div. Proc. ASCE, Vol. 91, (1) April 1965.

(60) Holmes, M. "Ph.D. Thesis" University of Bristol, 1958.

(61) Odquist, F. "On the effective width of reinforced plane plates" Royal Swedish Air Board, Translation No. 5, 1948.

(62) Allen, D.N. de G., and Severn, R.T., "Composite action between Beams and slabs under transverse load." The struct. Engr. Vol. XXXIX, No. 5. May 1961.

(63) Yuille, I.H. "Shear lag in stiffened plating" Trans. Inst. of Naval Architects, Vol. 97, 1955.

(64) Timoshenko, S. and Gordier, J.N., "Theory of Elasticity", McGraw Hill Book Co. N.Y. 1951.

(65) Kemp, A.R., "Composite steel-concrete floor systems" Ph.D. Thesis September, 1966. University of Cambridge.

(66) Bresler, B., and Pister, K.S., "Strength of concrete under combined stress". Proc. A.C.I. 55, September, 1958.

(67) Goode, C.D., and Helmy, M.A., "The strength of concrete under co shear and direct stress". Magazine of concrete Research, Vol. 19, No. 59, June 1967.

(68) Davies, J.D., "Structural Concrete" The Macmillan Co. New York, 1

(69) Johnson, R.P., "Ultimate strength Design of sagging moment re

composite beams" Technical report no. S/11. August 1967. Cambridge University.

(70) B.S. Code on "Composite construction in structural steel and concrete" C.P. 117, part 2 for bridges, 1967.

(71) ACI-ASCE Committee 333, "Tentative recommendations for design of composite beams and girders for buildings." Jl. of ACI Dec. 1960.

(72) Brendel, G., "Strength of the compression slab of T-beams subject to simple bending" Jl. of ACI. Jan. 1964. Proc. Vol. 61. no. 1

(73) B.S. code of practice, C.P. 117 part 1. 1965. Composite construction in structural steel and concrete.

(74) Barnard, P.R., "On the collapse of Composite Beams" Ph.D. Thesis, University of Cambridge, September, 1963.

(75) Massonnet, C., Methode de calcul des ponts a poutres multiples tenant compte de leur resistance a la torsion (Method of calculation of bridges with several longitudinal beams, taking into consideration their torsional resistance). Zurich, International Association for Bridge and Structural Engineering. Publications. Vol. 10, 1950.

(76) Morice, P.B., and Little, G., "Analysis of right bridge decks subjected to abnormal loading". Cement and Concrete Association, London (1956).

(77) Rowe, R.E., "Concrete Bridge Design" John Wiley and Sons, Inc. N.Y.

(78) Sawko, F. and Saha, G.P., "Ultimate Load Analysis of Bridge Decks". Building Science, Vol. 2. November 1967. Pergamon Press Oxford. London, New York, Paris.

(79) Reynolds, C.G., "The strength of prestressed concrete grillage Bridges" Technical Report TRA/268 (1967). Cement and Concrete Association, London.

(80) Siess, C.P., and Viest, I.M., "Tests of Continuous Right I. Beam Bridges" University of Illinois Engineering Station Bulletin Series No. 416.

(81) Richart, F.E., and R.W. Kluge, "Tests of Reinforced concrete slabs subjected to concentrated loads" University of Illinois Bulletin 314, June 10, 1939.

(82) Base, G.D., "Some tests on punching shear strength of reinforced concrete slabs". Cement and Concrete Association, London.

(83) Short, A., and Thomas, F.G. "Studies of Bridge-deck systems III. Tests on Model slab-and-girder bridge-deck systems". National Building Studies. Research Paper 37, H.M.S. Office, London, 1963.

(84) Newmark, N.M., Siess, C.P., and Penmann, R.R., "Tests of Simple Span right I-Beam bridges". University of Illinois Bulletin 363.

(85) Teychenne, D.C., "Proc. Symposium on Mix Design and quality control of concrete. 1954." Cement and Concrete Association, London.

(86) Whitney, C.S. "Ultimate strenth of R.C. Flat slabs, Footings, Beams and Frame Members without shear reinforcement". Journal of ACI. Oct. 1957. No. 4. Vol. 29.

(87) Yitzhaki, D., "Punching strength of Reinforced Concrete Slabs" Journal of ACI, May 1966.

(88) Moe, J. "Shearing strength of reinforced concrete slabs and footings under concentrated loads" Portland Cement Association Research and Development Department Bulletin D 47.

(89) Hendry, A. W., "Elements of Experimental stress Analysis". Perganon Press, 1964.

(90) Soane, A.J.M., "Automatic strain Recording Equipment" "The Analysis of Interconnected shear walls" Ph.D. Thesis, 1966, University of Edinburgh.

(91) Siess, C.P., Viest, I.M., and Newmark., "Small scale Tests of shear Connectors and Composite T-Beams" University of Illinois Engineering Expt. Station Bulletin 396.

(92) Hendry, .A.W., and Jaeger, L.G., "The Analysis of Grid Frame works and Related Structures". Chatto and Windus, 1958.

APPEDIX 1

Computer programme for calculating Ultimate Moment of Composite Beam allowing for strain-hardening

Notation

As = Area of steel section, sq.in,

af = Ratio of flange area to area of steel section,

aw = Ratio of web area to area of steel section,

D = Depth of Composite section, in,

t = Thickness of slab, in,

B = Width of flange, in,

L = Length of span of beam, in,

fy = Yield stress of steel in beams, tsi,

E = Young's Modulus, tsi,

r = Ratio of strain at strain-hardening to strain at first yield,

s = Ratio of Young's Modulus E to strain-hardening modulus E_{sh},

Ar = Area of longitudinal reinforcement at top of slab, sq.in,

fyr= Yield stress of reinforcing steel, tsi,

cr = Cover to the centre of longitudinal reinforcement, in,

fcc= Cylinder strength of concrete, psi,

ecu= Concrete edge strain,

v1 = α' as given by Eq.(2.2),

v2 = β as given by Eq.(2.3),

Be = Effective width, in,

n1 = Depth of neutral axis from top of slab, in,

eu = Curvature, in^{-1},

n = Ratio of N.A. Depth to depth of Composite section,

fyy= Stress at top of steel section, tsi,

fs = Strain-hardening stress, tsi,

ae, as as shown in Fig.3.5,

eyy= Strain at top of steel section,

ey = Strain in steel at first yield,

ee = Strain at bottom of steel section at Ultimate moment,

C = Total compressive force, tons,

T = Total tension in steel, tons,

l = Distance of T from interface, in,

zp = Distance of C from interface, in,

jd = l+zp =Lever arm, in,

Mp =MU = Ultimate moment, ton-in,

WU = Ultimate load at mid span, tons.

PROGRAMME

```
***A
CIE 015/0000 0006 MU REDDY
OUTPUT
0 LINE PRINTER 1000 LINES
EXECUTION 3 MINUTES
COMPILER AA

begin
real As,af,aw,as,ap,ae,D,d,t,fy,E,r,s,Ar,fyr,fc,fcc,c
     ecu,v1,v2,B,Be,L,k,k1,f,g,ee,ey,eyy,u,fs,fyy,P1,c
     P2,F1,F2,np,nf,C,T,l,zp,MU,WU,n,c
     A1,B1,cr,Mp,jd, cu,n1
integer m,i
  m=0
  read(As,af,aw,D,t,B,L)
1:read(fy,E,r,s,Ar,fyr,cr)
  m=m+1
  newpage
  caption $beam$A
  print(m,2,0)
  caption $==========
  newlines (2)
  i=0
2:i=i+1
  read (fcc)
  if fcc=-1 then ->1
  if fcc=-99 then stop
  if i=1 then ->21
  if i=2  then ->22
  read(ecu,v1,v2)
  ->3
  21:ecu=.004-fcc/6.5e6
     v2=.5-fcc/79950
     v1=(3897+.35*fcc)/(3200+fcc)
    ->3
```

```
  22:read(ecu,v1,v2)
  3:caption #D$=$
  print (D,2,2)
  caption $$ fcc $=$
  print (fcc,4,0)
  caption $$$$ ecu $=$
  print (ecu,1,5)
  caption $$$$ v1 $=$
  print (v1,1,3)
  caption $$$$ v2 $=$
  print (v2,1,3)
  fc=fcc/2240
  Be=(1-.525*v1*B/(v2*L))*B
  d=D-t
  k=As*fy/(v1*Be*D*fc)
  k1=Ar*fyr/(v1*Be*D*fc)
  f=D/d;ey=fy/E;u=ecu/ey;g=t/D
  A1=2*s*u- aw*f*k*((u+r)*2-s*(1+u)*2)
  P1=2*u*k*((1-k1/k)*s-(u+r)*(af+aw*f)c
  -s*(1+u)*(af-aw*f*g))/A1
  P2=k*u*2*((2*af+aw*f)+g*s*(2*af-aw*f*g))/A1
  np=(P1+sqrt(P1*2+4*P2))/2
  fyy=u/np*(g-np)*fy
  B1=2*s*u-aw*f*k*(u+r)*2
  F1=2*u*k*((1-k1/k)*s-(u+r)*(af+aw*f))/B1
  F2=k*u*2*(2*af+aw*f)/B1
  nf=(F1+sqrt(F1*2+4*F2))/2
  if fyy>fy then ->4
  n=np
  caption #steel$is$partially$elastic#
  ->5
4:n=nf
  fyy=fy
  caption #steel$is$fully$plastic#
5:fs=fy/s*(u/n-(u+r))
  as=1-n*(u+r)/u
  if fs>0  then  ->55
  fs=0
  as=0
55:ap=n*(r-1)/u
   ae=n*(fy-fyy)/(u*fy)
  eyy=fyy/E; ee=ecu*(1-n)/n
 caption $$ Be $=$
 print(Be,2,2)
 n1=n*D
 cu=ecu/n1
caption $$ n1 $=$
print(n1,2,2)
caption $$ cu$=$
print (cu,0,7)
```

```
C=v1*Be*fc*n*D+Ar*fyr
T=As*fy+af*As*fs+aw*As*as*f*fs/2-af*As*(fy-fyy)c
  -aw*As*ae*f*(fy-fyy)/2
  l=(As*fy*d/2+af*As*fs*d+aw*As*as*f*fs/2*(d-as*D/3)c
  -aw*As*ae*f*(fy-fyy)/2*ae*D/3)/T
  zp=(v1*Be*fc*n*D*(g*D-v2*n*D)+Ar*fyr*(g*D-cr))/C
  jd=l+zp
  MU=T*jd
  WU=MU*4/L
  Mp=As*fy*(D-d/2)+af*As*fs*D+aw*As*as*f*fs/2*(D-as*D/3)c
  -af*As*(fy-fyy)*t-aw*As*ae*f*(fy-fyy)*(ae*D/3+t)/2c
  -v1*Be*n*D*fc*v2*n*D-Ar*fyr*cr
caption $$$n$=$
print(n,1,3)
caption $$ fyy $=$
print (fyy,2,2)
caption $$ fs $=$
print (fs,2,2)
caption $$ ae $=$
print (ae,1,3)
caption$$ as $=$
print (as,1,3)
caption $$ eyy $=$
print (eyy,1,5)
caption $$ ey $=$
print (ey,1,5)
caption $$ ee $=$
print (ee,2,5)
newlines (2)
caption $$ C $=$
print (C,5,2)
caption $$ T $=$
print (T,5,2)
caption $$ l $=$
print (l,2,2)
caption $$ zp $=$
print (zp,1,2)
caption $$ jd $=$
print (jd,2,2)
caption $$ MU $=$
print (MU,6,2)
caption $$ Mp $=$
print(Mp,6,2)
caption $$ WU $=$
print (WU,3,2)
newlines(2)
->2
end of program
```

DATA FOR BEAMS A_1 TO A_6 (Table 3.1)

```
    13  .333  .333  18  6  48  216
15.35  13000 11.3  21  3.07  15.25  1.313
3635
3635  .0038  1  .5
3635  .0038  .925  .5
3635  .0038  .85  .5  -1
14.74  13300  4.6  17.7  .306  15.25  1.156
4220
4220  .0038  1  .5
4220  .0038  .925  .5
4220  .0038  .85  .5  -1
16.95  13200  1  21.15  .306  15.25  1.156
3030
3030  .0038  1  .5
3030  .0038  .925  .5
3030  .0038  .85  .5  -1
16.36  13400  1  10.66  .306  15.25  1.156
3880
3880  .0038  1  .5
3880  .0038  .925  .5
3880  .0038  .85  .5  -1

15.34  13300  1  10.66  .306  15.25  1.156
5010
5010  .0038  1  .5
5010  .0038  .925  .5
5010  .0038  .85  .5  -1
 14.87  13700  2.4  17.7  .306  15.25  1.156
5040
5040  .0038  1  .5
5040  .0038  .925  .5
5040  .0038  .85  .5  -99
***Z
```

DATA FOR BEAMS AICB TO BIIICB (Table 7.1)

```
1.18  .333  .333  4.5  1.5  12  72
20.09  13400  1  30  .0492  26.8  .3125
4450
4450  .0038  1  .5
4450  .0038  .925  .5
4450  .0038  .85  .5  -1
20.09  13400  1  30  .0492  26.8  .3125
4320
4320  .0038  1  .5
4320  .0038  .925  .5
4320  .0038  .85  .5  -1
20.09  13400  1  30  .0492  26.8  .3125
5340
5340  .0038  1  .5
5340  .0038  .925  .5
5340  .0038  .85  .5  -1
15.60  13200  13  62.5  .0492  26.8  .3125
4370
4370  .0038  1  .5
4370  .0038  .925  .5
4370  .0038  .85  .5  -1
15.60  13200  13  62.5  .0492  26.8  .3125
5310
5310  .0038  1  .5
5310  .0038  .925  .5
5310  .0038  .85  .5  -1
15.60  13200  13  62.5  .04952  26.8  .3125
4750
4750  .0038  1  .5
4750  .0038  .925  .5
4750  .0038  .85  .5  -99
***Z
```